NAVAL SHIP RESEARCH AND DEVELOPMENT CENTER
Washington, D.C. 20034

[redacted]

[redacted]

CRITICAL REVIEW OF FRACTURE AND FATIGUE ANALYSIS

by
O. Lomacky and H. Vanderveldt

[redacted]

STRUCTURES DEPARTMENT
RESEARCH AND DEVELOPMENT REPORT

March 1972

Report 3655

Report 3655

CRITICAL REVIEW OF FRACTURE AND FATIGUE ANALYSIS

The Naval Ship Research and Development Center is a U. S. Navy center for laboratory effort directed at achieving improved sea and air vehicles. It was formed in March 1967 by merging the David Taylor Model Basin at Carderock, Maryland with the Marine Engineering Laboratory at Annapolis, Maryland.

Naval Ship Research and Development Center
Bethesda, Md. 20034

MAJOR NSRDC ORGANIZATIONAL COMPONENTS

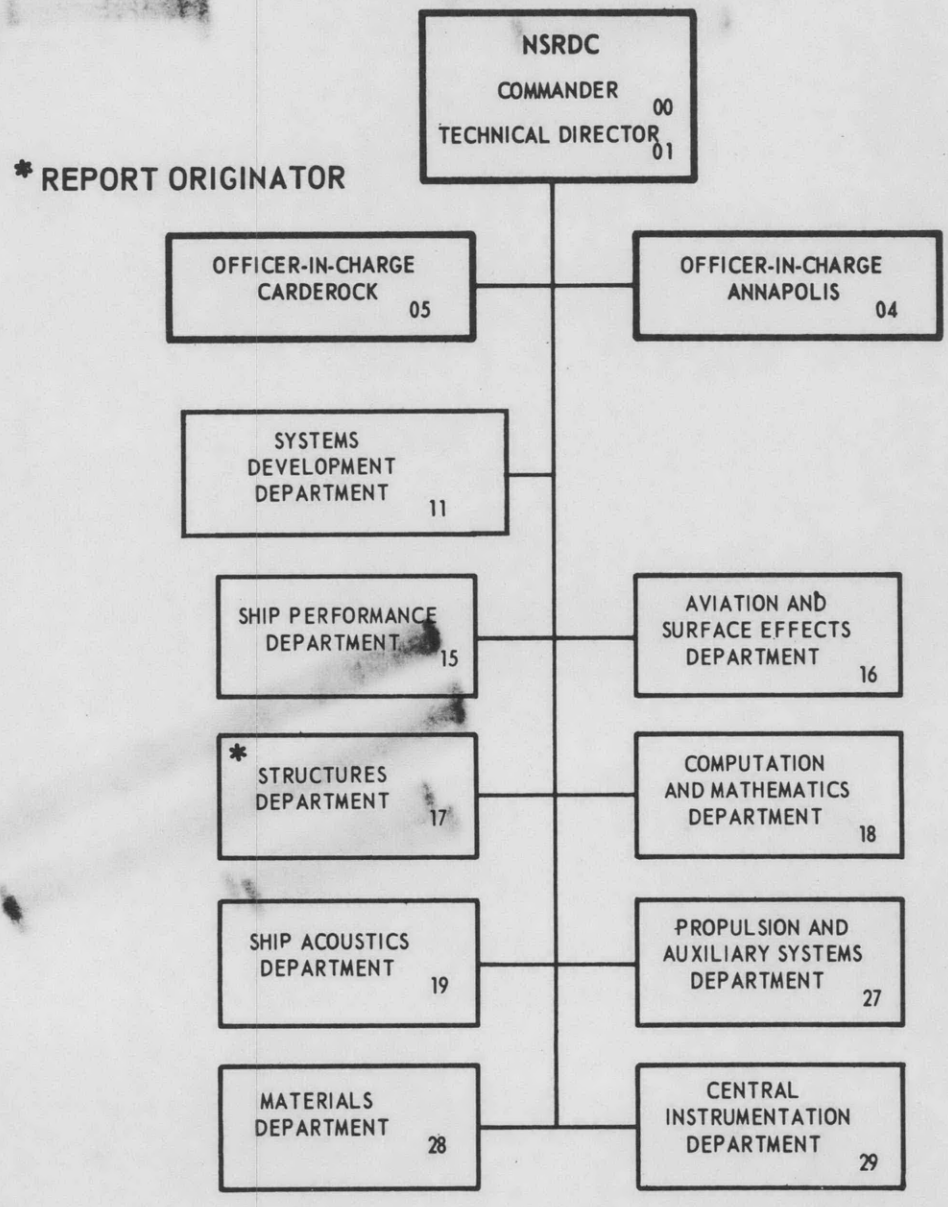

DEPARTMENT OF THE NAVY
NAVAL SHIP RESEARCH AND DEVELOPMENT CENTER
WASHINGTON, D.C. 20034

CRITICAL REVIEW OF FRACTURE AND FATIGUE ANALYSIS

by

O. Lomacky and H. Vanderveldt

March 1972

Report 3655

TABLE OF CONTENTS

Page

ABSTRACT 1

ADMINISTRATIVE INFORMATION 1

PREFACE 1

STRESS ANALYSIS NEAR STATIONARY CRACKS AND FRACTURE CRITERIA UNDER MONOTONIC LOADING 4
- INTRODUCTION 4
- ELASTIC ANALYSIS 5
- ELASTIC-PLASTIC ANALYSIS 17
- FRACTURE CRITERIA UNDER MONOTONIC LOADING 37

SUBCRITICAL CRACK INITIATION AND GROWTH 63
- INTRODUCTION 63
- CRACK GROWTH UNDER MONOTONIC LOADING 70
- CRACK INITIATION UNDER CONSTANT AMPLITUDE CYCLIC LOADING 75
- CRACK PROPAGATION UNDER CYCLIC LOADING 87
- CUMULATIVE DAMAGE ANALYSIS 119
- BIAXIALITY EFFECTS, MODE II AND COMBINED MODE DEFORMATION 132
- CRACK INITIATION AND GROWTH UNDER CYCLIC COMPRESSION 140

ENVIRONMENTAL EFFECTS 150
- INTRODUCTION 150
- FUNDAMENTAL STRESS CORROSION APPROACH 152
- FRACTURE MECHANICS APPROACH 156
- SOME SPECIFIC METALS AND ENVIRONMENTS 176

SUMMARY 182

REFERENCES 241

LIST OF FIGURES

Page

Figure 1 - Basic Modes of Crack Extension 187

Figure 2 - Polar and Rectangular Components of Stress Around Crack Tip 187

Figure 3 - Local Coordinate System of Crack-Border Stress Components 187

Figure 4 - Shell Element with Elliptical Flaw under General Loading 188

Figure 5 - All-Around Bending of Straight Crack in Flat Plate 188

Figure 6 - Magnitude of Local Stresses in Reissner Plate 189

Figure 7 - Internally Pressurized Cylinder with a Through Crack 189

Page

Figure 8 - Stress Intensity Ratio P_e versus λ (Tension) 190

Figure 9 - Stress Intensity Ratio P_b versus λ (Bending) 190

Figure 10 - Elliptical Crack Embedded in a Wall Subjected to Uniaxial Tension 191

Figure 11 - Magnification Factor for Stress Intensity Factor for Two Coplanar Cracks in Infinite Solid Subjected to Uniaxial Tension 191

Figure 12 - Slip Line Field Near a Crack Tip in a Plane Strain 192

Figure 13 - Small Scale Yielding Formulation 192

Figure 14 - Crack in Two-Dimensional Deformation Field 192

Figure 15 - Details of the Very Near Tip Deformation in Plane Strain 193

Figure 16 - Extent of the Elastic-Plastic Boundary for Increasing Loading in Plane Strain 194

Figure 17 - Ramberg-Osgood-Type Stress-Strain Relation 194

Figure 18 - Values of I versus n (for Equation 23) 194

Figure 19 - Angular Variations of Stresses and Strains at the Tip of a Tensile Crack for Plane Strain 195

Figure 20 - Angular Variation of Stresses and Strains at the Tip of a Tensile Crack for Plane Stress 195

Figure 21 - Stress Characteristics and Stress Distribution at the Tip of a Tensile Crack in a Perfectly Plastic Material for Plane Stress 196

Figure 22 - Dugdale-Barenblatt Model for Plane Stress Yielding 196

Figure 23 - Variation of Plastic Zone Size and Crack Opening Displacement with Applied Stress for Centrally Notched Plate 197

Figure 24 - The Plastic Strain Intensity Factor as a Function of the Applied Stress for Tensile Loading 197

Figure 25 - Fully Plastic Flow Fields in Tension (Plane Strain) 197

Figure 26 - Slant and Square Fractures as a Result of the State of Stress 198

Figure 27 - Crack-Propagation in PMMA under Compression 199

Figure 28 - Crack Propagation for Arbitrarily Inclined Cracks in Brittle Plates under Uniform Tension 199

Figure 29 - Stress Components Referred to Principal Axes of Crack under Combined Shear and Normal Loading 200

Figure 30 - Critical Initiation Stress for Large Scale Yielding, Tension 200

Figure 31 - Elastic-Plastic Stable Crack Extension and Final Instability, from Antiplane Shear Theory 201

Page

Figure 32 - Fracture Mechanics Definition of $\tilde{R}$-Curve Features in Terms of Rising $\mathcal{G}$ to the Point of Instability ($\mathcal{G}_c$) 201

Figure 33 - Total Strain as a Combination of Two Linear Relations 202

Figure 34 - Relation between Percent of Life to Crack Initiation N_o and Fatigue Life N_f 202

Figure 35 - Cyclic Stress-Strain Curves for SAE 1018 Steel at Various Numbers of Cycles 203

Figure 36 - Stress and Strain Distributions in Notched Specimen under Controlled Strain Amplitude 204

Figure 37 - Stress and Strain Distributions in Notched Specimens under Controlled Force Amplitude 204

Figure 38 - Variation of ΔK_I with N_o, for Flaws in Butt-Welded 3/4-Inch-Thick HY-80 Steel Strips 205

Figure 39 - Comparison of Theoretical Crack Growth of 0.010-Inch with First Observation of 0.010-Inch Fatigue Cracks in Notched Sheets of 7075-T6 Aluminum 205

Figure 40 - Surface Lengths versus Number of Cycles of Repeated Load for HY-80 Plate Specimens Cycled Zero-Tension ($\bar{R} = 0$) and Tension-Compression ($\bar{R} = -1$) 206

Figure 41 - Plastic Superposition for Unloading 206

Figure 42 - Plasticity Estimates near Monotonically and Cyclically Loaded Cracks in Plane Strain 207

Figure 43 - Fatigue Crack Growth Curve on Log-Log Coordinates 207

Figure 44 - Stress-Intensity-Growth Rate Spectrum with Two Regimes and Definitions in Table 2 208

Figure 45 - Specimen Configuration and Result of Crack Propagation Studies on 7075-T6 Aluminum Plates Loaded Tension 209

Figure 46 - Fatigue Crack Propagation Data for Specimens Cycled Zero-to-Tension ($\bar{R} = 0$) and Fully Reversed Tension-to-Compression ($\bar{R} = -1$) 212

Figure 47 - The Plastic Blunting Process of Fatigue Crack Propagation According to Laird (1967) 212

Figure 48 - Typical Random Load Trace Showing Derivation of RMS and Associated PSD Diagram 213

Figure 49 - Examples of Statistical Counting Methods 213

Figure 50 - Idealized Crack-Growth Behavior under Two-Level Loading 214

Figure 51 - Cyclic Stress and Stress Ratio for Block-Loading Problem 214

Page

Figure 52 - Hypothetical Cyclic Strain Histories at a Notch 215

Figure 53 - Crack Extension Pattern of an Initially Slanted Crack in a Tension Plate 215

Figure 54 - Compressive Specimen Design 216

Figure 55 - Compressive Specimen Fatigue Data 216

Figure 56 - Qualitative Notch Stress-Notch Strain under Compressive Cycling 217

Figure 57 - Predicted Fatigue Curves for Notched Compression Specimens with No Residual Stress 218

Figure 58 - Predicted Fatigue Curves for Notched Compression Specimens with Initial Residual Stress 218

Figure 59 - Specimen Configuration and Results of Crack Propagation Studies on 7075-T6 Aluminum Plates Loaded in Compression 219

Figure 60 - Important Processes that Operate to Affect Stress Corrosion Cracking 220

Figure 61 - Film-Rupture Model 221

Figure 62 - Mechanochemical Model 221

Figure 63 - Adsorption Model 221

Figure 64 - Brittle Film Model and Resulting Fracture Surface 222

Figure 65 - Mechanism of Stress Corrosion Cracking 222

Figure 66 - Potential-pH Diagram and Stress Corrosion Cracking of Brass in Ammoniacal Solutions 223

Figure 67 - Determination of σ_{NSCC} for 4340 Steel Using Three Different Specimen Configuration 224

Figure 68 - Determination of K_{ISCC} for 4340 Steel Using Three Different Specimen Configuration 224

Figure 69 - Fracture Specimens 225

Figure 70 - Crack Extension Due to Stress Corrosion 227

Figure 71 - Crack Growth Rates versus Stress Intensity for H-11 Steel in Humidified Argon 227

Figure 72 - Comparison of Actual and Predicted Crack Growth Rates for Hydrogenated D6aC Steel 228

Figure 73 - Subcritical Crack Growth in Molecular Hydrogen at Atmospheric Pressure and Humidified Argon, H-11 Steel 228

Figure 74 - Oxygen and Subcritical Crack Growth in Humidified Nitrogen, H-11 Steel 228

Page

Figure 75 - Hydrogen-Oxygen Mixtures and Subcritical Crack Growth, H-11 Steel 228

Figure 76 - Subcritical Crack Growth in Different Water, Water Vapor Hydrogen, and Oxygen Environments, HY-11 Steel .. 229

Figure 77 - Crack Tip Idealization Considering Corrosion Product Wedging Action 229

Figure 78 - Suggested Method of Analyzing the Effect of Environment on Fatigue Crack Growth Rate 230

Figure 79 - Fatigue-Crack Growth in 18 Ni (250) Maraging Steels Tested in Dehumidified Argon and Hydrogen 230

Figure 80 - Fatigue Crack Propagation of 7075-T6 Alclad Aluminum in Wet and in Dry Air High Load Frequency 231

Figure 81 - Effect of Load Frequency for 2024-T3 Alclad Aluminum in Wet Air 231

Figure 82 - Fatigue Crack Propagation of 2024-T3 Alclad Aluminum in Dry Argon 232

Figure 83 - Crack Extension by Alternating Shear in a Singly Grooved Tensile Specimen 232

Figure 84 - Comparison of Crack Tip Extension after Two Load Cycles in Air and in Vacuum 233

Figure 85 - K_{ISCC} Data for Several Alloy Steels 233

Figure 86 - Stress-Corrosion Crack Growth Rate of AISI 4340 Steel in Salt Water as a Function of Stress Intensity 234

Figure 87 - Corrosion Fatigue Cyclic Crack Growth Rates in HY-80 Steel as a Function of Frequency 234

Figure 88 - Time-Based Crack Growth Rates in 4340 Steel as a Function of Frequency 235

Figure 89 - Effect of Frequency on the Crack Growth Rate of 12 Ni-5 Cr-3 Mo Maraging Steel in a 3-Percent NaCl Solution 235

Figure 90 - Stress-Corrosion Crack Growth Rates for Aluminum Alloys as a Function of Stress Intensity 236

Figure 91 - Summary of Stress Corrosion Cracking Resistance Index for Titanium Alloys in 3.5-Percent NaCl Solution 237

LIST OF TABLES

Page

Table 1 - Criteria for the Extension of Axial Through Cracks in Unstiffened Pressure Vessels 238

Table 2 - Summary of Cyclic Crack Growth Data 239

Table 3 - Stress Corrosion Characteristics of Some Titanium Alloys 240

NOTATION

a	Crack depth or minor semiaxis of semielliptical flaw
a_{cscc}	Critical crack depth under conditions of stress corrosion
C, C_1	Empirical constants associated with Equations (51) and (52) respectively
$2c$	Crack length or major axis of semielliptical flaw
D	Ductility measured in terms of area reduction in uniaxial tensile test
D_f	Diffusivity of hydrogen
d	Average facet size
$\frac{da}{dN}$ or $\frac{d(2c)}{dN}$	Crack growth rate
E	Young's modulus
E_S	Secant modulus
E_T	Tangent modulus
f_{ij}	Angular functions characterizing stress variations around crack tip
G	Shear modulus
$\mathcal{G}$	Crack extension force
$\mathcal{G}_c$	Critical crack extension force
J	Energy integral evaluated around crack tip in accordance with Formula 12
K_c	Critical stress intensity factor (fracture toughness)
K_e	Threshold value of the stress intensity factor under conditions of constant amplitude fatigue
K_f	Fatigue strength reduction factor
$(K_I)_{EC}$	Effective stress intensity factor in compression
$(K_I)_{eff}$	Effective stress intensity factor in tension
K_{Ic}	Plane strain K_c
K_{ISCC}	Critical threshold value of the stress intensity factor under conditions of stress corrosion (monotonic load)

K_t	Theoretical (elastic) stress concentration factor
K_I, K_{II}, K_{III}	Stress intensity factors in Modes I, II, and III, respectively
K_σ	Plastic stress intensity factor
K_ε	Plastic strain intensity factor
$\hat{K}_\varepsilon$	$\Delta \varepsilon_T \sqrt{a}$
m, m_1	Material constants associated with Equations (51) and (52)
max	Maximum value of the quantity
min	Minimum value of the quantity
$\overline{N}$, n	Strain hardening coefficients
N	Number of load cycles
N_o	Cycles to crack initiation
N_f	Cycles to failure
n_j	Number of load cycles applied at σ_j^{th} stress level
Q	Applied load
R	Extent of plastic zone along the direction of crack plane
$\overline{R}$	Ratio of the minimum to the maximum stress intensity of the loading cycle or ratio of the minimum to the maximum stress of the loading cycle
$\tilde{R}$	Fracture resistance of ductile materials; see Figure 32
R'	Extent of intensely strained region near the crack tip
R_m	Radius of cylindrical shell
R_{max}	Maximum extent of plastic zone
R_o	Defined by Equation 36
r, θ	Polar coordinates with the origin at the crack tip
t	Plate or shell thickness
u, v, w	Displacement in x, y, and z directions, respectively
V	Velocity of dissolution at the crack tip
x, y, z	Cartesian coordinates
$\overline{z}$	Empirical material constant, see Equation (42)

α	A geometric factor dependent on flaw geometry
β	Angular orientation of the initial crack plane
γ_f	Fracture shear strain
γ_f^p	Critical plastic shear strain
γ_o	Yield strain in shear
γ_s	Surface energy
Δ	Indicates range difference between maximum and minimum values of the quantity that follows
δ_t	Crack tip opening displacement (C.O.D.)
$(\delta_t)_c$	Critical crack tip opening displacement
ε_E	Elastic strain
ε_e	Effective strain
ε_f	Fracture tensile strain
ε_m	Mean strain
ε_o	Yield strain
ε_p	Plastic strain
ε_r, ε_θ, $\varepsilon_{r\theta}$	Strain components referred to polar coordinates, r, θ
ε_T	Total strain
$\bar{\varepsilon}_T$	Quantity defined by Equation (83)
ε_x, ε_y, ε_z	Strain components referred to x, y, z coordinates
ε_1, ε_2, ε_3	Principal strains
μ	Poisson's ratio
ρ	Radius of blunted crack
ρ_m	Characteristic microstructural dimension
$\tilde{\sigma}$ $\tilde{\varepsilon}$	Dimensionless stress and strain
σ_e	Effective stress
σ_f	Fracture stress
σ_{ij}	Components of stress (i, j = x, y, z)

σ_m	Mean stress
σ_o	Yield stress
σ_r, σ_θ, $\sigma_{r\theta}$	Stress components referred to polar coordinates r, θ
σ_t	Tangential stress
σ_u	Ultimate stress
σ_x, σ_y, σ_z, σ_{xy}, σ_{xz}	Stress components referred to xyz coordinates (see Figure 3)
σ_1, σ_2, σ_3	Principal stresses
σ_∞	Nominal applied stress
τ_o	Yield stress in shear
(c)	When typed above the symbol it indicates cyclic property of the quantity

ABSTRACT

The state of knowledge in fracture and fatigue analysis is reviewed in order to provide a technical background for the development of fatigue design procedures for submarine hulls. Special emphasis is placed on the analytical fracture mechanics approach. Results are presented for the stress and strain distribution near the crack tip. Current fracture criteria and subcritical crack initiation and propagation laws are summarized including the environmental effects.

ADMINISTRATIVE INFORMATION

This work was supported by the Naval Ship Systems Command (NAVSHIPS) funded under Subproject SF 35.422.210, Task 15055.

PREFACE

NSRDC recently initiated studies aimed at the development of submarine hull structural reliability analysis. The first task summary report (Lomacky, 1970) outlined the relevant background and anticipated milestones.* It was concluded that in contrast to successful ventures into the utilization of computer-based numerical methods in the solution of pressure hull stability and general stress analysis problems, the methodology for rational quantitative fatigue and fracture analysis under hydrostatic loading was yet to be developed.

As a first step toward the development of suitable quantitative procedures for the prediction of the fatigue performance of submarine hulls, it was decided to conduct an assessment of existing analytical methods as applied to specimens under controlled laboratory conditions. In view of the statistical aspects of the fatigue phenomenon, it was recognized that limited supplementary testing of large-scale models will continue to be required (at least for the purpose of initial verification of the reasonableness of proposed analytical models), but it was hoped that some

*References are listed alphabetically, starting on page 241.

previously unexplored approach could be identified which offered the highest potential for correlating the behavior of small laboratory specimens and complex structures. It became clear that traditional methods based solely on numerous variants of the concept of S-N curves had the least chance of success. The reason for this shortcoming is not too surprising since such approaches generally make no attempt to discriminate between three stages of the fatigue life of the structure (crack initiation, growth, and final instability) and often tend to attribute the scatter of the experimental results *solely* to statistical effects. On the other hand, an approach based on fracture mechanics with due allowance for its limitations and possible need to combine it with other approaches (especially in regard to the crack initiation phase) does offer more promise in meeting the stated objective. In any event, such view finds increasing recognition in the aerospace and pressure vessel industries where the dominant design stress is of tensile character. Here, it must be admitted that the applicability of fracture mechanics to *externally* pressurized hulls remains to be demonstrated. Nevertheless, if an entirely plausible hypothesis is adopted that the fatigue phenomenon in compressively loaded structures is due in large measure to the pressence of localized residual tensile stress, then the methodology of fracture mechanics developed for the tensile loading case does become germane. However, one should not minimize the difficulties involved in the development of suitable analytical models to account for the interaction between the externally applied pressure and the localized residual tensile stress field.

Within this framework, let us defer the discussion of on-going and future NSRDC programs until subsequent publications* and outline the specific objectives and scope of this report. As indicated above, our intent is to provide an outline of the most noteworthy features and limitations of the existing analytical methods assessed in light of available experimental data with an emphasis on the fracture mechanics viewpoint. No

---

*These include computer-oriented methods of crack stress analysis, assessment and development of crack initiation and propagation laws, and conduct of supporting experimental programs, and a probabilistic approach to reliability against fatigue and fracture.

attempt is made to cover details of the mathematical methods and results since these can be found in the original papers and review papers referenced in the text. Instead, our aim is to provide a critical overview of the entire field--the significant results that have been achieved and the alternate avenues of approach and problems to be solved while bearing in mind the need to study the feasibility of the ultimate application of these methods to submarine pressure hulls. We have confined ourselves largely to the discussion of the continuum (macroscopic) approach although metallurgical factors are certainly important and may be explicitly recognized in macroscopic fracture criteria at some future date by the inclusion of some substructure parameters. Material anisotropy, strain rate effects, and geometric nonlinearities stemming from finite strains and displacements are generally not considered. Commencing with the review of elastic and, later, elastic-plastic *analyses* of stationary cracks, we continue with the discussion of some of the common fracture criteria under monotonic loading. Subcritical crack initiation and growth under sustained and cyclic loading are then considered including the cumulative damage theories and the discussion of environmental effects.

We hope that this report will serve as a useful source of background information both for those who are interested in some specialized aspects of the general problem and for those who are interested primarily in gaining an up-to-date perspective of the entire field for the purpose of identifying areas of future research. Although the ultimate application of these methods to submarine hulls has been emphasized, the underlying rationale is also applicable to surface ships and other vehicles. Background in solid mechanics, particularly the elastic-plastic analysis, is helpful in reading the text although an effort was made to keep the mathematical level accessible to a wide circle of readers. Finally, in such a rapidly changing field, it is entirely possible that some significant theoretical treatment and/or basic experimental work may have been unintentionally overlooked.

STRESS ANALYSIS NEAR STATIONARY CRACKS AND FRACTURE CRITERIA UNDER MONOTONIC LOADING

INTRODUCTION

At low stress levels where inelastic behavior is confined to a small region in the immediate vicinity of the crack tip, the stress intensity factors provide an extremely useful one-parameter characterization of the local deformation field. Consequently they have been widely used to correlate stable and unstable crack extension of laboratory specimens with crack extension in large-scale structures. Our discussion of the elastic analysis is concerned primarily with the available solutions (and their limitations) for the stress intensity factors for various flaw configurations, assuming that the nominal stress fields are unaffected by the presence of the crack.

Although elastic analysis along the lines discussed above may be quite sufficient in many instances, some form of plasticity calculation may be required for better modeling of material behavior. Consequently, after first elaborating on the need for such analyses, we shall discuss some of the methodology that has developed in recent years; it ranges from fairly simple "plasticity corrections" to fairly complex methods which may combine an analytical approach with numerical (finite element) procedures.

So far our discussion has been concerned entirely with the stress analysis aspects. However, the strength analysis is equally important, for the purpose of formulating design criteria. This consists of the prediction of applied stress level and crack size combinations which lead to fracture for given material properties. In other words, a fracture criterion is required, preferably on a macroscopic, continuum level. It turns out that under certain restrictive conditions, fracture criteria can be formulated and successfully applied in terms of one-parameter characterizations (such as critical crack opening displacement, critical stress intensity factor, etc.); in such instances, detailed knowledge of the crack tip deformation field is unnecessary. On the other hand, such detailed knowledge may turn out to be necessary but insufficient unless the microstructural aspects and prior deformation history are also considered. The discussion of these topics will be concluded by a review of some of the recently proposed fracture criteria intended specifically for pressure vessel application.

ELASTIC ANALYSIS

Linear elastic solutions for crack tip stresses are available for a wide variety of configurations. Typically, cracks are idealized as planes of discontinuity with zero radii of curvature at the crack tip.* Figure 1 shows the three basic modes of crack motion. In two-dimensional formulation, cartesian coordinates system, x, y, and polar coordinate system r,θ are used as shown in Figure 2. A generalization to the three-dimensional case and curved crack borders is given in Figure 3. In the latter case, the stress components are shown with reference to the *local* coordinates system, forming a trihedral such that the x-axis is normal to the crack contour, the y-axis is perpendicular to the crack plane, and the z-axis is directed along the tangent to the edge of the crack.** In two-dimensional cases (plane stress or plane strain), the stress at a point near the crack tip can be expressed in terms of the position variables r,θ, whereas in the three-dimensional problems with curved crack contours, an additional position variable is introduced to specify the location on the crack border.

Utilizing index notation, the elastic stress field near the crack tip may be written in the characteristic form (see Paris and Sih, 1964)

$$(\sigma_{xx} = \sigma_x,\ \sigma_{yy} = \sigma_y,\ \sigma_{xy} = \tau_{xy} \text{ etc})$$

$$\sigma_{ij} = (2\pi r)^{-1/2} \left(K_I\, f_{ij}^{(1)}(\theta) + K_{II}\, f_{ij}^{(2)}(\theta) + K_{III}\, f_{ij}^{(3)}(\theta) \right) + \text{other terms non-singular at the crack tip} \qquad (1)$$

Here, K_I, K_{II}, and K_{III} are the stress intensity factors introduced by Irwin (1957) to designate the three modes of crack deformation and $f_{ij}(\theta)$ are dimensionless functions that depend only on the orientation angle θ.

---

*Finite crack tip radii must be considered in connection with crack blunting effects in fatigue, in stress corrosion, and in studying fracture on a microscale. Solutions for blunted cracks in two-dimensional cases are given by Creager (1966).

**This definition breaks down where the crack border forms a sharp corner. Such corners constitute special singular points where the stress field is not well defined. See further discussion of this point on page 10.

For example for Mode I, $\left(f_{ij}^{(2)}(\theta) = f_{ij}^{(3)}(\theta) = 0\right)$ $f_{ij}^{(1)}(\theta)$ may be written as follows:

$$f_{xx}^{(1)}(\theta) = \cos\theta/2\,[1 - \sin\theta/2 \sin 3\theta/2]$$

$$f_{yy}^{(1)}(\theta) = \cos\theta/2\,[1 + \sin\theta/2 \sin 3\theta/2] \qquad (2)$$

$$f_{xy}^{(1)}(\theta) = \sin\theta/2 \cos\theta/2 \cos 3\theta/2$$

The displacements can be expressed as linear functions of the stress intensity factor and exhibit an $r^{1/2}$ dependence on the distance from the crack tip. As an example, for Mode I, the plane strain displacement v in the y direction is given by

$$v = \frac{K_I}{G}\,[r/2\pi]^{1/2} \sin\theta/2\,[2 - 2\mu - \cos^2\theta/2] + \text{other terms nonsingular at the crack tip} \qquad (3)$$

where μ is the Poisson ratio, and G is the shear modulus.

For various configurations of cracked solids, the effects of loading and geometry are contained entirely in the stress intensity factors. In three-dimensional cases with curved crack boundaries, the expressions for K_I, K_{II}, and K_{III} also contain a position variable which locates the particular point on the crack border. However, the expressions for $f_{ij}(\theta)$ are the same as for the two-dimensional problems.* Characteristic features of all linear elastic solutions (with the possible exception of an unknown effect of sharp corners in crack boundaries to be discussed later) are the singularity in the stress field and $r^{1/2}$ dependence of the displacement fields, which leads to the prediction of unbounded stresses and zero crack opening displacements at the tip. It should be noted that although the stresses arising from the singular terms of Equation (1) predominate in the immediate

*Except for some bending solutions for through cracks in plates and shells obtained on the basis of approximate (classical) thin plate or shell theory. See discussion on page 13.

vicinity of the crack tip, the nonsingular terms of the complete solutions may become important if either the stress or strain field ahead of the crack tip is to be calculated, as required in some fracture criteria. For such problems, complex function theory and/or eigenfunction expansions in two-dimensional problems and a potential function approach in three-dimensional problems should prove useful. These approaches have been discussed by Sih and Liebowitz.

For two-dimensional problems and a limited number of three-dimensional cases, Paris and Sih (1964) provide an excellent compilation of expressions for stress intensity factors developed until 1964. However, cases may arise for which the stress intensity factors are yet unavailable or else are difficult to obtain analytically. One example of such a problem is the combined mode deformation. This may arise in the case of branched cracks where Modes I and II are involved. Another example is a surface crack embedded in a nonuniform residual stress field. Of particular interest to submarine hull application are axisymmetric cracks located near structural discontinuities such as hull penetrations and ring stiffeners. Finite element procedures have recently been applied to solve two-dimensional problems (Kobayashi et al, 1968 and Chan, 1968). However, an inherent difficulty of the finite element method, as proposed by those investigators, is the inability of constant strain elements to follow the steep gradients at the crack tip resulting from the stress singularity; a good deal of judgment on the part of the analyst is required. In order to compensate for this difficulty, Chan obtained the stress intensity factors by linear extrapolation to the crack tip; however, this procedure may not be sufficiently accurate in all cases.* Clearly, special treatment of the elements at the crack tip is required if accurate estimates are desired.

To this end, Ostergren (1968) and Levy (1970) used quadrilateral elements for Mode I elastic-plastic analysis at the crack tip. These elements featured r^{-1} singularity, and thus provided better approximation to

---

*We shall discuss these problems in future status reports in connection with the description of current work at NSRDC.

the strain field gradients than the conventional finite elements. (We shall discuss the Ostergren study in greater detail in connection with the plastic analysis.) Similarly Wilson et al (1968) and Hilton and Hutchinson (1969) used special circular elements at the crack tip.

The usefulness of two-dimensional (plane stress, plane strain, and axisymmetric computer programs) finite element analysis can be extended to surface cracks in shells. In particular, approximate solutions to circumferential cracks in spherical and cylindrical shells and long longitudinal cracks in cylindrical shells may be obtained.

In contrast to the two-dimensional problems, the number of solutions for three-dimensional cases is rather meager. The simplest case from the point of view of mathematical tractability is the class of problems dealing with cracks embedded in infinite solids. However, even for this case the existing solutions are restricted to elliptical cracks* (or to the degenerate case of penny-shaped cracks or to parabolic cracks.)**

Kassir and Sih (1966) gave the solution for uniform shear or uniform normal loading of an embedded elliptical crack (this was treated earlier under more restrictive conditions of uniform tension by Green and Sneddon (1950). An important result was that the crack border stress state can be expressed in the form analogous to two-dimensional problems with the same angular dependence (functions $f_{ij}(\Theta)$ of Equation (1) and in terms of the three stress intensity factors. In general, all three modes are operative at the crack border. Furthermore, the state of stress at the crack border is that of plane strain,*** $\sigma_z = \mu(\sigma_x + \sigma_y)$.

---

*It should be noted however that the emphasis on elliptical cracks seems well justified at least under fatigue loading since it appears from the experimental work of Randall (1966) that even surface cracks of irregular initial geometries show a tendency to grow to elliptical shape under cyclic loading.

**Shah and Kobayashi (1968) showed that for deep surface cracks which can be idealized geometrically by parabolic shape, the stress intensity factors were higher than the stress intensity obtained for similarly oriented elliptical cracks of comparable area.

***This is also the case for parabolic cracks in an infinite medium (Shah and Kobayashi, 1968).

Green and Sneddon (1950) and Smith et al (1967) give solutions for arbitrary normal loading at embedded penny-shaped or elliptic cracks.

The three-dimensional problems concerned with surface flaws in shells are of more practical interest. The importance of surface flaws in a pressure hull stems from several considerations. First, fabrication processes increase the probability that large flaws will be present at the surface rather than at the interior of the plate. Second, the maximum applied stress is usually found at the surface because of bending effects. Third, the free surface magnifies the stress intensity factors. Finally, the deleterious environment is readily available at the surface and may lead to an increased rate of crack propagation, as will be discussed later in the section dealing with environmental effects.

As pointed out previously for very long flaws, the problem may be reduced to a two-dimensional formulation. On the other hand, in the case of surface flaws of finite length, the three-dimensional aspects of the problem lead to severe complications. Figure 4 shows an elliptical surface flaw (with minor and major axis given by 2a and 2c, respectively) in a shell element of thickness t subjected to some general loading at some distance away from the crack. The loading is represented by the extension forces N_y, N_x, the in-plane shear stress N_{xy}, the out-of-plane shear forces Q_y and Q_z, the bending moment M_y and M_z, and the twisting moments M_{yz}. For the sake of simplicity, we assume that the plane of the crack is normal to the middle surface of the shell. Since an analysis under such general conditions has not been attempted, let us review the following available solutions which may serve as useful idealizations in special cases.

1. Surface flaw in a semi-infinite elastic solid where $a/_t \to 0$.
2. Surface flaw in plates of finite thickness.
3. Through crack in a plate.
4. Through crack in a shallow shell.

Before any discussion of the above cases, we should note a general limitation of the existing methods. Analytically, the stress intensity factors are obtained as the coefficients of the leading singularity. As discussed above for smooth crack borders and linear elastic fracture mechanics, the leading singularity is of the type $r^{-1/2}$. However, as

pointed out by Sih (June 1969), the order of singularity* (the value of the negative exponent of r) is not known at this time for the point where the crack border joins the free surface (for $\phi = 0$, $z = \pm c$ in Figure 4), and hence a precise definition of stress intensity factor at such a location cannot be given but can only be inferred from the solutions for embedded flaws. This also leads to difficulty in the construction of numerical solutions. As discussed previously, the knowledge of a singularity is important in the selection of special finite elements at the crack tip. Further, it cannot be claimed *a priori* that the effects of such a singularity can be ignored along the crack border away from the singular point. Consequently, the accuracy of existing three-dimensional analytical and numerical solutions is subject to some uncertainty until this point is resolved.

Returning now to the discussion of the specific solutions to the four classes of problems as defined above, we note that the existing analytical solutions to the surface crack in a semi-infinite medium subjected to an arbitrary loading are limited to cracks of semicircular shape. The solution by Smith et al. (Dec 1967, Part 2) constructed from their previous analysis for an embedded crack (Dec 1967, Part 2), is only an estimate in the sense that the correction for the free surface was calculated in an approximate manner using the Schwarz alternating technique and the Love (1927) solution for loads applied at the free surface. It was found that an intensification of about 20 percent in the stress intensity factor occurs at the free surface.

Analytic solutions for stresses near the surface flaws in plates of finite thickness are presently not available, although many estimates for the stress intensity factors have been proposed. Irwin (1962) was the first to propose an approximate formula for a semielliptical surface flaw in a plate under tension. The estimate was based on the previous Green and Sneddon (1950) work (embedded elliptical flaw) with corrections for the two free surfaces ($x = o$ and $x = t$ of Figure 4) derived from heuristic arguments based on the results of the edge-notched two-dimensional

---

*Singular problems of the three-dimensional theory of elasticity are discussed by Sih and Liebowitz (1968).

specimen. Better estimates required for deep surface flaws were subsequently found for the case of bending by (Kobayashi and Moss, 1969) as well as extension (Smith, 1966; Kobayashi and Moss, 1969; and Kobayashi, 1965). Approximate plasticity corrections are usually also incorporated in such estimates.

Numerical solutions for surface flaws in plates (including plasticity aspects) featuring three-dimensional finite elements are presently under way at Brown University (Marcal et al., 1970) under contract to the Atomic Energy Commission. Earlier, Ayres (1968) attempted to solve such problems by means of the finite-difference methods. However, in the extension case, he could obtain only the stresses at some distance away from the crack tip (possibly because of the inability of the finite difference scheme to take the stress singularity into account and also because of a very crude definition of the crack contour). Repeated attempts at NSRDC to utilize Ayres computer program for obtaining the solution to the bending problem were not successful. Finally, in connection with the numerical solution of three-dimensional crack problems, one should be prepared for considerable computer running times so that parametric studies based on such computer analyses would be prohibitive at this time. For this reason, we have attempted to establish the range of validity of various estimates of stress intensity factors for three-dimensional surface flaw problems (including plasticity corrections) based on Smith (1966), Kobayashi and Moss (1969), Kobayashi (1965) and Irwin (1962). Such estimates as well as a discussion of the related computer program (developed to facilitate such computations) are reported informally by DeYoung in enclosure (1) to NSRDC letter Serial 70-720-780 of 28 August 1970.

Although the first appearance of a through crack in a submarine pressure hull would normally be considered as a terminal point of the useful life, the discussion of through cracks of finite length is useful because it illustrates the effect of shell thickness and curvature on stress intensity factors, and these effects may turn out to be important for *deep* surface flaws. To begin, let us examine the case of all-around bending by moment M_0 of a straight crack in a flat plate as shown in Figure 5. The origin of coordinates x,y,z is taken at the crack tip on

the midplane of the plate. Both Knowles and Wang (1960) and Hartranft and Sih (1969) used the Reissner thick plate theory* to show that the surface layer on the tension side may be viewed as behaving locally at the crack tip as if the plate were being stretched by uniform in-plane loads. The expressions for in-plane stresses σ_x, σ_y, and σ_{xy} were found to be in the form of Equation (1), with the out-of-plane shear stresses σ_{yz} and σ_{zx} remaining finite as $r \to 0$.

The stress intensity factor K_I was given** by

$$K_I = \frac{12z}{t} \Phi M_0 \sqrt{\pi c} \tag{4}$$

where the plot of functions Φ is shown in Figure 6, for various values of the Poisson's ratio, as a function of the dimensionless ratio $t/c\sqrt{10}$, where t is the thickness. We note at the tension face ($z = t/2$) that without the correction factor Φ, the result for K_I is the same as that for an infinite plate with a through crack subjected to an applied loading $\frac{6 M_0}{t^2}$. Figure 6 shows that the stress intensity factor increased 62 percent for Poisson's ratio of 0.3 as the plate thickness increased from zero to one-tenth of the crack length, thus illustrating dramatically the dependence of crack tip stress on the thickness.***

We have described the main features of this solution in order to emphasize that the results based on thick plate theory are in sharp contrast to earlier solutions based on classical thin plate theory (Williams,

---

*The theory takes into account the effect of shear deformation on bending (Reissner, 1945).

**Factor $\sqrt{\pi}$ does not appear in (Sih and Liebowitz) but was introduced here to conform with the usual definition of K_I expressed in Equation (1).

***Recent studies of Hartranft and Sih (1969) and Sih (December 1969) also indicate dependence of the stress intensity factor on plate thickness in plates with through cracks subjected to uniform extension. It will be recalled that the conventional formula $K_I = \sigma_\infty \sqrt{\pi c}$ indicates no such dependence.

1961; Erdogan and Sih, 1963; and Sih et al., 1962). First, the angular dependence of in-plane stresses differed from the dependence shown by $f_{ij}^{(1)}(\theta)$ of Equation (2). It should be noted that $f_{ij}^{(1)}(\theta)$ is reflected in the solutions for the plane problems, crack problems in an infinite medium, and solutions based on the Reissner theory. Secondly, the ratio of σ_x to σ_y at $\theta = 0$ depended on the Poisson's ratio; in contrast, the plane extension theory and the Reissner theory yield unity. Finally, the transverse shear stresses σ_{yz} and σ_{zx} approached infinity as $r \to 0$ but remained bounded in the Reissner formulation.

Some comments on such discrepancies seem in order. The inherent difficulties which arise in the application of classical plate theory to crack problems stem from the fact that the two boundary conditions at the crack surface for normal shear and twisting moment are replaced by a single, statically equivalent condition, i.e., the Kirchhoff effective shear. Such replacement is usually justified in thin plate and shell bending problems by invoking the St. Venant principle. However, such justification cannot be used if stresses in the *vicinity* of the crack tip are of interest. Although the use of the Reissner theory removed the foregoing difficulties of classical plate theory, the analysis still contained several limitations. First, the crack surface interference was ignored. This is not objectionable provided the bending solution, which is to be superimposed on the plane extension is sufficiently small to prevent crack closure on the side where the bending stress is compressive. Secondly, the in-plane stress variation was allowed to vary linearly over the entire plate thickness, and the out-of-plane stress σ_z was assumed to vanish. Thus the plane strain conditions ($\sigma_z = \mu(\sigma_x + \sigma_y)$) that should be expected (on the basis of the results from embedded flaws discussed previously) in the interior of the plates is violated.

Hartranft and Sih (1969) have recently proposed an alternative three-dimensional formulation for plates of finite thickness under combined extension and bending. The formulation permits nonlinear stress variations through the thickness, a nonzero σ_z value, and the satisfaction of plane strain conditions in the interior of the plate. However, the stresses at the plate *surface* can still be estimated only approximately because of

the difficulty of obtaining the solution at the singular corner formed at the intersection of the crack plane and free surface; this has been discussed earlier in connection with part-through crack problems.

We conclude the discussion of through cracks with a brief reference to the effects of shell curvature corrections on elastic stress intensity factors. In contrast to the plate problems, bending and extension stress in cracked shells are coupled. For this reason, the expressions for stress intensity factors are rather complicated and have not been obtained in closed form. In addition, solutions are based on the existing classical thin shell theory and consequently suffer from deficiencies similar to those described in connection with the classical bending theory of cracked plates.* Utilizing classical shallow shell theory, Folias (1964, 1965, 1967) has solved the problem of a symmetrically located or a line crack in a spherical shell and the problem of cylindrical shell with either an axial or a circumferential crack. The applied loading in each case was internal pressure. Later, Catanach (1967) extended the Folias (1965) solution to a wider range of crack and shell parameters. We reproduced the Catanach results for the stress intensity factors in order to illustrate the effect of shell curvature; see Figure 7. It shows a long, open-ended cylindrical shell of radius R_m and thickness t subjected to internal pressure p and containing a longitudinal through crack of length 2c. The shell stress intensity factors $(K_I)_S$ for the outer and inner shell surfaces are given by**

$$\begin{aligned} (K_I)_S &= (P_e + P_b)\, K_I \quad \text{outer surface} \\ (K_I)_S &= (P_e - P_b)\, K_I \quad \text{inner surface} \end{aligned} \tag{5}$$

where K_I is the stress intensity factor for a through crack in an infinite plate under tension σ_∞ and is defined by

$$K_I = \sigma_\infty \sqrt{\pi c} \quad ; \quad \sigma_\infty = \frac{p\, R_m}{t} \tag{6}$$

---

*Also, as in the case of combined bending and extension of cracked plates crack closure effects are not considered, i.e., extensional effects predominate.

**A complete solution (including nonsingular terms) for the stress field *ahead* of the crack tip was not obtained although an approximate estimating procedure was suggested.

and where the stress intensity ratios P_e and P_b (computed from an eight-term solution) reflect the extensional and bending effects and are shown in Figures 8 and 9 as functions of the crack-shell parameter λ, where

$$\lambda = \frac{c\sqrt[4]{12(1-\mu^2)}}{\sqrt{R_m t}} \tag{7}$$

The numerical results were felt to be accurate to λ values of 2.2, although an experimental check on the $(K_I)_S/K_I$ ratio using an aluminum cylinder and a plexiglass plate model yielded only a fair agreement with theoretical analysis. Finally, since the analysis is based on infinitesimal displacement theory, it cannot be applied to problems where bulging occurs at the crack in the form of large radial displacements (comparable to shell thickness).

Although, as mentioned earlier, the problem of surface flaws is of primary concern, the possibility of crack initiation from interior flaws must also be taken into consideration.* Such flaws are three-dimensional defects in the form of inclusions or voids, but for the purpose of simplification, they may be idealized as surfaces of discontinuity. If the cracks are sufficiently small in comparison to the shell thickness and also sufficiently far removed from the free surfaces, the stress intensity factor may be estimated from the various solutions for embedded cracks described earlier.** Otherwise, modifications to the embedded flaw solutions are required. To our knowledge, the only available analysis of this problem (still to be verified by experimental work) appears in the work of Kobayashi et al. (1965). Figure 10 shows an elliptical crack with major axis 2c (parallel to the two bounding surfaces of the plate) and

*For example, fatigue cracks may initiate from the interior of welds (Lawrence and Radziminski, 1970).

**For an elliptical crack, Shah and Kobayashi (paper submitted for publication in J. Eng. Fract. Mechanics) recommended that the distance to the free surface be at least 3a where 2a is the minor axis of the ellipse located in the thickness direction of the plate. This work should also permit an assessment of the effects of the free surface on the stress intensity factors for embedded flaws in plates under bending and/or extensional stresses.

minor axis 2a under applied tensile stress σ_∞ acting in the direction normal to the crack surface. The plate is assumed to have a half-thickness of unity. The major axis of the crack is located at distance e with respect to the centerline of the plate. For the crack embedded in an infinite solid, the stress intensity factor on the minor axis as obtained by Irwin (1962) is given by

$$K_I = \frac{\sigma_\infty}{\Phi} \sqrt{a\pi} \tag{8}$$

where Φ is the complete elliptic integral of the second kind represented as

$$\Phi = \int_0^{\pi/2} \left[1 - \frac{c^2-a^2}{c^2} \sin^2 \theta\right]^{1/2} d\theta \tag{9}$$

and ranges, depending on the flaw geometry, from 1.0 (infinitely long, shallow flaw) to $\pi/2$ (penny shaped flaw).

For the flaw configuration shown in Figure 10, the maximum stress intensity factor occurs at point N (closest point to the free surface) on the minor axis and is expressed as

$$K_I = \alpha\beta\sigma_\infty \sqrt{a\pi} \tag{10}$$

where α is a correction factor due to the curvature of the ellipse and β is a correction factor due to the eccentricity of the crack with respect to the middle surface of the shell. The correction factor β is estimated from the plane strain solution of a straight, through crack in a plate. The correction factor α represents an attempt to correct for the curvature of the crack based on an analogous problem of two adjacent collinear cracks in an infinite solid (Kobayashi et al., 1965). Tabular values given for the magnification factor $\alpha = \alpha\left(a/c, \frac{1-e}{a}\right)$ range from 1.0 for a line-like flaw ($a/c \to 0$) for all values of eccentricity e to 0.52 for $a/c = 0.60$ and $\frac{1-e}{a} = 1.025$. The magnification factor β, resulting from the eccentricity at the crack, ranged from 1.600 (for $a/c = 0.65$ and $e/c = 0.30$) to 1.087 (for $a/c = 0.25$ and $e/c = 0.45$). It would appear from the above that the upper bound on the overall correction factor is

approached by the correction due to eccentricity alone for long elliptical cracks. For a specific case of a/c = 0.25 and e/c = 0.45, the stress intensity factor is about 12 percent above the value which is uncorrected for the proximity of the free surface and finite plate thickness (Equation (8)).

So far we have been concerned with the determination of stress intensity factors for single flaws. However, a question which must arise in the formulation of realistic acceptance criteria is whether some limit* should be placed on the proximity of flaws which acting singly may be tolerable from the standpoint of not violating the permissible stress intensity factors. For two-dimensional problems involving collinear through cracks in plates (and crack arrays), solutions for the stress intensity factor can be obtained from Sih and Liebowitz (1968) and are also discussed by Packman (1968). However, in the case of flaw interaction in a three-dimensional solid, the only available (and approximate) solution appears in Kobayashi et al. (1965) and is concerned with the problem of two equal coplanar elliptical cracks in an infinite medium subjected to uniform tension (normal to the crack plane) at infinity. The magnification factors K_N/K_I are plotted versus the separation distance y_o/a in Figure 11; K_N is the maximum stress intensity factor at the minor axes (points N and N') and K_I is given by Equation (8). We note that for y_o/a of less than 2.5, the interaction effect can become quite significant especially for pencil-like flaws ($a/c \to 0$).

ELASTIC-PLASTIC ANALYSIS

As discussed in the early work of McClintock and Irwin (1964), interest in the plasticity aspects of fracture mechanics originated from some of the inadequacies of purely elastic analyses. Specifically some type of plasticity analysis is required in the following cases:

---

*Specific suggestions for establishing rejection standards for various crack geometries and interaction of multiple flaws on the basis of elastic fracture mechanics are presented by Payne (1964).

1. A description of stress or strain field is required when the local plasticity is beyond the small-scale yielding range. As defined by Rice in the Journal of Applied Mechanics (1968), small-scale yielding occurs when the plastic zone size is small in relation to the characteristic geometric dimensions of the specimen, i.e., crack length, plate thickness, etc.* For the small-scale yielding range, the elastic stress intensity factor controls not only the surrounding elastic stress field but also the size of the plastic zone and the crack opening displacement. As the load is increased to what will be referred to as large-scale yielding range,** at least for nonstrain hardening materials, one-parameter characterization of the local deformation field may no longer be possible. As will be discussed later, dependence on the overall specimen geometry (for example, single- or double-edge notched) may have to be taken into account for large-scale yielding. A large- rather than a small-scale yielding is more likely to occur for submarine hulls.

2. A detailed description of stress and strain history in the immediate vicinity of notches and crack tips may be required in the formulation of stable or unstable fracture criteria under monotonic loading. It may also be required in the study of fatigue propagation dependence on the load history (crack blunting and fatigue "damage" accumulation ahead of the crack) and for fatigue initiation criteria.

3. The specimen "thickness effect" may have to be accounted for in determining fracture toughness. In contrast to elastic fracture mechanics, plastic analysis shows significant differences in the pattern of local deformation fields between the two extreme idealizations of plane strain and plane stress. In reality, practical shell thicknesses fall between these two extremes and can thus be considered to be in the realm of three-dimensional elastic-plastic formulation.

---

*An approximate estimate of the maximum extent of plane stress plastic zone size R_{max} may be obtained from the elasticity solution from the formula $R_{max} = 1/\pi\ (K_I/\sigma_o)^2$ where σ_o is the uniaxial yield stress. Plane strain R_{max} is roughly one-half as large. More precise estimates will be discussed in connection with plane stress and plane strain calculations.

**In the absence of strain hardening, this may reach the fully plastic limit load condition if prior fracture does not occur.

Despite interest in plasticity aspects of crack analysis, the number of available solutions for the cases of greatest interest (Mode I) is rather limited. Ideally, since plastic deformations are dependent on loading history, one would like to have the solutions based on incremental theory of plasticity. This would permit the possibility of accurate analysis of unloading and/or change of ratios between the stress components under monotonically increasing loads (due to stress redistribution) and particularly in the study of cyclic plasticity under fatigue loading. In addition, one needs the provision for large plastic strains and geometry changes since crack blunting does turn out to be important in stress corrosion and load sequence effects. However, with the exception of several finite element solutions and hybrid finite element-analytical methods to be discussed later, analytical solutions are based on the deformation theory of plasticity and finite strains* at the crack tip are yet to be taken into account.

We shall now discuss what appear to be the most significant features of Mode I analysis for the two extreme idealizations of plane strain and plane stress under conditions of small-scale yielding.** The usefulness of the small-scale yielding formulation is that the crack may be viewed as semi-infinite in extent, and thus the results from such plasticity analysis can be applied to a wide range of geometries if the elastic stress intensity factors are known. Possible extension to large-scale yielding and some of the features of limit load analysis are then considered. At NSRDC, DeYoung has summarized the approximate plasticity corrections for surface flaws in plates (published informally; see footnote to page 11).

---

*A finite element approach presently underway includes provision for large displacements but not for finite strains at the crack tip (Visser et al., 1969 and Visser and Tuba, 1969). The complicating feature appears to be the current lack of constitutive equations involving noninfinitesimal plastic strains.

**The most recent and comprehensive review of the mathematical aspects of elastic-plastic fracture mechanics appears in Volume II of Fracture (Rice, 1968).

Plane Strain

It will be recalled that the condition of plane strain requires that the displacement normal to the x-y plane (z-direction) of Figure 1 vanish and that the displacements u and v in the x- and y-directions, respectively, be independent of z. Consequently, the strains ε_{iz} (i = x, y,z) vanish.

Some preliminary observations on the general features of the stress pattern around the crack tip emerge from the slip line theory (Prager and Hodge, 1968).* On the assumption that (1) plastic strain incompressibility can be specified, (2) plastic strains are large in comparison to elastic strains, and (3) the crack tip is completely enclosed within a plastic zone, the slip field can be constructed as shown in Figure 12. It can be shown (Rice, J. Appl. Mech., 1968) that the polar and rectangular stress components within the triangular Regions A and B (bounded by 45 degree slip lines) and the central fan Region C are as follows:

$$\begin{aligned} &\sigma_x = 2\,\tau_o\ ,\ \sigma_y = \sigma_{xy} = 0 && \text{Region A} \\ &\sigma_x = \pi\,\tau_o\ ,\ \sigma_y = (2+\pi)\tau_o\ ,\ \sigma_{xy} = 0 && \text{Region B} \\ &\sigma_r = \sigma_\theta = (1+3\pi/2 - 2\theta)\tau_o\ ,\ \tau_{r\theta} = \tau_o && \text{Region C} \end{aligned} \qquad (11)$$

where τ_o is the yield stress in shear related to the uniaxial yield stress σ_o by the formula $\sigma_o = 2\tau_o$ for Tresca material and $\sigma_o = \sqrt{3}\,\tau_o$ for a von Mises material. For all three regions, the stress σ_z (normal to x,y-plane) is given by the plane strain condition $\sigma_z \approx 1/2(\sigma_x+\sigma_y) = 1/2(\sigma_r+\sigma_\theta)$.

Two significant results appear from this analysis. First, the hydrostatic stress buildup occurs only *ahead* of the crack tip where σ_y is increased by $\pi\sigma_o/2$ (Tresca condition) above the uniaxial tensile yield σ_o. Second, it can be shown that the large strains can occur only** in the fan

---

*It will be recalled that the slip field constitutes an orthogonal set of lines oriented in the direction of principal shear stress.

**We shall discuss later how this statement needs to be qualified when crack blunting is taken into account.

region C *above* and *below* the crack where the shear strain $\gamma_{r\theta}$ exhibits $\frac{1}{r}$ singularity (in contrast to $\frac{1}{\sqrt{r}}$ singularity of the elastic solution). However, explicit formulas for the *angular* dependence of strains cannot be given since (in contrast to the strain-hardening solutions to be discussed later) angular distribution of strains in perfectly plastic material is not unique.

Although the assumptions on which the slip field was constructed may seem somewhat restrictive, it appears that the general features of the solution do retain their validity after these assumptions have been relaxed. In particular, Rice (J. Appl. Mech., 1968) has concluded that the elastic-plastic boundary could cut sharply into the crack tip in Regions A and B without invalidating the stress field. Additional insight into the plastic deformation around the crack tip and its relation to the elastic stress intensity factor can be obtained from Rice's small-scale yielding analysis. Figure 13 shows the crack formulation for such an analysis (plane strain or plane stress problems). The actual specimen configuration in the vicinity of the finite crack (not necessarily an edge notched specimen), as shown in Figure 13, is modeled by a semi-infinite crack in an infinite plate with the stress boundary conditions at "infinity" specified from purely elastic analysis, i.e., stress intensity factors. As mentioned previously, such an approach is permissible only if the plastic zone size is small in comparison to the plate dimensions and the dimensions of the crack. Before formulas for the size of the plastic zone and the crack opening displacement are presented in terms of the elastic stress intensity factor, the Rice concept of a path independent integral J should be introduced. The integral J is defined by*

$$J = \int_{\Gamma} \left(W\, dy - \vec{T} \cdot \frac{\partial \vec{u}}{\partial x}\, ds \right) \tag{12}$$

---

*Its application is restricted to linear and nonlinear elastic materials or in cases where the deformation theory of plasticity is applicable (unloading is not permitted).

where Γ is *any* curve surrounding the crack tip starting from the lower crack surface and terminating at the upper crack surface (as is shown in Figure 14).

W is the strain energy density,

$\vec{T}$ is the traction on Γ, and

$\vec{u}$ is the displacement on an arc element ds along arc s.

When J can be evaluated from the applied elastic stress field, Rice has shown that for small-scale yielding J is equivalent to the Irwin energy release rate* $\mathcal{G}$ used for linear elastic materials. Earlier, Irwin (1960)--who was the first to recognize the significance of the elastic stress intensity factor--had also derived the relations between the elastic stress intensity factors and $\mathcal{G}$. Thus, if K_I is the elastic stress intensity factor** in Mode I, we have

$$J = \mathcal{G} \quad \begin{matrix}\text{(small-scale yielding} \\ \text{or linear elastic)}\end{matrix} \tag{13}$$

where $\mathcal{G}$ is given by

$$\mathcal{G} = \begin{cases} \frac{1-\mu^2}{E} K_I^2 & \text{for plane strain} \\ \\ \frac{K_I^2}{E} & \text{for plane stress} \end{cases} \tag{14}$$

A generalization to combined mode loading in plane strain can be written in the form

$$J = \mathcal{G} = \left(\frac{1-\mu^2}{E}\right)\left(K_I^2 + K_{II}^2\right) + \frac{1}{2G} K_{III}^2 \tag{15}$$

---

*$\mathcal{G}$ can also be interpreted as the crack extension force (Irwin, 1960).

**Equations (14) and (15) provide additional means for computing the elastic stress intensity factor since J can easily be computed from the elastic stress fields at a large distance away from the crack tip. See, for example, Chan et al. (1968) for the application of this approach to the finite element method.

Because of the equivalence between J and $\mathcal{G}$, the important features of the plastic deformation at the crack tip, such as the plastic zone size and the crack opening displacement, can be expressed either in terms of K_I or J. However, in contrast to the elastic K_I (or $\mathcal{G}$), the use of J as a controlling parameter is not restricted to the small-scale yielding range as will be discussed.

Combining the slip field analysis and the J integral approach, Rice obtained an approximate extent $R(\theta)$ of the elastic-plastic boundary as given by

$$R(\theta) = R_{max} \cos[2(\theta-\pi/2)] \tag{16}$$

where the maximum distance R_{max} occurring at $\theta = \pi/2$ was given by*

$$R_{max} = \frac{3J}{2\sqrt{2}\ (2+\pi)\tau_o\ \gamma_o} = \frac{3(1-\mu)K_I^2}{\sqrt{2}(2+\pi)(2\tau_o)^2} = 0.29\left(\frac{K_I}{2\tau_o}\right)^2 \text{ for } \mu=0.3 \tag{17}$$

where γ_o is the yield strain in shear. The crack opening displacement δ_t was defined as the total separation distance at $\theta = 3\pi/4$ (the boundary between the Regions A and C of Figure 12) between the upper and lower crack surfaces at the tip. Mathematically, the concept of crack opening discontinuity at the crack tip arises from the idealized sharp crack model with unbounded shear strains at the tip. On physical grounds, δ_t may be viewed as crack surface separation very *near* the tip of the crack blunted by increasing load as shown** in Figure 15. The Rice approximate analysis yields

$$\delta_t \approx \frac{2J}{(2+\pi)\tau_o} = \frac{2(1-\mu)^2}{(2+\pi)\tau_o}\frac{K_I^2}{E} = 1.9\ \gamma_o\ R_{max} \tag{18}$$

---

*This turns out to be $R_{max} = 0.29\left(\frac{K_I}{\sigma_o}\right)^2$ and $R_{max} = 0.21\left(\frac{K_I}{\sigma_o}\right)^2$ for Tresca and von Mises materials, respectively.

**We shall elaborate shortly on the further significance of Figure 15.

The validity of the above approximations was confirmed by the finite element solution of Ostergren (1968). A noteworthy feature was the use of quadrilateral elements which reproduced the r^{-1} singularity at the crack tip and permitted direct calculation of the crack opening displacement δ_τ. In order to check the Rice results, the calculations were performed in the small-scale yielding range for elastic-perfectly plastic material, but in principle, the analysis could be extended to the strain-hardening case,* to large-scale yielding, and to cyclic loading (without crack closure). One interesting result of the Ostergren calculations, shown in Figure 16, is an indication of the shape and direction of growth of the plastic zone with increasing load. The increasing load is reflected in the increasing values of the ratios K_I/K_{o_I} where K_{o_I} is the stress intensity factor just sufficient to cause initial yielding in the element at the crack tip. We note that the growth is approximately in the $\pi/3$ direction, with the shape of the zone showing increasing departures from symmetry about the $\pi/2$ line as the load is increased.

Influence of Strain Hardening on Plane Strain Plasticity

Analytical results discussed so far were based on the assumption of of an elastic-perfectly plastic stress-strain curve. We shall now consider the effect of strain hardening as discussed by Hutchinson (1968, and April 1968) by Hilton and Hutchinson (1969), and by Rice and Rosengren (1968). For plane strain, only the very near tip solutions** were obtained based on the deformation theory of plasticity and an assumption of elastic-plastic

---

*It should be noted however that the singularity at the crack tip is no longer r^{-1} for strain-hardening materials but, depends on the strain-hardening exponent (see Equation (20)). Thus the results may be in error in the immediate vicinity of the crack tip.

**The near tip solutions represent only the first term of the series approximation to the complete solution. The complete solution has not yet been found analytically although the finite element analysis by Swedlow (1965, 1969) and by Kobayashi et al. (1970) has been carried out. These analyses used conventional finite elements without any special provision for the crack tip; hence the results near the crack tip cannot be expected to be entirely accurate.

incompressibility. Hutchinson (1968) utilized the Ramberg-Osgood tensile stress-strain curve for several n values with $\alpha = 0.02$ in the form:

$$\varepsilon = \sigma + \alpha \sigma^n \tag{19}$$

shown in Figure 17

where σ is the uniaxial tensile stress nondimensionalized by the initial yield stress σ_o,

ε is the uniaxial strain nondimensionalized by the corresponding yield strain ε_o, where $\varepsilon_o = \sigma_o/E$,

E is the initial (elastic) slope of the stress strain curve, and

α,n are material constants.

For the case of plane stress, plane strain, and antiplane shear, the near tip stress field σ_{ij}, the strain field ε_{ij},* and the von Mises stress σ_e were expressed in the form:

$$\sigma_{ij}(r,\theta) = K_\sigma \, r^{-1/n+1} \, \tilde{\sigma}_{ij}(\theta)$$

$$\varepsilon_{ij}(r,\theta) = K_\varepsilon \, r^{-n/n+1} \, \tilde{\varepsilon}_{ij}(\theta) \tag{20}$$

$$\sigma_e(r,\theta) = K_\sigma \, r^{-1/n+1} \, \tilde{\sigma}_e(\theta)$$

$$K_\varepsilon = (K_\sigma)^n$$

Here, stresses σ_{ij} and σ_e have been nondimensionalized by the initial yield stress σ_o, and the strain components ε_{ij} have been nondimensionalized by the corresponding yield strain ε_o. Also K_σ and K_ε are defined as plastic stress intensity and strain intensity factors respectively and $\tilde{\sigma}_{ij}(\theta)$ and $\tilde{\varepsilon}_{ij}(\theta)$ are dimensionless functions of angle θ. The stress intensity factor K_σ has been normalized by dividing by the yield stress σ_o and the strain intensity factor K_ε has been normalized by dividing by the yield strain ε_o. The forms of the dimensionless angular functions differ depending on the state of stress (plane strain, plane stress, or

*It is assumed that the elastic strain near the crack tip may be neglected in comparison to the plastic strains.

antiplane shear) but are independent* of the applied load level or specimen geometry; thus, they are analogous to functions $f_{ij}(\theta)$ of Equation (1) for purely elastic formulation.

It was shown that the plastic stress intensity factors for small-scale yielding can be directly related to the elastic stress intensity factors** K_I in the form

$$K_\sigma = C_n\left(\frac{K_I}{\sigma_o\sqrt{\pi}}\right)^{\frac{2}{n+1}}, \quad K_\varepsilon = (K_\sigma)^n \tag{21}$$

The coefficient C_n is expressed in the form

$$C_n = \begin{cases} \left(\frac{\pi}{I\alpha}\right)^{\frac{1}{n+1}} & \text{for plane stress} \\ \left(\frac{\pi}{I\alpha}\,(1-\mu^2)\right)^{\frac{1}{n+1}} & \text{for plane strain} \end{cases} \tag{22}$$

where I depends on the strain-hardening exponent as well as on the state of stress (plane stress or plane strain). Values of I as a function of n are plotted in Figure 18. Equation (21) is not valid for large-scale yielding which will be discussed later.

Some comments on the most noteworthy features of plane strain hardening solutions seem to be in order.

First, let us note the angular dependence of stress and strain fields (referred to polar coordinates r, θ) as reflected in the dimensionless functions $\tilde{\varepsilon}_{ij}(\theta)$, $\tilde{\sigma}_{ij}(\theta)$ and $\tilde{\sigma}_e(\theta)$. Figure 19 shows these functions for two values of coefficient n. As in the perfectly plastic case (approached by high values of the exponent, in this case n = 13), maximum strains occur

---

*For elastic-perfectly plastic materials, $\tilde{\varepsilon}_{ij}$ may depend on the load level.

**Recall that K_I reflects the crack geometry and applied load level.

above and below the crack. Second, ahead of the crack (θ = 0 degrees) the ratio of σ_θ, the maximum tensile stress, to the yield stress σ_e is approximately equal to 3.8 for n = 13 and increases to about 6.6 for n = 3 in contrast to the ratio of $\frac{2+\pi}{\sqrt{3}}$ = 2.95 achieved for the perfectly plastic solution and the von Mises condition (Equation (11) in Region B) of Figure 12. These results are observed from Figure 19 if we note that along any radial lines (θ = constant), the ratio of any stress σ_{ij} to the uniaxial yield stress is given by $\tilde{\sigma}_{ij}/\tilde{\sigma}_e$. Rice and Rosengren (1968) speculate that such high ratios may be somewhat in excess of the actual values because of possible inaccuracies stemming from the incompressibility assumption.

Finally, the stress and strain singularities and the effect of crack blunting deserve some comments. We recall that the singularities which lead to the prediction of unbounded strains in the perfectly plastic idealization and the prediction of unbounded strain and stress fields for elastic (Equation (1)) and strain hardening (Equation (20)) cases, are all based on the assumption of infinitesimal strains in the vicinity of a sharp crack. The crack is assumed to retain this geometry during the loading process. By contrast, perfectly plastic idealizations in the sharp crack analysis lead to the prediction of crack opening discontinuity δ_t at the crack tip. In reality, intense plastic deformation results in blunting and the appearance of crack tip as shown in Figure 15a. Rice and Rosengren (1968) observed that the slip line field discussed in connection with sharp crack analysis needs to be modified in a very small region D ahead of the crack.* The size of this region is on the order of twice the crack opening displacement as shown in Figure 15a. As reported in a more recent paper by Rice and Johnson (1969), consideration of the blunted cracks

---

*To get an appreciation for the numbers involved, let us assume high strength steel with σ_o = 220 ksi and K_I = 150 ksi $\sqrt{\text{in}}$, E = 30 x 10^3 ksi. Thus, from Equations (17) and (18), the size of region D turns out to be on the order of 50 microns. This is already on the scale where microstructure may have to be taken into account. In this connection, the discussion of fracture as observed at various scales of observation ranging from the continuum to the atomic level can be found in McClintock and Irwin (1964).

results in the appearance of intensive (but bounded) strains in Region D in contrast to the prediction of slip line theory based on initially sharp crack geometry. The effect of increasing strain hardening was also found to decrease the blunting of the crack.

Figure 15c shows the tensile stress $\sigma_y(x,o)$ ahead of the crack normalized by twice the yield shear stress τ_o (for the strain-hardening law shown in Figure 15b). The computations were carried out by assuming sharp crack geometry and using a single-term approximation for various values of the coefficient, where $\bar{N} = 0$ corresponds to the perfectly plastic case. In the report by Rice and Johnson 1969, it was shown that the blunt crack analysis does confirm the expectation of falloff in stress (as indicated by the dashed line in Figure 15c for $\bar{N} = 0$) occurring for all values of $\bar{N}$.

Plane Stress

Mathematically, the definition of plane stress in the x-y plane of Figure 2 requires the vanishing of both the out-of-plane normal stress σ_z and the out-of-plane shear stresses σ_{zx} and σ_{zy}. From the standpoint of elastic-plastic fracture mechanics, such a state of stress is *approached* at some distance ahead of the crack when the dimension of the plastic zone is either comparable to or larger than the plate thickness. In the vicinity of the crack tip, the problem is essentially three-dimensional in nature; nevertheless, the plane stress analysis for thin sheets provides fairly accurate gross measures of plastic deformation such as the crack opening displacement, and plastic zone size. What is perhaps equally important is that plane stress analysis indicates significant departures from the deformation pattern predicted by plane strain theory. This point is obscured in either purely elastic analyses or pseudoelastic analyses with plastic zone corrections (to be discussed later), and one might expect the deformation pattern for practical plate thickness to fall somewhere in between the plane stress and plane strain predictions.

Experimental observations have indicated that two patterns of plastic deformation are possible for plane stress. The first pattern was observed in cracked aluminum plates (Gerberich, 1964); plastic deformations presented a diffused pattern, and the extent of the plastic zone in the direction normal to the plane of crack propagation was comparable to or

larger than the extent in the direction of the crack extension. The second pattern was observed on silicon iron (Rosenfield et al., 1965); the plastic zone was confined to a long narrow strip* in the direction of the crack extension and was associated with necking ahead of the crack and development of a through-the-thickness shear lip. Without dwelling on the hypothesis** advanced for the physical explanation for the alternate plane stress deformation patterns, we shall present the two corresponding mathematical models, namely, the analysis of Hutchinson, appropriate for the diffuse pattern, and the Dugdale model, appropriate to the strip type of deformation.

Hutchinson's analysis (1968 and April 1968) reveals that for materials which strain harden according to Equation (19), the near tip fields are given by Equation (20), with the plastic stress and strain intensity factors in the small-scale yielding range defined by Equations (21) and (22). Figure 20 shows the angular dependence of the stress and strain fields as reflected in the dimensionless functions $\tilde{\sigma}_{ij}$, $\tilde{\varepsilon}_{ij}$, and $\tilde{\sigma}_e$. For the sake of comparison, Hutchinson's results for perfectly plastic materials are given in Figure 21. The solution for the perfectly plastic case was constructed on the basis of the slip line field also shown in Figure 21 and by inference from the strain-hardening solution. Here Regions OAB, OBC, and OCD, as defined by radial lines shown in Figure 21, represent regions with three sets of relations between θ and the stresses σ_r, σ_θ, and $\sigma_{r\theta}$. Although a unique solution for the strain field is not possible for the perfectly plastic case, it was found that unbounded strains (1/r singularity) are possible only ahead of the crack in Region OCD and that $\varepsilon_r(\theta)$ vanishes for all regions. As can be seen from the comparison of results for the strain-hardening case, these features of the perfectly plastic solution are approached by the low strain-hardening solution (n = 13), as should be expected.

---

*The width of the strip is on the order of the plate thickness.

**It was suggested that materials (Rice, 1968 and Drucker and Rice, 1968) that obey the Tresca yield condition produce a strip-type plastic zone whereas von Mises materials lead to diffuse patterns of plastic deformation.

Several comments should be made on the comparison of the above results and the plane strain results discussed earlier (see Figure 19). First, the tensile stress ahead of the crack is much smaller than in the case of plane strain. In fact, for the perfectly plastic solution, the ratio of σ_θ at $\theta = 0$ computed by plane strain analysis to the corresponding quantity computed by plane stress is $1 + \pi/2$. This ratio decreased for increasing strain hardening.

On the other hand, as can be seen by comparing Figures 19 and 20, plane stress leads to large strains *ahead* of the crack rather than above and below as predicted by sharp crack plane strain analysis.

The Dugdale* model (Dugdale, 1960) representing the second type of observed plastic deformation is shown in Figure 22. Here, yielding is viewed as being confined to a narrow strip directly ahead of the crack. The material surrounding the crack is considered to be elastic, and the analyses for the determination of the length R of the plastic zone and the crack opening displacement are performed entirely by elastic calculations. This is accomplished (Rice, 1965) by considering that the actual crack is extended by the amount R with the extended crack propped open by yield stresses (or stresses in excess of initial yield for strain-hardening material) and by requiring that the stress field be bounded at the outer tip of the plastic zone. In the absence of strain hardening, this condition leads to the width R of the plastic zone as given by**

$$R = \frac{\pi}{8}\left(\frac{K_I}{\sigma_o}\right)^2 \tag{23}$$

At the physical crack tip ($x = o$, $y = 0$) for the sheet of thickness t and for the linearly strain-hardening material defined by

---

*It is also referred to as the Dugdale-Barenblatt (Barenblatt, 1962) model.

**This formula is restricted to the small-scale yielding range and for the configuration of Figure 22, represents only the first term of the complete solution (see footnote on page 33) expanded in Taylor's series (Drucker and Rice, 1968).

$$\sigma = \sigma_o + E_T \varepsilon_p \tag{24}$$

(where σ and ε_p are uniaxial tensile stress and plastic strain, respectively, and E_T is the tangent modulus of the plastic portion of the curve) the crack opening displacement δ_t is given by

$$\delta_t = \frac{\sigma_o t}{E_T}\left[\left(1 + \frac{2 E_T J}{t \sigma_o^2}\right) - 1\right]^{1/2}$$

$$= \frac{\sigma_o t}{E_T}\left[\left(1 + \frac{2 E_T K_I^2}{E t \sigma_o^2}\right) - 1\right]^{\frac{1}{2}} \tag{25}$$

(small-scale yielding)

In the second form, the plane stress relation between J and K_I, Equations (13) and (14), have been utilized.

In the special case of elastic, perfectly plastic material ($E_T = 0$), Equation (25) takes the form* of

$$\delta_t = \frac{J}{\sigma_o} \; ; \; \delta_t = \frac{(K_I)^2}{E \sigma_o} \qquad \text{(small-scale yielding)} \tag{26}$$

Comparing Equations (23) and (17), we note that the maximum extent of the plastic zone R_{max} for plane strain is about 74 percent of the plane stress value for a Tresca material and about 53 percent for a von Mises material.** The crack opening displacement δ_t for plane strain is about 70 percent of

---

*The first of these equations is analogous to the formula proposed by Wells (1963) with J replaced by $\mathcal{G}$ interpreted as the crack extension force.

**Etching studies of Hahn and Rosenfield (1966) suggest a figure of about 50 percent.

the plane stress value for a Tresca material and about 61 percent for a von Mises material, as can be seen by comparing Equations (18) and (26). In attempting to assess the accuracy of the Dugdale model, Kobayashi et al. (1968) measured the normal strains and crack opening displacement in the vicinity of the crack tip in centrally notched states of ductile materials by means of moire fringe technique. They found that although the crack opening displacement compared favorably with the results of the Dugdale model, the prediction for normal strains differed significantly from the experimentally observed values.

Large-Scale Yielding and Limit Load Analysis

The previous discussion of plane strain and plane stress was mainly concerned with the analysis of small-scale yielding where the gross plasticity features can be expressed entirely in terms of the elastic stress intensity factor. It will be recalled that in such a formulation, the crack is viewed as being semi-infinite in extent with the plasticity confined to a very small region in comparison to the actual crack length.

We shall now consider some aspects of the two-dimensional plasticity solutions where the loads are increased into the large-scale yielding range, culminating in fully plastic limit load distributions. Here, the elastic stress intensity factor loses its significance, and one must deal with finite crack lengths and specific configurations. In addition to discussing the various approaches, we shall also attempt to assess the range of validity of some specific small-scale yielding solutions.

The extension of fracture mechanics into the large-scale yielding range may be approached from three points of view. The first is an approximate method based on the Rice (1968) concept of path independent energy integral J introduced in Equation (12). The second, developed by Hilton and Hutchinson (1969), is based on earlier studies of Hutchinson (1968) and employs plastic stress intensity factors. Hutchinson utilizes a combination of the finite element method and knowledge of the character of near tip stress fields as specified by Equations (20) to obtain plastic stress intensity factors. The third method is based entirely on the finite element technique. This last category includes the work of Swedlow (1965,

1969), Kobayashi et al. (1970), and a possible extension of the Ostergren (1968) and Levy (1970) analyses into the large-scale yielding range. Before comparing their principal factors, we will briefly review only the first two methods; since the important features of finite element analysis have been discussed in connection with small-scale yielding.

Turning first to the J integral formulation, we recall that for small-scale yielding, J is identical to the Irwin (linear elastic) energy release rate $\mathcal{G}$, as defined in terms of K_I by means of Equation (14). For large-scale yielding, the value of J can only be *approximated* (Rice, 1968) by the use of crude models of yielding near the crack tip or else by inference from the known results of large-scale yielding Mode III analysis.* Although such models may be inaccurate in detail, we would still expect a fairly accurate prediction of overall energy absorption as measured by J. Specifically, after an approximate value of J has been obtained, Rice suggests that it can then be used to obtain more detailed features of the plastic deformation near the crack tip, by substituting the value of J into the formulas of previous sections, namely, Equations (17), (18), (25), and (26).

The range of accuracy of small-scale yielding solutions may now be judged by examining the results obtained (Rice, 1968) from the analysis of a semi-infinite plate with a central crack of length 2c loaded by a remote stress σ_∞, as shown in Figure 23. The analysis was performed using the Dugdale model for elastic, perfectly plastic material with yield strength σ_o. The curves show the results for the ratios** R/c and $\pi G\delta_t/(\kappa+1)\sigma_o c$, corresponding to the plastic zone size R, nondimensionalized by one-half crack length c and crack tip opening displacement δ_t, respectively, as a function of the dimensionless ratio $\sigma_\infty\ \sigma_o$ where

$$\kappa = 3 - 4\mu \text{ for plane strain}$$
$$\kappa = \frac{3 - \mu}{1 + \mu} \text{ for plane stress} \qquad (27)$$

*Alternately, J can be calculated with the aid of numerical (finite element) methods. (See Chan, et al, 1968).

**For large-scale yielding R is no longer given by Equation (23) (where $K_I = \sigma_\infty\sqrt{\pi c}$ for the configuration of Figure 23) but by $R = c[\sec(\pi\sigma_\infty/2\sigma_o)-1]$ (Rice, 1968).

The two solid lines are the values obtained for large-scale yielding; both results for small-scale yielding fall on a single dashed line. We note that although κ can assume either a plane stress or plane strain value, the appropriateness of the Dugdale model for plane strain can be questioned in view of our previous discussion on plane strain plasticity (as well as for some materials in plane stress). Nevertheless, for the cases where the Dugdale model is sufficiently accurate, the curves show that the small-scale yielding solutions break down when the ratio of the applied stress to yield stress is about 0.5.

In principle,* the plastic stress intensity factor approach can be used for either the plane stress or the plane strain problem; to date, results have been published only for the plane stress calculation (Hilton and Hutchinson, 1969) for the configuration shown in Figure 23. Strain hardening according to Equation (19) and Figure 15 is assumed but $\alpha = 1$. The starting point of the analysis is Equation (20). The angular variation of the stress and strain fields remain as shown in Figure 20; however in contrast to the small-scale yielding solution represented by Equations (21) and (22), large-scale yielding analysis yields the solutions for the stress and strain intensity factors** in the form

$$K_\sigma = f\, c^{\frac{1}{n+1}} \quad , \quad K_\varepsilon = f^n\, c^{n/n+1} \tag{28}$$

*Plane strain calculations are presently underway as reported to us in a private communication by Professor Hilton.

**As in the case of Equations (20) and (21) K_σ and K_ε have been normalised by dividing by the yield stress σ_o and the yield strain ε_o, respectively.

where functions $f = f(\sigma_\infty/\sigma_o)$ have been calculated up to (σ_∞/σ_o) ratios of 0.9. The calculations were performed using a combination of the finite element technique to connect the near tip stress field governed by Equation (20) with the applied uniaxial stress field σ_∞. (This technique should also be applicable to the treatment of cracks in finite bodies.) Figure 24 shows the ratio of the plastic strain concentration factor K_ε (obtained from large-scale yielding) to the strain intensity factor $(K_\varepsilon)_{s.s.y}$ (obtained from the small-scale yielding solution, Equation (21) as a function of the ratio σ_∞/σ_o for high and low strain-hardening materials represented by n = 3 and n = 9, respectively. The small-scale yielding solution is substantially correct until the ratio of applied stress to yield stress reaches about 0.5. Even up to this value, the accuracy of the small-scale yielding solution is interesting in view of the fact that at an applied stress level of one-half the yield stress, the maximum extent of the plastic zone is already on the order of 40 percent of the half-crack length.

We shall now summarize the principal factors of the three techniques for Mode I large-scale yielding analysis, namely, the J integral formulation, the Hilton and Hutchinson plastic stress intensity factors, and the finite element analysis approach of Ostergren, Levy, Swedlow, and Kobayashi. All of these methods are based on infinitesimal strain assumption and ignore crack blunting. However, since the Ostergren-Levy analysis uses the Marcal general computer program, it may be possible to extend the analysis to include the feature of finite displacements at the crack tip. In addition, such analysis in the absence of crack closure may provide the means for studying cyclic plasticity, a feature not available in J integral or plastic stress concentration factor methods. It is also superior to the Swedlow and Kobayashi finite element programs in that it minimizes the numerical difficulties at the crack tip. Both the J integral and Hutchinson technique are based on the assumption of elastic as well as plastic incompressibility at the crack tip.

Further, the J integral and the Hutchinson method* are limited to the deformation theory of plasticity, whereas finite element methods are not. The Hutchinson method is further restricted to strain-hardening materials, although perfect plasticity solutions may be approached by selecting sufficiently high values of the exponent n. It is probably the most accurate method for strain-hardening materials and for obtaining *elastic* stress intensity factors.** On the other hand, the J integral approach, although approximate in nature, may in simple cases be evaluated without recourse to a finite element program and permits the use of the formulas obtained previously for small-scale yielding. In short, it appears that all of the above methods have both advantages and drawbacks and that the usefulness of a particular method will ultimately depend on how the results will be used in the fracture criterion.

We shall conclude the review of plastic analyses by noting some aspects of plastic limit load solutions. Such solutions are useful since they can be obtained from slip line theory fairly readily in some cases and can then be used to construct upper bounds*** for the load-carrying capacity of notched plates of nonhardening materials as the applied stress fields approach yield condition. In addition, these solutions lend emphasis to the statement made earlier that for nonhardening materials, there is no single parameter to replace the elastic stress intensity factor in large-scale yielding. The details of the stress fields near the crack, in particular such features as the hydrostatic yield stress elevation, depend on the overall specimen configuration. Thus, for single-edge and internally notched plane strain specimens, no stress elevation due to triaxiality occurs, and the net section stress is, in fact, the uniaxial yield stress.

---

*At least for the plane stress and plane strain cases.

**This approach is being investigated in current NSRDC programs.

***For tough material, the failure load may be governed by net section yielding.

On the other hand, deep double-edge notched specimens in plane strain result in appreciable hydrostatic stress elevations* as shown in Figure 25.

Thus, although specific edge-notched and internally notched specimens can be designed to have the same elastic stress intensity factors, the correlation in terms of fracture load is expected to decrease as the applied stress level is increased into the large-scale yielding range approaching the limit (fully plastic) condition. More experimental as well as analytical work in this field is clearly needed.

FRACTURE CRITERIA UNDER MONOTONIC LOADING

Before a discussion of specific criteria, a few comments seem warranted on the general differences between brittle versus ductile fracture. This will be followed by a review of the currently used fracture criteria appropriate to the idealized brittle fracture and to the conditions of ductile fracture in small-scale yielding. We will then consider the difficulties associated with such fracture characterizations in large-scale yielding which may well necessitate intensive studies on the feasibility of including microstructure in some fashion in the fracture criteria. Furthermore, we will describe some of the current research on microstructural models as well as some aspects of the effect of biaxiality and combined mode deformation. Finally, we will examine the relevance of the above criteria to the formulation of general criteria for the design of pressure vessels.

Our concern will be with the *initiation* of crack extension under monotonic loadings; the onset of crack extension, however, does not necessarily signify unstable crack propagation leading to failure. Thus even in brittle materials, crack initiation may be followed by crack arrest. Stable crack growth under monotonic loading and the criterion for the stable-unstable transition will be deferred to the section on subcritical crack growth.

---

*These results are the same as for the slip line construction for *any* crack in plane strain in small-scale yielding, as given in Figure 12 and Equation (11). No significant hydrostatic elevations can occur for corresponding plane stress cases.

Brittle versus Ductile Fracture Mechanisms

The criteria for brittle fracture, which are defined here as taking place under the idealized conditions of complete absence of plastic deformation, require only the knowledge of current state of stress. The problem is not significantly altered by the presence of a large population of open small flaws with assumed size distribution and random orientation. Since fracture initiation is regarded as a point event,* failure criterion for a given flaw population under a complex applied state of stress can be obtained on the basis of a *single* hypothetical flaw** of random size and orientation by "extremizing" the orientation angle and the crack size. The observed fracture load under a simplified uniaxial tension test is then used as the material constant. This procedure was followed, for example, by Griffith (1925) utilizing the uniaxial macroscopic tensile strength to obtain a fracture criterion under biaxial stress conditions. In such a formulation, the "size" effect in brittle fracture is then simply due to the larger probability of finding flaws of critical size in larger volumes of material.

By contrast, ductile fracture may occur by a variety of mechanisms or their combinations. Because of the plastic flow (no matter how localized), the entire deformation history of the region in the vicinity of the crack tip may be important. Specifically, dependence on the past loading or thermal history may lead to a local reduction of ductility. Thus, Griffith-type energy balance criteria applied to ductile materials in terms of critical energy release rate $\mathcal{G}_c$ (equivalently expressed) through K_I by the use of Equation (14) and based on the current state of

---

*As yet, there has been no experimental demonstration of the relevance to brittle fracture of the so-called microstructural theories (Eringen, 1968) which attempt to take into account stress gradients on the micro-scale.

**Unless the stress interaction with adjacent flaws (or notches) is to be taken into account. The basic strength criterion, however, remains to be based on the achievement of critical tensile stress at a point.

stress can only describe the conditions *necessary* for crack propagation to continue (or conditions for crack arrest) but cannot (at least in principle) provide *sufficient* information for predicting crack initiation.*

In view of the above complications, it is not surprising that no general criterion for ductile fracture seems to be now available; however, several qualitative descriptions and simplified analytical models based on microstructural mechanisms have been offered. In addition to the effects of metallurgical factors, anisotropy, and previous loading history, experimental and theoretical studies emphasize the importance of transverse stress (triaxiality) on ductile fracture. Since our discussion in this report is concerned mainly with the effect of mechanical constraint (as reflected in the geometry of the structure) as opposed to the effect of metallurgical and/or temperature transition aspects, a brief discussion of the qualitative aspects of triaxiality at the tip of the crack should prove useful. For this purpose we shall review the experimental studies which Broek (1966) performed on the slant to square fracture transition of aluminum plates with central through cracks.

Figure 26a shows the state of stress near the crack tip in terms of the Mohr circle representation for the two extreme idealizations of plane stress and plane strain with conditions of plasticity at the crack tip. The assumption of vanishing of the transverse stress σ_3 in the plane stress case and the relation $\sigma_3 = \mu(\sigma_1 + \sigma_2) \approx 1/2(\sigma_1 + \sigma_2)$ for plane strain leads to different orientations of the planes of the maximum shear stress, τ_{max}, as shown in Figure 26b. Broek postulates a fracture mechanism based on void initiation, growth, and coalescence. This seems to be a plausible model for materials which contain large brittle inclusions. Cracking of inclusions leads to the formation of small cracks (voids) ahead of the main

*For example, Mylonas (1966, 1967) points out that a crack initiation barrier in the form of the exhaustion of local ductility must be overcome in *addition* to meeting the running crack condition expressed by the energy balance. This point is often obscured in the conventional linear elastic or pseudoelastic approach to fracture.

crack front which join or grow to a certain size (ductile enlargement) and are followed by unstable coalescence and extension of the main crack front. Void initiation and growth in the Broek model depend on the magnitude of the shear stress; hence the planes of the *maximum* void density are oriented along the planes τ_{max}. On the other hand, void coalescence leading to crack growth depends on the tensile stress acting on the planes of maximum void concentration. The difference of orientation of the planes τ_{max} between the plane stress versus plane strain thus leads to a difference in the direction of crack propagation as shown in Figure 26c. Broek then offers a tentative hypothesis for the *gradual* change from the fully square fracture (plane strain) to the fully slant fracture (plane stress) as the plate thickness is reduced. The orientation of the planes of maximum void concentration and the magnitude of maximum tensile stress acting on such planes also change as the condition approximating plane stress at the surface of the plate changes to a condition approximating plane strain on the interior of plates of finite thickness.* Although the Broek model appears quite plausible qualitatively, the quantitative description of fracture transition is presently lacking.

Idealized Brittle Fracture Criteria

In the absence of plastic deformation, the condition for fracture initiation (according to Griffith, 1925) is governed by the "attainment of specific tensile stress at the edge of one of the cracks." In the Griffith formulation, the flaws were idealized as planar elliptical cracks having a

---

*On the other hand, analytical studies of Sih et al. (1966) and the finite element analysis of Levy (1970) on *elastic* stress distribution near the tip of through cracks in finite thickness plates under uniform extension have shown that the condition of plane strain prevails throughout the *major* section of the plate thickness. Only near the surfaces of the plate (referred to as the boundary layer) does the stress distribution *approach* the plane stress condition. Similar three-dimensional treatment of the elastic-plastic aspects would be helpful since an earlier analysis of Ayres (1968) by finite difference methods cannot be expected to be accurate near the crack tip.

small but finite radius of curvature at the tip. Under Mode I deformation, where the crack extension remains in the original crack plane, an energy criterion was also formulated by Griffith (1921) in terms of the concept of free surface energy γ_s. Orowan (1947) demonstrated that the Griffith energy criterion based on an elliptic crack front gives a fracture initiation stress that differs only by a numerical factor from the maximum stress criterion if a reasonable approximation for surface energy is assumed. Since the experimental determination of γ_s is a rather complicated task, the energy criterion can be written equivalently in terms of the critical energy release rate* $\mathcal{G} = \mathcal{G}_c$ which, in turn, can (for sharp cracks) be expressed in terms of the elastic stress intensity factor K_I (see Equation (14)). However in the use of energy criteria in terms of $\mathcal{G}$, the details of crack tip stress fields, and particularly the connection to Griffith maximum stress criterion, are obscured. More specifically, in comparing the energy criterion with the maximum stress criterion, difficulties arise when the crack is modeled as a slit** (customarily employed in fracture mechanics formulation), leading to the prediction of infinite stress at a crack tip. In such a case, Hahn and Rosenfield (1968) suggested that the concept of critical stress intensity factor K_{Ic} may be linked to the maximum tensile stress criterion by writing the condition for rupture when a critical normal stress σ^+ occurs at a fixed distance r^+ from the crack tip. This leads to the form***

$$K_{Ic} = \sigma^+ \sqrt{2\pi r^+} \tag{29}$$

---

* $\mathcal{G}$ can be obtained directly by an experimental procedure based on compliance measurements (Srawley and Brown, 1964).

** The equivalence of energy criterion and cohesive forces model of Barenblatt (1962) was demonstrated by Rice (1968). Here the prospective fracture surfaces ahead of the sharp crack tip are permitted to separate and the stresses are assumed to be bounded at the crack tip. Fracture occurs when the crack tip opening displacement reaches a critical value.

*** We make no attempt at this point to identify K_{Ic} with the *plane strain* fracture toughness.

Equation (29) shows that K_{Ic} may now be regarded as a material constant (independent of specimen geometry) defined in terms of two other material constants σ^+ and r^+. For the case of Mode I loading, the condition for fracture in terms of applied loading and crack length is then obtained by simply equating the computed stress intensity factor K_I to K_{Ic} determined from material tests. In principle, the determination of material constant K_{Ic} could be made on the basis of a single test for perfectly elastic materials. For Mode I loading, since K_I can be expressed in terms of energy release rate $\mathcal{G}$, the use of the energy criterion versus maximum stress criterion (as expressed by Equation (29)) leads to the same prediction. A difference in the two approaches does arise under conditions of biaxial loading, where the cracks propagate in directions other than the original crack plane. Here, the importance of the local maximum stress criterion rather than an energy criterion was confirmed by the experimental studies of Guinand (1961) and Erdogan and Sih (1963). In the Guinand tests, crack extension occurred in the direction of the compressive load as shown in Figure 27. As the crack grew, the stress concentration at the tip of the crack was reduced, and eventually led to crack arrest; in contrast, macroscopic energy considerations would have allowed continued growth in the direction of the original crack, as pointed out by McClintock (discussion of a Erdogan and Sih paper, J. Basic Eng., December 1963).

The direction of crack extension in an applied biaxial stress field depends on the orientation of the principal tensile stress at the tip of the crack, as demonstrated by Erdogan and Sih. Figure 28a shows a plate of brittle material (plexiglass) under applied tensile stress σ_∞ featuring an inclined through crack of length 2c oriented at an angle β with the applied load direction. The fracture angle $\theta = \theta_o$, which defines the plane of crack extension, is determined by maximizing the tangential stress σ_θ acting on that plane at a point located by the coordinates r,θ from the origin.* This, in turn, implies the vanishing of the shear stress $\sigma_{r\theta}$ as computed from the addition of the stress fields from K_I and K_{II} mode contributions.

*See Figure 2 for a description of the stress components.

Thus utilizing Equations (1) and the Griffith maximum stress criterion at some point r, θ and given the critical stress intensity factor K_{Ic}, the onset of crack initiation and the fracture direction $\theta = \theta_o$ can be determined from the equations

$$\cos \theta/2 \left[K_I \cos^2 \frac{\theta}{2} - \frac{3}{2} K_{II} \sin \theta\right] = \sqrt{2\pi r}\, \sigma_\theta = K_{Ic}$$

$$\cos \theta/2 \left[K_I \sin \theta + K_{II} (3 \cos \theta - 1)\right] = 2\sqrt{2\pi r}\, \sigma_{r\theta} = 0 \tag{30}$$

Since K_I and K_{II} can be obtained as functions of the applied load, crack length, and initial crack orientation, the second equation leads directly to the determination of fracture direction $\theta = \theta_o$ for given K_I and K_{II}. The results for the infinite plate configuration of Figure 28a are shown in Figure 28b; the experimental results were in excellent agreement.* Eliminating θ from the first of Equations (30) permits the construction of a failure interaction curve as a function of K_I, K_{II}, and K_{Ic} as plotted in Figure 28c together with the experimental values. We note that such a theoretical fracture interaction curve based on the maximum stress criterion gives conservative results (at least for plexiglass). An alternate criterion for biaxial loading was proposed by Erdogan and Sih in the form of a quadratic function of K_I and K_{II} as

$$a_{12} K_I^2 + a_{12} K_I K_{II} + a_{22} K_{II}^2 = \text{constant} \tag{31}$$

where a_{11}, a_{12}, and a_{22} are material constants. We note that at least the shape of the curve predicted by Equation (31) seems to provide a better fit for the experimental results of Figure 28c.

Studies on brittle fracture criteria in three dimensions appear to be limited to the work of Kassir and Sih (1967). They used the energy

*As we shall see later, this analysis is questionable when yielding at the crack tip is to be taken into account.

approach (by analogy with the two-dimensional formulation) to express the condition for propagation of an elliptical crack in an infinite body subjected to the generalized three-dimensional tensile and shear loading at infinity in terms of the Griffith surface energy γ_s. Such a criterion is not particularly useful for application to design because of difficulties in measuring y experimentally, but the analysis did lead to several significant conclusions. First, the critical shear stress acting on the plane of the crack and the required critical tension normal to the plane of the crack increased rapidly as the ratio of the major to the minor axis approached unity. Second, the condition for fracture was found to be independent of the two tensile stresses parallel to the plane of the crack at infinity. Third, from the general expression for the fracture stress σ_{cr} of a three-dimensional solid with an embedded penny shaped flaw (a=c), the ratio of the fracture stress of a crack in a three-dimensional solid to the fracture stress of a through crack in plane strain was equal to $\pi/2$. This indicates that bulk constraining improves the brittle strength of material.

Up to now, our discussion of brittle fracture has been limited to cases where the cracks remain open during loading. In a submarine pressure hull, this may represent the situation of residual tensile stress acting in the vicinity of open cracks before hydrostatic loading is applied. From the standpoint of submarine hull application, it is of interest to consider either fully or partially closed cracks during the loading (compressive) part of the cycle, where normal and frictional stress are transmitted across the surface. Here, the available references which may be relevant appear to be limited primarily to the work of McClintock and Walsh (1963) which was aimed at the development of failure criteria in rocks.* The impetus for their study was the fact that the actual compressive strength of brittle materials with random flaw distribution was seldom eight times the tensile strength as predicted by the Griffith maximum local tensile stress criterion. In fact, many experimental results showed values far above those

*The work of Bieniawski (1967) may also be mentioned. However his work was concerned more with the failure *mechanisms* in rock crack *arrays* than with the study of localized failure at a specific crack.

predicted by Griffith, leading to the supposition that the effect of normal force and the frictional effects on the crack surface led to the lowering of the stress concentration factor and hence to an increase in strength.

The McClintock formulation is essentially a modified Griffith stress criterion. As shown in Figure 29a, the mathematical model is an elliptical through crack (having a major axis of 2c and a minor axis of 2a) in a plate under generalized plane stress condition with biaxial loading represented by σ_1 and σ_2 (tension or compression). The crack is oriented at an angle β with respect to the principal applied stress σ_1. Equivalently, as shown in Figure 29b, we can refer the applied stresses to the coordinate axes x and z, directed along the axes of the ellipse. Now in contrast to the Griffith formulation, normal stress σ_n and shear stress σ_f are applied to the crack surface when stresses σ_x, σ_z and τ_{xz} are applied at some distance away from the crack. McClintock postulated that the relation between σ_n and σ_x may be obtained by assuming that after applied stress σ_x has reached a certain critical value σ_c, the crack will close (at least at the ends) and that any further increase in σ_x will cause an equal increase in σ_n. The frictional stress σ_f is found by assuming that in order for the crack to grow, the applied frictional stress (σ_f which is proportional to the current normal stress σ_n and the coefficient of friction μ_f) must be overcome.

Summarizing, $\sigma_n = 0$ for the tensile case where $\sigma_x > 0$ or for the compressive case $|\sigma_x| < |\sigma_c|$
and

$$\sigma_n = \sigma_x - \sigma_c \text{ for } |\sigma_x| \geq |\sigma_c|$$
$$\sigma_f = -\mu_f \sigma_n \text{ for } |\tau_{xz}| > \sigma_f \qquad (32)$$

Analogous to the Griffith procedure but including σ_n and σ_f, McClintock proceeded to find the maximum tangential stress on the periphery of the ellipse in terms of the applied stresses and crack orientation. Then in addition to the applied stresses σ_1 and σ_2, the expression for the maximum stress contains the angle β, the crack closure stress σ_c, and the assumed coefficient of friction μ_f. Assuming further that flaws of all orientations are equally likely, the next step is to maximize the expression for critical

stress in terms of β and express the failure criterion in terms* of $(\sigma_i)_\infty$ the applied *tensile* stress (i.e., for a special case when $\sigma_1 = (\sigma_i)_\infty$ and $\sigma_2 = 0$) required for fracture initiation.** Agreement with the experimental results was obtained if the crack closure stress was negligible ($\sigma_c \quad 0$) and if the coefficient of friction μ_f was nearly unity. Although the McClintock analysis represents an important start toward the solution of problems involving crack closure, some of the possible shortcoming of this approach must also be mentioned. First, the modeling of the crack as an ellipse in a plane stress field with a small but finite radius of curvature at the crack tip, rather than as a slit in a three-dimensional body,*** is open to question. In fact, McClintock discussed the discrepancy† between the strength prediction under biaxial conditions using the slit versus the narrow ellipse model, and indicated that agreement with the experimental results depends on the character of the applied stress.†† Additional difficulties involve the assessment of the frictional coefficient μ_f, the stress required for crack closure under the most general biaxial loading condition, the necessity for specifying critical *local* tensile stress in the case where fracture criterion for a single crack is required (rather than a criterion for an assumed random flaw population which can be related to applied uniaxial fracture initiation stress $(\sigma_i)_\infty$), and finally the appraisal of the crack blunting effect.

---

*Paul (1968) used a similar approach to calculate fracture loads and crack extension directions under unequal biaxial compression by assuming an open elliptical crack in a plate.

**Using $(\sigma_i)_\infty$ as the applied value observed in the uniaxial tension test, the explicit dependence on maximum allowable *local* tensile stress and the crack dimensions was bypassed.

***Fracture mechanics approach.

†This discrepancy between predictions based on the slit and the ellipse model under biaxial loading was also investigated by Cotterell (1969). In his opinion, the difficulty stems from the wrong method of approaching the limit (sharp crack) in at least one of the above models. Intuitively, one would expect that both models should lead to identical results in the limit.

††Combined tension and shear as in Erdogan and Sih studies versus biaxial compression as in the McClintock and Walsh studies.

Ductile Fracture

As noted previously, the presence of plastic deformation at the crack tip enormously complicates the task of finding a general fracture criterion. Nevertheless, the success of elastic-plastic continuum models in predicting fracture in the small-scale yielding range for materials with the same deformation history and initial state must be acknowledged. Fracture criteria in this range are generally expressed in terms of a one-parameter characterization. Here the attempt is to predict fracture initiation on the basis of some general feature of crack tip plasticity without attempting to delve explicitly into the fine details of localized peak stresses or strains. The discrepancies between the predictions of the various criteria appear mainly in the large-scale yielding range. This is not surprising since (as discussed in the section on elastic-plastic analysis), such plasticity features as the plastic zone size and crack opening displacement are uniquely related to the stress intensity factor K_I on the small-scale yielding range. However, the small-scale yielding approximation appears to be valid only for an applied load level less than about 50 percent of the general yield load (Hilton and Hutchinson, 1969).

In what follows we will first summarize the main features of two such criteria for Mode I tensile deformation: (1) the critical stress intensity factor and (2) the critical crack opening displacement concept. The discussion will omit a less commonly proposed criterion based on the critical plastic zone size and a criterion recently proposed by Beeuwkes (1968, 1969) where crack blunting, fracture stress, and ductility are taken into account. In conjunction with improved methods of elastic-plastic analysis now underway (Kobayashi et al., 1970) for the purpose of extending its applicability combined with supporting experimental programs, the Beeuwkes criterion shows promise of encompassing brittle as well as ductile behavior for a variety of materials. We shall also postpone the discussion on stable crack growth in Mode III as well as the discussion of two-parameter characterization based on critical strain and critical length parameter since corresponding work on Mode I has apparently not been explored.

In conjunction with Mode III, we shall also review the concept of fracture resistance curves (R-curves) appropriate for Mode I brittle and ductile fracture characterization since the definition of crack instability in such analyses is quite similar to the definition employed in the Mode III analysis. Some of the current work on more fundamental approaches to ductile fracture based on the consideration of microstructural mechanisms will then be reviewed. In addition, biaxial effects and combined mode deformations will be discussed. Finally, we will conclude by examining some of the criteria based on fracture mechanics considerations that have been proposed for pressure vessel application.

Critical Stress Intensity Factor

According to this criterion, fracture initiation takes place when the computed stress intensity factor* K_I reaches the critical value K_c defined as the material constant. As stated, this criterion represents a generalization from the brittle fracture concept discussed previously. The meaning of K_C as a "material constant" requires further elaboration. We have noted in the discussions on the elastic-plastic analysis that the computed elastic stress intensity factor K_I completely describes the local plastic deformation in the small-scale yielding range in the crack opening mode. Now if a series of tests is conducted on specimens of various thicknesses, designed so that the computed value of K_I remains constant, the computed critical value of $K_I = K_c$ at which fracture initiation takes place will be observed to decrease with increasing plate thickness** until

---

*Although the subscript I denotes Mode I only, the discussion at least in principle also applies to Mode II and Mode III.

**With the exception of sheets in the foil thickness range where a decrease in sheet thickness is associated with a decrease in toughness.

a lower bound is approached. This lower bound, denoted by $K_C = K_{Ic}$, is commonly associated with the approach to the plane strain condition* and is independent of further increase of the plate thickness. Hahn and Rosenfield (1968) demonstrated that K_{Ic} does indeed appear to be a material constant at least in the small-scale yielding range. On the basis of a simplified elastic-plastic model and the use of maximum strain criterion, the following relation was proposed between K_{Ic} and the ordinary tensile properties

$$K_{Ic} \approx \sqrt{\frac{2}{3} E \sigma_0 \varepsilon_f n^2} \qquad (33)$$

where E is the Young's modulus,

σ_0 is the yield stress,

n is the strain-hardening exponent obtained from the true-stress versus true-strain curve of the form $\sigma = k\varepsilon^n$ (k is a constant), and

ε_f is the true strain at fracture of a smooth tensile bar.**

Although the above expression is somewhat approximate,*** it was shown to lead to good agreement with experimentally measured K_{Ic} values for a wide variety of titanium and steel alloys with the exception of cases for which n was very low (e.g., n = 0.013 as for 18-percent nickel maraging steel). We also emphasize that the application of this formula must be restricted to the small-scale yielding range, which Hahn and Rosenfield imply is valid up to the applied load to yield stress ratio of about 0.7; but as noted earlier, a ratio of about 0.5 seems to be favored by other investigators.

---

*This interpretation of K_{Ic} may have to be revised in the light of the analysis referred to in the footnote on page 40. It appears that for *any* plate of finite thickness containing a through crack, the plane strain condition is satisfied (at least from purely elastic analysis) in the major portion of the plate thickness adjacent to the crack tip.

**Correlation between K_{Ic} and n was also found by Krafft (April 1964).

***For example the factor of 3 in the denominator reflects only approximately the actual reduction in ductility (reduction of ε_f) due to strain triaxiality in the plane strain zone ahead of the crack.

As described above, K_{Ic} constitutes a lower bound of toughness. For the other extreme, i.e., where plane stress conditions are approached and the plastic zones are on the order of the plate thickness, Hahn and Rosenfield (1968) suggested a formula similar to Equation (33) to evaluate the upper bound in the form

$$(K_C)_{\text{Plane stress}} \approx \sqrt{\frac{1}{4} E \sigma_0 \ell^*_{(n,t)} \varepsilon_f} \tag{34}$$

where all the symbols are defined in Equation (33) except that $\ell^*_{n,t}$ is the width of the plastic zone in the direction of the applied load at the onset of cracking and is roughly equal to the plate thickness t.

Here, subscripts n and t associated with $\ell^*_{(n,t)}$ (increases with increasing n) denote the dependence of the plastic zone width on the strain hardening exponent n and the plate thickness t. The accuracy of Equation (34) is presently uncertain, and Hahn and Rosenfield recommend further work to improve the estimates of plane stress K_C.

The most that can be said at present for plates in the intermediate thickness range is that the value of K_C is presumably bracketed between K_{Ic} and K_C plane stress. Thus, for intermediate thicknesses, Irwin et al. (1967) suggested an empirical formula

$$K_C^2 = K_{Ic}^2 (1 + 1.4 \beta_{ic}^2) \tag{35}$$

where $\beta_{ic} = \frac{1}{t}\left(\frac{K_{Ic}}{\sigma_o}\right)^2$.

Clearly, since both Equations (34) and (35) include the dependence on plate thickness t, then K_C determined in this manner cannot be considered a true material constant, thus demonstrating the need for formulating the ductile fracture criteria in terms of more basic material properties. We shall later return to this question in connection with the discussion of micro-structural models of fracture mechanics.

Having already discussed the determination of the governing K_C (the "material constant"), let us briefly review the computation of K_I in terms of applied load and specimen geometry to which K_C is to be compared. As discussed in connection with the methods of elastic-plastic stress

analysis, K_I can be identified with the *elastic* stress intensity factor for the small-scale yielding range. On the other hand, the Hilton-Hutchinson plastic stress intensity factors K_σ (discussed on page 34) may be substituted for K_I* for the large-scale yielding range. However, we also recall that at present only the plane stress plastic stress intensity factors have been calculated and those only for the case of a single configuration, i.e., an infinite plate with a through crack under remotely applied tension. Until further work becomes available in this area, the Irwin semiempirical corrections for large-scale yielding effects should be used (McClintock and Irwin, 1964 and Irwin et al., 1967). Irwin assumed that the plastic zone at the crack tip may be taken into account by postulating an effective crack length. The physical crack length was assumed to be increased by an amount corresponding to one-half of the plastic zone size R_{max}. Additional simplification is that the estimate of plastic zone size was based on a perfect plasticity Mode III model, which predicts a circular plastic zone of radius R_o. Accordingly, the plastic zone correction R_o was estimated by

$$R_o = \frac{1}{2\pi}\left(\frac{K_I}{\sigma_o}\right)^2 \qquad \text{for plane stress}$$

and (36)

$$R_o = \frac{1}{4\sqrt{2\pi}}\left(\frac{K_I}{\sigma_o}\right)^2 \qquad \text{for plane strain}$$

The need for plastic analysis is thus bypassed by utilizing the Irwin correction. If closed-form elastic solutions for K_I in terms of the crack size are available, then R_o can be computed with terms of K_I substituted

---

*In principle, plastic stress intensity factors can be used in the small-scale yielding range, where they can be directly calculated from the elastic stress intensity factors (see Equation (21)) and strain-hardening properties. However, at least for the configuration and materials shown in Figure 30, there is apparently no difference in fracture initiation stress computed from the methods based on either K_σ or $(K_I)_{elastic}$ below the applied stress to yield stress ratio of about 0.5.

in the solution, and the "effective" K_I can then be readily calculated.* On the other hand, an iterative method must be used when the "effective" stress intensity factors are computed by numerical procedures.

Crack Opening Displacement $(\delta_t)_c$

This criterion states that fracture initiation for a sequence of sheets with identical thicknesses takes place when δ_t, the opening displacement at the crack tip, exceeds a certain critical value $(\delta_t)_c$ independent of the crack length. This criterion was originally proposed by Wells (1963) in connection with plane stress fracture studies on nonhardening materials. Calculation of δ_t in terms of the applied load level and crack size may be performed for the two extreme cases of plane stress and plane strain using the methods discussed in connection with elastic-plastic stress analysis. Here, we shall confine ourselves to general comments on the limitations of $(\delta_t)_c$ fracture characterization. First, because of the dependence on plate thickness, $(\delta_t)_c$ cannot be regarded solely as a material constant. In this respect $(\delta_t)_c$ shares the shortcomings of the K_C concept for finite thickness plates. Second, experimental difficulties arise in the measurement of $(\delta_t)_c$ near the crack tip. Some of the available measurements have been summarized by Hahn and Rosenfield (1968) for the two extreme cases of plane stress and plane strain. However, for intermediate thickness plates, where on the basis of plane stress and plane strain solutions δ_t may be expected to vary through the thickness, not even an empirical formula (analogous to Equation (25) for K_C) appears to be available. Third, as pointed out by

---

*As an example, for an infinite plate with a through crack of length 2c subjected to a remote tensile stress σ_∞, the elastic stress intensity factor is given by $K_I = (K_I)_{elastic} = \sigma_\infty \sqrt{\pi c}$. For plane stress, we add the R_o correction to the crack size and have $K_I = \sigma_\infty \sqrt{\pi \left(c + \frac{1}{2\pi} \left(\frac{K_I}{\sigma_o} \right)^2 \right)}$. By solving for $K_I = (K_I)_{effective}$, we obtain

$$(K_I)_{effective} = \frac{\sigma_\infty \sqrt{\pi c}}{\left[1 - 1/2 \left(\frac{\sigma_\infty}{\sigma_o} \right)^2 \right] 1/2} = \frac{(K_I)_{elastic}}{\left[1 - 1/2 \left(\frac{\sigma_\infty}{\sigma_o} \right)^2 \right] 1/2}$$

McClintock and Irwin, a crack opening displacement criterion is not likely to be universally consistent with the local stress-strain criterion *ahead* of the crack.* Finally, as discussed in connection with the fully plastic solutions and in McClintock (1965) large differences in stress and strain patterns can exist for crack configurations with the same displacement and similar elastic fields (see Figure 25).

Comparison of K_c and $(\delta_t)_c$ Approaches

We conclude the discussion of the stress intensity factor versus the critical crack opening displacement fracture criteria under Mode I tensile loading by comparing the criteria on the basis of the theoretical results obtained by Hilton and Hutchinson for plane stress fracture calculations of centrally notched infinite sheets. The applied fracture initiation stress $(\sigma_i)_\infty$ (nondimensionalized by the initial yield stress σ_o) is plotted in Figure 30 in terms of the nondimensional ratio $\left(\frac{(K_I)_{elastic}}{\sigma_o\sqrt{\pi c}}\right)$ as computed by three fracture criteria based on alternate methods of calculating the load-induced stress intensity factor K_I and the concept of the critical stress intensity factor K_C. The straight line represents the small-scale yielding (and linear elastic) solution fracture criterion $K_I = (K_I)_{elastic} = K_C$. The curves marked n=3 and n=9 were obtained using the Hutchinson plastic stress intensity factors $K_I = K_\sigma = K_c$ for the two strain-hardening stress-strain curves shown in Figure 28. The dotted curve represents the fracture criterion for elastic, perfectly plastic material ($n \to \infty$) using the Irwin plasticity correction $(K_I) = (K_I)_{effective} = K_c$. Although the initiation stress based on the critical crack opening displacement $(\delta_t)_c$ is not shown, according to Hilton and Hutchinson, the results would fall between the predictions for n=9 and the Irwin formula. It would appear from the curves that when the small-scale yielding

---

*It was pointed out that the displacement criterion is not sufficient without stating in how small a region the fracture displacements are concentrated. Alternatively, two parameter fracture criterion based on the notion of critical strain $\gamma_f p$ at distance ρ from the crack tip can be used as will be discussed on page 70.

solutions are used to predict large-scale yielding behavior, the validity extends approximately up to the $\frac{(\sigma_i)_\infty}{\sigma_o}$ ratio of 0.5.

Similar comparisons for the plane strain case are presently unavailable. The Rice (1968) calculations for antiplane shear (Mode III) stress indicate that the differences in the applied fracture initiation stress based on the critical crack opening displacement, the critical elastic stress intensity factor, and the critical plastic zone size criteria increase significantly as loading is extended beyond the small-scale yielding range. The McClintock and Irwin analysis for Mode III also shows that there is no one parameter (irrespective of the test specimen configuration) at high stress levels which corresponds to critical stress intensity factors, critical plastic zone size, or critical crack opening displacement that can be used to correlate fractures. However, the relevance of antiplane shear loading to the plane strain case is at present uncertain, and it may well turn out that the agreement between the Irwin plasticity correction approach, the plastic stress intensity, and the crack opening displacement criteria will be at least as good as shown in Figure 30. Nevertheless, additional comparisons for configurations other than the centrally notched plates should be performed before general conclusions can be made regarding the agreement between various one-parameter fracture criteria. Such calculations appear necessary in view of the difference in plastic stress-strain fields for various crack configurations under the applied stress conditions approaching general yield (as discussed on page 36).

Microstructural Models

Some of the current work on more fundamental approaches will now be discussed. One microstructural mechanism to which we have alluded earlier is the mechanism of void growth and coalescence. Such mechanism may well model the situation in which cracking of weak phases or inclusions

occurs at a low stress level* and is then followed by void initiation and growth. A start toward the analytical modeling of such problems was recently proposed by McClintock (1968) using a somewhat artificial model of the plastic continuum with three orthogonal sets of cylindrical voids. He postulated a fracture criterion based on strictly ductile plane strain enlargement of holes. Failure occurs when the cell walls touch. A delamination type of fracture as well as the normal types were considered. In addition, the dependence on past deformation was included. An approximate analytical expression of the criteria was stated in terms of the applied strain required to produce coalescence of cylindrical voids of given size and spacing. Rice and Tracey (1969) recently contributed to this line of investigation by considering the expansion of isolated spherical voids (thus modeling the void geometry somewhat more realistically) under a triaxial strain system.

Both investigators found that the growth rates were significantly elevated by the stress triaxiality. Specifically, McClintock found that the required (applied) critical true strain $\bar{\varepsilon}_f$ at which the expansion and the eventual linking of long cylindrical voids takes place decreases drastically with increasing ratios of $\frac{\sigma_{max} + \sigma_T}{\sigma_o}$. Here σ_{max} is the normal applied stress (in the direction of the cylinder axis), σ_T is the transverse stress (normal to the cylinder axis), and σ_o is the yield stress. This means that the true strain to fracture observed under simple tension tests conducted on round bars of ductile metals far exceeds the maximum strain achievable ahead of the crack under plane strain condition, where the stress triaxiality is much higher. The reduction of ductility due to triaxiality as calculated using McClintock's model** is presented by Hahn and Rosenfield (1968) for several configurations. These are a round tensile bar, pure plane stress, plane stress with necking, and the plane strain case. In the

---

*Such modeling may be appropriate to the toughness studies of welds discussed by Chin (1969). On the other hand, where cracking of the brittle phases or inclusions is the governing process, a local brittle fracture criterion based on the stress over a region of the order of the inclusion spacing may be considered to be more appropriate (McClintock, 1965).

**Similar conclusions were reached by Rice and Tracey in their study of a spherical void model, this emphasizes the pitfalls of basing fracture criteria on the fracture strain observed in standard uniaxial tensile tests.

extreme case of plane strain, the ratio of $\frac{\sigma_{max} + \sigma_T}{\sigma_o}$ turned out to be 4.7 (as compared to the maximum of 1.7 for a round tensile bar), and the resulting true strain to fracture decreases to about 10 percent of the corresponding value for the round bar. Hahn and Rosenfield question such enormous reduction in ductility near the crack, yet in their computation of K_{Ic} as presented in Equation (33), the critical strain to fracture near the crack was taken as only one-third of the tensile test value. Strain hardening was found to lead to a significant increase in the fracture strain that can be tolerated for *given* triaxiality,* thus indirectly confirming earlier studies of Krafft (1964).

Although the above studies provide a useful start, the complete analytical modeling of ductile fractures is yet to be developed. Such modeling will have to include void stress field interaction as well as interaction with the stress field of the main crack. Brittle (unstable) coalescence of holes, as contrasted to coalescence due to purely ductile enlargement, must be included. Finally, possible embrittlement due either to fabrication and welding or to the previous loading history must be considered.

The importance of local strain history was emphasized by the studies of Mylonas and Kobayashi (1969) on notched prestrained mild steel. Loss of ductility occurred following the prestrain in *tension or compression* and thus could not be attributed merely to the presence of residual tensile stress. According to Mylonas and Beaulieu (1969), the effect of residual tensile stress on fracture may have been unduly emphasized at the expense of considering the local reduction of ductility following hot or cold prestraining.

In conclusion, the need for future research aimed at the development of comprehensive microstructural fracture criteria, as distinguished from conventional one-parameter characterizations discussed previously,

---

*On the other hand, as noted in the Rice and Tracey paper, strain hardening increases the stress triaxiality ahead of the main crack, thus complicating the picture.

can best be summarized by quoting from Rice (1968): "Ultimately a fracture criterion in terms of local average stress and strain history over a small region with characteristic microstructural dimensions is desired."

As a start, possibly a simple, history-independent, two-parameter fracture criterion could be developed for the Mode I loading case analogous to the Mode III fracture criterion proposed by McClintock and Irwin (1964). It states that fracture initiation takes place where a critical plastic shear strain γ_p^c is reached at a certain microstructural distance ρ ahead of the crack. Here, ρ could represent the characteristic microstructural dimension such as the grain size, inclusion spacing, etc.

Approaches based on the notion of the critical microstructural cleavage stress $\bar{\sigma}_\rho$ and, alternately, on a notion of critical local plastic extension strain $\bar{\varepsilon}_p$ were recently proposed by Wilshaw et al. (1968) and Tetelman and Wilshaw (1969). However, each criterion was found to have a restricted range of applicability. Thus, a $\bar{\sigma}_\rho$ criterion was found to apply to low-temperature cleavage of mild steel, whereas a $\bar{\varepsilon}_p$ criterion was appropriate both for cleavage in the transition temperature region for low and medium strength steel and for dimpled rupture in high strength materials. Judging from the state of the art, comprehensive microstructural fracture criteria will not be available for some time; at present, therefore, recourse must be made to approximate formulas (such as the K_C or $(\delta_t)_c$ approaches). Correlations must then be based on configurations with similar crack tip stress fields, similar microstructures, and deformation histories, and comparable ratios of applied stress to yield stress.

Biaxiality Effects and Combined Mode Deformation

The difficulty of formulating ductile fracture criteria under uniaxial applied tensile loading is compounded by the presence of applied stress biaxiality and even more so for the combined mode of deformation existing when the cracks are inclined in the direction of applied uniaxial stress. Regrettably, no doubt because of the analytical complexities, this problem has received scant attention. Biaxiality studies on surface flaws have been devoted to experimental observations related to the attempt to correlate the results with uniaxial specimen data rather than to the

development of explicit biaxial fracture criteria. Thus an investigation conducted for the primary purpose of studying fatigue under biaxial loadings (Crosby et al., 1969) introduced elliptical surface cracks of various dimensions in the axial direction of internally pressurized cylinders fabricated from high strength aluminum ($K_{Ic}/\sigma_o \approx 0.5$). In addition an axial load was applied and varied to produce several values of the stress biaxiality, and the loading was increased until fracture occurred. Fracture toughness K_{Ic} was calculated on the basis of the observed size of critical cracks using the Irwin surface flaw formula corrected for finite plate thickness and for plasticity effects. The recorded data indicated an apparent increase in K_{Ic} with increasing ratios of crack depth to shell thickness. However, the effect of biaxiality, if any, could not be deduced because the experimental data were rather limited. Thus it cannot be established to what extent the failure to obtain a uniform value of K_{Ic} was due simply to the shortcomings of the approximate K_I formula, stress biaxiality, to the effect of prior fatigue damage at the crack tip,* or to some combination of these factors.

Good correlation between the uniaxial and biaxial K_{Ic} data were obtained by Tiffany et al. (1966) in a study of cylindrical pressure vessels fabricated from titanium and aluminum alloys. However, a generalization to other situations may not be warranted since the tests were conducted at cryogenic temperatures and, therefore, under fairly brittle conditions $\frac{K_{Ic}}{\sigma_o} \approx 0.3$ and in the small-scale yielding range.

Apparently, the first published attempt to explicitly include applied tensile stress biaxiality in fracture mechanics criteria was that

---

*Very little data are available on the effect of previous cyclic deformation on K_{Ic}. Recently, Mager (1970) found the effect of precracking procedures on K_{Ic} test results for A533 Grade B steel to be significant especially when precracking and K_{Ic} testing were performed at different temperatures. Earlier Srawley and Brown (1964) recommended that the nominal net section stress be kept below 50 percent of yield in the fatigue crack preparation of conventional fracture specimens. For the pressurized cylinders under consideration, the applied cyclic stress was fairly close to nominal yield stress.

by Valluri (1965) on a thin sheet of width 2W with a centrally located crack of length 2c. He assumed that the external loading σ_2 was in the direction parallel to the crack extension and that σ_1 was in the direction normal to the crack extension. He further assumed that the stress strain curve of the material followed the Ramberg-Osgood strain-hardening law as expressed by Equation (19). However, in order to conform closer to Valluri's notation we rewrite Equation (19) in an alternate form (without nondimensionalization).

$$\varepsilon = \frac{\sigma}{E} + \bar{c}\left(\frac{\sigma}{\sigma_s}\right)^n \tag{37}$$

where ε and σ are the uniaxial strain and stress, respectively, and $\bar{c}$, σ_s and n are the experimental constants.* His fracture criterion (analogous to the Griffith energy balance formulation) was based on the assumption of stable crack growth followed by instability, with unstable crack extension occurring when the elastic strain energy release rate exceeds the plastic energy dissipation rate.

The fracture criterion was written in the form:

$$\sigma_n = \frac{\sigma_{pu}\,(1-\bar{\alpha}+\bar{\alpha}^2)^{-1/2} + 1}{1 + \dfrac{A\lambda(1-\bar{\lambda})\,(1 + 0.595\,\bar{\lambda}^2)}{1 + \left(\dfrac{1-\bar{\alpha}/2}{1-\mu\bar{\alpha}}\right)(1-\bar{\alpha}+\bar{\alpha}^2)^{n/2}\,\bar{c}n\dfrac{E}{\sigma_o}\left(\dfrac{\sigma_{pu}}{\sigma_o}\right)^{n-1}}} \tag{38}$$

where σ_n is the nominal net section stress,

A is the factor dependent on the specimen width and the crack tip radius to be determined from uniaxial tests,

$\bar{\alpha}$ is σ_2/σ_1 and

$\bar{\lambda}$ is a/w.

The term σ_{pu} is an approximate plastic stress at the crack tip when only the uniaxial stress σ_1 is applied. Valluri proposed an expression

$$\left(\frac{\sigma_{pu}}{\sigma_o}\right)^{n+1} = \left\{42.7\left(\frac{n+1}{nc}\right)\frac{\sigma_o}{E}\right\} - 1 \tag{39}$$

for an estimate of σ_{pu}.

*Specifically, if σ_s is identified with 2 percent offset, yield stress σ_o is then $\bar{c} = 0.002$.

The trend predicted by Equation (38) leads to a decreasing of the biaxial fracture stress with increasing $\bar{\alpha}$ for tensile loads and when compared with the uniaxial strength (with the maximum decrease associated with $\bar{\alpha} = 0.5$). It should be recognized, however, that Equation (38) is derived on the basis of fairly crude assumptions possibly leading to serious errors in the estimate of the plastic energy dissipation. First, plastic energy dissipation was assumed to be confined to a strip along a 60-degree radial line associated with the location of the maximum σ_y stress of the *linear-elastic* fracture mechanics solution. Thus, a Mode I elastic-plastic analysis was not attempted. Secondly no attempt was made to perform a crack blunting analysis,* and the form of the dependence of the crack tip radius on the load was assumed rather arbitrarily. Where the material follows the Dugdale strip-type yielding, better estimates of plastic energy dissipation could undoubtedly be obtained by using the procedure suggested by Goodier and Field (1963). Finally, the plastic deformation in the vicinity of a quasistatically extending crack which may precede the event of fracture instability is not necessarily identical to that existing in the vicinity of a stationary crack.**

In short, the validity of the Valluri approach appears questionable especially in view of recent experimental evidence, e.g., the work of Kibler and Roberts (1968) on thin centrally notched sheets fabricated from 6061-T4 and 6061-T6 aluminum and plexiglass loaded in biaxial tension under both static and cyclic loading conditions. Deferring the discussion of fatigue aspects until a later section, let us note some of their conclusions regarding the observed value of the apparent fracture toughness K_c in the presence of applied tensile stress components parallel to the crack face. They found that the biaxial tensile stress field *increased*** the fracture toughness compared to the toughness measured under the conditions of remotely applied uniaxial loading normal to the crack face. Further, they concluded that

---

*Provisions for crack blunting *and* biaxiality are made in the Beeuwkes (1968, 1969) criterion.

**This will be discussed in the section on subcritical growth analysis.

***In other words in the presence of biaxial stress the load in the direction normal to the crack had to be increased in order to cause fracture.

existing elastic-plastic models germane to the plane stress condition are inadequate to explain such behavior. They felt that the most promising approach would be to utilize the Hilton-Hutchinson plastic stress intensity factors (see page 25) suitably modified* for the case of biaxial loading.

Ductile fracture criteria have not been attempted for the more complex situations, including combined mode deformation. What does emerge on the basis of some experimental observations is that for combined mode deformation, the direction of crack propagation can deviate appreciably from the prediction based on brittle fracture theory.** This was demonstrated in the course of studies conducted at Westinghouse (Wilson et al., 1968) on through cracks in 7178-T651 aluminum plates. The cracks were inclined at various angles to the direction of applied tensile load (combined Mode I and II loading). The direction of crack extension was observed to be approximately normal to the loading direction regardless of the initial crack inclination. Also, contrary to the expectations of brittle fracture, propagation in the direction of maximum shear (pure Mode II deformation) has been observed in biaxial loading tests*** conducted at Syracuse University (Liu and Lal, 1969).

Application of Ductile Fracture Criteria to Pressure Vessels

In view of the various limitations associated with current fracture criteria for plates with flaws, it is not surprising that the fracture criteria for internally pressurized vessels continue to be based, to a great extent, on semiempirical formulas. The applicability of such formulas to

---

*We were informed by Professor Hilton that this work is underway and that his analysis does confirm the findings of Kibler and Roberts.

**We recall that for brittle fracture (see Figure 28), the direction of extension from a sharp crack takes place along a plane on which the tangent stress σ_θ is maximum and the shear stress $\sigma_{r\theta}$ vanishes. For Mode I loading, such direction can be shown to coincide with the direction of the original crack plane. Note that this is not the direction associated with the maximum tensile stress σ_y, which is found within an element located by $\theta = 60$ degrees (see Figure 2 for orientation of coordinate systems.)

***Unstable fracture was preceded by slow crack growth in fatigue.

submarine pressure hulls, where high applied biaxial compressive stress is expected to exist, is at best uncertain. Here, the possibility of pure shear-type crack propagation, as observed by Liu and Lal on plates with through cracks is at least conceivable (although it has not been reported in pressure vessels). On the other hand, the likelihood of high tensile residual stress* due to forming or welding does provide justification for examining fracture criteria for internally pressurized vessels based on Mode I extension.

It was mentioned previously that some of the experimental data for internally pressurized vessels containing shallow surface flaws in the small-scale yielding range indicate good agreement with fracture criteria based on the K_c concept and that they compare favorably with uniaxial data. Whether this will continue to be the case for deep surface flaws in the large-scale yielding range is presently unknown. It is conceivable, however, that in lieu of a single fracture criterion, a set of criteria each restricted to a certain range of crack depth to thickness ratio and material parameters may eventually be adopted. Such an approach may resemble the recommendations made recently by Hahn et al. (1969) in proposing fracture criteria for Mode I extension for axial through cracks in cylindrical pressure vessels. For this reason, these criteria (backed by considerable experimental data) deserve some discussion.

Hahn et al. recommend three criteria with specified ranges of applicability as summarized in Table 1: (1) a fracture criterion intended mainly for low and medium toughness materials with relatively long cracks, (2) a plastic flow stress criterion for short cracks in tough materials, and (3) a modification of (1) for relatively thin-walled containers. Underlying all three criteria is the utilization of the Folias (1965) elastic analysis of cylindrical shells with through cracks, coupled with approximate plasticity corrections based on the Dugdale model for flat plates.

---

*Whether the residual tensile stress can be treated simply as remote load-induced stress is open to question. In any event, since the residual stress may approach uniaxial yield, the small-scale yielding analysis with the utilization of the elastic stress intensity factor is uncertain.

Criteria (1) and (3) are based on the concept of critical stress intensity factor K_c where K_c is determined preferably from the fracture tests of the plate with the *same thickness* as the pressure vessel (otherwise thickness corrections should be applied to K_{Ic}, as for example in Equation (35)). The second criterion is deemed appropriate to large-scale yielding and is based on failure occurring when the local flow stress $\bar{\sigma}$ is exceeded rather than when the toughness measure K_c is exceeded.* There is some uncertainty as to the relationship between the uniaxial yield stress σ_o and the ultimate stress σ_u, particularly for strain-hardening materials. This accounts for the various formulas proposed for $\bar{\sigma}$ in terms of σ_o and σ_u as shown in Table 1. Although biaxiality is not included explicitly in these criteria, one would expect it to play some role in the determination of $\bar{\sigma}$. The need for the third criterion arose when the experimental results for very thin vessels failed to show the dependence on R_m/t ratio predicted by the Folias analysis. Consequently, a semiempirical correction was introduced to bring the first criterion into better accord with the experimental data. Finally, in regard to the second criterion, we wish to reemphasize the point made by Hahn et al., namely, that *localized* large-scale yielding at the crack can occur while the nominal membrane stress is still well below the yield stress.

SUBCRITICAL CRACK INITIATION AND GROWTH

INTRODUCTION

Up to now we have been concerned with the prediction of the stress state near stationary cracks. Accordingly, the discussion of fracture was confined to the criteria for crack initiation under monotonic loading from an assumed preexisting crack. It was noted, however, that the onset of crack extension does not necessarily lead to unstable (catastrophic) crack propagation. In fact slow crack growth under Mode I monotonic loading and predominantly under conditions approaching that of plane stress has been

---

*Such a criterion is important from the practical standpoint since for tough materials, experimental determination of K_c is subject to considerable uncertainty.

observed in ductile materials (Clark, 1968 and Broek, 1968). Consequently, the stress analysis of slowly extending cracks and the appropriate fracture criteria in terms of the required conditions for stable advance, are of interest, as well as the conditions for defining stable-unstable transition and crack arrest. A theoretical analysis for Mode I crack extension under rising load is presently unavailable,* but the analysis of Mode III extension (McClintock and Irwin, 1964 and Rice, 1968) does indicate a significant difference in the plastic strain distribution in the vicinity of a running crack, as opposed to the strain distribution near a stationary crack. In the submarine pressure hull, steady-state growth (apart from cyclic loading effects) under conditions approaching plane strain is likely to be enhanced by the presence of a corrosive environment. For these reasons, anticipating a similar analysis for Mode I in the section that follows, we begin with the discussion of the main features of Mode III analysis of stable crack extension under monotonic load. This discussion will be considered with a review of similar concepts arising from the resistance curves approach proposed for Mode I fracture analysis.

As might be expected, the analysis of stable crack initiation and growth under either cyclic or a combination of cyclic and steady-state loading is on the higher level of difficulty. Here, the residual stress arising in ductile materials due to the load reversal, alternate blunting and resharpening of the crack tip, and the effect of cycling on the material properties near the crack tip tend to complicate the picture. In view of the above, it is not surprising that the prediction of fatigue life in a submarine pressure hull represents such a formidable challenge even without considering the additional complications of *initial* residual stresses (due to welding and fabrication), stress raisers at structural discontinuities,

---

*With the exception of the elasto-plastic numerical analysis recently carried out by Kobayashi et al. (1970). Advancing yield lobes and the stress distributions ahead of the extending crack under constant applied load were found to be approximately the same as the initial yield lobe and the initial stress distribution, respectively. It should be noted however that the analysis employed conventional finite elements so that the detailed plasticity features at the crack tip could not be assessed.

nonuniformity of material and structural geometry, and the variability in load-induced stress and load sequence effects. What is possibly less readily appreciated is that even if the applied stress range, the initial residual stress (presently determinable experimentally only at the surface) level, and the static material properties were known fairly accurately, the cyclic life of the hull could not be predicted quantitatively with a high degree of confidence from the information provided by many of the conventional laboratory specimens.*

For the purpose of this review, we are confining the discussion to what appear to be the most serious limitations of the two conventional laboratory specimens: (1) the constant stress range specimen designed to provide information in terms of the conventional S-N diagram** and (2) the constant strain range specimen designed to provide information in terms of the applied strain range (with the stress range allowed to vary) required for a given fatigue life. We will also consider the energy interpretation of the S-N specimen.

What makes the first specimen impractical as a design prediction tool is that given the conditions of high stress/low cyclic life fatigue (associated with the conditions representative of the submarine hull), the major portion of the life (at least for the surface flaws) is spent in crack propagation. Thus, not only the crack initiation period and the total cyclic life but also the rate of growth of the crack as a function of the applied stress level and material properties should be important factors in determining the acceptance standards and the required inspection schedule. Further, it is clearly important to know whether the fatigue life should be expected to be terminated as a result of leakage resulting from the through-the-thickness subcritical growth or from the achievement of the catastrophic (unstable) crack size. This type of information is not

---

*We are not questioning the merits of these specimens as comparative material rating methods. Our concern here is with the applicability of these tests to the design for finite fatigue life or for the assessment of the residual strength of the structure as defined by its capacity to resist static or dynamic overloads in damaged condition at any time during the cyclic life.

**Here S represents the stress amplitude (at zero mean stress) and N the corresponding number of cycles to "failure."

readily extracted from the conventional S-N curve, regardless of whether a notched or unnotched specimen is used. The usefulness of the constant strain range specimen is somewhat greater, particularly for both the crack initiation predictions and (as will be discussed later) the construction of some theoretical crack propagation models.

Aside from the inability to provide information on the component phases of the fatigue process, there are other difficulties in even attempting to generalize the results from a specific laboratory specimen (constant stress or constant strain range type) to the prediction of crack initiation or propagation in a full-scale hull. The nominal stress or strain range is controlled in smooth laboratory specimens. But the presence of localized cyclic plastic deformation in the neighborhood of notches in the full-scale structure requires an estimate of the relation between the *local* strain range and the specified *nominal* stress range using plastic stress concentration factors calculated, preferably, from the cyclic rather than static stress-strain curve.*

The usual approach for notched laboratory specimens is to try to circumvent this problem by using the so-called fatigue strength reduction factors** which are either obtained from tests or are estimated on the basis of relevant experience. Obviously, the notch sensitivity factors for full-scale hulls cannot be easily obtained, and so it is rather a formidable task to obtain the local strain or stress range at a notch near a structural detail in a hull for the purpose of relating it to the

---

* A cyclic stress-strain curve represents the plot of strain amplitude versus the required stress amplitude obtained from stable hysteresis loops generated from constant strain range specimens. For materials classes as cyclic strain hardening, the cyclic stress range is greater than would be predicted on the basis of the static stress-strain curve; whereas the reverse is true for cyclic strain softening. Extended discussion of the phenomena is given, for example, in Younger (1966) and Manson (1965). It will be discussed further in connection with Figures (35), (36) and (37).

**The fatigue strength reduction factor K_f is defined as the ratio of the endurance stress S_e of smooth specimen to that of a notched specimen. Conceptually, S_e is defined as the stress amplitude below which no fatigue damage occurs. In terms of the S-N diagram, S_e is taken as the point where the curve becomes parallel to the N (fatigue life) axis. For materials which do not exhibit definite endurance stress, S_e is taken to correspond to extremely long lives ($N \approx 10^8$ cycles).

corresponding range of a smooth specimen. Also, the ability of any small-scale laboratory specimen to duplicate the notch effect (stress/strain triaxiality) in a full-scale structure is questionable.

The energy criterion for fatigue prediction of small-scale specimens also warrants consideration. Morrow (1964) gives a comprehensive review of this approach (up to 1964). Here we will mention only the most noteworthy features. The first hypotheses (Morrow, 1959) assumed that the total energy to fracture in fatigue was constant and equal to the area under the true stress-strain curve.* The monotonic stress-strain properties were used to obtain the energy dissipated per cycle. Further steps in the development appeared to be the use of plastic strain hysteresis energy (Morrow, 1960) and the use of cyclic rather than monotonic stress-strain properties (Feltner and Morrow, 1961).**

At this point the basic shortcoming of the energy concept developed for smooth laboratory specimens should be summarized in terms of its usefulness for predicting the total life of notched specimens and, ultimately, of full-scale structures. The crack propagation life is generally rather short for smooth laboratory specimens. This means that in a smooth specimen, the energy is dissipated primarily on initiation and growth of macrocracks and may thus be justifiably assumed to be distributed (at least on the macroscopic level) fairly uniformly throughout the cross section. However, when the macrocrack propagation*** aspects need to be considered, it is the plastic-energy absorption near the vicinity of the crack tip which serves as the important energy sink and not the energy absorbed by the entire specimen. This distinction becomes even more important for full-scale structures where several macrocracks may be propagating simultaneously. Finally, even in the crack initiation phase, the energy dissipation in

---

*Essentially this is also the premise of the Bement-Pohler (1966) and Stowel (1966) theories.

**Morrow has also concluded on the basis of an extensive analysis of experimental data that the total plastic strain energy required to cause fatigue fracture should be considered not as constant but as increasing with decreasing stress amplitude with increasing life.

***In fact the need to study local energy dissipation near the crack tip and to employ fracture mechanics parameters is recognized in the 1964 paper by Morrow.

some small region near the notch, where the dominant macrocrack eventually appears, would seem to be a far more relevant criterion than the energy dissipated by the entire specimen.

In short, all of the phenomenological approaches described above (the S-N curve, constant strain range data employed in conjunction with the fatigue strength reduction factors, and the application of global energy methods to full-scale structures) suffer from inherent limitations, and more sophisticated analytical methods are clearly required. Unlike the methods already mentioned, they should be capable of treating the three phases of the fatigue life on the phenomenological level, namely: (1) crack initiation, (2) crack propagation, and (3) final instability leading to fracture. Let us now consider at first in very general terms the extent to which the fracture mechanics approach can fulfill these three requirements.

In recent years following the paper of Paris and Erdogan (1963), good correlation for crack propagation rates under constant amplitude cyclic stress range for various crack configurations was obtained in terms of the range of the stress intensity factor. Such an approach to random loading has been investigated by Paris (1964), Rice et al. (1965), and Smith (1965). It appears that the fracture mechanics approach may also be applicable to the prediction of fatigue crack growth in pressure hulls although better understanding is needed of such factors as the effects of crack closure, combined mode deformation, biaxiality, initial and load-induced residual stress,* high mean and cyclic stress levels (in terms of applied stress to yield stress ratio), and transient effects due to the load sequence.

The crack propagation phase is expected to constitute the major portion of cyclic life under the condition of low cycle fatigue in a submarine pressure hull, but better understanding of crack initiation from

---

*In particular, it appears that the magnitude and distribution of the initial residual stress must be considered as a random variable and that, at best, some bounds may be assumed. The randomness of the residual stress could, however, be treated by the methods of the probabilistic structural mechanics (presently underway at NSRDC) provided that the capability is first achieved to predict crack growth under specific assumed distribution.

notches or preexisting flaws would be helpful in at least defining the lower bound and/or notch acuity below which the cracks are not expected to initiate and hence influence fatigue life. This information could then be used in establishing reasonable acceptance and inspection standards and in deciding where to truncate the stress level in the service life spectrum simulation tests conducted on large scale fatigue models. Here the conventional fracture mechanics approach is less applicable since it implies both that preexisting cracks (assumed to have zero radius at a crack tip) are expected in the structure and that all are assumed to propagate from the very first load cycle. Nonetheless, the fracture mechanics approach recently proposed by Foreman (1968) does attempt to predict the crack initiation period from flaws having a finite root tip radius and to define a limiting crack size which has no effect on the cyclic life. The concept of the threshold stress intensity factor range for nonpropagating cracks (analogous to the concept of the endurance stress observed in S-N curve) has also been suggested (Paris, 1970 and Bates and Clark, 1968).

The critical crack size which terminates* the subcritical crack growth in fatigue can be determined by utilizing the fracture mechanics approach under the restrictions discussed previously in connection with monotonic loading. Here, some uncertainty does exist in assessing the effect of prior cyclic deformation on the fracture toughness as discussed previously. Fleck and Anderson (1969) found that in some cases, the critical cyclic stress intensity factor for 7075-T6 aluminum sheets was approximately 70 percent of the static value. On the other hand, no appreciable evidence of cyclic loading history on fracture toughness was observed by Tiffany et al. (1966) for pressure tanks of aluminum alloy 2219-T87 with surface flaws tested under cryogenic conditions.

We defer the discussion of environmental effects until later and begin with a review of some of the analytical aspects of steady-state growth under monotonic load in an assumed inert environment. This is followed by a consideration of amplitude cyclic loading in connection with current analytical approaches to crack initiation and crack propagation

*The number of cycles required to propagate the crack from the initial value to the critical size is obtained by integrating the growth rates (crack propagation law).

under predominately tensile loading. The current approaches to the problem of cumulative damage under variable amplitude loading are then briefly reviewed. We then continue with a review of some aspects of biaxial and combined mode fatigue. Finally, we conclude with an assessment of the limited data bearing on the crack initiation and growth under cyclic compressive loading.

CRACK GROWTH UNDER MONOTONIC LOADING

The original analysis of steady-state quasi-static growth in Mode III deformation was presented by McClintock and Irwin (1964). Later, Rice (1968) generalized the analysis by presenting the results in terms of the plastic zone requirement* rather than in terms of the elastic energy release rate $\mathcal{G}$ (or equivalently in terms of the stress intensity factor). As mentioned earlier, elastic stress intensity factors cease to be a meaningful measure of the crack tip plasticity beyond small-scale yielding. In summary, the significant conclusions of Mode III analysis are as follows:

1. In order for stable crack growth to *proceed*, an increasing plastic zone (and increasing load) extending ahead of the advancing crack is required so that local fracture requirements ahead of the crack tip are satisfied.

2. Unstable crack propagation** is attained when the dimension of the plastic zone, as calculated for a given load and a stationary crack size, coincides*** with the calculated requirement for the plastic zone size of a moving crack.

We shall now elaborate on the two ideas expressed above. The plastic zone shape for Mode III deformation is found to be a circle of radius R_o, centered at the crack tip. For a stable crack extension to occur, the local fracture criterion must be met. The criterion is postulated in the form of a critical plastic shear strain γ_f^p (fracture

*We recall that for small-scale yielding, plastic zone size may be expressed in terms of the stress intensity factor.

**This refers to the condition where no further load increase is required to maintain quasi-static load extension.

***As defined by the point of tangency of the two curves (see Figure 31) and further discussion below.

ductility) to be attained at a certain microstructural dimension ρ_m from the crack tip (two-parameter fracture characterization). Now the respective plastic zone sizes required to *initiate* fracture and to *maintain* quasi-static steady-state extension are, respectively, Rice (1968) and Drucker and Rice:

$$(R_o)_{\text{initiation}} = \rho_m \, (1 + \gamma_f^p/\gamma_o)$$

$$(R_o)_{\text{steady state}} = \rho_m \exp\left(\sqrt{1 + 2\,\gamma_f^p/\gamma_o} - 1\right) \tag{40}$$

where γ_o is the yield strain in shear. The ratio of steady state to initiation zone size increases rapidly with fracture ductility, being 3 when $\gamma_f^p = 10\,\gamma_o$ and 170 when $\gamma_f^p = 50\,\gamma_o$. Rice has also shown that the plastic zone dimension required to quasi-statically increase the crack length by a distance ℓ is a universal monotonically increasing function* $R_o^f(\ell)$ of ℓ (for a given fracture ductility γ_f^p and characteristic microstructural dimension ρ_m). This curve labeled as $R_o^r(\ell)$ is shown as a heavy line in Figure 31 where we measure ℓ from the initial crack length c_o. On the other hand, the extent of the plastic zone for *fixed* load values (and stationary crack) given by load parameter Q as a function of the total crack depth is shown in Figure 31 as a family of curves starting from the origin. The point of tangency contact with curve $R_o^f(\ell)$ defined by a particular member of this family defines the point of crack instability.**

Some discussion on the possible relevance of the above analysis to the subcritical crack growth and fracture in Mode I seems to be in order. As mentioned earlier, a complete analysis for Mode I, analogous to the Mode III loading, has not been carried out.***

---

*See Rice (1968) for the explicit form of this function.

**Analytically, we refer to the point where the slope $dQ/d\ell = 0$.

***Rice did present a start on the problem of plane strain which indicated that the form of strain distribution for steady-state advance differs from that of the stationary crack with monotonic loading.

However it should be mentioned that a similar approach in defining the event of crack instability was considered earlier by Irwin (1960), Krafft et al. (1961), and Srawley and Brown (1964) for Mode I and was based on the notion of "resistance" ($\tilde{R}$) curves and elastic* crack extension force $\mathcal{G}$.**

The need for an extension of such an approach *beyond* the linear elastic formulation to obtain a quantitative characterization of fracture of materials in the immediate toughness range where a limited amount of crack extension may precede catastrophic instability has recently been emphasized by Pellini and Judy (1970). Hence it may be useful to outline*** some of the main concepts of such an approach although it must be admitted that at present it remains largely conceptual. We begin by showing in Figure 32 a plot quite similar to that shown in Figure 31. In this case, however, instead of representing the plastic zone size, the ordinate represents the crack extension force $\mathcal{G}$ (defined in terms of K_I by Equation (14)) and the crack resistance $\tilde{R}$. The essential idea is that for a given initial crack size, as $\mathcal{G}$ is increased during the test (by increasing the applied stress σ_∞) it is opposed by the corresponding increase of the resistance $\tilde{R}$ at the crack tip. Further, beyond a certain load value (dependent on the material) the resistance increases as a *consequence* of small, stable crack extension ℓ from initial length c_o. As Srawley points out, the situation is somewhat analogous to the ordinary tensile test where for a strain-hardening material, increasing load Q is required to continue the deformation e into the plastic range until the ultimate load is reached as computed with the aid of the tangency condition $dQ/de = 0$. Analogously, the equality between $\mathcal{G}$ and $\tilde{R}$ is continued until the instability condition $\mathcal{G} = \mathcal{G}_c$ is reached. Beyond that, $\mathcal{G}$ increases at a faster rate than $\tilde{R}$ so

*We recall that the term crack extension force and the elastic strain energy release rate are often used interchangeably. The first term is to be preferred since it can in principle be extended beyond linear-elastic formulation.

**The similarity extends only to the definition of onset of unstable crack propagation embodied in the second conclusion given on page 70. *Localized* fracture criterion ahead of advancing crack is not utilized to characterize the $\tilde{R}$ curve analytically due no doubt to the lack of precise elastic-plastic analysis similar to the preceding analysis for Mode III.

***A more detailed review is contained in the work of Srawley and Brown.

that the applied critical stress $(\sigma_\infty)_c$ corresponding to $\mathcal{G}_c$ does represent the maximum stress that can be sustained by the specimen for a given initial crack size.

Bearing in mind general concepts discussed above, let us return to Figure 32 and to the specific problem of a centrally notched "infinite" plate containing an initial through crack of length $2c_o$ and loaded by remotely applied stress σ_∞. Here, the family of straight lines starting from the origin (analogous to a family of curved lines shown in Figure 31) represent $\mathcal{G}$ as a function of current half crack length c and the applied stress level σ_∞. Recalling the relations between K_I and $\mathcal{G}$ and the K_I formula appropriate for this configuration, we have $\mathcal{G} = \pi(\sigma_\infty)^2 c/E'$ where $E' = E$ for plane stress and $E' = E/1-\mu^2$ for plane strain. Curves labeled $\tilde{R}_3$, $\tilde{R}_2$, and $\tilde{R}_1$ correspond to the crack extension resistance characterizing the materials in the range from extremely frangible (brittle) to extremely nonfrangible. Actually, explicit dependence of $\tilde{R}$ on the stress level, crack size, geometry, temperature, and loading rate has not been established except that according to the postulate proposed by Krafft (1961), $\tilde{R}$ appears to be primarily a function of the magnitude of crack *extension* $\ell = c - c_o$ and only secondarily a function of the initial crack size $2c_o$. In any case, as mentioned above, $\mathcal{G}$ is equal to $\tilde{R}$ until the event of crack instability and can be established for a particular specimen from compliance tests as discussed by Srawley and Brown. For extremely brittle materials represented by $\tilde{R}_3$, catastrophic crack propagation (instability) takes place before any appreciable crack extension from the initial crack can occur. On the other hand, for extremely nonfrangible materials characterized by $\tilde{R}_1$, an appreciable crack growth (and, consequently, appreciable plastic energy absorption) takes place before final instability. In any case, the general condition for instability is given by

$$\tilde{R}\Big|_{\sigma_\infty = (\sigma_\infty)_c} = \mathcal{G}\Big|_{\sigma_\infty = (\sigma_\infty)_c}$$

and (41)

$$\frac{d\tilde{R}}{dc}\Big|_{\sigma_\infty = (\sigma_\infty)_c} = \frac{d\mathcal{G}}{dc}\Big|_{\sigma_\infty = (\sigma_\infty)_c}$$

As discussed above, it is assumed that $\mathcal{G}$ is a linear function of c, as follows from the idealization of small-scale yielding for an "infinite" plate configuration. Also, instability is defined in terms of rapid (unstable) crack extension. Alternate interpretation is also possible. Thus recent analysis and associated experimental work on 2024-T3 and 7078-T6 Al alloys shows (Vasquez and Paris, 1970) that the load instability may for some materials be associated with the rapid extension of plastic zone which may be *followed* by a rapid crack extension. Further, an attempt was made in the above paper to include the case of large-scale yielding by including the Irwin plasticity and finite specimen corrections; both effects lead to $\mathcal{G}$ becoming a nonlinear function of the crack length (analogous to a family of curved lines starting from the origin in Figure 31).

Undoubtedly, more work is needed in this area, particularly in terms of quantitative characterization of $\tilde{R}$ curves. However, future investigations should be coupled with advances in elastoplastic stress analysis near stationary and quasi-statically extending cracks (similarly to the Mode III analysis discussed previously) in order to provide better understanding of the essential features of crack initiation, stable advance, stable/unstable transition, and crack arrest.

Let us conclude by examining some of the aspects of the subcritical crack growth in Mode I under monotonic loading apart from the problem of fracture characterization discussed above in connection with the $\tilde{R}$ curve approach. In terms of relevant experimental evidence, Johnson and Paris (1968) report that incidence of stable crack growth in the inert environment under *constant* load* (analogous to creep deformation) has been observed, as well as crack growth under rising load. It does seem, however, that steady-state stable growth in the inert environment has been observed only in plane stress or else in mixed plane stress-plane strain conditions with a corrosive environment being primarily responsible for such growth in plane

*Some of these data were obtained on 18 Ni (250) maraging steel (Li et al., 1966).

strain. An analysis of plane-strain, steady-state crack growth along the lines leading to Equation (30) and graphical construction of Figure 31 would no doubt be useful since there is some doubt as to whether the principal features of Mode III analysis also appear in Mode I. Thus, the experimental result of Hahn et al. (1969), based on a *simulated*[*] steady-state growth in plates under tension and the observed pattern of plastic deformation on unloading, indicates that, in contrast to above analytical predictions for Mode III, the plastic zone sizes appear to be the same for quasi-statically moving cracks as for stationary cracks. Also, the numerical analysis of Mode I by Kobayashi et al. (1970) tends to support the Hahn conclusion insofar as the gross plasticity features are concerned although the details at the crack tip remain unclarified. Finally, the existence of the subcritical crack growth under sustained or rising load in submarine hulls has not been reported (as distinguished from the growth under actual load reversal), but it cannot be entirely ruled out. If such slow, steady-state growth (analogous to creep deformation) can occur during loading or at *sustained* load with or without corrosive environment, it would raise further questions as to the sufficiency of the conventional **"fatigue tests" conducted at comparatively high cyclic frequencies and short hold times at constant pressure.**

CRACK INITIATION UNDER CONSTANT AMPLITUDE CYCLIC LOADING

Recall that from an engineering point of view, the fatigue life of a structural detail can be roughly visualized as follows: (1) a crack initiation phase terminated by the appearance of macrocracks, (2) a macrocrack propagation phase, and (3) final instability associated with the period when the dominant crack reaches a critical size. In the pressure hull fabricated from ductile materials, the occurrence of the third phase may be replaced by the appearance of a stable through crack leading to

---

[*]Some questions could be raised in regard to the accuracy of the experimental techniques.

leakage. It must be admitted that the line of demarcation between crack initiation and crack propagation is rather difficult to define for several reasons. First, the appearance of a macrocrack is preceded by the propagation and coalescence of many macrocracks, so that this period can also be viewed in terms of crack propagation. Second, the definition of the macrocrack initiation period is related to the type of the specimen and to the sensitivity of the crack detection system. Thus, the Applied Research Laboratory at United States Steel defines the initiation life as the number of cycles required to produce 0.019-in.-long fatigue cracks (Boblenz and Rolfe, 1966). Schijve (1967) associates the initiation life with the appearance of a 1 mm (0.0394-in.-long) crack; Manson and Hirschberg (1966), and Forman (1968) favor a 0.010-in.-length definition.*

The lack of a clear distinction between the crack initiation and propagation phases of the fatigue process (combined, possibly, with the lack of necessity in a particular application to make such a distinction) may be one of the reasons why some investigators continue to treat the fatigue problem only in terms of the total number of cycles for through cracking. Although such an approach may be quite satisfactory for small structural components (particularly for low stress-high cyclic life application), it is inadequate for such complex structures as a submarine pressure hull. Here, an estimate of the initial size of cracks and their rates of growth are required for rational reliability predictions, acceptance standards, and scheduling of inspection periods. In addition, such information is required to assess the residual strength of the hull (its capacity to resist static or dynamic overloads in a damaged condition) at any time during its operational life.

In discussing crack initiation, we must distinguish between two situations. The first is the case of a crack originating from an assumed flaw-free geometric surface discontinuity (notch of finite root radius) designed or fabricated into the structure. Notch in this context may include smooth transition sections and holes. In the second case, actual preexisting defects in the form of surface scratches, internal weld defects,

*Manson and Hirschberg found that for their specimen (notched round bar), a 0.010-in.-long surface crack corresponded to 0.003 in. in depth. Their initiation and propagation analysis were based on the development and subsequent propagation of 0.003-in. deep cracks in the radial direction.

or undercuts are assumed to be present, and the problem reduces to the prediction of the number of cycles required to initiate or maintain crack *extension* from the above defects. The problem of nonpropagating cracks, studied by Frost (1960) also falls within the second category.

The conventional approach to the first class of problems is to use stress or strain concentration factors to relate the observed initiation life of a notched specimen to that of a smooth specimen.

The simplest variant of this approach is to use elastic stress concentration factors; the more sophisticated method is to employ cyclic stress-strain curves and plastic strain concentration factors. An implicit assumption common to the above methods is that the nucleation period is dependent only on the maximum local stress or strain range,* regardless of the stress gradients, statistical size effects, stress or strain triaxiality, etc.** In this connection, Schijve (1967) pointed out that the attempted correlations between smooth and notched specimens overlook the difference in the amounts of highly stressed volume*** between smooth and notched specimens. This means that from the statistical point of view, the cracks can nucleate in a much larger volume in the unnotched specimens. His observation was confirmed by tests on smooth and notched specimens of aluminum alloy under axial tension; correlation between the crack initiation periods could not be obtained when the calculated stress at the notch was made equal to the applied stress in the smooth specimen. (The

---

*When the work on the manuscript was essentially completed, the authors have learned of a new approach which was the product of stress and strain ranges as the correlating parameter between the smooth and notched specimens. This procedure appears to be markedly superior to the conventional methods and is summarized in the work of Morrow et al (1970).

**The concept of equivalent strain is sometimes used to account for triaxiality as will be discussed later.

***An indirect way of taking this factor into account is to use K_f, the fatigue strength reduction factor (see page 66) instead of K_t, the elastic stress concentration factor in the notch stress analysis.

actual crack initiation period for notched specimens was much longer than predicted.) On the other hand, Schijve noted generally good correlation* for macrocrack propagation rates.**

The question has not been resolved as to whether maximum stress or strain range criterion should be used for crack initiation. Use of the strain range would seem to be a more appropriate index, however, since the stresses at the notch are generally in the plastic domain. For this reason, our discussion of the notch factor approach to crack initiation is confined to the correlation methods based on the strain range.

In regard to the second class of problems, a recent paper by Forman (1968) employs the fracture mechanics approach for dealing with the prediction of crack extension from sharp (or blunt) initial flaws. Here, the effect of plasticity at the crack tip is only indirectly recognized in the computation of the modified stress intensity factor. On the other hand, such an approach is considerably simpler than the localized strain range computation, and comparisons of the two methods to the existing experimental data for blunt cracks (notches) would undoubtedly prove useful.

We shall now consider in greater detail the approaches based on the notch strain range and the approach based on the fracture mechanics parameter.

Notch Strain Range Method

Since the application of this method to notched specimens requires knowledge of the crack initiation period for a given strain range of a smooth specimen, some discussion of the fatigue life of a smooth specimen as a function of the strain range seems warranted.

---

*As indicated by the required number of cycles to grow macrocracks from the initial length of 0.1 to 1 mm in a smooth laboratory specimen and in small and large notched specimens (utilizing the stress intensity factor approach).

**In this connection, note the Freudenthal (1969) comments on the relative insensitivity of crack propagation rates to microstructure. By contrast, the duration of crack initiation phase seems to be strongly affected by the metallurgical factors.

By running axial tensile fatigue tests on smooth laboratory specimen of hourglass shape for a wide variety of materials, Manson (1965) confirmed the generality of the so-called Manson-Coffin* law for low cycle fatigue, which states that the cyclic life N_f is related to the plastic** cyclic strain range by the formula

$$\Delta \varepsilon_p = (N_f/D)^{\bar{z}} \tag{42}$$

where z is a material constant and D is the ductility measured by a uniaxial tensile test and is defined by

$$D = \log \left(\frac{1}{1 - RA}\right) \tag{43}$$

where RA is the percentage reduction in area.

Several points need to be made about Equation (42). Manson obtained this relation from axial tests where the mean strain*** was zero and the total transverse (diametral) strain range was maintained constant. When the total axial strain range (deduced from the knowledge of stress range, diametral strain range and elastic constants) was plotted against fatigue life on the log-log plot, a curved line† resulted as shown in Figure 33. Now the total strain range $\Delta\varepsilon_T$ is composed of the elastic component $\Delta\varepsilon_E$ and the plastic component $\Delta\varepsilon_p$. The elastic strain range is computed as the stress range divided by the elastic modulus where the plastic strain range

---

*As will be discussed subsequently, the application of this equation is not limited to crack initiation studies under constant amplitude loading. It is also used in several crack propagation and cumulative damage theories.

**Gross (1963) claimed that the total strain range $\Delta\varepsilon_T$ rather than $\Delta\varepsilon_p$ provides better correlation. See footnote † below.

***Manson (1966) proposed that the effect of tensile mean strain ε_m can be taken into account by rewriting Equation (42) in the form

$$\Delta \varepsilon_p = \left(N_f/(D-\varepsilon_m)\right)^{\bar{z}}$$

†On the other hand, the data obtained by Gross (1963) on a cantilever plate bending specimen indicated a straight-line relationship leading to the form $\Delta \varepsilon_T N^k$ = constant. It appeared that a value of k of about 1/3 represented a good approximation for all materials tested.

is obtained by subtracting the calculated elastic strain range from the total strain range. Manson showed that both the elastic and the plastic components can be approximated by straight lines on the log-log plot, thus leading to the exponential relationship of the general type represented by Equation (43) connecting either $\Delta\varepsilon_E$ or $\Delta\varepsilon_p$ with the cyclic life. As shown in Figure 33, the curve of the total strain range becomes asymptotic to the elastic line at high cyclic life and to the plastic line at low cyclic life.

It should be noted in connection with the above discussion that in the Manson tests, cyclic life was defined as the specimen separation. In contrast, Coffin (1954) used the first sign of a visible crack as the terminal point of the test. Using the Manson definition of N_f, the coefficient $\bar{z}$ for a wide variety of materials turns out to be about -0.6; using the Coffin definition yields approximately -0.5. In the low-cyclic fatigue range that is of interest to the submarine application (i.e., between 10^4 and 10^5 cycles) and for the smooth specimen under consideration, the distinction between initiation and total life is insignificant (at least for the materials considered in Figure 34). As shown in Figure 34, the crack initiation period N_o for such a range of interest constitutes at least 90 percent of the fatigue life N_f. Finally, Equation (42) may be used to predict the fatigue life of a smooth specimen (knowing or estimating the material constants $\bar{z}$ and D) in terms of the *total* axial strain range by making use of the method of universal slopes proposed by Manson (1965). Essentially, it is an empirical law, derived on the basis of observations on a wide variety of materials, for relating the total strain range to its plastic and elastic strain components and static strength properties as written in the form

$$\Delta\varepsilon_T = \Delta\varepsilon_p + \Delta\varepsilon_E = 3.5\,\frac{\sigma_u}{E}\,N_f^{-0.12} + D^{0.6}\,N_f^{-0.6} \qquad (44)$$

where σ_u is the ultimate tensile stress in pounds per square inch.

Having obtained the plot of cycles to crack initiation as a function of the total strain range for the smooth specimen either by using Equation (44) or preferably by a series of cycling tests represented by a plot similar to Figure 33, the designer is then faced with the problem of

determining the local strain range at the root of the notch for the structural detail under consideration. This may turn out to be a rather complicated task and merits an extended discussion.

In principle, the local strain can be obtained by multiplying the nominal strain by the strain concentration factor. If the stresses at the notch remain in the elastic domain, the distinction between the stress and strain concentration factors disappears, and the formulas of Peterson (1953) and Neuber (1946) can be used for a wide variety of notch configurations. However, elastic stress fields are extremely unlikely in the vicinity of notches in regions of high residual and/or load-induced stresses, and so at least an approximate plastic analysis is generally required. Such approximate procedure may involve the use of the plastic stress concentration factors proposed by Hardrath and Ohman (1953) and the monotonic stress strain curve in the form*

$$\bar{K}_\sigma = \frac{\sigma_{max}}{\sigma_\infty} = 1 + (K_t - 1)\frac{(E_s)_o}{(E_s)_\infty} \tag{45}$$

Here, σ_{max} is the maximum notch stress, σ_∞ is the applied (nominal) stress, and K_t and $\bar{K}_\sigma$ are the elastic and plastic stress concentration factors, respectively. $(E_s)_o$ and $(E_s)_\infty$ are the secant moduli calculated from

$$(E_s)_o = \frac{\sigma_{max}}{\varepsilon_{max}}, \quad (E_s)_\infty = \frac{\sigma_\infty}{\varepsilon_\infty} \tag{46}$$

where ε_{max} and ε_∞ are, respectively, the maximum notch strain and ε_∞ the nominal strain. For a given notch geometry and the applied stress state, K_t may be obtained from Peterson and Neuber. $\bar{K}_\sigma$ and $(E_s)_\infty$ may be computed by an iterative process or a graphical procedure (Manson and Hirschberg, 1966) for a given uniaxial stress-strain curve. The strain concentration $\bar{K}_\varepsilon$ can then be obtained from

$$\bar{K}_\varepsilon = \frac{\varepsilon_{max}}{\varepsilon_\infty} \tag{47}$$

---

*These authors have generalized the equations developed by Stowell (1950) for the specialized case of stress concentration near a circular hole in a plate under uniaxial tension. It should be noted, however, that plane stress conditions appropriate to thin plates are assumed. Also the plastic stress and strain concentration factors discussed here should be distinguished from K_σ and K_ε introduced in Equation (20).

We note that this approach is limited to the deformation theory of plasticity; although for specialized configurations more precise solutions based on the incremental plasticity theory have been developed (for example the work of Davis, 1963). The solution for cases where K_t is not available can be obtained by numerical or experimental methods. Finally, in order to take into account the stress gradient effect K_f is used instead of K_t. Although K_f can be easily obtained from laboratory data on simple notched specimens, such modification does not appear to be particularly useful for pressure hull application because of the obvious difficulty in estimating K_f.

As described above, the $\bar{K}_\varepsilon$ estimate is an attempt to assess the plasticity effects by using only the first* loading portion of the *monotonic* stress-strain curve. For the case of materials which exhibit considerable cyclic hardening or softening, however, it should be observed that such an approach may be doubtful. The complications which may arise in such a case are not generally recognized and can best be illustrated by discussing the experimental work of Blatherwick and Olson (1968) on the cyclic strain redistribution in double-edge notched plate fatigue specimens fabricated from SAE 1018 steel. First, smooth cylindrical test specimens were used to obtain the static and cyclic material properties shown in Figure 35. The effect of cyclic softening or hardening can be obtained by observing the hysteresis loops which were obtained by subjecting these specimen to the controlled strain range alternating between extension and compression strains. As shown in Figure 35 for the strain range of ±1350 μin./in., the observed stress range decreased from ±39.4 to ±29.2 ksi after 1000 cycles, thus indicating a cyclic softening material property. By selecting other strain ranges and recording the corresponding stress ranges, a cyclic stress-strain curve can be obtained and compared to the monotonic curve as shown in Figure 35. Since the compressive part of the cycle was the same** as

*This restriction does not apply when cyclic stress-strain curves are used (see Manson and Hirschberg, 1966)

**In connection with tests run on other materials, Younger (1966) noted that the Bauschinger effect noted following the first load reversal tends to disappear when the stabilized cyclic hysteresis loop is reached, leading to the speculation that eventual stress level symmetry may be a general material characteristic.

the tensile, half, only the tensile portion of the cycle is shown. The numbers on the curves represent the number of cycles of the repeated strain, with 10^4 cycles being associated with a stable condition.

Figure 36 shows the results for stress and strain distributions in the notched specimen as a fraction of the distance from the centerline of the plate and the number of cycles. In these tests, the strain amplitude of the notch was held constant, leading to a reduction of the stress and strain amplitude in the rest of the specimen as the cycling progressed.* For contrast, Figure 37 shows the stress and strain redistribution across the specimen when the axial load range is maintained constant. Here, the strain amplitude at the notch decreases, and the stress distribution tends to be equalized as the cycling progresses. One can speculate that an increase of the strain range at a notch may be expected for the cyclic strain-hardening material.

We have described the main features of the Blatherwick-Olson work in order to emphasize possible inaccuracies inherent in calculating the strain range at the notch by the use of static stress-strain curves and the plastic strain concentration factor. Unless cyclic hardening or softening is negligible, such an approach can at best predict the strain amplitude at the end of the maximum load stage of the first cycle.** Nonetheless, because of the analytical difficulties associated with prediction of the "shakedown" (stabilized) strain range, elastic stress concentration factors and static stress-strain curves are commonly used. Thus a simplified approach toward calculating the "shakedown" strain range at a nozzle in a pressurized vessel was used by Pickett and Grigory (1967) and yielded good agreement with the experimental data. The simplifications entailed the use of the elastic stress concentration factor, the static strain-stress curve during the first load cycle, and the approximate cyclic stress-strain relations for subsequent cycles as proposed by Stowell (1966).

---

*Stresses were computed by utilizing recorded strain measurements and the cyclic stress-strain curve of Figure 35.

**Further discussion of notch strain histories are contained in the section on biaxiality effects.

Attempts have been made (Manson and Hirschberg, 1966 and Younger, 1968) to utilize cyclic stress-strain curves for initiation *and* crack propagation for a small notched specimen; however, aside from the frequent lack of knowledge of K_f required for the implementation of such an approach, the relevance of the initial stress concentration factors for the subsequent macrocrack propagation phase is questionable. Ideally, a complete elastic-plastic stress-strain history analysis at the notch root is required; particularly desirable is one that takes into account the changing material properties as the cycling progresses. Although such computations are not beyond present analytical capability,* they generally require complex computer programs and, consequently, simplified approaches analogous to those used in Pickett and Grigory (1967) should be further explored.

Additional complications are also involved in the practical application of the cyclic strain range material data to the calculation of the crack initiation life at notches in submarine pressure hulls. First, calculation of the local strain range at the notch may involve initial tensile residual stress as well as the load-imposed stress. Thus, in contrast to the fully reversed strain range commonly utilized in the characterization of the material, nonzero mean strain may be present at the notch. Second, the calculation of the "shakedown" strain range is also complicated because of the presence of initial residual stress.** Finally, the effect of applied stress biaxiality (to be discussed later) may have an important effect on initiation life, as discussed by Pickett and Grigory in connection with the reported experimental data on pressure vessels.

---

*Manson (1966) discusses in detail several methods ranging from the cyclic plasticity computations utilizing cyclic stress-strain curve and a computer program to more approximate methods. A numerical elastoplastic analysis (utilizing static stress-strain curve) has also been used to establish a hysteresis loop (Marcal and Turner, 1965).

**The inability of several current theories to take these factors into account will be discussed in connection with compressive loading fatigue.

Stress Intensity Factor Method

As will be discussed later,* the stress intensity factor range has been used quite extensively to correlate the crack growth rates in full-scale structures with that of laboratory specimens. Forman (1968) proposed that ΔK_I can also be used to correlate crack initiation period for cracks originating from sharp or blunt flaws. A similar approach was also subsequently utilized by Jack and Price (1970). The example of application to sharp embedded flaws shown in Figure 38 is based on experimental data (Munse et al., 1964) for embedded defects in butt-welded 3/4-in.-thick HY-80 steel under zero to tension applied cyclic loading. The initial defects in the form of porosity, slag, inclusions, or drilled holes were all idealized as penny-shaped flaws of radius a. Although the effect of initial residual welding stress, which was undoubtedly present, was not considered, it can be seen that the experimental data for crack initiation as detected by radiographic techniques does show correlation in terms of ΔK_I. It should be noted that the crack initiation period for these specimens represented from about 50 to 90 percent of total cyclic life.

So far we have discussed the possible usefulness of the ΔK_I concept for cracks emanating from (idealized) initially sharp internal flaws. Forman also proposed that data on the number of cycles to crack initiation from flaws having a finite initial root radius may be correlated in terms of the relative stress intensity factor $\Delta K_I/K_a$ where K_a is defined by

$$K_a = (r_p/R_o)\, K_c \tag{48}$$

Here r_p is the extent of the plastic zone at the tip of a blunt notch, K_c is the critical stress intensity factor (fracture toughness) for a sharp crack, and R_o is the normalizing factor** defined by Equation (36) for plane stress.

*ΔK_I is the difference between the maximum and the minimum K_I in the loading cycle. As we shall see later, this definition is intended primarily for tensile load application and consequently problems in the interpretation arise whenever complete or partial crack closure occurs during part of the cycle as, for example, in the reversed bending case.

**It will be recalled that R_o represents a crude estimate of the plastic zone extent for sharp cracks.

As discussed in connection with the fracture criteria, K_c depends on the plate thickness as well as on material properties.

The calculation of r_p was based on the elastic analysis (Creager, 1966) of stresses in front of the blunt crack, with the extent of the plastic zone being determined by the point where the elastic stresses satisfy a yield criterion. Such calculations give, of course, only a very crude estimate of the yield zone size under *monotonic*[*] loading and can at best be applied to the small-scale yielding range. The test results obtained on 7075-T6 aluminum sheet for zero to tension cyclic loading were subsequently interpreted in terms of $\Delta K_I/K_a$ versus N_o (cycles to initiate 0.010-in. fatigue crack) correlation as shown in Figure 39. Essentially, three types of notch geometry were tested: (1) a centrally notched plate ($\bar{\rho} = 0$, $\beta = 90$ deg), (2) a notched circular hole with $\beta = 90$ deg and (3) a notched circular hole with $\beta = 45$ deg. Here $\bar{\rho}$ represents the hole radius and β the notch orientation with respect to the direction of applied stress σ_∞. Notch radius ρ was varied along with the initial crack size c. Experimental results (shown in Figure 39 by solid points) represented the cases where plastic deformation was calculated at the crack tip; open points represented elastic deformation. It can be seen that the envelope of the test results was rather wide, but that nevertheless, the trend of the data does indicate correlation with $\Delta K_I/K_a$. In view of the variety of the configurations tested, such scatter is not too surprising and is probably narrower than would have been obtained using other correlating methods that do not attempt to take into account the specific notch configurations and crack tip plasticity. Finally, the dashed curve in Figure 39 represents the cycles to initiate a 0.010-in. crack computed by the Forman crack

---

[*] Forman (1968) also presents a table for the relative plastic zone size r_p/R_o as a function of the nondimensional initial root radius ρ/R_o for the cases of plane stress and plane strain.

propagation equation (to be discussed later), in which it is assumed that the crack growth begins in the very first load cycle and reaches 0.010 in. after N_o cycles.

It appears that the theoretical curve obtained from crack propagation equations is a good lower bound representation of the data. Forman reached similar conclusions utilizing the above approach in his analysis of the test results obtained by Manson (1965) for 2014-T6 aluminum alloys, where held the appearance of a 0.0025-in.-deep crack was regarded as the crack initiation.

CRACK PROPAGATION UNDER CYCLIC LOADING

We have reviewed some of the approaches to the crack initiation problem and noted that a considerable portion of the crack initiation period may be viewed in terms of the microcrack propagation if the scale of the observations is sufficiently reduced. In what follows we assume that a dominant macrocrack has already formed and that the problem is then reduced to predict its stable rate of growth until reaching critical crack size, as defined by some fracture mechanics parameters discussed previously.

It is instructive to list some of the factors that may have an effect on the rate of growth. These are:

1. Geometry - size, shape, and orientation of the crack and the specimen dimensions.

2. Stressing conditions - magnitude, sequence, and character of applied stress level (or strain); ratio of the mean to the cyclic component; biaxiality; and initial residual stress and its cyclic dependence.

3. Material properties - static tensile test data, cyclic stress-strain curves, fracture toughness, and microstructural properties - possibly as influenced by the previous deformation history.

4. Environmental effects - temperature and electrochemical properties of the media.

The above list could be supplemented by the test frequency effect; however, a discussion of this variable will be deferred until the section on the environmental effects because of the apparent intimate connection between frequency and environment.

We will first summarize some of the qualitative features of the effects of the first three factors listed above, as revealed by the experimental observations on Mode I propagation in simple uniaxial tensile specimens.* This will be followed by a review of the current state of elastic-plastic analysis under reversed loading as contrasted to the analysis under monotonic load discussed previously. We will then conclude by assessing some of the current analytical approaches to the crack propagation as applied to constant amplitude cycling.

Some Experimental Observations

Here we summarize some of the important observed qualitative features of the crack growth and speculations that have been advanced on the relative influence of the geometry, stressing conditions and material properties.

Most of the observations of the rates of growth have been obtained for Mode I propagation of edge or through cracks in thin plates, thus reducing the crack growth characterization to one dimension and description in terms of the crack depth (or length) alone. This being the case, the primary geometrical factor apart from the crack size is the specimen thickness. Now in view of the observed sensitivity of the fracture stress to the plate thickness under the conditions of monotonic loading, such sensitivity would also be expected to appear in the case of subcritical crack growth. However, although some increase in crack growth rates with the increased plate thickness has been observed by Schijve (1967) and by Fleck and Anderson (1969), Frost and Denton (1961) have found that the rates were practically insensitive to plate thickness.**

---

*It should be noted here that although most of these observations were conducted in air and thus ostensibly do not involve corrosive environment aspects, it has been argued that air should not necessarily be considered as an inert medium. Further discussion of this point will be found in the section dealing with environmental effects.

**Fleck and Anderson noted dependence on plate thickness, with the cracks in thick plates growing at a faster rate but primarily *before* the transition to the slant mode (to be discussed later) took place.

In assessing the effect of stressing conditions the transitions that have been observed both in the fracture mode and in the crack growth rates are of considerable interest but are presently not well understood. Wilheim (1966) observed the transition on centrally notched aluminum plates from the flat (90-deg orientation of the fracture surface to the loading direction) to the slanted mode with shear lip formation (as in the static fracture tests of the ductile material), where the slanted mode was associated with the higher growth rates. The transition to higher growth rates occurred in a fairly narrow region of the stress intensity factor range, and even after the transition to shear lip mode occurred, the propagation could be forced back into the flat mode by decreasing the stress intensity factor.

Such transitions (from flat to slant mode) are sometimes thought of as the transition from plane strain to plane stress (Schijve 1967). On the other hand, the change from the flat to the slant mode need not be accompanied by a change of growth rates, as observed by Hertzberg and Paris (1965). On the basis of his tests, Clark (1968) concluded that the transition to high crack growth rates is not associated with the transition from plane strain to plane stress but rather with the approach of the stress intensity factor range to that stress intensity level at which subcritical crack growth would have occurred under rising monotonic loading. Finally, there is evidence (Wei, 1970 and Feeney et al., 1969) that at least for some materials the transitions are strongly dependent on the environment. Clearly, further work is needed on this facet of the problem.

In addition to the observed transition effects at high stress levels (more precisely, high stress intensity factor levels), abrupt transitions in growth rates have also been observed at extremely low stress levels (Paris, 1970; Bates and Clark, 1968; and Gross, 1970). Paris found a fairly abrupt transition from 10^{-9} to 10^{-7} in. per cycle at extremely low growth rates in 9310 steel within a very narrow stress intensity factor

range. This phenomenon led him to propose the concept of a threshold stress intensity range ΔK_e below which crack growth rates are negligible.*

Continuing with the discussion of the qualitative aspects of stressing conditions, we find that the effect of mean load on crack growth has not been answered to our complete satisfaction. (The load *fluctuation* is commonly accepted as a primary variable). Especially in need of clarification is the effect of negative $\bar{R}$ values. $\bar{R}$ is the ratio of the minimum to the maximum stress of the cycle, and negative values thus correspond to testing between tension and compression. Empirical laws based solely on the stress intensity factor *range* correlation show distinct layering,** with the higher crack growth rates associated with increasing $\bar{R}$. It has been argued with respect to the negative values of $\bar{R}$ that since the crack surfaces can be assumed to be closed during the compressive portion of the cycle, the compressive portion of the stress range should have no effect on the rates of growth. This implies that the growth rates for the negative values of $\bar{R}$ should be identical with $\bar{R} = 0$ for the same value of the tensile stress range.

Although this assumption appears to be borne out by experimental results on some materials, it does not appear to be universally true. Thus, Illg and McEvily (1959) and more recently Hudson (1969) found that although the compressive portion of the cycle did not seem to affect the crack growth rates for 7075-T6 alloy, the cracks in 2024-T3 alloy grew faster in tests with $\bar{R} = -1$ than in tests with $\bar{R} = 0$ for the same tensile stress range. Another demonstration of the possible adverse effect of the compressive portion of the cycle was provided by a recent Naval Research Laboratory study (Crooker, 1971) on 9Ni-4Co-0.2C, HY-80 quenched-and-tempered steels and Ti-6Al-4V alloy. Fully reversed tension-compression and zero-to-tension cyclic tests were run on plate specimens containing embedded surface cracks.

---

*This should not be confused with the threshold stress intensity factor K_{ISCC} associated with sustained loading to be discussed in connection with environmental effects.

**See, for example, Figure 59 given later in this report.

The data showed an increase in fatigue crack growth rates due to tension-compression cycling ($\bar{R}$ = -1) as compared to cycling under zero to maximum tension ($\bar{R}$=0). Figure 40 shows the effect for HY-80 steel in terms of the plot of the surface length of the crack (2c) as a function of the number of cycles N. Note that both the initiation (extension from starter notch) and the subsequent propagation were accelerated by the compressive portion of the cycle. We will later discuss the interpretation of Figure 40 in terms of the ΔK_I semiempirical crack propagation law based on ΔK_I correlation.

When the formulation of any crack propagation theory is being considered, the question that needs to be posed is whether crack growth is continuous (occurring in every cycle) or whether there is a possibility that intermittent growth and delays or accelerations can occur. The experimental evidence shows that growth does appear to be continuous for low growth rates* (less than say 10^{-4} in./cycle) and that it can be correlated with the striation spacing (Bates and Clark, 1968 and Hahn et al., Dec. 1969) observed on the fatigue surface.**

At high growth rates on the other hand, the crack can advance by intermittent bursts (Bates and Clark) aided by the crack nucleation ahead of the main crack front. Another instance of discontinuous growth as directly related to the load sequence effect has been observed by Hardrath (1964) for programmed loading tests conducted on 7075-T6 aluminum alloy. He found that a change of cycling stress from 0 to σ_1 to 0 to σ_2 resulted in delays*** when $\sigma_2 < \sigma_1$ and immediate adjustment to σ_2 level when $\sigma_2 > \sigma_1$.

---

*This regime corresponding to low stress and low crack growth rates was characterized by Hahn as Regime No. 1. Regime No. 2 corresponds to high-stress and high growth rate of the spectrum usually greater than 10^{-5} in./cycle. (See Figure 44 which will be discussed later in greater detail).

**It should be noted here that the phenomenon of striations appears to be connected with environmental effects at least for some materials in low growth range since striations were found to be entirely absent when fatigue tests were carried out in vacuum on 2024-T3 aluminum alloy (McClintock and Pelloux, 1968 and Pelloux, 1969).

***Acceleration in the rate of crack propagation when the second stress was higher than the first were also reported (Jacoby, 1965), but the effects were claimed to be quite small compared with the effects observed when the second stress was lower than the first one.

Here it is difficult to interpret the sequence effect solely in terms of the load amplitude and the maximum load changes since both were changed. More revealing in this respect are the data obtained by McMillan and Pelloux (1967) who ran random and programmed load tests on 2024-T3 aluminum with sequences of (1) constant maximum load with variable fluctuating load ranges and (2) constant fluctuating load range with variable maximum loads.

For the first type of test, they found (1) that there was no marked advance in crack front when the fluctuating load changed from one level to another and (2) that after a change of fluctuating load, the spacing of the striations for the next load amplitude sequence reached a stable and uniform value on the first cycle of the new load amplitudes. However, the sequence was shown to be quite important for the second type of test and led to retardations following the high load, thus indicating the dependence of crack growth on the prior as well as the current maximum stress level. Finally, the effect of random loading sequence was observed to lead to higher crack growth rates* than in nonrandomized program loading sequence with variable maximum load. However, when the maximum load was kept constant, the growth rates were the same as for programmed loads.

The relative importance of various material properties is not entirely clear at present, particularly the properties measured in a conventional static test (yield stress, Young's modulus, ductility, and ultimate strength). Experimental data has been analyzed by Hahn et al., Dec. (1969) on a variety of materials with a wide range of yield strength and ductility; they showed a relative insensitivity of crack growth to such variables in the low-crack growth, low-stress regime. Most significant material properties in this range appeared to be the cyclic stress-strain properties** directly ahead of the crack tip. The transition point between the low and

---

*Cross-overs between constant amplitude and random loading (with various maximum load) behavior were observed by Smith (1965) when data were compared on the basis of time averages of the stress intensity factor. Random loading rates were higher at the low stress intensity levels and lower at high levels than for constant amplitude loading.

**These could be measured by the cyclic stress-strain curve discussed previously.

the high growth regions is apparently dependent on the Young's modulus.* Dependence on the static yield stress and microstructure, appears to be more pronounced in the high stress, high-growth rate regime than in the low-growth region.

At extremely high growth rates when the critical crack size is being approached, the toughness as measured by the critical stress intensity factor would appear intuitively to be an important factor although direct experimental assessment of this effect alone is lacking.**

In conclusion, we emphasize that some of the observations made solely on the basis of geometric and material parameters may be modified by environmental effects that were generally not considered in the above discussion.

Elastic-Plastic Analysis under Cyclic Loading

Our previous discussion of the elastic-plastic stress distribution near the crack tip assumed that the applied load is either maintained constant or is increased monotonically. In addition, with the exception of the discussion of the McClintock and Rice analyses of stable Mode III growth, we have assumed that the cracks remain stationary. Now some difference between the plastic strain distribution in front of a growing crack as opposed to that of the crack which remains stationary under a load reversal would appear probable in view of the known general dependence of the plastic strain on the entire deformation history. Thus at a given point ahead of the crack tip, the local plastic strain and hence the size of the plastic zone surrounding the crack tip would appear to be a function of the previous as well as the current crack length.

Limited experimental data obtained by Hahn et al. (December 1969) on Fe-3Si steel (under plane strain) showed that at least the sizes of the plastic zones of a cyclically loaded growing crack and a monotonically

---

*Bates and Clark also stress the importance of Young's modulus in normalizing the growth rate of the various alloys.

**Fracture toughness has been included in empirical equations proposed by Forman and discussed later.

loaded stationary crack are essentially the same if the cracks are loaded to the same peak stress intensity factors. Hahn noted, however, that the fatigue plastic zone does display larger regions of intensely strained* material, and this is consistent with the idea of superposition and accumulation of deformation from the previous crack positions.

In what follows, we shall confine ourselves to a review of some of the main features of the approximate method of elastic-plastic analysis near stationary cracks under reversed loading. The discussion of the state of deformation ahead of the *growing* crack cannot be entirely divorced from the local fracture criterion required for continuous crack extension and therefore will be discussed later in connection with the review of the crack propagation laws.

The method of plastic superposition provides an approximate approach to the problem of stress fluctuation near the crack tip under reversed loading. It is based on the assumption of the proportionality** of the plastic flow and is thus restricted to cases for which (simplified) deformation theory of plasticity is applicable. It was originally applied for special cases by Hult and McClintock (1956), Paris (1964), and Dixon (1965) and was generalized by Rice (1967). The assumption of proportionality was shown to be fairly accurate at least for the plane stress case by Dixon's experiments on thin, centrally cracked copper sheets under tension to tension reversed loading and utilizing photoelastic coating. Rice speculated that, barring both the compressibility effect on plane strain yielding and transitions from in-plane deformation to 45-deg shear bands, the inaccuracies in the proportional flow assumption would be expected to be insignificant for the case of large plane strains. However, in addition to assuming the validity of proportional flow, an assumption which is perhaps more important in the analysis that follows is that crack blunting by plastic deformation may be neglected.

---

*Strains in excess of 5 percent.

**This means that the components of plastic strains remain in a constant ratio to each other during loading and unloading in the plastic domain.

To illustrate the main ideas,* let us consider Figure 41, which shows a cracked body of nonwork hardening material that was first subjected to the maximum remote tensile stress σ_∞ and then unloaded by $\Delta\sigma_\infty$ load increment. Strain distribution due to loading σ_∞ may be obtained by the methods of elastic plastic stress analysis discussed earlier. When load reversal occurs, reversed plastic flow leads to the formation of the reversed plastic zone of width $R^{(c)}$ embedded in the original zone of plastic deformation of width R created by the initial monotonic loading. The effect of unloading (assuming the validity of proportional flow and absence of crack closure) is to simply reverse the direction of stresses in the flow region creating a zone of residual compressive stress. The changes in stresses, strains, and displacements due to the load increment $-\Delta\sigma_\infty$ can then be obtained from the original monotonic solution with σ_∞ replaced by $-\Delta\sigma_\infty$ but with the yield stress σ_o and strain ε_o replaced by twice their values for static loading. The replacement of σ_o by $2\ \sigma_o$ is required in order for the stresses to have the correct magnitude and direction in the reversed zone where the changes due to load reduction are subtracted from the effects of the original monotonic loading. Reloading by $+\Delta\sigma_\infty$ then restores the original state so that the stress and strain distributions repeat themselves under an applied fluctuating tensile stress $(\sigma_\infty-\Delta\sigma_\infty)$ $\pm\Delta\sigma_\infty$.

The degree of sophistication in applying the above ideas of plastic superposition is, of course, dependent on the sophistication in the original monotonic solutions. Dixon applied the analysis to plane stress strain hardening as well as to the perfectly plastic case by assuming that the stress and distribution in the plastic zone can be obtained directly from the elastic solutions for sharp crack. For example, he gave the strain component ε_x (referring to Figure 2 for the designation of the strain components) for the loading part of the cycle as

$$\varepsilon_x = (E/E_s)^{1/2}\ \varepsilon_{xo} \tag{49}$$

---

*This part of the discussion is based entirely on Rice (1967).

and the strain increment $\Delta\varepsilon_x$ for unloading as

$$\Delta\varepsilon_x = (E/E'_s)^{1/2} \Delta\varepsilon_{xo} \tag{50}$$

where the secant moduli E_s and E'_s are obtained from the effective stress/strain curve of the material as a function of the effective (Von Mises) stress and effective stress increment. Also ε_{xo}, $\Delta\varepsilon_{xo}$ are the strains and strain increments computed from the linear elastic solution. For loading and unloading, appropriate (loading and unloading) stress-strain curves should be used to obtain E_s and E'_s, respectively. A suitable modification was proposed for nonwork hardening, elastic-perfectly plastic materials.

A more sophisticated approach would be to modify for the cyclic loading the small-scale cyclic yielding, monotonic solutions of Rice and Hutchinson for elastoplastic analysis, including the effect of strain hardening as discussed in the first part of this report. In particular, since the crack opening displacement (COD) δ_t is an important parameter, the approach based on Rice's monotonic loading solutions may be preferred to the simplified treatment proposed by Dixon, which does not permit direct calculation of the COD.

Several important implications stem from such superposition analyses. The first is that for a given peak stress intensity level $(K_I)_{max}$, the reversed plastic zone size $R^{(c)}$ in cycling from zero to $(K_I)_{max}$ and then back to zero ($\Delta K_I = (K_I)_{max}$) is one-quarter of the corresponding plastic zone size R obtained in the monotonic loading excursion* up to $(K_I)_{max}$. As pointed out by Rice (1967), it also means that the range of small-scale yielding solutions obtained for monotonic loading is doubled for cyclic deformations. If, for example, a certain monotonic small-scale yielding solution is found to be valid up to a certain ratio of remote stress to yield stress, then doubling the yield stress, in effect, doubles the range of usefulness of monotonic solutions for the cyclic loading. It should be repeated however that Hahn's limited experimental observations on Fe-3Si steel do not seem

*This follows, for example, from Equation (17) by substituting $2\sigma_o$ for σ_o.

to bear out the idea that the reversed plastic zone is only one-quarter of the monotonic zone; in fact the two zones appeared to be nearly the same. This by itself does not necessarily invalidate the plastic superposition analysis since the question of appropriate yield stress to use in the cyclically work-hardened material near the crack tip has not been resolved. In any event, doubling the static yield stress also leads to the residual COD $\delta_t^{(c)}$ (and compressive residual strains) at the crack tip of one-half the maximum displacement after the load has been reduced to zero.* Finally, the analysis indicates that the cyclic stress/strain *fluctuations*, cyclic plastic zone size, and displacements depend *only*** on the load *fluctuations* and are independent of the maximum load.

Figure 42 presents a concise summary of some of the *gross* features of plane strain plasticity in small-scale yielding near monotonically and cyclically loaded stationary cracks. The summary is based on the idea of plastic superposition discussed in this section, on theoretical work on monotonic loading, and on the Hahn etching studies. Note that (1) the cyclic yield stress σ_c is substituted for the static yield stress $\sigma_o^{(c)}$ in the cyclic zone descriptions and (2) according to Hahn's studies, (R_{max}) cyclic $\approx (R_{max})$ static.

To summarize the limitations of the above analyses, we emphasize that a simplified (history independent) plasticity theory has been used and that both crack blunting under cyclic loading and crack closure effects have been neglected. In principle, existing finite element computer programs which utilize incremental plasticity theory developed for the monotonic loading problems could also be applied to load reversal problems (provided that the crack closure does not occur); however, the running time may be considerable. More important, the effect of crack blunting and finite strains and displacements near the crack tip should be studied. As

---

*This follows, for example, from Equation (18) by substituting $2\sigma_o$ for σ_o.

**However, Rice's approximate calculations indicate that when crack blunting due to high load *is* taken into account, the strain range ahead of the crack under subsequent low load cycling is reduced. This may bear on the crack delays in sequence loading discussed earlier.

discussed in connection with the monotonic loading analysis, crack blunting has a very important effect on the strain distribution in the immediate vicinity of the crack tip. In cyclic loading, the effect of crack retardation (or acceleration) following the change of the maximum loading is thought to stem largely from this effect. Further, the effect of partial crack closure on the stress distribution should be studied. The possibility of incomplete crack closure has been mentioned as a possible explanation for the effect of the compressive portion of the loading cycle on the crack growth, at least for some materials under fully reversed loading. Finally, there is a need to utilize cyclic rather than static stress-strain relations* in the computations in order to account for the hardening or softening of the material which occurs ahead of the crack tip as a result of cyclic deformation.

Crack Propagation Laws

Many theories of fatigue growth have been proposed in recent years. The recent literature also contains several excellent reviews of this field, namely, the papers by Paris and Erdogan (1963), Rice (1967), Erdogan (1968), and Pelloux (1969).

As observed by Paris and Erdogan, many of the proposed laws which were claimed to have been verified by experimental observations do not fit a broad range of data. In fact, Paris and Erdogan have shown that several quite dissimilar laws can be made to agree with the same test data although only over a limited range.

A general theory of fatigue crack growth which would take into account all of the factors and experimental observations discussed earlier is not yet available. Furthermore, not even a simplified elastic-plastic stress analysis under load reversal, discussed in the previous section, appears to be an essential part of the development of most of the proposed theories. In general, as was pointed out by Pelloux, the current theories

---

*Such equations could take the form (Tomkins, 1968) $\Delta\sigma = k\,\Delta\varepsilon_p^{\alpha}$ where $\Delta\sigma$ and $\Delta\varepsilon_p$ are the stress range and plastic strain range, respectively, and k, α are the material constants to be determined from the stable hysteresis loops previously discussed in connection with the crack initiation aspects.

may be divided into four groups: (1) semiempirical laws, (2) theoretical laws based on the kinematic concept of crack opening displacement (COD) translated into fatigue extension, (3) theoretical laws based on the concept of (plastic strain) damage accumulation ahead of the crack tip, and (4) laws derived from the dimensional analysis.

In what follows we will discuss some of the main features of these laws, starting with the semiempirical type, which presently enjoy the widest application.

Semiempirical Laws. Here the attempt is to correlate a range of experimental data by means of some fundamental parameter reflecting the applied stress (strain) and crack size and the "material constants." It should be observed that the material constants are selected generally as curve-fitting parameters and do not refer to fundamental material properties as determined for example from static uniaxial tensile tests.*

Presently, such fundamental parameters appear to be the stress intensity factor range which seems to be restricted to the small-scale yielding application and the recently proposed strain intensity factor which is presumably also valid in the large-scale yielding range. Let us now examine both of these concepts in some detail.

Stress Intensity Factor Correlation. The earliest example of a semiempirical law expressing the relation between the crack growth rate (a is the current crack depth and N the number of cycles) and the range in the stress intensity factor ΔK_I is the formula proposed by Paris (1964) in the form

$$\frac{da}{dN} = C(\Delta K_I)^m \; ; \text{ where } \Delta K_I = (K_I)_{max} - (K_I)_{min} \qquad (51)$$

For through cracks, the surface crack length (2c) is used in lieu of depth a in the above equation.

---

*In fact, as pointed out, for example by Hahn et al., Dec. 1969, these curve-fitting parameters may depend on the stress range, the material, the test environment, and the exact details of the testing procedure.

Most of the current data on the material characterization with respect to fatigue crack growth (in terms of depth or surface length) is presently obtained by cycling in tension between $(K_I)_{max}$ and $(K_I)_{min} = 0$ and reported in the above form. Ordinarily, the crack growth in terms of da/dN versus ΔK_I is shown in the log-log coordinates, in which case the exponent m (representing the slope of the curve) and coefficient C are selected as curve-fitting constants.

The usefulness of the ΔK_I correlation between various laboratory specimens and the full-scale structures has been amply documented.* However, some of the limitations of Equation (51) should also be recognized. Apart from restriction to the small-scale yielding range, they concern the transitional effects discussed earlier, the maximum stress effect and uncertainty in the application to the tension-compression loading cycle.

Let us begin with the discussion of the transitional effects which preclude the use of a *single* power law relation represented by Equation (51) to describe the full range of crack propagation rates, ranging from extremely slow rates (say 10^{-8} in./cycle) to fast rates (say 10^{-3} in./cycle). A general qualitative description of the transitional effects has already been mentioned in connection with the discussion of the experimental observations. Specifically, with reference to the applicability of Equation (51), it should be noted that its applicability is confined to the central regions within the upper and lower inflection points** of Figure 43. Furthermore, even within this central region, Hahn et al. (December 1969) claim that on the basis of their recent assessment of the crack growth data on a wide variety of materials *two* power laws yielding two different values of the exponent m should be used. The two regimes are shown schematically in Figure 44, which also defines the symbols used to characterize the transitions. Table 2 from Hahn et al. provides a useful

---

*See, for example, Tiffany and Masters, 1969.

**The lower inflection point is associated with the approach to the threshold stress intensity factor and the upper inflection point with the approach to crack instability. This curve is taken from Crooker and Lange (1969) based on the summary of recent work as reported by Paris and Wei (1969) and Johnson (1969).

summary of both the cyclic growth data for a wide variety of steels and the source from which the data was compiled. We note that in Regime No. 1 the value of the coefficient m is approximately 2, whereas the high growth in Regime No. 2 is associated with an m value generally exceeding 4. The compilation is mainly for growth in air (except as noted) under zero to maximum tension loading. The coefficient C for Regime No. 1 turns out to be approximately $8/(E)^2$. The corresponding value for Regime 2 is not given by Hahn et al., and the original sources listed in Table 2 must be consulted to obtain this information.

The effect of maximum stress, which increases the growth rate for the same value of the range ΔK_I, has been incorporated in the equations proposed by both Forman et al. (1967) and Roberts and Erdogan (1965). Both equations have been observed (Hudson, 1969 and Crooker and Lange, 1968) to reduce the scatter observed in the experimental data when Equation (51) is used. In addition, Forman's equation includes the feature of asymptotic approach to instability associated with the approach to the critical crack size, thus reproducing the trend of the upper* portion of the curve shown in Figure 43; because of this feature, it may be conceptually preferred to the equation of Roberts and Erdogan. Forman's equation is given in the form

$$\frac{da}{dN} = \frac{C_1 (\Delta K_I)^{m_1}}{(1-\bar{R})K_c - \Delta K_I} \tag{52}$$

*We shall note later in connection with the discussion on environmental effects that Forman's equations can also be modified to account for the lower portion of the curve, i.e., the approach to the threshold value.

where a is the current* crack depth, K_c is the critical stress intensity factor, and

$$\bar{R} = (K_I)_{min}/(K_I)_{max} = \frac{(K_I)_{min}}{(K_I)_{min} + \Delta K_I} \tag{53}$$

The curve fitting parameters C_1 and m_1 are generally different from C and m of Equation (51) and must be obtained by experimental procedures in which K_c and $\bar{R}$ are known. So far only the values have been reported for 7075-T6, 2024-T3 aluminum alloys (Forman et al., 1967) and 9Ni-4Co-0.25C steel (Crooker and Lange, 1968). In principle, C_1 and m_1 should be *independent* of $\bar{R}$ ratio and thus obtainable by testing at a single $\bar{R}$ level.** That this is indeed the case at least for some materials under specific loading conditions may best be illustrated by referring to recent work of Hartman and Schijve (1970). In addition, the above work also points out instances under specific environmental and testing frequency conditions where the Forman equation *cannot* be made to fit the data (as well as the possibility of incorporating the feature of the threshold ΔK_e value into the equation).

We shall defer the latter aspects of the problem until the section on the environmental effects and confine ourselves for the present to the case where good correlation with the data was obtained by Hartman and Schijve, 1970 on 7075-T6 clad aluminum sheets tested in dry air at fairly high frequency (approximately 3400 cycles/min). (The previous specimen configuration and stress cycle definitions are shown in Figures 45a and 45b, respectively.) The data are plotted in Figure 45 on log-log scale first in terms of 1/2 d(2c)/dN versus ΔK_I. We note that the straight line relationship predicted by Equation (51) is not observed; there is a distinct layering of the data with higher growth rates associated with higher $\bar{R}$ ratios. Figure 45c shows the same data replotted on log-log scale now using $[1/2\ d(2c)/dN]\ [(1-\bar{R})K_c - \Delta K_I]$ as an ordinate and ΔK_I as abscissa.* Now as predicted by Equation (52), the data for various R ratios does fall close to the straight line relationship.

---

*If the crack extension within a particular load cycle is sufficiently small, $\bar{R}$ may be expressed equivalently in terms of the ratio of the minimum to the maximum stress of the cycle as utilized on page 90 and in Equation (73) given later.

**This would permit the use of the existing data for $\bar{R} = 0$ together with the knowledge of K_c to establish values of C_1 and m_1.

associated with higher $\bar{R}$ ratios. Figure 45 shows the same data replotted on log-log scale now using $[1/2\ d(2c)/dN]\ [(1-\bar{R})K_c - \Delta K_I]$ as an ordinate and ΔK_I as abscissa.* Now as predicted by Equation (52), the data for various $\bar{R}$ ratios does fall close to the straight line relationship.

The uncertainty in the use of a ΔK_I correlation with respect to the tension-compression cycle has already been discussed to some extent in connection with the experimental observations. Specifically, with respect to application of Equation (52), it remains an open question as to what extent ΔK_I should include the compressive portion of the cycle, which in the case of the fully reversed loading ($\bar{R} = -1$) would make the load range twice the maximum load. Here, an inconsistency in resolving this question appears among various investigators. Thus by comparing his equation with the experimental data of Illg and McEvily, Forman did use the compressive portion of the cycle (negative R values); whereas in contrast Hudson (1969) and Crooker and Lange (1968) neglected the compressive portion in analyzing their results. Until this problem is satisfactorily resolved, it may be in the interest of conservative design (although probably excessively conservative) to include the compressive range in the calculation of da/dN according to the Forman equation. When $\bar{R} \leq 0$, it can be shown that the ratio υ between the predicted crack propagation rates calculated with and without the compressive portion of the cycle is $(1 - \bar{R})^{m_1-1}$. The largest discrepancy occurs for fully reversed loading ($\bar{R} = -1$) in which case $\upsilon = 2^{m_1-1}$.

If the effect of the compressive part of the cycling, considered to be fully effective, is interpreted in terms of Equation (51) where the mean load effect is not explicitly considered, then $\upsilon = (1-\bar{R})^m$. In this case for the fully reversed loading, the growth rates obtained for zero to tension loading would have to be multiplied by the factor of 2^m (or thus by a factor of 16 for the value of m = 4) to yield the growth rates for fully reversed loading. This turns out to be an excessively conservative estimate on the basis of the previously mentioned test results obtained by

---

*For this sheet thickness, $K_c = 149\ \text{kg-mm}^{-3/2}$.

Crooker (1971). The data shown in Figure 40 are replotted in Figure 46 in terms of the crack growth rate versus ΔK_I correlation for $\bar{R} = 0$ and $\bar{R} = -1$. On the basis of this plot and similar plots for other materials tested in their study, Crooker and Lange recommend that in applying Equation (51) to the design situations of fully reversed tension-compression cycling, only the tensile portion be used in calculating ΔK_I but that the crack growth laboratory data obtained under the conditions of zero-tension loading be increased by 50 percent to compensate for the effect of the compressive loading.

Strain Intensity Factor Correlation. We have observed in the previous discussion of the monotonic loading that the elastic stress intensity factor no longer characterizes plastic deformation in the vicinity of the crack tip when the applied stress is in the large-scale yielding range. In the discussion of the simplified elastic-plastic stress distribution under load reversal, we mentioned that the region of applicability of the ΔK_I concept for *cyclic* plasticity may be higher* although the evidence is presently insufficient to fully support such a conclusion pending more precise analytical and experimental work. In any event, a recent study by McEvily (1969) demonstrated that at least for one material (OHFC copper), the stress intensity factor correlation is no longer feasible when the net section stresses exceed the yield stress. An approach to be described below was suggested to cope with the problem of meaningful correlation parameter to replace ΔK_I in the large-scale yielding range.

*We recall that this results from the doubling of the static yield stress.

McEvily's attempt to correlate crack propagation data obtained for unnotched cylindrical specimens tested under controlled net section strain range* (full reversal with zero mean strain) with data obtained on centrally notched sheets under fully reversed stress gave a specific impetus to the development of the strain intensity factor concept.

Several important conclusions were reached. First, at high stress levels the rate of growth was no longer a single-valued function of the stress intensity factor (the rate also depended on the applied stress level). Second, at the above stress levels, correlation could not be obtained between cylindrical and plate data in terms of the stress intensity factor. This led to the proposal that the data be correlated by means of the strain intensity factor $\hat{K}_\varepsilon$ expressed as

$$\hat{K}_\varepsilon = \Delta \varepsilon_T \sqrt{a} \tag{54}$$

where $\Delta \varepsilon_T$ is the total (applied) strain range and a is the crack depth for edge notched specimen and half-crack length for centrally notched plate. For a given applied stress range, the total strain range was obtained by adding the elastic strain range component (obtained by dividing the applied stress range by Young's modulus) to the plastic strain range obtained from the cyclic stress-strain curves for a given applied net section stress range. It was then found that the apparently dissimilar data from the two specimens could be correlated in terms of the strain intensity factor.

Furthermore, by plotting the entire range of data obtained by testing specimens (from low to high stress levels) in terms of the strain intensity factor, a transition was observed from growth dependence on the

---

*Earlier work utilizing the applied strain range as a controlling parameter in low-cycle fatigue crack propagation is contained in the papers of Manson (1965) and Crooker and Lange (1967). Manson proposed a form $d(2c)/dN = \beta_1(\Delta \varepsilon_p \sqrt{c})^s$, where 2c is the crack *length* and, β_1 and s are material constants, and $\Delta \varepsilon_p$ is the applied plastic strain range. In the special case when s = 1, the integration of this equation reduces to the Manson-Coffin law expressed in Equation (41). Crooker and Lange proposed a similar form $d(2c)/dN = \beta_2(\Delta \varepsilon_T)^{\alpha_1}$, where $\Delta \varepsilon_T$ is the *total* strain range and β_2, α_1 are the material constants.

fifth power of the strain intensity factor when the net section strains are in the elastic range to the second power dependence when net section strains are in the plastic range.

Although the McEvily approach does seem to offer a convenient correlation method to be used in the plastic range, its validity for other materials and configurations must be demonstrated.* Specifically, the use of the same formula for the strain intensity factor for the two different configurations represented by plates with central cracks and cracked cylindrical specimens deserves closer examination.**

Theoretical Models Based on Crack Opening Displacement (COD). Crack propagation equations in this category are based on the idea that the crack extension occurs solely as a result of irreversible plastic flow at the crack tip. Such mechanisms of crack growth were postulated by McClintock (1963), Laird (1967), McClintock and Pelloux (1968), and Pelloux (1969). Specifically, Laird's model, which also attempts to account for the striation spacing, envisions the growth as occurring as a result of the plastic blunting process shown in Figure 47 and described as follows.

Initially, as a small tensile load is applied to the cracked specimen, slip zones of intensive plastic deformation at the crack tip occur at 45 deg to the plane of the crack.*** When the maximum tensile load is

---

*The author claims that it can also be used instead of K_I in the elastic range. In the elastic range, the strain concentration factor for centrally notched plate is obtained by dividing the stress intensity factor by $E\sqrt{\pi}$. This procedure permits a first order correlation of growth data for the same alloys of differing Young's moduli.

**We note that in contrast to the strain concentration factor K_ε introduced in Equation (20) for hardening materials, $\hat{K}_\varepsilon$ is not obtained from the actual analytical solution for the strain distribution near the crack tip but is instead defined somewhat arbitrarily by Equation (54).

***Although, in fact, analytical and numerical plane strain yielding solutions lead to diffuse plastic zones (as shown for example in Figure 16), Rice (1967) feels that the discrete yielding slip lines at 45 deg to the sharp crack can be used to model the *gross* features of plastic flow.

reached, the crack blunts to a semicircular shape. Application of compressive loading (load reversal) forces part of the newly formed circular surface into the plane of the crack. Partial buckling at this surface also occurs and results in the formation of another notch configuration similar to the appearance of the original crack tip. In fact, such a plastic blunting* process was observed by McEvily et al. (1963) in polymer specimens which exhibit considerable ductility.

Theoretical equations based on the basic idea of crack tip displacement mechanism were developed among others by McClintock (1963), Frost and Dixon (1967), McClintock and Pelloux (1968), Tomkins (1968), and Weertman (1969). Probably the most general formulation is that by McClintock since it can be used in either the large- or the small-scale yielding range.** He suggested that crack growth be related to the cyclic crack opening displacement $\delta_t^{(c)}$ by the proportionality constant ω (smaller than unity) in the form

$$\frac{da}{dN} = \omega \, \delta_t^{(c)} \tag{55}$$

Let us now examine some specific forms which Equation (55) may take for small-scale and large-scale yielding ranges.

Small-Scale Yielding. Here $\delta_t^{(c)}$ may be expressed as a function of the square of the stress intensity factor. For the particular case of plane strain yielding (Von Mises criterion) for *monotonic* loading, Equation (18) yields

$$\delta_t = 0.613 \frac{(K_I)^2}{\sigma_o E} \tag{56}$$

---

*A somewhat simpler mechanism which can proceed in the absence of striations was proposed by McClintock and Pelloux (1968). They envision the crack as remaining sharp and propagating as a result of irreversible COD due to alternating shear flow at the crack tip. This model can account for the absence of striations observed in some tests. The crack advance per cycle is equal to one-half of the crack opening displacement.

**See discussion in the Appendix of the paper by Laird (1967).

Now we recall from our previous discussion of plastic superposition under load reversal that for the change of the stress intensity factor ΔK_I, the cyclic crack opening displacements $\delta_t^{(c)}$ may be obtained from Equation (56) in the form

$$\delta_t^{(c)} = 0.613 \frac{(\Delta K_I)^2}{2 \sigma_o E} \tag{57}$$

This leads to

$$\frac{da}{dN} \approx \omega \frac{(\Delta K_I)^2}{4 \sigma_o E} \tag{58}$$

We noted earlier that Hahn et al. (December 1969) objected to identifying σ_o with the static yield stress and argue that the cyclic yield stress $\sigma_o^{(c)}$ appropriate to the intensely strained region near the crack tip be used as shown in Figure 40.* They assumed that $\sigma_o^{(c)} = 2 \sigma_o$ and then by comparing Equation (58) to a wide range of experimental data, found that ω varies from approximately unity to about 0.2. McClintock found, by using a simplified expression for $\delta_t^{(c)}$ (assuming the applicability of Mode III formula) and $\sigma_o^{(c)} = \sigma_o$, $\omega = 1/2$, that Equation (55) correlated reasonably well with the observed striation spacings for 7178 aluminum alloy (as indicated in his discussion of the Laird paper).

In conclusion it should be mentioned that the above dependence of the crack propagation rate on the square of the stress intensity factor does correlate approximately with the experimental findings reported for Regime No. 1 (see Figure 44) and is thus in general accord with the semi-empirical laws in that range.

Large-Scale Yielding. In this domain (net section stresses may approach yield), we have noted that the monotonic small-scale yielding

---

*It was also suggested that the cyclic yield stress near the crack tip for all materials approaches a common level $\sigma_o^{(c)} = \frac{E}{100}$ and that this might explain the relative insensitivity of crack propagation in Regime No. 1 (Figure 44) to static yield stress.

solutions generally underestimate the crack opening displacement.* For the case of fatigue loading, work by Rooke and Bradshaw (1969) indicated that the COD was proportional to the fourth** power of the stress intensity factor (in contrast to the second power dependence predicted by small-scale yielding solutions). Such observation does correlate with the value of m changing from 2 to generally at least 4 in going from the low to high stress regimes of Figure 44.

We recall from our discussion of the monotonic loading that an estimate of the COD in the large-scale yielding ranges may be obtained by using the Rice path independent J integral instead of K_I in the appropriate formulas, although presently the accuracy of such an approach would be questionable if applied to fatigue loading.

Theoretical Models Based on "Damage Accumulation." Crack propagation theories based on some variant of fatigue damage accumulation were proposed among others by Head (1953), McClintock (1963), Krafft (1971), Lehr and Liu (1969), and Fleck and Anderson (1969). The basic mechanism is envisioned as stable crack growth controlled by localized rupture *ahead* of the crack tip. In such an idealization, the possibility is ignored that secondary growth may start from nucleated cracks and extend toward the main crack. As commonly described, the process based on rupture occurring *ahead* of the crack tip is idealized as follows.

A typical fatigue element (which may have a finite microstructural dimension rather than being simply a point) is postulated at some distance r rupture at*** or ahead of the crack tip, but within the zone of reversed plasticity $R^{(c)}$. As the crack extends, the element experiences increasing amplitudes of plastic strain. In a sense, the plastic strain being accumulated within the element is analogous to the damage stored within a smooth laboratory specimen subjected to controlled strain cycling. However, in contrast to the conventional laboratory strain range specimen, the above

---

*Note for example Figure 23.

**Their work is also discussed by McEvily (1969) in terms of the connection of COD to the strain intensity factor.

***This pertains to the model proposed by Krafft (1971) based on the notion of tensile instability of a ligament having a process zone diameter d_T, the growth per cycle being equal to the process zone diameter.

fatigue element experiences a given strain range only during one cycle, since the crack is assumed to be propagating continuously. Thus the strain range increases due to both the decreasing distance of the element from the crack tip and to the increasing stress intensity factor resulting from the larger crack. Fatigue failue within the element ensues when the accumulated plastic strain reaches a saturation point. The saturation point is determined by using the fatigue data obtained from constant strain range of smooth laboratory specimens in conjunction with some cumulative damage theory to account for the variable amplitude strain cycling of the element. The number of cycles which an element may thus tolerate is, in turn, related to the crack propagation rate, which then determines the number of cycles required for the main crack front to reach the element.

As may be expected, the above model is more difficult to translate into mathematical terms than is the case for the COD model; the latter requires essentially only the computation of the cyclic COD. Specifically, the development of the crack propagation equations implementing the damage concept requires:

1. An exact solution for the cyclic plastic zone and the plastic strain range ahead of the advancing crack. The crack blunting effect which produces, under cyclic loading, a zone of length $R^{(c)}$ with intense deformation should also be considered (see Figure 42).
2. Cyclic stress-strain relations of the material.
3. Localized fracture criterion expressing fatigue life of the conceptual element in terms of the number of cycles of constant amplitude plastic strain superimposed on a given mean plastic strain.
4. Cumulative damage rule expressing the relationship between the failure (crack initiation) under constant and variable amplitude cycling.

The above outline lists ideal requirements which are not completely within the scope of current analytical capabilities. For this reason, current crack propagation laws based on the damage concept employ various

assumptions and approximations. Thus, when confronted with the discrepancy between predicted and observed crack growth, it is difficult to decide whether the discrepancies stem from the inadequacy of the basic concept or from the oversimplifications with respect to any of the above features required for implementation.

Let us now briefly review some common forms of such crack propagation laws and indicate where some of the important assumptions have been made.*

First, let us consider McClintock's equation as modified by Pelloux (1969) in the form

$$\frac{da}{dN} = \frac{7.5}{16} \frac{(\Delta K_I)^4}{\varepsilon_f E^2 \sigma_o \rho_m} \tag{59}$$

where ρ_m is a characteristic microstructural dimension representing the inclusion spacing and ε_f is the true fracture strain obtained from conventional static tensile tests. Two main assumptions are as follows:

1. The plastic strain amplitude ε_p at some distance from the crack tip was expressed as a function of the static yield strain and the plastic zone size in turn based on the small-scale yielding solution for Mode III under monotonic loading. The solution was assumed to be applicable to the Mode I and the conversion to *cyclic* plasticity was made by doubling the *static* yield stress σ_o in accord with the idea of plastic superposition discussed earlier.

2. The fatigue failure criterion was assumed to be given by the Manson-Coffin law (see Equation (41)) rewritten in the form

$$N^{1/2} \varepsilon_p = \varepsilon_f/2 \tag{60}$$

---

*With the exception of some features of the derivation by Hahn et al. (December 1969) to be discussed later, the crack propagation laws that follow are based on sharp crack solutions, i.e., blunting effects are neglected.

In the application of Equation (60) to variable amplitude cycling, fracture ahead of the crack was assumed to have occurred in N cycles when an accumulated plastic strain ε_p averaged over a microstructural region of size ρ_m satisfied an assumed cumulative damage rule

$$\int_o^N 4 \left(\frac{\varepsilon_p}{\varepsilon_f}\right) dn = 1 \tag{61}$$

Recently, Lehr and Liu (1969) proposed the forms*

$$\frac{da}{dN} = \left(\frac{D^{0.6}}{\varepsilon_o^{(c)}}\right)^{1/\bar{z}} \frac{\bar{R}^{(c)}}{1-\bar{\beta}/\bar{z}} \quad \text{for } (1-\bar{\beta}/\bar{z}) > 0 \tag{62}$$

and

$$\frac{da}{dN} = \left(\frac{D^{0.6}}{\varepsilon_o^{(c)}}\right)^{1/2} \sum_{i=1}^{\bar{n}} \left(\frac{r_i}{R^{(c)}}\right)^{-\bar{\beta}/\bar{z}} \Delta r_i \tag{63}$$

$$\text{for } (1-\bar{\beta}/\bar{z}) \leq 0$$

The meaning of various terms in Equations (62) and (63) may best be explained by discussing basic simplifications introduced in the derivation, mainly with respect to *a priori* assumption of both the cyclic strain distribution ahead of the crack and the localized fracture criterion. They are as follows:

---

*More complex expressions derived along similar lines were quite recently obtained by Fleck and Anderson (1969). The equations contain dependence of crack extension on the maximum stress intensity factor, stress intensity factor range, fracture toughness K_c, and tensile and cyclic material properties.

1. Cyclic plastic strain amplitude ε_p at a distance r from the crack tip was *assumed* to be given by

$$\varepsilon_p/\varepsilon_o^{(c)} = (r/R^{(c)})^{\bar{\beta}} \tag{64}$$

where $R^{(c)}$ is the plastic zone width, $\varepsilon_o^{(c)}$ is the yield strain obtained from *cyclic* stress-strain properties, and $\bar{\beta}$ is a negative constant characterizing the singularity of the strain distribution. The choice for the numerical values of $\bar{\beta}$ was apparently guided by the results of the finite element solution obtained by Swedlow et al. (1965) for monotonic loading. It showed that $\bar{\beta}$ was -1/2 for a σ/σ_o ratio not exceeding 0.2 (applied stress to yield stress ratio) and decreased to about -0.7 for a σ/σ_o ratio of approximately 0.8. We recall from our discussion of monotonic elastic and strain-hardening solutions that $\bar{\beta}$ should be -1/2 for the perfectly elastic case and should approach -1 for the perfectly plastic case.

2. The fracture criterion for constant strain range was taken to be the Manson-Coffin law (Equation (41)), which defines the material constants D and $\bar{z}$. Miner's law with its inherent simplifications (to be explained later in connection with the cumulative damage theories) was utilized to account for the cumulative damaged absorbed in each increment Δr_i of the crack advance through the cyclic plastic zone of length $R^{(c)}$ with $\bar{n} = R^{(c)}/\Delta r_i$ as the total number of such increments.

Let us now examine some of the general implications of Equations (62) and (63). First, we note that the static test ductility as measured by D and the cyclic yield strain $\varepsilon_o^{(c)}$ are included. Second, the dependence of $\frac{da}{dN}$ on ΔK_I as implied by Equation (62) is of interest. In the case where the ratio σ/σ_o is small, $\bar{\beta} \approx -1/2$ and, utilizing $\bar{z} = -0.6$ as a fairly representative value, we note that Equation (62) becomes applicable. In such a case, the growth rate becomes proportional to ΔK_I^2.

On the other hand, as the applied stress increases $\bar{\beta} \to -1$--Equation (63) becomes applicable, and now the growth rate (through the dependence on $\bar{\beta}/z$ exponent of the plastic zone size) may depend on at least the third power of the stress intensity factor. We should recall, however, that analytical solutions for the coefficient of strain singularity yield $\bar{\beta} = -1$ for elastic perfectly plastic material regardless of the stress

level, and this would in turn imply that Equation (63) rather than Equation (62) should always be used (with $\bar{z} = -0.6$) for nonhardening materials. When applied to 7075-T6-Al, 2024-T4-Al, AM250 stainless steel, and 18Ni(300) maraging steel, the use of simplified Equation (62) yielded an unconservative prediction when compared with the experimental data.

We conclude the discussion of crack propagation laws based on the damage concept by presenting simplified expressions derived by Hahn et al. (December 1969). Assuming that the crack extension rate is constant while the crack is propagating through the plastic zone and utilizing the expressions of Figure 42, we obtain the number of cycles of plastic straining experienced by the material ahead of the crack as:

$$\eta = \frac{R^{(c)}}{\frac{da}{dN}} \approx \frac{0.03\ (\Delta K_I)^2}{\left(\frac{da}{dN}\right) 4\left(\sigma_o^{(c)}\right)^2} \tag{64}$$

and

$$\eta' = \frac{R'^{(c)}}{\frac{da}{dN}} \approx \frac{(\Delta K_I)^2}{\left(\frac{da}{dN}\right) 4E\ \sigma_o^{(c)}} \tag{65}$$

where η is the number of cycles of plastic strain (assuming that the critical fatigue element is located just at the outer edge of the plastic zone) and η' is the number of cycles of large plastic strains (assuming that the critical fatigue element is located just at the edge of a heavily strained region). Now, rewriting the Manson-Coffin law of Equation (60) in the form

$$N^{1/2}\ \overline{\Delta \varepsilon_p} = \varepsilon_f \tag{66}$$

where $\overline{\Delta \varepsilon_p}$ is now an *average weighted*[*] value of the plastic strain range, we obtain from Equations (64) and (65)

$$\frac{da}{dN} \approx \frac{0.03\ \overline{\Delta \varepsilon_p}\ \Delta K_I^{\,2}}{4\ \varepsilon_f^{\,2} \left(\sigma_o^{(c)}\right)^2} \qquad \text{(small strains)} \qquad (67)$$

$$\frac{da}{dN} \approx \frac{\overline{\Delta \varepsilon_p}^{\,2}\ \Delta K_I^{\,2}}{4\ \varepsilon_f^{\,2}\ E\ \sigma_o^{(c)}} \qquad \text{(large strains)} \qquad (68)$$

For reasons which are not entirely clear, Hahn et al. suggest that $\overline{\Delta \varepsilon_p}$ for the small strain case may be estimated as $\overline{\Delta \varepsilon_p} = 4\ \bar{\sigma}_o^{(c)}/E$ and for the large strain case as $\overline{\Delta \varepsilon_p} \approx 0.5$ (inferred from the Rice and Johnson (1969) crack blunting solution for monotonic loading).

Whether Equation (67) or Equation (68) is more appropriate remains to be determined. However, indirect evidence is provided by approximate calculations of Fleck and Anderson and Lehr and Liu[**] indicates that the greatest amount of damage is accumulated in the immediate vicinity of the crack tip. This would strengthen the case for using Equation (68), which is based on large strain accumulation.

Comparison of COD versus Damage Accumulation Model. General assessment of the relative merits of the two theoretical models seems to be in order insofar as they account for the observed qualitative and

---

[*] This accounts in an approximate fashion for the change of the strain amplitude as the crack advances. In Equation (64), all the cycles required to propagate the crack to the edge of the plastic zone are considered whereas in Equation (65) the damage is assumed to be accumulated only in traversing the large strain region.

[**] Based on the simplified models of sharp crack geometry.

quantitative features of the crack growth. An excellent discussion along these lines is given by Hahn et al. (December 1969). Only the principal features are summarized here.

First, let us consider the low growth Regime No. 1 of Figure 44. Although neither model is entirely satisfactory, the COD mechanism seems to be in better accord with most of the observations (specifically as summarized in Table 2). Thus the observed dependence of growth rate on the second power of the stress intensity factor can be obtained from either model as indicated, for example, in Equations (58) and (67).

Despite the predictions of such equations, the actual insensitivity of the growth rate to the static yield stress may be accounted for by arguing that the cyclic yield stress $\sigma_o^{(c)}$ in the immediate vicinity of the crack tip may be relatively invariant for many materials and may, as indicated earlier, approach a common value ($\sigma_o^{(c)} \approx E/100$). The observed absence of the ductility dependence may similarly be explained by arguing that ε_f should be the ductility as influenced by the complex state of stress (degree of triaxiality) ahead of the crack tip instead of the ductility as measured in smooth bar static tests.* Possibly the strongest argument against the damage theory can be found in our discussion of the lack of load sequence effects in some of the tests by McMillan and Pelloux (1967). When the maximum load was kept constant and only the load amplitude changed, then from the implications of the damage theory one would expect a *gradual* adjustment to the new amplitude; instead, a stable and uniform value of crack propagation, as measured by the striation spacing, was achieved on the very first cycle of the new load amplitude. However, it should be observed that the point in favor of the damage theory may be the observed increase of crack propagation in the presence of hostile environment, which could be rationalized more easily in terms of the effect of environment on ductility rather than on the yield stress and thus on the blunting mechanism.

---

*In this connection, we should recall our discussion on page 56 regarding the effect of triaxiality on ductility.

With respect to the crack propagation under high stress conditions (specifically in Regime No. 2), the actual mechanism is not well defined. McClintock and Pelloux (1964) speculate that some combination of the two mechanisms may be involved. Such a mechanism may be envisioned as including tearing near inclusions and growth of secondary cracks which join with the main crack growing by the regular striation spacing mechanism. Thus, although crack propagation laws based on either the damage (see Equations (63) and (59)) or the COD concepts (see discussion on page 109) may be derived in such a way as to at least predict the growth dependence on the fourth power of the stress intensity factor (in agreement with the general experimental observations in Regime No. 2), their range of applicability is somewhat uncertain. The uncertainty is caused either by the various mathematical simplifications in their derivations or by the fact that the actual fatigue process under high stress conditions may proceed by a more complex mechanism.

Dimensional Analysis Theories. Crack propagation equations derived from the application of dimensional analysis were obtained by Frost and Dugdale (1958), by Rice (1961), and most recently by Yang (1967) and Liu (1961).

Basically, the procedure is to start with a list of variables that may have a bearing on the crack propagation rate. It is essential that *all* the variables be listed, and herein lies the main difficulty of this approach since in the application, quite dissimilar laws may result, depending on which variables are listed and which are omitted.*

As an example, if according to Liu we assume a plane strain case (thus the plate thickness is not a variable) with the maximum stress equal to the stress range ($\sigma_{max} = \Delta\sigma = \sigma_\infty$) and restrict the relevant variables to σ_∞, 2c, σ_o, ε_o, ε_f, n, and da/dN (where σ_o and ε_o are respectively the

*The idea is to seek a functional relationship between the variables by first expressing them in terms of three basic dimensions of force, length, and time. The next step is to obtain relations of the dimensionless combinations of variables. This is done by solving a set of algebraic equations (expressing the equality of powers of basic dimensions on both sides of the equation) for the unknown exponents of the variables.

static yield stress and strain, ε_f is the fracture strain, and n is some measure of strain hardening), then we obtain

$$\frac{d(2c)}{dN} = c\ f_1\ (\sigma_\infty/\sigma_o,\ \varepsilon_o,\ \varepsilon_f,\ n) \tag{69}$$

where f_1 is a dimensionless function of the arguments. Equation (69) expresses linear dependence of the crack propagation rate on the current crack length 2c, which is in accord only with a limited range of experimental data.*

On the other hand, Rice assumes that the dependence of d(2c)/dN on the stress and the current crack length enters solely through the dependence on the stress intensity factor range ΔK but that an *additional* parameter ρ_m characterizing the microstructure** should be included and obtains

$$\frac{d(2c)}{dN} = \frac{\Delta K_I^2}{\sigma_o^2}\ f_2\ [\Delta K_I^2/\rho_m\ \sigma_o^2,\ \varepsilon_o,\ \varepsilon_f,\ n] \tag{70}$$

where now f_2 is a dimensionless function of the variables. Equation (70) may be adjusted to fit a variety of the semi-empirical laws discussed previously.

Finally, Yang obtains the form

$$\frac{da}{dN} = c\ f_3\left[\sigma_\infty/\lambda_1\ ,\ \frac{1}{E}\ ,\ \frac{d\ \sigma_\infty}{dt}\ ,\ \frac{dN}{dt}\right] \tag{71}$$

where f_3 is a dimensionless function of the gross section stress σ_∞, the modulus E, the stress-time derivative $d\ \sigma_\infty/dt$, the test frequency dN/dt, and λ_1, a physically undefined "material constant."

---

*For example Regime No. 1 of Figure 44.

**For example, ρ_m could represent grain size of inclusion spacing.

Clearly, the range of possible laws emerging from the manipulations of the dimensional analysis is quite large, depending on the selection of variables. Such an approach appears to be quite useful for deriving a semiempirical law to fit a given range of experimental observations but not for obtaining a general crack propagation law to fit a broad range of data.

CUMULATIVE DAMAGE ANALYSIS

The previous discussion concerned various aspects of crack initiation and propagation under constant amplitude strain or stress cycling. However, spectrum loading must often be considered in estimating the fatigue life of actual structures. Consequently we are confronted with two intimately related problems, namely (1) modeling and possible simplification of load history in terms of parameters assumed to be significant for the fatigue damage and (2) selection of an appropriate cumulative damage theory in terms of the above parameters.

Although a detailed analysis of various aspects of load history characterization is beyond the scope of this report, some general comments on this problem are appropriate. They will be followed by a short digression into the various measures of fatigue damage with reference to loading sequence effects before taking up the discussion of two alternate analytical approaches to damage analysis. The first approach is based on the cumulative damage theories. Such theories generally attempt to predict only the total life of the structure under spectrum loading based on the information provided by the conventional S-N diagrams (or strain range fatigue life data). The second approach is based on the utilization of crack propagation data and the analysis already discussed in connection with constant amplitude cycling.

Load History Analysis

An essential first step in deciding on the fatigue life estimates for a structure or a structural component is the decision as to the degree of randomness in the anticipated load history. Such a decision should preferably be made on the basis of representative load-history records that are sufficiently detailed to provide the relevant statistical information. Such information is seldom available in practice, particularly for the

submarine hull depth excursions. It would appear at first that the statistical approach is not germane insofar as depth excursions are concerned because operational capabilities and/or restrictions permit the hydrostatic loading to be predicted (at least within a limited time span) in contrast, for example, to the gust or wave loading. On the other hand, when viewed over the entire projected life of the hull, the question does arise as to whether one should not, as a practical matter, view the problem in some statistical sense since the exact sequence of load peaks cannot be readily predicted. One could, of course, take what appears to be a conservative approach and design for some particular number of full depth excursions. However, there are other difficulties in addition to the obvious problem of rationalizing a particular choice of "equivalent" full depth constant amplitude cycles. First, initial residual stress must be considered as well as load-induced stress. Since only approximate bounds can be given, residual stress should probably be characterized as a random variable (which may also be cycle dependent), thus providing additional impetus for placing the problem in the probabilistic context. Second, crack initiation and propagation may depend on the mean as well as on the fluctuating stress, and this may lead to time as well as cyclic dependence of the fatigue damage especially when the environmental effects are taken into account. In any event, it would appear that if crack growth estimates are to be made over a long time span, some estimates of the mean load and some statistical description of fluctuations about the mean would be useful. Let us now consider some methods by which such characterizations may be performed.

Figure 48a shows a hypothetical stress-time history at some structural point of interest (with stress regarded as a random variable). The stress may be considered to be made up of two components: (1) the mean stress which may be estimated or preferably calculated by obtaining the area under the stress-time curve and dividing by the time interval of interest and (2) a fluctuating component which may be considered as a random variable. Characterization of the fluctuating component may then be performed by either the power spectral density (PSD) approach or statistical counting techniques.

The PSD approach utilizes the theory of random processes. The basic ideas as applied to fatigue testing are discussed at length in two papers by Swanson (1968), and the applications to crack propagation analysis are presented in Paris (1964), Rice et al. (1965), and Smith (1965). Essentially, starting from a given stress-time history (as shown in Figure 48a), one can calculate first the mean square and then the root mean square (rms) of stress over a given time interval and express the wave form by means of a frequency decomposition (PSD plot) analogous to harmonic analysis.* Additional important parameters that can be obtained from the original signal (by counting *all* the peaks following mean level crossings) are the irregularity factor R_i, defined as the ratio of mean level crossings with positive slope to peaks (R_i = 1 for constant amplitude cycling), and the clipping ratio, defined as the maximum value of a signal to rms in the interval of interest.

A great deal of valuable statistical information similar to that extracted from the counting techniques (to be discussed later) can also be extracted from PSD analysis. On the other hand, all information on load sequence is lost. This does not necessarily constitute a serious objection to the PSD analysis if the service life is to be considered over a very long time span since the sequence effects can be assumed to average out in such a case. A more serious objection to the PSD approach stems from the fact that cumulative damage theories expressed in the parlance of PSD analysis are presently unavailable. As noted previously, the attempts to correlate crack growth data under random loading with crack growth data under some *single* "equivalent" constant amplitude loading on the basis of

---

*The PSD plot contains all wave form information as well as overall intensity level. Thus frequencies are related to the reciprocal of the curvature of the signal. As an example frequencies f_1, f_2, f_3, shown in Figure 48b are related to the reciprocal of the curvatures of the corresponding portions of the time history plot of the signal in Figure 48a. The overall intensity of the signal is characterized by its mean square (or rms) and is equal to the area under the PSD plot. For a given signal, a PSD analysis (leading to the plot similar to Figure 48b) may be performed in the laboratory using specialized equipment that contains analog filters.

equivalent rms value were not successful.* Nevertheless, if the time under load** is important as well as the magnitude and number of load peaks (or reversals), then an analysis on the basis of continuous loading (such as the PSD history method) may eventually turn out to be preferable to a statistical counting technique which ignores the time scale entirely. Schijve (1961) discussed statistical counting techniques at length and reviewed seven alternate methods. In this technique only the *number* of occurrences is counted based on some rather arbitrary assumptions as to the relative importance of various occurrences. The character of the occurrences may be the peak values, ranges, or crossings of a certain level in positive or negative directions. The results are presented by means of the statistical frequency of occurrence and provide little if any information on the sequence. Figures 49a and 49b are examples of such techniques based on the peak counting methods. Only the maximum peaks above the mean level crossing are counted in Figure 49a. In Figure 49b, variations (i.e., all local peaks) are counted in Figure 49b; however one may decide to neglect a maximum or minimum value preceded or succeeded by a value that differs from it by a specified amount. The simulation of such data for programmed loading commonly assumes that each peak is to be considered as a fictitious "cycle" that passed through zero on either side of the peak. On the other hand, the *differences* between the successive peak values are counted in the range count method shown in Figure 49c. The range is considered to be positive when a minimum is followed by a maximum and negative if the inverse has occurred. Although (in contrast to the previous method) indirect information on the load variations is provided, any information on the absolute magnitude of *peak* loads is lost. If the maximum load does play an important part in the fatigue process, then such a method is clearly unacceptable.*** When such range count method is used

---

*This despite the fact that such correlations were found to be quite good between the crack growth rates under various *random* loading histories with radically different wave forms (Rice et al., 1965).

**See the discussion on environmental effects on page 172.

***This difficulty is avoided by more elaborate counting procedures referred to as the range-mean count (Schijve, 1961).

in attempting to design an "equivalent" programmed loading, each rise or fall (negative r values) is to be considered as a part of complete "cycle."

In conclusion, the merits of a particular counting method or continuous load analysis depend more on decisions regarding the significance of various parameters in fatigue damage than on the sophistication of the statistical analysis. Thus if the stress corrosion effects are felt to be important, then a continuous load history analysis should be attempted because fatigue crack propagation in a hostile environment may depend on the wave form and the loading frequency (and hence on the total time under the load). On the other hand, if the time frame is relatively unimportant and only the number and magnitude of the stress excurions (cycles) are felt to be significant, then a statistical counting technique such as the range or range pair counting method is sufficient. If in addition the peak load effect on the crack propagation is to be considered, then even more elaborate counting techniques would be justified.

Measures of Damage

Before considering cumulative damage theories, some review seems appropriate on just what constitutes fatigue damage, particularly in regard to those aspects that can be observed or defined on the continuum level. Let us consider some of the possible effects of previous cyclic deformation on the subsequent cyclic life in terms of its crack initiation, propagation, and final crack instability phases.*

First, in regard to the crack initiation we would expect to find the relevant information from the strain cycling of smooth specimens where crack propagation is generally only a small portion of the total life. We have already mentioned in the discussion of the crack initiation under constant amplitude strain cycling and in the review of the theoretical crack propagation models based on the damage accumulation that the Manson-Coffin

---

*We prefer to examine fatigue life in terms of its various phases rather than in terms of conventional S-N diagrams. It should be mentioned, however, that from the viewpoint of S-N curves, an additional aspect of prestressing is its effect on the endurance stress which can be either reduced or increased depending on the material (Manson, 1964).

law (Equation (42)) may be viewed as defining the tolerance of the material to irreversible plastic strain accumulation. On the macroscopic level, the damage may also be viewed in terms of the effect of the strain cycling on the yield stress and ductility and may be measured by the cyclic stress-strain diagrams (cyclic strain hardening or softening). On the microscopic level, such cyclic damage may be interpreted as microcrack nucleation and coalescence.

Freudenthal (1969) observed that the actual *mechanism* of damage (prior to appearance of macrocracks) and accumulation depends on cyclic strain amplitude and concluded that the damage produced by strain cycles of different amplitudes cannot be additive. Thus one would expect a possibility of pronounced sequence effects in fatigue life under two-level amplitude straining, and these have, in fact, been observed by Wood and Reimann (1964), who subjected smooth specimens of copper and brass to high and low strain amplitudes of alternating torsion. They found that damage was particularly severe in cases where the high amplitude followed low amplitude cycling (with an amplitude ratio of about 20). On the other hand, Manson's tests (1965) on aluminum and titanium with much smaller amplitude ratios did not show appreciable sequence effects, leading to the speculation that linear addition rules may be sufficiently accurate at least in the case of the consecutive strain cycles of *comparable* order of magnitude.

Second, with respect to crack propagation aspects, an obvious but by no means only criterion of fatigue damage is the current crack size. In addition, the residual stresses at the crack tip, the crack blunting (or sharpening), and the "conditioning" of the material ahead of the crack (including some aspects of the premacrocrack initiation damage discussed above) may be important when the effect of previous cycling history on the current rate of crack growth is to be taken into account. Finally, as discussed previously, cyclic deformation may have an adverse effect on fracture toughness, thus shortening the crack propagation phase and consequently the entire fatigue life.

Cumulative Damage Theories

As might be expected, the development of fatigue damage theories under spectrum loading is handicapped by the lack of completely satisfactory mathematical models of the fatigue process even under constant amplitude stress or strain cycling. Consequently, such theories are generally based on rather abstract theoretical models in which "damage" is not clearly defined in terms of the various physical aspects of the crack initiation, propagation, and terminal crack instability phases discussed previously. Essentially, the attempt is to predict the *total* fatigue life under the conditions of variable amplitude cycling from conventional S-N curves data coupled with some assumptions (to be discussed below) in regard to the way in which damage is accumulated under a constant amplitude cycling and also in regard to the degree of interaction between the various load cycles. Kaechele (1963) gives an excellent review of such theories (until 1963), and so we shall confine ourselves to some general comments before proceeding to discuss alternate approaches based on the notion of separating the crack initiation and crack propagation phases.

Quoting from Kaechele, we may classify the cumulative damage theories (in terms of the assumptions referred to above) as follows:

> "Cumulative-fatigue-damage theories can be *stress-dependent* or *stress-independent*. That is, the amount of fatigue damage produced by a specified fraction of the number of cycles that would produce failure can be the same for all stress amplitudes (stress-independence) or different (stress-dependence).
>
> There can be *interaction* or *interaction-free* theories. The course of damage at one stress amplitude may be changed by applying other stress amplitudes (interaction), or it may be unaffected (interaction-free)."

The simplest theory which is both stress-independent and interaction free was proposed by Miner (1945). It is also occasionally referred to as Palmgren-Miner linear damage accumulation theory due to an earlier independent derivation by Palmgren (1924). The basic assumptions are as follows:

1. At a given applied stress level σ_j, the fatigue damage incurred after n_j cycles is proportional to the cycle ratio n_j/N_j where N_j is the fatigue life at σ_j level (as obtained from the S-N curve data). For Specimens cycled at different stress levels, the amount of fatigue damage (percent of life consumed) is equal if the respective cycle ratios are equal (stress independence).

2. The total damage absorbed in a sequence of stress levels is equal to the sum of damages incurred in each cycle during the sequence (interaction-free). Thus if N is the total number of cycles accumulated in a sequence of k stress levels with a particular stress level σ_j applied during n_j cycles, the failure condition is given by*

$$\sum_{j=1}^{k}\left(\frac{n_j}{N_j}\right) = 1 \quad ; \quad N = \sum_{j=1}^{k} n_j \tag{72}$$

The Miner theory has often been criticized because of drastic simplifications inherent in the above assumptions (to be discussed below). When compared to the experimental results, the sum of the cycle ratios of Equation (72) has often been found to be either greater or smaller than unity (depending on the mean stress, specimen shape, material, load sequence, etc.) thus leading to either conservative or unsafe prediction. Nevertheless, when compared to more elaborate cumulative damage theories reviewed by Kaechele, it does have the advantage of simplicity and--what is equally important--it compares at least as well with the experimental results (Crichlow et al., 1962).

The controversy regarding conditions under which the Miner rule is applicable has not yet been resolved. By means of probabilistic analysis, Saunders (1969) recently claimed that Equation (72) may apply under far more general conditions than expressed in Assumptions 1 or 2 and that, in fact, it predicts *mean* fatigue life under both programmed and random loading spectra when both the stress dependence and cycle interaction effects are taken into account. In any event, although a probabilistic approach has much to commend itself and is in fact being explored in the NSRDC hull

---

*For variable amplitudes *strain* cycling the same formula applies. In fact we have made use of it in the discussion of some of the theories of crack propagation under constant amplitude cycling based on the damage accumulation ahead of the crack tip. When applied to strain cycling, N_j can be obtained from the experimental results on specimens cycled to failure under constant strain amplitude or can be calculated from the Manson-Coffin law (Equation (42)).

reliability program (Lomacky, 1970; Ang and Amin, 1970; and Lomacky et al., 1970) our concern in this report is primarily with the deterministic analysis. It is from this standpoint that the Miner rule will be examined in terms of its plausibility with respect to both the crack initiation and crack propagation phases.

First, in regard to crack initiation, we have mentioned previously that under the loading conditions and for materials utilized by Manson (1965), linear damage accumulation theories may be considered fairly accurate. Specifically, when the cycle ratio summation was performed for the two level fully reversed cyclic strains (smooth bars), it turned out to be close to unity irrespective of the sequence. Nevertheless, Equation (72) may not hold if there is a great difference in cyclic strain amplitudes due to the different mechanisms of damage accumulation associated with high and low strain amplitudes as discussed previously. Second, with respect to crack propagation, it is easy to rationalize why the Miner rule may be suspect if interpreted literally in terms of damage accumulation in the form of crack length. To this end, consider a hypothetical example considered by Manson (1965). Figure 50a shows the plot of relative crack length in cycles obtained under two stress levels acting alone with the life of 100 cycles and a cyclic life of 1000 cycles obtained respectively under high and low stress conditions. The high stress curve OAB must terminate in a shorter crack length than the low stress curve OA'B'C'. Now consider Figure 50b which shows the relative crack lengths replotted as functions of the percentage of fatigue life at each stress level. Thus, a relative crack length of 4 units represents 100 percent of fatigue life for high stress cycling and only 75 percent of life for low stress cycling. Now consider a loading sequence of cycling along curve OAB until 50 percent of life at this stress level is used; this corresponds to the relative crack length of unity to be followed by low stress cycling until failure occurs. Now since the crack length of unity already corresponds to 75 percent of fatigue life at the low stress level, the cycles that can be tolerated following the high load constitute 25 percent of fatigue life at this stress level. Performing the Miner summation as shown in Figure 50b

thus leads to the cycle ratio summation of 0.75. On the other hand, if the low stress level was applied first until the crack of unity was formed, a cycle ratio summation of 1.25 would be obtained.

It would appear from this example that high-low sequence is more damaging than low-high sequence, since in the first case, smaller number of cycles can be tolerated at the second level for a given number of cycles at the first level. However, it must be remembered that, aside from the assumptions of the Miner theory, crack length cannot be regarded as a *sole* criterion of damage and that the blunting of crack tip and creation of favorable compressive residual stresses could actually make the high-low sequence more favorable. In fact, this effect has been observed in two level tests reported by Hardrath and Naumann (1959) and Hardrath (1964).*

To conclude this review of the cumulative damage theories, we should mention that several new theories of cumulative damage have been proposed since the publication of the state of the art survey cited above. Of particular interest is the double linear damage rule recently proposed by Manson et al. (1967). In this approach, fatigue life is recognized as being made up of crack initiation and crack propagation stages and the Miner rule is applied to each phase separately, thus recognizing to some extent the lead sequence effects. In the Manson approach** as well as in other new theories (Sorensen, 1967 and Mattawi, 1969) the emphasis remains on the prediction of fatigue life (or on the duration of initiation *and* propagation phases) rather than on the assessment of residual strength at any time in the loading history. Since, from the fracture mechanics point of view, the residual strength of the structure does depend primarily on

---

*On the other hand, we recall from earlier discussion that no sequence effects were observed in some programmed loading tests conducted by Pelloux. This may be one of the reasons why the Miner theory does, at least in some cases, provide reasonably good estimates of the fatigue life despite the apparent oversimplification.

**So far the Manson method has been applied only to round bars in fully reversed strain cycling and entails the use of semiempirical equations for predicting the duration of crack initiation and propagation phases.

the instantaneous crack length, we shall now discuss some of the approaches to crack propagation analysis under programmed loading.

Crack Propagation under Programmed Loading

We shall conclude this survey of cumulative damage analysis by focusing attention on prediction of crack growth under variable amplitude loading. Here, the attempt is to utilize directly the results obtained for the constant amplitude cycling.

Consider the application of previously discussed crack propagation laws, as for example Equation (52), to the fixed block loading shown in Figure 51. There is a *specified* sequence of blocks in which the stress ratio $\bar{R}$ and the applied stress range $\Delta\sigma_\infty$ (defined in Figure 51) remain fixed in each block. If it is assumed that the crack extension which occurs between each trough and peak value of the stress is small compared to the instantaneous value of the crack length, then $\bar{R}$ as defined in Figure 51 becomes identical with $\bar{R}$ defined in Equation (53), i.e.,

$$\bar{R} = \frac{(\sigma_\infty)_{2p-2}}{(\sigma_\infty)_{2p-2}} \quad \frac{(K_I)_{2p-2}}{(K_I)_{2p-1}} \tag{73}$$

where $(K_I)_{2p-2}$ and $(K_I)_{2p-1}$ are respectively the maximum and the minimum stress intensity levels corresponding to a particular loading cycle N = 2p. Thus given the initial crack length, an expression for calculating K_I, the material constants C_1, m_1, (defined in Equation (52)), and fracture toughness K_c (Equation (52)) may be integrated for each cycle to calculate the crack length following the application of a specific block loading sequence as well as the number of cycles at which crack instability $K_I \rightarrow K_c$ occurs. This approach was followed in the development of computer programs by (Forman et al. (1967), Forman and Hudson (1967) and at NSRDC (reported

informally by DeYoung).* Here the key assumption is that there is no interaction between the stress levels in the sense that the growth rate adjusts itself immediately to the current stress intensity level.

When crack propagation laws and/or experimental data developed for constant amplitude loading are applied to the prediction of crack propagation under service loading, some probabilistic considerations may be involved. We shall consider below two methods which have been proposed for this purpose.

The first approach requires the use of a computer program for block loading analogous to the one described above in conjunction with the idealization of the loading history. The idealization consists of representing the actual loading by S distinct stages; each stage may consist of several constant amplitude stress cycles characterized by different maximum stress and stress ranges. The total number of cycles at a particular stress level k may be determined from the estimated service loading profile by some statistical counting technique. The order of application of each of the stages is then randomized** along with the percent of visitations to a specific k^{th} stress level in each stage until all the cycles in all N stages are used up. This establishes a specific loading profile for which the computer program as described above may be utilized to obtain an estimate of the final crack size. The process is then repeated using different sets of random numbers, thus leading to different sequences (and final crack sizes) until sufficient data are obtained to establish the mean and the standard deviation of the final crack size (Packman et al., 1968).

The second approach (Christensen, 1965) to the estimate of crack growth under random loading makes direct use of the idea of linear damage accumulation and the results from constant amplitude cycling. The load

---

*We do not discuss methods based on attempted correlations between crack growth rates under random loading with growth rates under some *single* "equivalent" constant amplitude loading. As indicated earlier, such an approach was found to be inadequate.

**This can be done by using the table of random numbers.

history is analyzed to establish mean and rms levels and to estimate a probability distribution of the loading peaks. The continuous distribution curve of the peaks is divided into a discrete number of steps, and the proportion of the total cycles (total number of cycles is assumed to be known) at each peak level can then be estimated. Thus, in effect, the actual loading history is replaced by a weighted sum of the constant amplitude cycles. Starting from a given initial crack size, the number of random load cycles required to advance the crack by a given amount is then obtained from the linear superposition of crack growth rates under discrete loading. Thus by setting

n_r = number of random load cycles to propagate a crack from ℓ_o to ℓ_i,

n_s = number of cycles under discrete $\bar{s}$ loading level where $\bar{s}$ = ratio of peak load to rms load, and

$p(\bar{s})$ = probability density function,*

then

$$\frac{1}{n_r} = \int_o^\infty \frac{p(\bar{s})d\bar{s}}{n_s} \tag{74}$$

In the actual application, the above integral may be replaced by a discrete summation of the contributions from each stress cycle within a given stress interval $\Delta \bar{s}_i$. The utilization of this method was shown to lead to a good agreement between the predicted and experimental results on 2024-T3 aluminum although further verification would no doubt be useful. Certainly, the basic idea of utilizing the superposition of constant amplitude growth rates** weighted in some manner to obtain the growth rate under random loading deserves further consideration.

---

*Christensen used the Rayleigh probability density function; however, the basic method should be applicable to other distributions.

**These could be obtained either from the crack propagation equations or from the actual experimental results from constant amplitude cycling as in Christensen.

BIAXIALITY EFFECTS, MODE II AND COMBINED MODE DEFORMATION

As in the case of the biaxial fracture criteria under monotonic loading, the relative importance of applied stress biaxiality for fatigue is not sufficiently understood. Specifically, the choice of an appropriate correlation parameter which would permit extrapolation of uniaxial specimen data to biaxial conditions likely to exist in service is an open question. It is readily acknowledged, for example, that the effects of material anisotropy become extremely important under the conditions of multiaxial fatigue (Christensen and Harmon, 1967), but this effect has not been explicitly recognized in any of the proposed correlation methods. Furthermore, any generalizations on the basis of given fatigue data are complicated by the fact that such data do not always discriminate between crack initiation, crack propagation, and crack instability phases.* Since the dominant mechanisms of the crack initiation phase differ from those of macrocrack growth, it seems doubtful that the same correlating parameter can be applied to both phases. Finally, difficulties in comparing existing uniaxial versus biaxial data are compounded by the fact that the specimen tested under nominally uniaxial applied stress (or strain) is, in fact, frequently subjected to various degrees of strain triaxiality in the vicinity of crack initiation.

In what follows we shall first review some of the most noteworthy aspects of biaxial fatigue on the basis of the apparent relevance of the observed data or proposed characterization methods either to crack initiation or to crack propagation phases.** This will be followed by a discussion of some qualitative features of Mode II and combined mode fatigue growth.

---

*The effect of stress biaxiality on fracture associated with crack instability has been discussed on page 57.

**We admit that the classification along these lines may in some instances appear somewhat arbitrary especially where it has not been used by the original investigators.

Crack Initiation

Since in crack initiation cyclic slip does appear to be an important factor, it appears natural to express the fatigue criteria in terms of some form of effective shear concept. Consequently, the Von Mises formulation, which is associated with the idea of octahedral shear stress, is often employed.* Let us now examine some of the merits of such an approach.

In the simplest situation where the shakedown strain range is known to be entirely elastic, Von Mises formulation may be expected to yield reasonably good correlation between uniaxial and biaxial data. An illustration of such analysis is contained in the work of Mattawi and is concerned with the low cycle fatigue life prediction of rotor blades. The state of stress was biaxial and the stress-strain response followed the curve shown in Figure 52. The plot is presented in terms of the equivalent stresses and strains. Here, equivalent stress σ_e and the equivalent plastic strain $(\varepsilon_e)_p$ are defined in terms of principal stresses σ_1, σ_2 and plastic strain components ε_{1p}, ε_{2p} by the relations

$$\sigma_e = \left(\sigma_1^2 + \sigma_2^2 - \sigma_1 \sigma_2\right)^{1/2}$$
$$\left(\varepsilon_e\right)_p = \frac{2}{\sqrt{3}} \left(\varepsilon_1^2 + \varepsilon_2^2 + \varepsilon_1 \varepsilon_2\right)^{1/2} \tag{75}$$

Total equivalent strain $(\varepsilon_e)_T$ is defined in terms of the total strain components ε_{1T}, ε_{2T}, ε_{3T} or alternatively in terms of equivalent elastic $(\varepsilon_e)_E$ and equivalent plastic strain $(\varepsilon_e)_p$ by means of the formulas

$$(\varepsilon_e)_T = (\varepsilon_e)_E + (\varepsilon_e)_p \tag{76}$$

or

*The American Society of Mechanical Engineers employs an alternative approach based on the *maximum* shear stress (criteria of Section III of the ASME Boiler and Pressure Vessel Code for Nuclear Vessels, ASME, 22, 1964). Here the plane of maximum range of shear stresses is first found on the assumption of elastic behavior; then it is assumed that fatigue life is a function of the mean as well as the range of shear stress on that plane.

$$(\varepsilon_e)_T = 2\left(\varepsilon_{1T}^2 + \varepsilon_{2T}^2 + \varepsilon_{1T}\,\varepsilon_{2T}\right)^{1/2}/\sqrt{3} \tag{77}$$

where

$$(\varepsilon_e)_E = 2(1 + \mu)\,\sigma_e/3E \tag{78}$$

First loading follows the curve 0-0'-1, unloading occurs along 1-2 leading to residual stress σ_R and residual strain σ_R respectively. Subsequent reloading follows loop 1-2-1-2. The cyclic strain range is then entirely elastic and is denoted in Figure 51a by $\Delta(\varepsilon_e)_E$. Corresponding stress range $\Delta\,\sigma_e$ is related to $\Delta(\varepsilon_e)_E$ and the principal stress increments $\Delta\,\sigma_1$, $\Delta\,\sigma_2$ by the formulas

$$\Delta(\varepsilon_e)_E = 2(1 + \mu)\,\frac{\Delta\,\sigma_e}{3E} \tag{79}$$

where

$$\Delta\,\sigma_e = \left(\Delta\,\sigma_1^2 + \Delta\,\sigma_2^2 - \Delta\,\sigma_1\,\Delta\,\sigma_2\right)^{1/2} \tag{80}$$

For a given strain range $\Delta(\varepsilon_e)_E$, the cyclic life N is computed from the expression analogous to Equation (60)

$$N\,(\Delta(\varepsilon_e)_E)^b = (\,2\,\varepsilon_f - 2\,\varepsilon_m)^a/4 \tag{81}$$

where ε_f is the equivalent fracture strain computed from the static test and ε_m is the equivalent mean strain (as defined in Figure 52a). The empirical exponents a, b could in principle be obtained from uniaxial cyclic tests. The proposed experimental relation appeared to be supported by experimental data on SAE 4340 steel alloy and aluminum casting material C355-T61. Mattawi also proposed a cumulative linear damage rule in the form

$$\sum_{i=1}^{k} (\Delta(\varepsilon_e)_E)_i^b \, \eta_i = (2\,\varepsilon_f - 2\,\varepsilon_m)^a/4 \qquad (82)$$

for variable amplitude (consisting of k strain range amplitudes) cycling about constant* mean strain ε_m.

Here η_i is defined as the number of cycles at cyclic strain range $(\Delta(\varepsilon_e)_E)_i$ imposed on a mean strain ε_m. Experimental verification of this equation by performing the Miner summations $\sum_{i=1}^{R} \frac{\eta_i}{N_i}$ (where N_i is the cyclic life at $(\Delta(\varepsilon_e)_E)_i$ strain level) from test results of smooth bars yielded values ranging from 0.56 to 1.37. Such variations for dual-level tests (k = 2) conducted at strain ranges which did not differ very greatly would tend to indicate that the proposed cumulative damage theory is in need of improvement.

The approach outlined above must be modified in a more general case when the plastic strain range needs to be considered. This is likely to be the situation at a notch when the strain range is controlled by the stress cycling of the surrounding elastic media. As an example, consider the strain history represented in Figure 52b. The initial loading proceeds along path 0-0'-1 whereas all subsequent cycling is assumed to follow the hysteresis loop 1-2-3-4-5.** For the sake of conformity with the notation of Figure 52a, we have also expressed the plot in terms of equivalent stress and strains. However, it should be noted that, strictly speaking, the deformation theory of plasticity is no longer valid in view of plastic unloading and subsequent reloading and consequently the term "equivalent" needs to be redefined. This means (accepting the Von Mises yield criterion)

---

*Mattawi also outlined the procedure to be used in strain cycling about a variable tensile mean strain which involves double summation.

**Further discussion of such loops in connection with the problem of crack initiation under the influence of residual tensile stress is shown later in connection with Figure 56.

that although Equations (76) and (75) remain valid, Equation (77) which expresses $(\varepsilon_e)_T$ in terms of total strain components and Equation (78) which expresses $(\varepsilon_e)_E$ in terms of effective stress should be modified to conform with the requirements of the incremental theory of plasticity.* Nevertheless, it is fairly common to compute the "equivalent" total strain range $\Delta\bar{\varepsilon}_T$ by taking the difference in the extreme values of the quantity

$$\bar{\varepsilon}_T = \frac{\sqrt{2}}{3}\left((\varepsilon_{1T} - \varepsilon_{2T})^2 + (\varepsilon_{2T} - \varepsilon_{3T})^2 + (\varepsilon_{3T} - \varepsilon_{1T})^2\right)^{1/2} \qquad (83)$$

on the right-hand side of Equation (83) corresponding to the extremes of the principal strain ε_{1T}, ε_{2T}, and ε_{3T}, assuming that the principal strains reach maximum or minimum values at the same time.

Regardless of which definition of the "equivalent" strain (in terms of total and/or plastic strain components) is eventually used, it is possible,** at least in principle, to obtain a hysteresis loop shown in Figure 52b by first calculating the hysteresis loop for each of the strain components by means of cyclic plasticity analysis.*** The principal remaining difficulty is the proper choice of the fatigue criterion to correlate uniaxial fatigue data with fatigue data under multiaxial conditions with due allowance for the effect of the mean strain. Here the experimental evidence is rather sparse and often contradictory. Thus Pickett and Grigory cite data obtained from the pressure vessel tests to support a correlation based on the use of the equivalent strain as defined above. Ives et al. (1966) also showed reasonable agreement between uniaxial and equibiaxial specimens when correlated on the above basis. On the other hand, evidence presented by Pascoe and deVilliers (1967) casts doubt on the general validity of such an approach.

---

*See, for example, Davis (1963) where the distinction between the deformation and the incremental theory definition of "equivalent" strain is discussed in context of a procedure suitable for numerical integration.

**See footnote on page 84.

***Alternately, the hysteresis loop may be established by experimental methods in terms of applied load versus total strain range.

To overcome the shortcomings of the above methods of correlation, Pascoe and deVilliers suggested that the "equivalent" total strain range* $\Delta\bar{\varepsilon}_T$ should be related to the fatigue life (as defined by the appearance of surface cracks) in the range of 10^2 - 10^4 cycles by means of the expression

$$\Delta\,(\bar{\varepsilon}_e)_T\, N^{\bar{\alpha}} = \bar{C} \tag{84}$$

By performing tests on smooth uniform specimens fabricated from two types of steel (yield stress values of 38 and 100 ksi, respectively) and varying the applied strain biaxiality, they found that the exponent $\bar{\alpha}$ and the coefficient $\bar{C}$ varied according to the state of strain (uniaxial, equibiaxial tension, or equal tension-compression).** Empirical rules were given to calculate $\bar{\alpha},\bar{C}$ from uniaxial tests. The experimental results indicated that for the same value of $\Delta\bar{\varepsilon}_T$ the condition of tensile strain equibiaxiality gave the shortest life.** Although the values of $\bar{\alpha}$ and $\bar{C}$ were approximately equal for the two steels (except when the inclusions were effective in shortening life) further experimental work would be useful to assess the validity of Equation (84) for other steels.

Crack Propagation

Experimental data that bear specifically on the effect of stress biaxiality on crack growth are extremely limited and somewhat contradictory. Nevertheless, existing data tend to support the view that the growth of cracks in Mode I is governed only by the tensile stress normal to the plane of the crack extension, at least as long as the conditions of small-scale yielding prevail. Thus Tiffany et al. (1966) and Crosby et al. (1969) found that growth rate correlated with the range of the stress intensity factor ΔK_I; these investigators did not detect any effect of biaxiality. On the other hand, Christensen and Harmon (1967) compared experimental uniaxial and biaxial data in terms of ΔK_I correlation and found that the

---

*Here the equivalent strain range was defined by taking the extreme values of $\bar{\varepsilon}_T$ defined in Equation (83).

**Mean strain was zero.

growth rate was much higher for biaxial load conditions. It is unfortunate that the conditions under which such data were obtained were not reported, particularly in view of the fact that later experimental work by Kibler and Roberts (1968) (previously discussed in connection with biaxial fracture) led to opposite conclusions on the effect of biaxiality on Mode I propagation. They compared crack growth rates from biaxial tensile loading* and the baseline data for uniaxial loading of centrally notched thin aluminum sheets under plane stress conditions and found that:

1. When the crack growth rate was plotted in terms of Equation (51), both the exponent m and the coefficient C decreased in the presence of biaxial loading compared to the baseline uniaxial data.

2. An improved fit to the data was obtained where fracture toughness K_c in Equation (52) was modified to reflect the effect of biaxiality as previously determined from the fracture tests.

Undoubtedly, more work is needed in this area, particularly for the problems of surface cracks in intermediate thickness plates under large-scale yielding conditions.

Modes II, III, and Combined Mode Deformation

Throughout our discussion on crack propagation aspects, we have assumed that the growth takes place entirely in the crack opening (tensile) mode and that the shear stresses on the plane of the crack extension are negligible. However, such idealized situation need not be representative of conditions in actual structures. Consider several examples. First, a situation can be conceived under a condition of unequal triaxial compressive (or tensile-compressive) stress where macrocrack extension in sliding modes (II or III) (pure shear) can proceed along a plane of maximum shear. Second, examination of some of the fatigue fracture paths near structural discontinuities shows that their direction is not always normal

---

*In some tests, the loading parallel to the crack face was held constant while in others it varied sinusoidually in phase with the dominant cyclic loading applied in the direction normal to the crack face.

to the direction of the applied stress. Finally, the locations where the cracks do propagate in the direction normal to the direction of the applied direct stress may also be the locations where high shear stresses have to be carried by the uncracked net section of the shell. In short, at least the essential features of either Mode II (pure shear) and combined Modes I and II (shear and tension) need to be examined.

Qualitative information bearing specifically on Mode II growth is provided by experimental evidence obtained by Liu and Lal (1969) in tests on HY-80, HY-130, and 18 Ni(180) maraging steel specimens. Under conditions of biaxial loading (equal tension-compression notched plate specimens), the growth of cracks by sliding was observed along the planes where nominally only the shear stresses occur. The phenomelogical aspects of crack growth rate in shear differed from those of Mode I growth. Specifically, in the initial period of growth, the growth rate appeared to decrease with crack length until a steady-state growth was achieved. The steady-state growth was followed by a period of increasingly rapid growth rate leading to fracture. Such behavior was attributed to the existence of frictional stresses on the crack surface and their effect on the effective stress intensity factor K_I. Because of the large-scale yielding effect, an empirical relation was proposed between the growth rate and the square of the crack sliding displacement (rather than between the growth rate and K_{II}).

Combined mode crack growth in the presence of K_I and K_{II} was studied by Kobayashi and Iida (1969). They determined propagation rates in 7075-T6 aluminum tension plates for central cracks initially oriented at various angles β to the width direction and subjected to uniformly applied cyclic tensile stress σ_∞. Figure 53 shows a typical initial cracks and the subsequent extension. In the course of the tests, they observed that the initially slanted cracks ($\beta \neq 90$ deg) rotated immediately and propagated in the direction where K_I is a maximum, as shown by the approach of the curved crack paths to the horizontal direction. K_I and K_{II} for both the initially straight cracks and the subsequent curved cracks were determined by the conventional (no special treatment at the crack tip) finite element computer program. Crack propagation rates plotted in terms of $d(2c)/dN$ versus ΔK_I for various values of K_{II} (including the reference case of $\beta = 90$ deg for which $K_{II} = 0$). It was observed that the presence of even a

small K_{II} significantly increased the crack growth rates.* However, because of the early rotation of the crack, the K_{II}/K_I ratio decreased as the crack size increased so that eventually the growth rate approached the rate for initially horizontal crack ($\alpha = K_{II} = 0$ for the same projected length 2c).

CRACK INITIATION AND GROWTH UNDER CYCLIC COMPRESSION

In previous discussion we have reviewed various analytical tools available for the interpretation of crack initiation and growth in laboratory specimens under conditions of applied tensile loading. However, it is the response under applied compressive loading that is of direct interest to the submarine designer. The question then arises as to what extent the analytical methods (and supporting experimental data) developed for tensile loading can be used or modified. For the sake of simplicity, we shall confine ourselves to the question of the applicability of the above methods to small laboratory specimens tested under compressive cyclic loading. Let us first, however, consider a question which may arise regarding the importance of multiaxial applied tension versus compression loading in the case where the dominant mechanism of crack initiation and growth appears to be governed only by the applied shear stress or strain along favorably oriented slip planes.

First, with regard to crack initiation in laboratory specimens, we recall that there is some support for the view that the common mechanism is that of the cyclic slip** and thus, in principle, that the distinction between applied tensile and applied compressive loading need not be made for the same value of equivalent shear strain.*** However such an approach is

---

*As an example, for K_{II}/K_I ratio of 0.217, the rate was nearly double the rate for $K_{II}/K_I = 0$.

**Although, alternately, initiation by means of cracking at the interface of the inclusions and the matrix is also possible.

***We should recall, however, our discussion of the experimental evidence presented by Pascoe and deVilliers. They found that although crack initiation did occur along the planes of maximum shear strain, the character of the biaxial strain (insofar as it effects the stress component normal to the slip plane) also needs to be considered.

not likely to be completely applicable to the real structures. This is because when defined in terms of *detectable* cracks (on the order of 1/32 in.), crack initiation for large structural elements is most likely to involve some prior propagation in the opening mode and so the entire character of the applied stress or localized residual stress needs to be considered. Also, with respect to macrocrack shear mode propagation (analogous to the type observed by Liu and Lal) the extent of friction on the crack surface is clearly dependent on the normal stress component; here too, the rate of crack propagation should be expected to depend on the state of the applied stress as well as on the magnitude of the shear stress component.

In contrast to the rather voluminous literature available on the interpretation of tensile loading fatigue in laboratory specimens, analogous work dealing specifically with compression cycling is virtually nonexistent. The following discussion is limited to two references which lend themselves to the interpretation of crack initiation and growth as being governed by localized residual tensile stresses with the stress fluctuations resulting from applied cyclic compressive loading. Such a view does find considerable support in terms of some of the fatigue phenomena observed for various large-scale models that simulate conditions in submarine pressure hulls

Crack Initiation in Notched Cylindrical Specimens

Compressive axial cycling and evaluation of the crack initiation data in terms of three fatigue theories was performed at Southwest Research Institute (DeHart et al., 1968). The specimen shown in Figure 54 was fabricated from 2 1/2 in.-thick HY-80 plate. Initial residual tensile stresses were introduced by first loading the specimen in axial compression to a value that was sufficiently high to cause compressive yielding at the notch.* Unloading of the specimens resulted in residual tensile stresses

*Detailed information on the measurements of through-the-thickness residual stress and crack propagation is presented by Pickett et al. No attempt was made to interpret the crack propagation data in terms of current crack propagation laws. However the crack growth data does permit some qualitative observations and these are discussed in a footnote to page 148.

near the notch that were approximately equal to the uniaxial yield stress. Attempts to experimentally determine the residual stress distribution through the thickness were not successful, and an approximate analytical procedure was used for this purpose. Two groups of specimens were tested by cycling at nominal stresses between zero and a specified compressive value that did not exceed initial preload.

The first group consisted of specimens which were preloaded according to the procedures described above, and the second group consisted of specimens which were stress relieved and furnace cooled subsequent to preloading. The residual tensile stress prior to cyclic load application was *assumed* to be zero for the second group of specimens. The notch strain range in the stress-relieved specimens after "shakedown" (as a function of the applied cyclic load) was established by measuring the stabilized strain loops. Such stabilization usually occurred within four complete cycles. Unfortunately the notch strain range was not measured for specimens which were not stress relieved; it was assumed to be the same (for the same value of the applied cyclic load) as for the stress-relieved specimens.

Figure 55 shows the crack initiation life as a function of measured notch strain range for the two groups of specimens. Also included is the plot obtained at the United States Steel Applied Research Laboratory (Boblenz and Rolfe, 1966) for fully reversed flexural strain cycling of smooth cantilever plate-type specimens.

Let us now interpret the test results in the light of two prediction methods. The first is based on direct utilization of available strain cycling fatigue data for smooth specimens (such as the U.S. Steel test data shown in Figure 55) and essentially involves only the estimate or direct measurement of the strain range at the notch. It appears that for cyclic lives greater than 2,000 cycles the U. S. Steel data does provide a fairly close although somewhat unconservative estimate of the fatigue life (for reasons on which we shall speculate later) when the notch strain range was measured for the specimen without initial residual stress; see Figure 55.

The second approach (followed by DeHart et al.) utilizes fatigue theories based on the static stress-strain curves. Prior to the comparison of the relative merits of such theories, a discussion of the stress history at the notch would be useful since it was first necessary to convert a given

notch strain range to an equivalent *notch* stress range in order to compare two of the above theories (specifically the theories of Stowell, 1966 and Bement and Pohler, 1966) to experimental results.

Figures 56a and 56b (taken from DeHart et al.) respectively show the qualitative longitudinal stress-strain history at the notch with and without the initial residual stress. For the case of no residual stress, the material was assumed to follow curve ABC in the loading part of the first cycle; point C corresponds to compressive yield stress σ_o. Unloading then follows path CDE to point E which represents the conditions at the notch after the first loading cycle. It is then assumed* that for continued cycling the stress and strain follow the loop EFCDE. The authors have used the measured strain range $\Delta\varepsilon$ and assumed cyclic stress-strain relations** proposed by Stowell (1966) to calculate the maximum cyclic stress σ_{max}. The notch stress was then assumed to vary between σ_{max} and σ_o. For the residual stress specimens (Figure 56b), the portion ABC represents the application of a large compressive preload that culminates in compressive yielding at the notch. Removal of the load along the path CDE is assumed to culminate in the notch tensile yield stress σ_o. Further cycling (assuming that the total strain range $\Delta\varepsilon$ is the same as for the same compressive *load* in stress-relieved specimens) under cyclic compressive load is assumed to follow path EFGHE. Stowell's cyclic stress-strain relations are then used to establish point G and to calculate σ_{min} (the compressive portion of the stress range $\Delta\sigma$).

Figures 57 and 58 compare the three fatigue theories with the experimental data (DeHart et al., 1968). We recall that both the Stowell and Bement-Pohler theories are based on the energy criterion of fatigue

*It is highly unlikely that point E remains the same (i.e., E will shift parallel to the strain axis) following the first loading cycle. Direct evidence that cyclic creep for these specimens does take place was provided by Pickett et al. Specifically, when measured notch strain was plotted as a function of the nominal compressive stress range, the maximum strain at the end of the cycle at which the stabilization (shakedown) of the strain range occurred was found to be larger than the maximum strain at the end of the first cycle. This phenomenon complicates the problem of calculating the mean strain associated with the stabilized strain range.

**Strictly speaking, Stowell's cyclic stress-strain relations are not based on the actual experimental determination of the hysteresis loop but were derived using in part the true stress-true strain tensile test data.

fracture; the energy required for fractures is assumed to be a known quantity obtainable from the static stress-strain curve.* The third theory is due to Manson (1954) as modified by Langer (1957). It attempts to predict fatigue life for a given cyclic strain range (mean strain is not considered) on the basis of fatigue data in the form of cyclic endurance stress and the static fracture strain. Figure 57 shows that of the three theories, that of Stowell best predicts initiation life for a specimen with zero initial stress.

For the case of specimens which were initially preloaded, Figure 58 indicates that all three theories give extremely poor correlation with the "apparent" experimental data. The word apparent is used here because, as mentioned above, the actual notch strain range in the preloaded specimens was not measured. Finally, in connection with the results shown in Figure 57 let us comment on the fact that U.S. Steel cantilever plate data provide a prediction that is reasonably close although somewhat unconservative. That the smooth specimen data overestimates the crack initiation may appear somewhat surprising in view of our earlier remarks on the test results of Schijve (see page 77).** We recall that in the above case correlation between unnotched and smooth specimens on the basis of equal stress at a notch resulted in overly conservative prediction of the initiation life of notched specimens. However in Schijve's tests both the notched and smooth specimens were loaded axially in tension and consequently the volume of the highly stressed material was much larger than in the notched

---

*Strictly speaking, the original derivations were based on the case of the nominal stress in unnotched *tensile* specimens and attempted to predict fatigue life based on the specimen separation rather than on the crack initiation at a notch. Recently an extension of Bement-Pohler theory to notched specimens utilizing nominal stress range in conjunction with elastic stress intensity factors was proposed by Garrison and Salive, 1970. Such modification would not change the prediction of Bement-Pohler theory as presented in Figures 57 and 58 since it would not reduce the difficulties involved in an estimate of the *notch* stress range from the experimentally determined notch strain range. On the other hand the use of *nominal* applied (compressive) stress range in lieu of the notch stress range would not be appropriate. This is because Bement-Pohler theory has been developed on the basis of eventual specimen separation (axial tension or bending). As will be discussed later in the specimen under consideration, following the crack initiation, an eventual crack arrest was achieved.

**Although it is conceivable that the difference in the specific experimental techniques of recording the crack initiation event may account for at least part of the difference in the experimental results.

specimens.* In our case, the smooth cantilever plate specimen does correspond more closely to the round notched bar in terms of the amount of highly stressed volume in tension.

It would appear from the results of the above investigation that if a reasonable prediction of the strain range at a notch can be made (or measured experimentally), the use of smooth specimen fatigue strain range data for crack initiation (especially if obtained under the conditions of similar strain gradients) may be preferable to the use of at least some of the fatigue theories based on the static stress-strain curve properties. Furthermore, it could be argued that in the specific case discussed above, the correlation between cantilever plate data and the notched bar could be further improved if the difference in the state of strain and the effect of nonvanishing mean strain in the notched bar could be taken into account. Thus assuming total strain incompressibility, we have for the state of strain in the cantilever plate specimen at the extreme fiber essentially $\varepsilon_x = \varepsilon$, $\varepsilon_y = \varepsilon$, and $\varepsilon_z = -2\varepsilon$ (Ives et al., 1966) where ε is the applied longitudinal flexural strain, ε_x and ε_y are the strains in the specimen surface. Here ε_x and ε_y are in the direction of ε and normal to ε, respectively, and ε_z is the strain normal to the specimen surface. The elastoplastic state of strain in round notched bars is presently unknown; in principle, it would be calculated by numerical elastic-plastic analysis or estimated by direct measurement of surface longitudinal or diametral strains. The results of such calculation could then be used to attempt correlation on the basis of equivalent strain** computed in accordance with Equation (83). Finally if the compressive mean strain could be estimated, its effect on the initiation could, in principle, be taken into account by using the fatigue theory proposed by Ohji et al. (1966). However, apart

---

*In fatigue crack initiation studies (Marcal and Turner, 1965) on thin shells in the form of expansion bellows, where the governing strain range was due to highly localized bending, good correlation was found with fatigue tests on plain parent material specimen. The parent material specimens were tested by flexural strain cycling, and so fatigue life correlation does appear to reflect the similarity in strain gradients.

**Utilizing such procedures, Ives et al. were able to correlate equibiaxial tensile strain cycling data with the data obtained from the cantilever plate specimen discussed above.

from the difficulty of estimating the compressive mean strain in the presence of cyclic creep, such theory has not yet received sufficient experimental validation to justify such a refinement.

Crack Propagation from Centrally Notched Aluminum Plates

Fatigue crack growth under compressive loading was recently studied by Hubbard (1969). Figure 59a shows a plate specimen fabricated from 7075-T6 aluminum alloy. Cracking originated from the ends of the machined notch. The following aspects of the investigation are of special interest:

1. Observations on the size of the plastic zone at the maximum compressive load and its relation to the residual tensile stress arising after unloading to zero load in the first cycle and after the crack had initiated and progressed a small distance.

2. Measurements of the crack growth rate and the use of such data in deriving the effective stress intensity factor and in constructing an approximate analytical model for crack loading.

3. Observations on crack arrest which results when the load cycle was modified to vary between the maximum and a specified nonzero minimum value of the compressive load instead of varying between the maximum and zero load.

Let us begin by summarizing the observations on the plastic zone size and the residual tensile stresses. The experimental data were obtained by means of photoelastic coating applied to both surfaces of the specimens. Photographs of the photoelastic fringe patterns were taken for specimens subjected to three load levels varying from zero to a maximum value. At each load level, observations were made at the maximum and zero load of the first cycle and after the crack had propagated a distance approximately equal to the initial plastic zone size. At the maximum load of the first cycle (compressive), the plastic zone showed a pattern similar to the diffused plane stress plastic zone observed by Gerberich (1964) in cracked aluminum plate and thus was similar in appearance to the schematic representation shown in Figure 42. However, as might have been expected, observed dimension R was much larger than the plane strain R shown in Figure 42. In fact, the observed dimension was approximately equal to the

diameter of Irwin's circular plastic zone idealization*
($R \approx 2\ R_o = 1/\pi\ (K_I/\sigma_o)^2$) with K_I obtained from the idealization of the actual notch configuration by a sharp 1/2-in. long central crack subjected to remote uniform stress field.

Of greater significance was the interpretation of the fringe patterns following load removal. Although neither the actual distribution of the tensile residual stress nor the extent of the (reverse) tensile plastic zone could be determined, Hubbard concluded that the extent of the residual tensile stress field region was slightly smaller than that of the compressive plastic zone at the maximum load. It could only be hypothesized that the average tensile residual stress was some fraction of the yield stress, with the actual tensile yielding confined to the immediate neighborhood of the notch tip. However he reached an important conclusion, namely that the overall distribution of the residual stress field remained as observed following the unloading of the first cycle; i.e., remained substantially unaffected by subsequent crack growth.** This conclusion was based on observations of the fringe patterns*** at no load after the crack had initiated and progressed a small distance.

Observations of the crack length 2c versus the number of cycles N for various values of the maximum load are presented in Figure 59. Note that data can be represented on the log-log plot by a straight line, thus yielding power relationship of the form

$$2c = C_2\ (N)^h \tag{85}$$

---

*This may seem somewhat surprising not only because Irwin's approximation was initially derived from Mode III analysis but also because the observations were presumably taken *before* fatigue crack extension from the initial notch (of unspecified root radius) took place. It should also be noted that such calculations would not be valid if partial crack closure occurred during the compressive cycle.

**With the possible exception of the immediate vicinity of the crack tip where the details of fringe patterns were obscured.

***We are assuming that there was no debonding in the coating. Otherwise this conclusion may not be valid.

where the positive constants C_2 and h depend on the load level.* Differentiation of both sides of Equation (85) with respect to N yields the relationship

$$\frac{d(2c)}{dN} = C_2 \, h \, N^{h-1} \tag{86}$$

indicating that the growth rate is a decreasing function of the number of cycles.** Equation (86) can now be related to Equation (51) obtained for zero to maximum tension loading on the basis of the following model. At the maximum compressive load, the crack surfaces are closed and no growth occurs. As the load is completely released, the crack surfaces are propped open and the crack tip is subjected to the unknown effective stress intensity factor $(K_I)_{EC}$. The stress intensity factor $(K_I)_{EC}$ is due to the action of *localized* residual tensile stress whose magnitude and spatial distribution can be estimated only crudely, as discussed above. Nevertheless the mechanism of crack growth can be envisioned as proceeding under an effective stress intensity factor range $(K_I)_{EC}$ and thus expressed by means of Equation (51) with $(K_I)_{EC}$ replacing ΔK_I. If the material constants C and m of

---

*As an example for 0-8000 lb load (corresponding to the net section stress of about 64 ksi), constants C_2 and h were found to be 0.429 and 0.0408, respectively.

**Thus, when the cracks have grown to a length of initial compressive plastic zone (and hence approximately to the extent of initial residual tensile stress field), the rate slowed down to approximately 10^{-7} in. per cycle. Similar effects were noted in two separate investigations of notched round bars subjected to mean compressive cyclic loading. In the first investigation already discussed in connection with crack initiation aspects (Figure 54), experimental data showed that the crack propagation had effectively stopped when a crack depth was reached that was approximately equal to the depth of residual tensile stress induced by the removal of high compressive preload. In the second investigation (Gerber and Fuchs, 1968), dealing with the interpretation of data of a similar specimen (fabricated from 7075-T6 aluminum), theoretical predictions of the extent to which cracking would be confined to the depth of residual tensile zone resulting from the unloading part of the compressive cycle were in general agreement with the experimental results.

Equation (51) are known, then $(K_I)_E$ can be evaluated by equating the right-hand sides of Equations (51) and by solving for $(K_I)_E$ in the form

$$(K_I)_{EC} = C_T N^{h_T} \tag{87}$$

where

$$C_T = \left(\frac{C_2 h}{C}\right)^{\frac{1}{m}} \quad ; \quad h_T = \frac{h-1}{m} \tag{88}$$

Figure 59c shows $(K_I)_{EC}$ plotted as a function of the crack length for the three load levels used in the experimental part of the study. The principal interest in the results of the above derivation is that they permit an assessment of approximate models to be described below. Such models can be envisioned for similar situations in which the residual stress field is not precisely known. Specifically, the concentrated force model described in Figure 59a was found to give reasonable agreement with the data shown in Figure 59c. The principal parameter in such a model* is the extent of the plastic zone R corresponding to the maximum load of the first cycle. The force P, assumed to be acting at the midpoint of the plastic zone, is calculated by multiplying R by the average tensile residual stress which in this case was assumed to be equal to one-half the yield stress. Since both P and its location $\bar{b}$ with respect to the plate centerline are assumed to be independent of crack length 2c, calculation of K_I in accordance with the formula (Irwin, 1957) written in Figure 59d leads to a general agreement with the trend of $(K_I)_{EC}$. This would not have been the case had K_I been calculated from a model of the centrally notched plate subjected to remote *tensile* fluctuating stress σ_∞ equal to yield stress σ_∞ as would appear in Figure 59b with the direction of σ_∞ reversed) since K_I would then behave as a monotonically *increasing* function of the crack length.

In conclusion, let us note those aspects of the investigation that deal with crack arrest. Hubbard found that after the crack had extended a

---

*The model must be restricted to cracks greater than one-half the notch length plus one plastic zone radius.

certain amount under zero to maximum compressive load, its further progress could be essentially arrested by modifying the load cycle to vary between a given maximum and a predetermined minimum compressive load. The minimum compressive load was calculated by reasoning as follows. At zero compressive load, the crack surfaces remain open due to the presence of a residual tensile stress which, in turn, results in the effective stress intensity factor $(K_I)_{EC}$ and can therefore be calculated directly from the observed growth rate as explained above. The minimum compressive applied stress σ_∞ required to keep the crack closed (and thus to prevent crack extension) was then calculated by utilizing the centrally notched model (shown in Figure 59b) and by equating the corresponding expression for the stress intensity factor to $(K_I)_{EC}$.

In summary, although the specific results of the above analysis may be restricted to the configuration shown in Figure 59, the underlying rationale (particularly as it pertains to the construction and assessment of analytical models from the experimental data on crack growth) may be applicable to a wide range of problems involving crack propagation under compressive loading.

ENVIRONMENTAL EFFECTS

INTRODUCTION

Considerable attention has been given to the problem of environmentally affected fracture processes. Stress corrosion cracking and interstitial embrittlement are among the more common environmental fracture processes. Although investigators of stress corrosion vary somewhat as to its exact definition, failure due to stress corrosion may be said to take place when a structural component fails in a certain environment under statically or dynamically applied tensile stresses that are below the anticipated fracture stress in the absence of that environment.

To date, the phenomena of stress corrosion have been studied using two fundamentally varying approaches. On the one hand, methods that originate from fracture mechanics are used by introducing some initial crack or flaw into the structure under study. On the other hand, methods are used that originate from the fundamental stress corrosionist, in which

case no initial flaw is introduced in the structure under study. In this context the word "structure" includes such components as single wires. To date, most, but certainly not all, of the effort has been concentrated on the study of fundamental mechanisms using initially unflawed specimens.

Despite the fact that stress corrosion cracking has been studied extensively for well over three decades, the complex nature of the phenomena that govern stress corrosion have thus far made it difficult to accurately define the term stress corrosion cracking. One of the earlier attempts (Sutton et al., 1945) to define stress corrosion cracking stated that it "implies a greater deterioration in the mechanical properties of the material through the simultaneous action of the static stress and exposure to corrosion environment that would occur by the separate but additive action of these agencies." Let it suffice at this point to indicate that stress corrosion may occur under conditions of residual and dynamic stresses as well. Part of the difficulty is a lack of understanding of the mechanism(s) of stress corrosion cracking.

Pugh (1966) has discussed some of the characteristics of stress corrosion cracking:

1. Cracking may be intercrystalline or transcrystalline.

2. The environments which cause stress corrosion cracking appear to be specific, i.e., well defined in their components.

3. Stresses which cause stress corrosion cracking must be tensile.

4. Stresses which cause stress corrosion may be static or dynamic.

5. Stress corrosion cracking appears to be fundamentally electrochemical in nature (this may not be accepted by all researchers in stress corrosion).

6. Stress corrosion cracking may occur in pure metals.

7. Stress corrosion may be related to the dislocation structure of the deformed material.

Although some of the above characteristics may be questioned or are subject to discussion, they are indicative of the nature of the problem of stress corrosion cracking. For a more detailed discussion the reader is referred to Pugh (1966).

Figure 60 shows some of the processes that play a role in stress corrosion cracking (Staehle, 1967). The complete stress corrosion cracking

processes shown there can be broken into four distinct events as follows: (1) a breakdown of the surface film followed by (2) the formation of a corrosion pit and (3) growth of the stress corrosion crack until such a depth that (4) a critical flaw depth is established and rapid fracture commences. It should be noted that hydrogen plays a very significant role, and investigators frequently distinguish between hydrogen embrittlement and stress corrosion cracking.

In the present discussion, it is desired to highlight some of the findings from the general area of stress corrosion, both past and present. First the fundamental stress corrosion point of view will be discussed, which consists of the electrochemical theory, the stress sorption models, and hydrogen embrittlement. This will be followed by a discussion of the approach which is derived from fracture mechanics. Finally, some specific metals and environments will be discussed.

FUNDAMENTAL STRESS CORROSION APPROACH

Several theories have been advanced to explain the mechanistic aspects of stress corrosion cracking. These theories are primarily concerned with the propagating crack. Only the major theories presently in vogue will be considered. They may be classed into two major categories, the electrochemical theory and stress sorption cracking theories (Uhlig, 1967). The electrochemical theory requires the material at the crack tip to be anodic so that the crack propagation can proceed by preferential anodic dissolution at the crack tip. Stress sorption cracking provides the justification for a brittle-type fracture (typical of stress corrosion cracking) in frequently ductile material. Finally hydrogen embrittlement will be considered separately from either of these categories.

Electrochemical Theory

The phenomena may be briefly described as follows (Uhlig, 1967): " • • • galvanic cells are set up between continuous intermetallic precipitates and adjacent metal at grain boundaries or through paths within the grains, the ensuing corrosion acting under stress to open up a crack." There are two models that are of main interest. They are described by Pugh et al. (1969) in some detail and will be outlined only briefly below.

The Film-Rupture Model. A passive film is assumed to form on the crack surfaces. This film then ruptures at the crack tip by continual plastic deformation which is caused by the applied stress. The crack tip, in turn, is subjected to localized anodic dissolution in which the crack walls act as cathodes. Champion (1948) and Logan (1952) have advocated this model. A sketch of the film rupture model is shown in Figure 61. The film rupture model appears quite satisfactory for certain cases of stress corrosion cracking but does have a number of drawbacks. In this model the crack is thought to propagate continuously by anodic dissolution.

The Mechanochemical Model. This model was first brought out by Hoar and Hines (1956). It differs from the film-rupture model primarily in that no film is formed at the crack tip. Because of the applied stress, the metal at the crack tip deforms and is anodic relative to the nondeforming metal on the crack walls. Consequently, anodic dissolution can occur at the crack tip and continuous crack propagation takes place. A schematic of this model is shown in Figure 62.

Stress Sorption Cracking Theories

The mechanism that governs the stress corrosion cracking in sorption cracking are not governed by a dissolution at the crack tip. On the contrary in these cases, the material at the crack tip (which is already severely strained due to the applied stresses) experiences a decrease in the surface energy so that under a tensile stress the Griffith criteria takes over and a brittle failure ensues. It is of interest to point out that these theories explain how a particular environment can cause a brittle failure. Some specific theories will be considered next.

The Adsorption Model. The critical species (attacking elements supplied by the corroding media) is absorbed by the strained bonds at the crack tip. This reduces the surface energy γ_s in the Griffith equation. The reduction in γ_s becomes such that in combination with a tensile stress, a brittle fracture becomes thermodynamically feasible. This idea as applied to adsorption was first proposed by Uhlig in 1959 and later emphasized by Coleman et al. in 1961. The process would appear to be

continuous but may be relatively slow, depending on the transport processes of the corroding agent at the crack tip. A schematic of this model is shown in Figure 63.

Brittle Film Model. The initial suggestion for this model came from Forty (1959). A brittle film is formed on the surface by the corroding media. This brittle film fractures under an applied tensile stress. The propagating crack will travel into the substrate before being arrested by plastic flow at the crack tip. Subsequently the brittle film again forms at the crack tip and the whole process is repeated. It is clear that the crack will propagate in a discontinuous fashion. The schematic of this model shown in Figure 64 was taken from Pugh et al.

Tunnel Model. A slip step is assumed to occur at the initial surface. From the slip step, tunnel corrosion occurs and leads to the formation of tubular pits such as shown in Figure 65a. These pits weaken the region and a localized ductile fracture occurs. The tunneling model was first suggested by Pickering and Swann (1963). The model advocates discontinuous crack growth.

Hydrogen Embrittlement

Although the mechanism of hydrogen embrittlement has not been established, various theories are being considered. The theories will not be considered under separate headings because some cover previously discussed models and some go into the area of fracture mechanics. The concepts have been enumerated by Johnson (1967).

One thought is that a reduction of hydrogen ions takes place at the crack surface. Hydrogen will subsequently enter into the lattice ahead of the crack tip. The fracture stress of the material will then be lowered as described in the adsorption model. Petch and Stables (1962) have described this in detail. Tetelman and Robertson (1962), considered that excess hydrogen precipitates in the material and causes voids. The hydrogen pressure in these voids builds up so high that the defects will grow by plastic deformation or cleavage. Application of external loads will cause void coalescence to create flaws of sufficient size to cause final failure. Finally, Johnson et al. (1958) suggested that hydrogen diffuses to regions

of high triaxial stress and then acts to reduce the theoretical cohesive or fracture strength of the material. Some of the aspects of hydrogen embrittlement will be considered in more detail when the fracture mechanics aspects are discussed.

Some Experimental Considerations

The preceding mechanisms are generally studied experimentally using smooth specimens. The use of smooth specimens has led to misleading results in some instances. A case in point is titanium where the smooth specimen showed immunity to stress corrosion cracking in water; however titanium proved to be rather sensitive to water when a precrack was introduced in the specimen (Brown, 1966). There are other disadvantages to using smooth specimens. The initiation and propagation of a stress corrosion crack are combined. Additionally the experimenter will not have good mechanical control, for example, when multiple cracking of the test specimen occurs.

On the other hand, there are some distinct advantages to using smooth specimens. The most prominent advantage is the simplicity of the specimen geometry and the associated ease of computations of results. Ability to control the environment of the corrosive media and to exercise control over the metallurgical conditions of the test specimen are also significant advantages, particularly for investigation of fundamental stress corrosion.

Effect of Potential and pH

Before proceeding to a discussion of the fracture mechanics approach to the problem of stress corrosion cracking, the role of the potential - pH diagram and some means of environmental control (cathodic and anodic protection) will be highlighted.

Potential - pH Diagram. The potential - pH diagram was developed by Pourbaix (1963). The diagram does not say that cracking due to stress corrosion *will* occur, but it does say that a reaction between the metal and the environment *can* occur thermodynamically for certain potential and pH combinations. Informative results in this regard were first obtained by

Mattsson (1961) for a brass-ammonia system. Figure 66 is a summary of Mattsson's description which was taken from Booker (1967). Care must be exercised in the application of the Pourbaix diagrams, however, in that the potential at the crack tip must be known. This potential may be different from the bulk solution. Brown and his collaborators have done significant work in this area (1969). They appear to have developed even more accurate methods for the determination of the pH at the crack tip (private communication, 1970). In conclusion, the value of the potential - pH diagram is quite considerable but its limitations must be recognized.

Environmental Control. Significant results have been achieved to date in the use of environmental control. Several different coatings to shield the metal from the environment have been used with varying degrees of success. In general the principal drawbacks to this method of protection are that the coating must be complete and must not itself enhance corrosion by gaseous entrapment or other forms of chemical reactions.

Cathodic and anodic protection are other popular means to shield against stress corrosion. Experts differ as to the extent to which this protection may be utilized, but it has been successfully applied. An example of the use of cathodic protection is in the AUTEC Toto II deep sea mooring system (Crisci and Foster, 1968). In cathodic protection (negative electrode), an external current is applied so that electrons are supplied to the electrode. This lowers the potential of the dissolving metal toward the equilibrium dissolution potential for metallic dissolution. Care must be exercised in the use of cathodic protection because it is usually accompanied by hydrogen evolution. Problems associated with hydrogen evoluation have been mentioned already; they will be discussed further in the paper later. Anodic protection (electrons are absorbed) has also been successfully used, e.g., carbon steels, stainless steels, and titanium alloys. Some insight on the subtleties of cathodic and anodic protection is given by Brown (1969).

FRACTURE MECHANICS APPROACH

Materials are generally covered with a protective film which must be broken down by the corrosive media before stress corrosion can attack the

material. After film breakdown, a corrosion pit can be formed. Under conditions conducive to further stress corrosion, this pit will grow until a final failure occurs at some critical stress intensity value. Consequently, initiation and "subcritical" propagation of a stress corrosion crack take place before a critical crack propagation occurs and may very well consist of a large portion of the total life of the component. Why then go to fracture mechanics (which utilizes precracked specimens)? The case of titanium, which was previously mentioned, is one case, for example, where it took a prenotched specimen to establish the sensitivity of titanium to stress corrosion. Aside from such a case, there are other significant factors which should not be overlooked. Use of the fracture mechanics approach (with a precrack) establishes the possibility of extending the fracture mechanics theory and developments to the field of stress corrosion. To assume the existence of a precrack in a structural component is not unrealistic since many materials contain inherent flaws. Also fatigue cracks may form and act as initiation sites for corrosion cracks. Basically, the initiation phase (corrosion pit) is eliminated by using the fracture mechanics approach.

The discussion that follows will cover the various aspects that relate fracture mechanics and stress corrosion cracking. The stress corrosion cracking stress intensity factor will be established and, through it, the fracture aspects will be highlighted. Hydrogen embrittlement will be discussed from the fracture mechanics point of view. Finally, the effects of fatigue, the interpretation of striation patterns, the influence of ambient pressure and the strain-hardening coefficients on stress corrosion cracking are presented.

The Stress Corrosion Stress Intensity Factor

The concept of a critical stress intensity factor has already been discussed in the section dealing with stress analysis near stationary cracks. This concept is extended in the present section to include the effect of stress corrosion on the stress intensity factor, resulting in a critical stress corrosion stress intensity value K_{ISCC}. The K_{ISCC} concept appears to be quite useful, but the actual determination of K_{ISCC} is not well defined. Evidence will be presented to show that "K_{ISCC}" is more

constant for a material than is the net stress when stress corrosion takes place. However some questions still remain, e.g., how long should a stress corrosion test be run to ensure that K_{ISCC} has been established? Certainly "intuition" on the part of the researcher helps, but it is a far cry from a definition of the time element. Possibly growth rates at certain levels of K_I are a more meaningful parameter although they may be discontinuous.* It should be noted that the limitations as to plane strain conditions and others apply equally in the case of stress corrosion.

Basically the approach in determining K_{ISCC} is straightforward conceptually. A number of fatigue precracked specimens of a given material are loaded to different levels of K_I (naturally less than K_{IC}) in a given environment. The specimens that fail have K_I values above K_{ISCC} and the remaining K_I values are equal to or less than K_{ISCC}. The K_{ISCC} thus determined is taken to be a material property. For practical reasons, the above concept is applied using the following modification "•••that fail *within some set amount of time* have K_I values above•••" Possibly the cracked wedge force panel, which will be discussed later, could be used as a stress corrosion test panel. Then if the stress corrosion test panel shows growth rates less than some preset rate at some crack length, then by convention that crack length could be used in the computation of K_{ISCC}. Additionally, the fatigue precracking load amplitude may cause a considerable effect. If low amplitudes of ΔK_I are used during precracking, the result may not be applicable to a structure with fatigue cracks initiated under high values of ΔK_I. Thus a number of important considerations remain unanswered and should have immediate attention in research programs.

Brown and Beachem (1967) presented strong evidence to indicate that K_{ISCC} is a material property. They tested various specimen configurations using 4340 steel. Two parameters were evaluated and compared with the time to failure. These parameters were the stress intensity K_I and the net section stress σ_N. Figure 67 shows the net-section stress versus the time

---

*These will be discussed later.

to failure; it shows clearly that there is a threshold value for the net-section stress but that this threshold value differs depending on the specimen geometry. However, it is clear from a plot of the stress intensity versus the time to failure (Figure 68) that a threshold value for the stress intensity K_{ISCC} exists which is the same regardless of the specimen geometry. An even more convincing demonstration of the significance of K_{ISCC} rather than σ_{NSCC} as a controlling parameter was presented by Smith et al. (1968). They noted that a center cracked wedge force panel would experience a decreasing stress intensity value and an increasing net section stress during crack extension under constant load up to a total crack depth equal to one-half the width of the specimen. Therefore, if the stress intensity decreases below K_{ISCC} (when a corrosive media is used), the crack should arrest if K_{ISCC} is the governing parameter for stress corrosion crack growth. But if the net section stress controls, the crack should not arrest. Crack arrest was found to occur. Consequently K_{ISCC} appears to be a reasonable parameter to use in discussing stress corrosion cracking behavior. A note of caution is in order in regarding use of the center cracked force panel to determine K_{ISCC}. Petrak (1970) has found discrepancies between the crack arrest and crack initiation values for the stress intensity under conditions of stress corrosion cracking. However, Petrak violated minimum thickness requirements, which was not true for the experiments by Smith et al.

Fracture Mechanics Aspects

Because of the similarity of the K_{IC} and the K_{ISCC} parameters in interpreting the behavior of the fracture of materials, computations based on linear fracture mechanics may be made in the case of stress corrosion cracking using K_{ISCC} instead of K_{IC}. The limitations of linear fracture mechanics still apply, but it should be noted that the stress levels under which stress corrosion may occur are frequently quite low and so that linear fracture mechanics may be properly applied. Some topics of particular interest in this section are the types of stress corrosion specimens and the analysis of the stress corrosion data from the viewpoint of fracture mechanics. Hydrogen embrittlement, the effect of stress corrosion on fatigue, and the influence of ambient pressure on stress corrosion will be discussed in separate sections. Finally the strain-hardening coefficients will be discussed.

Specimen Types. All stress corrosion cracking appears to occur in a manner described as a plane strain failure (Brown, 1970). The specimens that are used in fracture mechanics are designed to fail in plane strain. Consequently, those specimens may be utilized in the study of stress corrosion cracking without sacrificing the validity of the fracture tests. For these specimens, expressions are available that relate the value of the stress intensity K_I to the applied load and the dimensions of the fracture specimen. Figure 69 has been prepared to show some of the more frequently used specimen. Figure 69 is not complete,* but the more significant specimen geometries used in the testing of materials for stress corrosion cracking have been indicated together with terminology, geometry, and the equations used to determine K_I.

It is of interest to point out that the basic concept of these specimens is not identical, i.e., some are "time" dependent and some are "arrest" dependent. As an example of a time-dependent specimen, consider the cantilever beam specimen. A large number of notched specimens are loaded to differing K_I values and exposed to the environment under study. Then the lowest K_I values which does not cause failure in the environment within a certain time is the desired K_{ISCC}. The center cracked wedge force panel is an example of an arrest-dependent specimen. In this case, the specimen is loaded in the environment, and the crack length is measured at the point where the resulting crack growth is arrested. This crack length is used to compute a valid K_{ISCC} value, assuming that minimum size requirements have been met. Figure 68 shows that similar results are obtained from each specimen type.

Application of the Data. After a sufficient number of tests have established a value for K_{ISCC}, these data can now be used to determine critical flaw sizes in structures. The availability of information on the critical sizes of various types of flaws allows inspection procedures to be

*It should be noted that specimens such as the U-bent specimens are not included because they are not fracture specimens, even though they are used to study stress corrosion cracking.

established so that any critical or close to critical flaws can be found and remedial steps taken before a catastrophe occurs. Additionally, in the case of fatigue crack growth,* the amount of permissible crack growth can be established before a crack reaches a critical size so that the reliability of an inservice structure is known.

A practical example of such a procedure will be discussed for the case of a surface flaw subjected to a tensile load. From Irwin (1962), the maximum stress intensity K_I occurring at the inner axis of the semi-elliptical surface flaw may be calculated from

$$K_I = \left\{ \frac{1.2\ \pi\ \sigma_\infty^{\ 2}\ a}{\phi^2 - 0.212\left(\frac{\sigma_\infty}{\sigma_o}\right)^2} \right\}^{1/2}$$

where σ_∞ is the applied nominal stress, σ_o is the yield stress of the material and a is shown on Figure 69. ϕ^2 may be evaluated by means of the expression shown on Figure 69 or alternately approximated using a third order polynomial curve fit (unpublished results of DeYoung)

$$\phi^2 = 1 + 0.178\ \frac{a}{c} + 1.72\left(\frac{a}{c}\right)^2 - 0.426\left(\frac{a}{c}\right)^3 \qquad (90)$$

The critical stress intensity factor from the stress corrosion tests is K_{ISCC}. Using Equation (89), the critical crack depth a_{CSCC} may be found:

$$a_{CSCC} = \frac{\left\{\phi^2 - 0.212\left(\frac{\sigma_\infty}{\sigma_o}\right)^2\right\}}{1.2\ \pi\left(\frac{\sigma_\infty}{\sigma_o}\right)^2}\left(\frac{K_{ISCC}}{\sigma_o}\right)^2 \qquad (91)$$

Similar results may be found for other types of flaws that may be encountered. It should be noted that K_{ISCC} should be determined under conditions of plane strain, so that the determination of K_{ISCC} using one specimen type suffices and may be used as a material property. One word

---

*Fatigue crack growth will be discussed subsequently.

of caution, however: the precise stress corroding condition at the crack tip in a structure may not be duplicated in the test specimen! For example, the electrochemical interactions may influence the test specimen and the actual structure differently, particularly at the crack tip.

Crack Contour. Stress corrosion may cause a blunting or sharpening of the crack tip if the corroding mechanism is dissolution of the material at the crack tip. After such dissolution has caused a significant crack extension, the fracture may be governed by sharp crack fracture mechanics. Using a simplified analysis, such as delineated below, it is possible to establish whether the corrosion due to dissolution causes a blunter or a sharper crack. If it turns out that the crack tip becomes sharper due to the corrosion, then the sharp crack fracture analysis may be significant in analyzing the effect of such a corrosion flaw. However if the corrosion due to dissolution causes blunting, this would seriously challenge the sharp crack idealization of the fracture mechanics analysis. The preceding discussion assumes, of course, that the material properties are not changed extensively due to the corrosion.

The following analysis is due to Creager (1966). Considering Figure 70, assume that the horizontal component of the velocity of dissolution V_H is constant and that the velocity of dissolution V is a function of the applied stress σ_∞. Then

$$V_H = \frac{V(\sigma)}{\cos \phi} = \text{constant} \tag{92}$$

For r small in comparison to the semimajor diameter of the ellipse a, i.e., $\frac{r}{a} << 1$, it can be shown that $\cos \phi = \cos \frac{\theta}{2}$. Then Equation (92) may be rewritten as

$$V_H = \frac{V(\sigma)}{\cos \frac{\theta}{2}} \tag{93}$$

It has also been shown, however, that the tangential stress σ_t around the crack tip for the Mode I crack is given by

$$\sigma_t = \frac{K_I}{(\pi\rho)^{1/2}} \cos^2 \frac{\theta}{2} \tag{94}$$

Combining Equations (92)-(94) results in an expression for the velocity of dissolution in terms of the stress intensity and the tangential stress. The resulting equation is

$$V(\sigma) = V_H \frac{(\pi\rho)^{\frac{1}{4}}}{K_I^{1/2}} \sigma_t^{1/2} \tag{95}$$

The events at the crack tip are established by computing the derivative

$$\xi = \frac{d\left\{\frac{V(\sigma)}{\sigma_t^{1/2}}\right\}}{d\,\sigma_t} \tag{96}$$

No change occurs at the crack tip when $\xi = 0$, but a sharper crack results when $\xi > 0$ and the crack blunts when $\xi < 0$.

The foregoing analysis is based on a rather simple approach and has merit primarily in pointing out possible functional relationships. It should also be noted that the blunting is caused by stress corrosion and not by large deformations at the crack tip such as shown in Figure 15. The establishment of particular mechanisms will now be pursued in order to establish useful computational techniques.

Models of Stress Corrosion Cracking

Some theories to explain the mechanistic aspects of hydrogen embrittlement were indicated on page 154. They may be described, in short, as involving a lowering of the cohesive strength or a buildup of internal pressure in voids or, finally, a reduction in the surface energy. All three of these phenomena are said to be affected by the presence of hydrogen. Some analyses have been made and will be briefly reviewed below. These analyses were derived for cases of hydrogen embrittlement but they may be equally applicable to stress corrosion phenomena caused by other factors.

Analytical Time-to-Failure Computation. The principles of fracture mechanics will be utilized to establish failure criteria which may be used to compute the time to failure. This approach has been discussed by Tetelman (1967) and will be outlined below. Unstable fracture occurs at a

crack when the crack tip opening displacement δ_t reaches a critical value $(\delta_t)_c$. The crack tip strain $\varepsilon_{c.t.}$ can be related to the crack tip opening. displacement by the following equation

$$\delta_t = 2 \rho \varepsilon_{c.t.} \tag{97}$$

In Equation (97) ρ is the radius of the advancing crack. The crack opening displacement δ_t can also be related to the crack extension force $\mathcal{G}$. Fast fracture ensues when δ_t becomes a critical value which can be related to the critical stress intensity value and the fracture stress, σ_F. The resulting fracture stress is shown to be equal to

$$\sigma_F = \sqrt{\frac{E \sigma_o (\delta_t)_c}{\pi c}} \tag{98}$$

where 2c is the crack length. Equation (98) requires that $\sigma_F < \sigma_o$. Equation (98) can also be modified to give the resulting failure stress in terms of the critical crack extension force $\mathcal{G}_c$. But before doing so, it should be noted that relationships between the crack extension force and the characteristics of the flaw and the applied stress σ_∞ are given by

$$\mathcal{G} = \frac{\alpha \pi c}{E} \sigma_\infty^2 \tag{99}$$

where α is a geometric factor which varies for particular flaw geometries. At failure (for $\sigma_F < \sigma_o$), the values become critical and the failure stress is given by

$$\sigma_F = \sqrt{\frac{E \mathcal{G}_c}{\alpha \pi c}} \tag{100}$$

So far Equations (97)-(100) are derived from well-established fracture mechanics criteria. In order to introduce these concepts into stress corrosion analysis, consider Figure 71 (Johnson and Wilner, 1965). Such crack growth data permit computation of the time required for a crack to progress under corrosive conditions at varying levels of stress intensity if a certain functional relationship is assumed to describe dc/dt. Such a relationship may be determined empirically from Figure 71 for example.

Prior to a slow crack growth, some incubation time will be present. In fact the incubation time may make up a major portion of the total life time. Let this incubation time be denoted by t_i. Fast failure will be considered to occur when the crack reaches a critical size c_c. The starting flaw c_o will be taken as the depth of flaw obtained at the completion of the incubation time. Three types of stress corrosion crack growth relationship will be considered.

First, consider the crack growth rate to be constant, i.e., $dc/dt = A$. Then the total time to failure t_F is found by adding the incubation time t_i to the time t needed for the flaw to grow from c_o to C_i

$$t_F = t_i + t \tag{101}$$

The time t is found from

$$c_c - c_o = A \int_o^t dt \tag{102}$$

The critical flaw size c_c is given by

$$c_c = \frac{E\,\mathcal{G}_c}{\alpha\,\pi\,\sigma_\infty^{\,2}} \tag{103}$$

where $\mathcal{G}_c$ is determined from the critical value of the stress intensity K_c at which instability occurs; $K_c^{\,2} = E\,\mathcal{G}_c$ (assuming plane stress conditions and using Equation 14). Integrating Equation (102) and then substituting Equation (103) into (102), we can find the time t. Putting this t into Equation (101) results in the total time to failure for a constant rate of crack growth due to stress corrosion

$$t_F = t_i + \frac{1}{A}\left\{\frac{E\,\mathcal{G}_c}{\alpha\,\pi\,\sigma_\infty^{\,2}} - c_o\right\} \tag{104}$$

Equation (104) merits some discussion. Since the equation is based on an empirically established functional relationship, nothing is really said about the specific stress corrosion mechanism. Furthermore if the material has a threshold stress intensity below which no crack growth due to stress corrosion can occur, Equation (104) does not account for that.

Finally, when the applied stress intensity is equal to the critical stress intensity K_{ISCC}, catastrophic failure is assumed to occur; Equation (104) does not account for such an event.

A second approach is suggested by Figure 71 where it is noted that the rate of crack growth is a linear function of the stress intensity factor, i.e., $dc/dt = A' K_I$, which through the use of the definition of the stress intensity factor may be rewritten as

$$\frac{dc}{dt} = A' \sigma_\infty \sqrt{\alpha \pi c} \tag{105}$$

where A' is a constant.

Integration is straightforward as in the preceding case and using Equation (105) is given by

$$\int_{c_o}^{c_c} \frac{dc}{\sqrt{c}} = A' \sigma_\infty \sqrt{\alpha \pi} \int_o^{t_F} dt \tag{106}$$

The time t may be found after integrating Equation (106). Substituting t into Equation (101), the total time to failure is found for the case where the rate of stress corrosion is a linear function of the stress intensity. This total time is given by

$$t_F = t_i + \frac{1}{2 A' \sigma_\infty \sqrt{\pi \alpha'}} \left[\left\{ \frac{E \mathcal{G}_c}{\pi \alpha \sigma_\infty^2} \right\}^{1/2} - \sqrt{c_o} \right] \tag{107}$$

A third approach is suggested by the power laws of fatigue analysis. The assumption is made that the rate of crack growth is proportional to the square of the stress intensity factor. Although this assumption is not exactly representative of today's thinking in fatigue analysis and the stress corrosion problem may be due to noncyclic loading only, it is still a useful approach in the stress corrosion problem. Following the same procedure as for the last two cases,

$$\frac{dc}{dt} = A'' \sigma_\infty^2 \alpha \pi c \tag{108}$$

where A'' is a constant. Then

$$\int_{c_o}^{c_c} \frac{dc}{c} = A'' \sigma_\infty^2 \alpha \pi \int_o^{t_F} dt \tag{109}$$

so that by integrating Equation (109) and using (101), the total time to failure for the corrosion growth rate shown in Equation (108) is given by

$$t_F = t_i + \frac{1}{A'' \sigma_\infty^2 \pi \alpha} \ln \left\{ \frac{E \mathcal{G}_c}{\alpha \pi \sigma_\infty^2 c_o} \right\} \tag{110}$$

To summarize the preceding, it was shown how the principles of fracture mechanics can be utilized to compute the total time to failure under conditions of stress corrosion. The resulting equations are given in Equations (104), (107), and (110).

Acoustic Emission. The crack growth that occurs under conditions of stress corrosion cracking can be monitored through the presence of stress wave emissions (S.W.E.). Therefore the use of acoustic emission to accurately establish incubation time in stress corrosion cracking, such as for hydrogen induced cracking, becomes apparent. Gerberich and Hartbower (1967) have reported some results using this technique, and a few aspects of their investigation will be discussed below. The incubation time in question here is the time required for a crack to reinitiate from an initially existing fatigue precrack with stress corrosion cracking as the causative agent. In other words, the standard experimental fracture mechanics approach will be followed. During growth of the crack, the emissions may be monitored conveniently using acoustic detection methods. These experimental data may then be used to establish or verify some theoretical approach. One such analytical approach will be shown below and although some of the analysis is rather crude, it is certainly not an exercise in academic futility.

The discussion will be specifically concerned with hydrogen embrittlement. Hydrogen-induced cracking comes about because of the diffusion of the hydrogen atom into the lattice for a specific critical distance S* ahead of the crack tip. When the hydrogen concentration C becomes critical

(C_{cr}), then the matrix will fail over the distance S* when subjected to a load. Immediately at the new crack tip, the hydrogen concentration is assumed to be at the initial value C_o so that the diffusion process starts all over and repeats. It is assumed that the small crack advances S* occur at constant time intervals Δt_s. If the diffusivity D_f of the hydrogen into the lattice is known, then the buildup in C is governed approximately by

$$\frac{C_{cr} - C_o}{C_o} \cdot S^{*2} \approx 4 D_f \Delta t_s \tag{111}$$

Based on some experimental evidence, i.e., the average facet size observed in the electron microscope, a value for S* was obtained empirically and is given by

$$S^* \approx \frac{C_{cr}}{C_o} d \tag{112}$$

where d is the average facet size as observed in the electron fractographs. It should be noted that the diffusivity D_f can be reduced by an order of magnitude (or two) if hydrogen traps are present (Coe and Moreton, 1967). One necessary condition for local crack growth can be obtained by assuming that such an order of magnitude reduction occurs. Then the incubation time to initiate a local failure over a distance S* may be computed as

$$\Delta t_s \approx \frac{(C_{cr} - C_o) C_{cr}^2 d^2}{40 C_o^3 D_f} \tag{113}$$

In addition to Equation (113), a minimum stress level must be achieved. Such a minimum stress requirement is satisfied in terms of a critical crack tip displacement. It was also experimentally observed, however, that the cracks move in jumps that, for all practical purposes, are equal to the theoretical crack tip displacement. With this knowledge the crack growth rate dc/dt may be computed

$$\frac{dc}{dt} \approx \frac{\ell^*}{\Delta t_s} \tag{114}$$

where ℓ^* is the approximate jump distance. An approximate expression for ℓ^* is obtained by substituting the expression for the theoretical crack tip displacement into the relation between ℓ^* and the crack tip displacement.

The result is

$$\ell^* = \frac{K_I^2}{m \sigma_o E \pi \varepsilon_f} \tag{115}$$

where K_I is the stress intensity factor, $m \approx 1$ for plane stress and $m \approx 2$ for plane strain, and ε_f is the fracture ductility. Combination of Equations (113), (114), and (115) results in an approximate expression for the growth rate

$$\frac{dc}{dt} \approx \frac{40 K_I^2 C_o^3 D_f}{m \sigma_o E \pi \varepsilon_f (C_{cr} - C_o) C_{cr}^2 d} \tag{116}$$

The importance of Equation (116) is that it provides a theoretical picture of the stress corrosion process due to hydrogen embrittlement. Additionally the equation can be verified using acoustic emissions. One such comparison has been shown in Figure 72. This approach indicates another path which may be followed in an attempt to understand the phenomenon of stress corrosion cracking despite the fact that some significant approximations were used. It seems apparent also that without the use of acoustic emission detection equipment, the problem of studying initiation times and growth rate of a single crack is a formidable experimental problem.

Inhibiting Agents to Hydrogen Embrittlement. The corrosion effect of hydrogen on various high strength steels is affected by the availability of hydrogen to the corrosion process. For example, Johnson and Wilner (1965) found that relative humidity had a significant effect on the relation between the crack growth rate in H-11 steel and the stress intensity as shown in Figure 71. Note, however, that not much variation in growth rate with the stress intensity occurred for relative humidities above 56 percent. This is thought to be due to condensation at the crack tip. In other words, the crack tip is thought to be in a liquid (water) environment for relative humidities in excess of 56 percent, and so no significant changes

in crack growth rate would be expected among the higher humidities. Another study (Hancock and Johnson, 1966) showed the effect of pure hydrogen and additions of various mixtures of argon, nitrogen, and oxygen. Results of these studies have been presented in Figures 73-76. As shown in Figure 73, the effect of hydrogen is certainly dramatic compared to that of humidified argon. The effect of oxygen in combination with nitrogen (Figure 74), with hydrogen (Figure 75) and with argon (Figure 76) indicates the beneficial influence of oxygen in slowing down the process of hydrogen embrittlement. It is important to note in Figure 73 that the molecular hydrogen is at atmospheric pressure. When comparing the results of Figure 73 with similar results obtained in water or in an electrolytic charging condition, it is found that hydrogen at atmospheric pressure induces a more severe brittleness in high-strength steels. This observation led Johnson (1967) to the conclusion that the pressure mechanism* of hydrogen embrittlement is not operative in high strength steels.

Self-Stress. Stress corrosion cracking has certain requirements** that need to be satisfied. One of these is the existence of a tensile stress at the crack tip. The possibility of stresses induced by processes other than applied or residual stresses therefore becomes of great significance. Nielsen (1959) suggested that corrosion products at the crack tip could build up sufficiently so that a wedging action would establish the desired stress level at the crack tip. In fact, Pickering et al. (1962) measured stress levels of 4000 to 7000 psi caused by corrosion products in autoclave tests at 400 F.

More recently Vanderveldt (unpublished results, 1970) found that even with applied compressive stresses, tensile stresses at the crack tip could be introduced due to wedging action. The specific geometry used in a computer program is shown in Figure 77. Bending loads were applied as shown in Figure 77 so that the nominal bending stress at the outer fiber

---

*See page 154.

**See page 151.

equalled - 0.5 σ_o or so that the applied stress intensity at the crack tip equalled - 50 ksi $\sqrt{in.}$. Two wedges of d = 0.001 in. and d = 0.005 in. were studied. With d = 0.001 in., the resulting stresses at the crack tip were still compressive, but with d = 0.005 in., the stresses were tensile. Considering that the corrosion products can build up over a long period of time in many corrosion problems, the possibility of tensile stresses at nominally compressively loaded cracks becomes an alarming possibility. Hydrostatic pressure could force corrosion products into a crack and thus careful attention is warranted in this area particularly for submersibles.

Fatigue

The fatigue life of materials as determined from various types of tests is affected by the air in which the material is tested. This has been known for almost 40 years (Gough and Sopurith, 1932). Beyond that, the precise mechanism of corrosion in fatigue has been examined but is still not very well defined. Achter (1967) observed that the major effect of the environment for a number of metals is on the crack propagation phase rather than the crack initiation phase. On the other hand, Gross (1963) and more recently Schwab and Czyryca (1968) found that the crack initiation phase for a wide range of metals may be considerably shortened in the presence of salt water environment as demonstrated on the basis of smooth laboratory specimens. Studies of fatigue under conditions of stress corrosion indicate that the relative magnitude of ΔK_I with respect to K_{ISCC} is important. For example, Johnson and Paris (1968) noted that above the threshold K_{ISCC}, corrosion cracking is so rapid that it governs the life of the structure; furthermore, below the threshold, the phenomenon is more precisely described as an environment-accelerated fatigue crack. In addition, the frequency of the fatigue loading may be so high that the effect of corrosion on the fatigue is completely overshadowed by the effect of the fatigue in the absence of the corrosive environment.

It seems appropriate at this time to point out that at ultra-high testing frequencies, which are sometimes utilized in laboratory testing, the inertia effects of the environment alone might prevent an interaction between the material and the environment. Hence the use of laboratory data

on crack growth rates due to corrosion influenced fatigue obtained at high frequencies may not be conservative when applied to service life predictions.

Wei and Landes (1969) have recently suggested a simple quantitative method for estimating the effects of aggressive environments on fatigue-crack growth in high strength steels. This method will be briefly reviewed because of its obvious significance to the area of corrosion fatigue. It consists of the algebraic addition of the rate of fatigue crack growth in an inert reference environment $(\Delta a/\Delta N)_r$ to an environmental component which is computed from sustained-load crack growth data obtained in an identical aggressive environment and the load profile represented by $K_I(t)$ as shown in Figure 78.

Mathematically the concept is

$$\left(\frac{\Delta a}{\Delta N}\right)_c = \left(\frac{\Delta a}{\Delta N}\right)_r + \int_\tau K_I(t)\,\frac{da}{dt}\,dt \qquad (117)$$

where $\Delta a/\Delta N$ is the growth per cycle, the subscript c refers to the aggressive environment, and the subscript r refers to the reference environment; $K_I(t)$ is the load profile during a typical fatigue cycle, da/dt is the rate of environment induced crack growth under sustained stress intensity* (see Figure 78) and τ is the period of one fatigue cycle. Equation (117) has a number of interesting characteristics. The crack growth term for the reference environment need be determined only once and then can be used independent of the corrosive media. The $K_I(t)$ versus da/dt is a

---

*If there is a threshold stress intensity K_{ISCC} below which da/dt = 0, Equation (117) and Figure 78 imply that the growth rate $(da/dn)_c$ is not affected by the environment whenever $(K_I)_{max} < K_{ISCC}$. Gallagher (1970) indicates, however, that Equation (117) is not applicable in such a case since pronounced cyclic frequency effects have been observed in fatigue tests of HY-80 tested in a salt water environment between 0 and a maximum tensile load when $(K_I)_{max}$ was kept below K_{ISCC}. (See, for example, Figure 87 given later). Consequently future research should supply growth rates da/dt above and below K_{ISCC} as well as at K_{ISCC}. The need to develop semiempirical or analytical models to predict fatigue growth well below K_{ISCC} is needed if da/dt rates below K_{ISCC} cannot be supplied.

relationship determined under sustained stress intensity. Finally, it is clear that the frequency effect is considered since τ is dependent on the frequency. Wei and Landes compared their equation with experimental results and got remarkable agreement considering the fairly crude approach of their calculation. Some of their results have been reproduced in Figure 79.

A discussion on the role of environment was avoided in the previous discussion of empirical fatigue crack propagation laws. It can now be emphasized that such laws do not explicitly recognize the effect of the environment. Thus a given law may satisfactorily represent a broad range of data (as a function of cyclic and maximum load amplitude) under a given cyclic frequency and environment but fail to fit the data when the testing frequency and/or environment have changed. A case in point is the Forman equation discussed on page 101. Hartman and Schijve (1970) have found that such functional relationships cannot be made to fit the data at least for some materials under specific environmental conditions. In Figure 80 the straight line representing Forman's equation fails to predict the shape of growth rate curves in wet air although the equation does give an excellent representation for data from the same specimen for 7075-T6 aluminum when tested in dry air (see Figure 54).

The effect of cyclic frequency also influences the crack propagation considerably as has been shown in Figure 81. First, the influence of the wet air environment appears to cause a deviation from a straight line (as already shown in Figure 80). Second, the cyclic frequency is seen to affect the crack growth rates.

Hartman and Schijve have also shown the existence of a threshold value of stress intensity factor ΔK_e for this material.* More importantly, they showed how the lower inflection point in the growth data may be accounted for by modifying Forman's equation in the form:

$$\frac{da}{dN} = \frac{C_1(\Delta K_I - \Delta K_e)^{m_1}}{(1-\bar{R})\ K_c - \Delta K_I} \qquad (118)$$

---

*The concept of ΔK_e was introduced on page 90. It should be noted however that ΔK_e may depend on the testing frequency and environment as do other constants in the semiempirical equations. It may also depend on $\bar{R}$.

As shown in Figure 82 this leads to a linear plot. Such a form may also be applicable to other materials that exhibit an approach to the threshold value as reflected in the lower inflection point.

Fatigue Striations

Before proceeding to the next section, it is of interest to discuss fatigue striations that have been exhibited by some materials. An interesting explanation for the presence of striations has been forwarded by Pelloux (1969). In essence, he considers that striations are formed in ductile failures and consequently that the plasticity solution of the mechanics of deformation holds (McClintock and Pelloux, 1968). A crack such as pictured in Figure 83 will therefore extend due to an irreversible slip mechanism along lines AB or AC. If slip occurs along AC as shown, then some strain hardening will occur on that plane so that slip direction will change and proceed along AB. An alternating load experienced during fatigue loading can cause opening and closing of the crack surface (see Figure 84), so that oxidation might occur and prevent crack closure. Prevention of crack closure will enhance the formation of steps when the next cycle of loading is applied. Consequently, no steps should be observed in vacuum where no oxidation (corrosion) occurs. Pelloux verified his theory by experimental observations on some aluminum (2024 T3, 7075 T6) and titanium (Ti-6Al-4V) alloys.

Nielsen (1970) offered another explanation of the striation formation process. In short, he believes that striations are the result of corrosion tunneling. Consequently, it becomes apparent that care must be exercised in the interpretation of the striation patterns. If the Nielsen explanation is correct, then the existence of striations can be used to establish the corrosion mechanism in addition to the fact that corrosion did indeed occur.

Finally, the fractographic examinations that are used to establish the existence of striations must be done with a great deal of care. For example, the experimental handling of the fractographs can make a considerable difference. The inclination of the observation is important as indicated in a recent paper by Broek (1970). It may indeed become necessary to introduce the use of "tilt angle" fractographs in future fractographic analysis.

Ambient Pressure

The application of stress corrosion data to deep submergence vehicles is of prime interest to the Navy's deep submergence program. Yet, the data are rather scarce on the effect of ambient pressure on stress corrosion characteristics. De Hart and Liebowitz (1968) did an exploratory study on the effect of ambient pressure on the susceptibility of a material to stress corrosion. Their results appear to indicate that material may become less susceptible to stress corrosion at high ambient pressure (10,000 psi). It behooves the Navy to study the effect of stress corrosion at high ambient pressures.

Strain-Hardening Coefficient

Plastic flow will occur in the vicinity of the crack tip unless the material is perfectly brittle. Consequently, the effect of plasticity may play a significant role in the fracture process for most materials. Naturally, this influence extends into the realm of corrosion. Some recent work by Spretnak and Griffis (1969) indicates that plastic behavior at the crack tip may be significantly affected by corrosion processes. Similar phenomena were eluded to by Hahn et al (December, 1969). Details of the analysis by Hahn et al. were discussed earlier in this paper. Suffice it here to recall that two mechanisms of crack advance were discussed, namely (1) irreversible plastic blunting and (2) damage accumulation. Hahn et al. pointed out that corrosive environments greatly enhanced the crack growth rate in Region No. 1, i.e., the high-cycle, low-stress region. Based on this observation they concluded that the observed effect is easiest to rationalize in terms of rupture, i.e., damage accumulation. In addition, it will be recalled that environment-induced cracking does not give the appearance of a plastic failure but instead frequently looks like a brittle-type fracture.

In light of the above comments, it seems useful to point out the correlation between the strain-harding coefficient, plastic flow and fracture toughness as discussed previously on page 49. Useful future effort might be directed towards correlation studies of the effect of corrosion and its effect on the strain-hardening coefficient in the region immediately at the crack tip.

SOME SPECIFIC METALS AND ENVIRONMENTS

The available literature on stress corrosion studies that consider specific metals and environments is so voluminous as to force a considerable condensation of the material. The ASTM STP 425 deals with stress corrosion testing, the NACE Journal Corrosion, and various fracture mechanics journals such as Engineering Fracture Mechanics are just a few of the many references available. It is difficult to summarize the various studies concisely because at present there is no unifying theory which can tie the various results into a condensed package. Consequently, only some of the more prominent results will be pointed out.

Steels. High strength steels are susceptible to stress corrosion cracking, and such problems in high strength steel are usually due to a high favorability for hydrogen reduction. Consequently it may be said that hydrogen is the cause for the S.C.C. in high strength steels (Brown, 1969). Protective systems are used to prevent S.C.C. However, as will be pointed out again subsequently, cathodic protection is one approach that is not suitable for high strength steels.

The Navy has determined values of K_{ISCC} for various high strength steel alloys. Some of these are shown in Figure 85, which was originally presented by Sandoz (1970). The straight lines in Figure 85 establish critical crack depths for long surface flaws as determined from Equation (91) with $\sigma = \sigma_o$ and $\phi^2 = 1.0$. The interpretation of Figure 85 is straightforward for long surface flaws subjected to a tensile stress. For example, if available inspection techniques are capable of detecting only long surface flaws at least 0.01 in. deep, then only materials with characteristics that lie above the line a = 0.01 in. (as shown in Figure 85) will be acceptable.

Frequently data are given which show the crack growth rate as a function of various parameters. The effect of stress intensity on the rate of crack growth is of particular interest. A typical example is shown in Figure 86 (Peterson et al., 1967). Note in this last example that the load is statically applied and is not a fatigue load.

Some cases of crack branching in steels due to stress corrosion cracking have been observed. However it was found that K_{IC} had to be less

than twice K_{ISCC} for branching rather than rapid brittle fracture to occur in some high strength steels (Carter, 1969). This observation is significant since the branching mechanism is more efficient in absorbing energy than is available for brittle fracture.

In the manufacture of high strength steel pressure hulls, frequent use is made of welding. Consequently, the corrosion of weldments is an important aspect of submarine structures. The DSRV-2 pressure sphere was welded using HY-140. Tests were conducted on the weldments using synthetic sea water (Romine and Smith, 1968). The results indicated that the welds had a good resistance to stress corrosion cracking, i.e., the critical stress intensity of weldments under corrosion was within 3 percent of the critical stress intensity of the base metal.

Watkinson (1969) suggested that wrought steels based on nickel, molybdenum, and possibly vanadium might be advantageous with respect to the heat-affected zone hydrogen cracking.

An extensive survey (113 references) was recently published on the corrosion resistance of stainless steel weldments (Pinnow and Moskowitz, 1970). It noted that stainless steel weldment corrosion can be related to the metallurgical, chemical, and physical changes introduced during welding.

Stress corrosion effects also influence the behavior of high strength steels that are subjected to fatigue-type loading. For example, the Navy conducted studies on three high strength steels: 9 Ni-4 Co-0.25C, 12 Ni 180-grade maraging, and 18 Ni 200-grade maraging (Crooker and Lange, 1968). The K_{ISCC} was not found to correlate with the fatigue crack growth behavior. The power law of fracture mechanics was satisfied for fatigue crack growth of 9 Ni-4 Co-0.25C, and was approximately the same in air and in water. The power law also held for 12 Ni 180-grade steel but was different in air than in salt water. However the power law held for 18 Ni maraging in air but not in salt water.

Gallagher (1970) studied the effect of corrosion on fatigue crack growth with applied stress intensities above and below the K_{ISCC}. He used 4340 steel to study the behavior above K_{ISCC} and HY-80 steel to determine the effect below K_{ISCC}. Figure 87 shows the results for HY-80 and Figure 88 the results for 4340. The K_{ISCC} for 4340 was approximately 10 ksi - $\sqrt{\text{in.}}$ and the K_{ISCC} for HY-80 was believed to be above 200 ksi $\sqrt{\text{in.}}$

The effect of corrosion was cycle dependent for HY-80 steel at low frequency (< 10 Hz), but as the frequency of cycling increased, corrosion seemed to play a decreasing role during each cycle. The cyclic crack growth was cycle independent for the 4340 steel (ΔK_I was above K_{ISCC}) and simply approached the cycle-dependent behavior found in a vacuum. The effect of cycling above K_{ISCC} is thus seen to allow the environmental attack to control the rate of crack growth.

An interesting study in corrosion-fatigue crack propagation was also done by Barsom (1969). He noted that frequency had a considerable effect on the crack growth rate under a corrosive environment; e.g., see Figure 89. He found this effect for 12 Ni-5 Cr-3 Mo maraging steel in a 3-percent NaCl solution despite the fact that this material has a negligible strain rate sentivity. Barsom suggested the following relationship to predict the corrosion fatigue crack growth

$$\frac{da}{dN} = D(t)\ (\Delta \mathcal{G}) \tag{119}$$

where D(t) is a time- (or frequency-dependent) function which decreases in magnitude with increasing cyclic-stress frequency and ΔG is the range of the energy release rate. Recalling out discussion on elasto-plastic analysis we note that $\Delta \mathcal{G}$ may also be expressed in terms of the square of the stress intensity factor ΔK_I^2 or in terms of the cyclic crack opening displacement $\delta_t^{(c)}$. The effect of the inertia of the corrosive media may, of course, be one reason why less stress corrosion occurred at higher cyclic rates.

Barsom recently published additional corrosion studies (1970) dealing with 12 Ni-5 Cr-3 Mo steel which indicated that hydrogen embrittlement caused acceleration of a fatigue crack in a corrosive environment (3-percent NaCl). His results confirmed that cathodic protection was not effective on this high strength steel particularly as the crack depth increased. Figure 87 had indicated the same results for HY-80 steel. Barsom argued, furthermore, that hydrogen embrittlement accelerates corrosion-fatigue crack propagation because it affects the ductility of the material.

Freedman (1970) published data on 23 combinations of material (high strength ferrous alloys), heat treatment, and welding. He concluded that use of the WOL and SEN gave valid K_{ISCC} measurements in a relatively short time (<1000 hours) compared to long-duration corrosion tests (many months).

It should be noted however that Freedman did not appear to have controlled the electrochemical factors that are involved, e.g., the potential. He did take precautions, however, to ensure that the accelerated specimens were insulated from the container.

A final observation should be made on the use of fracture mechanics specimens in stress corrosion tests. The amount of information obtained in a single test can be significantly increased by use of stress wave emission monitoring (SWEM) methods (Reuter and Hartbower, 1970). The acoustic emission method is still in the infantile stage, although significant advances are being made by a number of investigators.

The present discussion has been limited to high strength steels because the ferrous materials that are of primary concern fall into that category. Naturally, the discussion has been quite condensed even with regard to high strength steel. Additional information dealing with specific environments, heat treatments, and material compositions (including low strength steels) may be found in a report by Gall (1970).

Aluminum Alloys

The problem of highlighting the stress corrosion aspects of aluminum alloys is no less formidable than it is for steels. In general the corrosion resistance of aluminum increases with increasing purity of the aluminum. The reason for this corrosion resistance of pure aluminum is that an aluminum oxide film forms on the surface. Application of a pure aluminum layer to the outside of an aluminum alloy will therefore enhance the corrosion resistance of the alloy. Increasing the thickness of the oxide layer will also reduce the chance of failure of the protective layers due to gouging or other means. Aluminum and its alloys can also be cathodically protected because of their electromotive characteristics.

Hyatt (1967) examined a number of aluminum alloys in a 3.5-percent NaCl solution and checked the crack growth rate at specific stress intensities. The results are shown in Figure 90. The need for evaluation of particular alloys under specific conditions is evident from Figure 90. Some specific comments useful to designers on individual aluminum alloy series have been made by Gall (1970). LaQue (1969) reported that at deep depths the ocean environment greatly accelerates the corrosive attack on

aluminum alloys. This definitely indicates the need for studying the effect of hydrostatic pressure on the stress corrosion cracking characteristics of aluminum and its alloys.

Feeney (1969) studied the effects of environment on the fatigue crack propagation characteristics of three aluminum alloys (2024-T3, 7075-T6, and 7178-T6). His principal results indicated that environmental sensitivity was most pronounced at small excursions of the stress intensity values, i.e., at small values of ΔK_I. Furthermore, the power law of fracture mechanics used to predict fatigue crack propagation characteristics could not always adequately describe fatigue crack propagation in these aluminum alloys. As indicated on page 173, Hartman and Schijve (1970) obtained similar indications for 7075-T6 and 2024-T3 Alclad aluminum as shown in Figures 80-82. Some of the references cited, e.g., Gall (1970) and LaQue (1969) will give a good starting point for obtaining specific behavioral properties of aluminum alloys. Underlying analytical considerations for aluminum alloys do not appear to exist except for general comments such as that by LaQue: "... preference should be given to alloys that do not release soluble copper or other heavy metal corrosion products." The power of the position in the electromotive or in the galvanic series of aluminum should always be considered in corrosion problems, as it should for any metal.

Titanium Alloys

Titanium is particularly attractive to the needs of the Navy because of its high strength-to-weight ratio. The stress corrosion characteristics of titanium and its alloys are not always acceptable, however. The nature of the corrosion process in titanium is not resolved; recent studies indicate that the process may be a discontinuous one, despite the possibility that the electrochemical mechanism may be the triggering device for the discontinuous process (Katz and Gerberich, 1970).

Regardless of the exact mechanism, three conditions must be met in order for stress-corrosion cracking to occur: an agressive environment, a flaw of sufficient size and acuity, and a stress of sufficient magnitude (Brown et al., 1965).

The Navy has conducted stress corrosion studies on a large number of titanium alloys (Judy and Goode, 1967 and Goode et al., 1967). Some of the results have been presented here. Table 3 shows the stress corrosion characteristics for some titanium alloys. K_{Ix} is the fracture toughness value obtained when testing in air. The environment used for the K_{ISCC} determination was a 3 1/2-wt-percent NaCl solution. Figure 91 shows a plot of K_{ISCC} values versus the yield strength for a number of titanium alloys. No results for weldments are given here, but they are available in Judy and Goode (1967). In general, however, the K_{ISCC} for welded material was lower than K_{ISCC} for the baseplate.

Some of the features in Table 3 and Figure 91 are worth emphasizing. Other mechanical properties shown there do not correlate with K_{ISCC} values. Results for K_{ISCC} obtained in simulated and actual sea water showed good agreement. It is of interest to note that all the alloys shown in Table 3 are subject to some degree of stress corrosion in a 3 1/2 percent by weight solution of NaCl. Furthermore, the results indicate that the presence of molybdenum as an alloying component improves the stress corrosion resistance of the titanium alloy. In fatigue on the other hand, when crack growth rates in air were compared with those in salt water, at least one alloy, Ti-7 Al-2.5 Mo, exhibited environmentally accelerated crack growth over a ΔK_I ranging from about 25 to 75 ksi $\sqrt{in}$. (Crooker et al., 1970). Although five out of six titanium alloys studied exhibited a low resistance* to fatigue crack growth in air, there was a marked absence of environmentally accelerated crack growth. In the same study (Crooker et al., 1970) a limited amount of fractographic analysis indicated that water vapor was not the probable cause for the low fatigue crack growth resistance of the titanium alloys studied, thus supporting the lack of influence of the environment. Finally, the effect of corrosion on the maximum compressive strength of various titanium alloy skin-stringer panels is discussed by Gardner and Royster, 1970.

---

*Crack growth rate (da/dN) data plotted as a function of stress-intensity factor range (ΔK_I) on log-log coordinates generally followed steep slopes ranging from 4:1 to 10:1.

In conclusion, it is emphasized that care must be exercised to ensure that stress corrosion investigations really study a general stress corrosion-dependent phenomenon and not some other event. To ensure that correct conclusions are reached, a knowledge of the precise alloy and the exact environment must be considered as well as the possible beneficial or degrading interaction between various elements of alloy and environment.

SUMMARY

This report contains a critical review of significant results that have been achieved in various aspects of fracture and fatigue analysis and indicates problems that still have to be solved. The emphasis throughout has generally been placed on the tensile loading of simple configurations; however, it is felt that such a review will also establish the required technical base for applications to the fatigue analysis of submarine hulls. Major elements of the report as well as some general conclusions are summarized below.

The first part of the report deals with the stress analysis and fracture criteria of plates and shells with stationary cracks. It begins with a description of the basic functional form of the stress distribution in the immediate vicinity of crack tips in an isotropic **elastic solid.** Such localized stress and deformation fields can be uniquely described with the aid of stress intensity factors which reflect both the crack geometry and the character of the applied loading. Significant progress has been achieved in recent years through an increased number of solutions that are available for determining the stress intensity factors. These range from the solution to problems of through cracks in plates and shells to those of embedded cracks in an idealized infinite medium. For problems featuring cracks in complex stress fields and/or structural details, however, recourse must be to numerical methods and mainly the finite element approach. Such techniques should preferably be coupled with an analytical insight into the general character of the expected solution in order to retain sufficient accuracy.

Some of the results from two-dimensional elastic-plastic analysis are reviewed for both the elastic, perfectly plastic and the strain-hardening

idealizations. Not surprisingly, the need for the application of hybrid analytical-numerical analysis mentioned above is manifest to a much greater extent than is the case for elastic problems. Further, the range of the applicability of elastic and the analogous concepts of plastic stress intensity factors in the characterization of gross plasticity features at the crack tip are examined. The most relevant of these features are the size and shape of the plastic zone and the crack opening displacement. When the ratio of the applied stress to yield stress is small, *elastic* stress intensity factors serve as extremely useful correlation parameters to describe the above plasticity features for various geometries. On the other hand, where the extent of the plastic deformation is large, elastic stress intensity factors lose this significance.

Not surprisingly, the analogous situation carries over to the problem of fracture *criteria* (concerned with the determination of critical load/crack size combination required to initiate crack extension) which are discussed subsequent to the above review of the essential features of stress *analysis*. Especially pronounced dependence on the specimen geometry appears when the plastic limit loads are approached. Thus, although one-parameter characterization (critical stress intensity factors, critical crack opening displacement, etc.) suffices in the case of brittle fracture or of small-scale yielding, further research is required to develop the ductile fracture criteria to cover the case of tough materials. Some of the investigations aimed at developing such criteria based on continuum approach but taking into account microstructural aspects are discussed. It appears that for some time in the future, reliance must continue to be placed on one parameter and/or semiempirical methods with due recognition as to the restrictions, conditions, and uncertainties under which they are to be applied. Related problems in ductile fracture concerned with biaxiality and combined mode deformation are particularly in need of clarification.

The second part of the report is concerned with the problem of subcritical crack growth under monotonic and cyclic loading. Some of the inadequacies of the conventional approach to fatigue are emphasized by comparing the application of conventional S-N diagrams (stress amplitude versus cycles to failure) to finite life (low cycle fatigue) and residual strength

prediction in *structures* with their utilization in the screening of materials. This is followed by a discussion of subcritical crack growth under monotonically increasing load due to out-of-plane shear loading. The purpose here is to highlight the need for a similar analysis for growing cracks and the conditions that define terminal crack instability in the tensile mode for tough materials. In this connection, the related concepts of R curves proposed for fracture characterization in Mode I for materials that can tolerate a significant amount of crack extension prior to fracture are also discussed.

Next, current analytical approach to the stress analysis of stationary cracks under cyclic loading is reviewed, particularly the inherent simplifications based on the idea of plastic superposition. Here the review emphasizes the need for full exploitation of numerical techniques which would permit better modeling of the material behavior (cyclic stress-strain curves) and geometric nonlinearities (for example the crack blunting). Eventually, the modeling of running crack under the influence of load reversal thus simulating the events in fatigue crack propagation should also be possible. Interpretation of crack initiation under cyclic loading by means of the localized strain range approach and the recently proposed method based on the stress intensity concept is then discussed. It is concluded that both approaches are in need of further examination. Crack propagation aspects of the fatigue problem are then discussed at length, starting from an overview of relevant experimental results. Crack propagation laws are examined ranging from the semiempirical type based on variants of ranges of stress or strain intensity factors correlations to those based on some of the proposed theoretical models. Such models are based on either the concept of crack tip opening displacement or on the concept of damage accumulation at or ahead of the crack tip. It appears that at present there is no universally applicable law which can encompass the full range of data and be expressible in terms of some fundamental material properties as, for example, those measurable in static tensile test. Nevertheless, the use of semiempirical crack propagation laws generated from the data provided by small (fracture mechanics type) specimens when used under appropriate restrictive conditions should provide a reasonable

estimate of the crack propagation in full-scale structures. There is undoubtedly a need for more research to better define the range of applicability of such semiempirical laws.

The problem of fatigue damage accumulation under variable amplitude loading is then discussed from the standpoint of statistical load history characterization as well as crack initiation and propagation. It is concluded that the conventional cumulative damage theories seem best suited to the prediction of crack initiation phase; crack propagation aspects are best treated via a fracture mechanics approach. It must be admitted, however, that additional work is needed to clarify the transient aspects of crack growth (acceleration and delays following the change of load amplitude) in programmed loading and average crack growth rates in random loading problems. As in the case of the monotonic loading, biaxiality and combined mode deformation are at present relatively unexplored.

Finally, crack initiation and growth are examined under applied cyclic compressive stress. It is concluded that to the extent that the particular material already has been characterized under applied tensile load, the assessment of fatigue damage is reduced primarily to the development of reasonable analytical models relating the fluctuation of local tensile residual stress to the fluctuations of the applied compressive loading.

The last part of the report is concerned with the important effects of the corrosive environment on fracture and fatigue. The stress corrosion theories developed using the fundamental electrochemical approach are briefly reviewed together with an indication of some of the advantages and disadvantages of this approach. This is followed by an analysis of the fracture mechanics approach. The stress corrosion stress intensity factor and the critical crack size under monotonic loading conditions are discussed. It is concluded that the critical stress corrosion stress intensity factor does provide a useful approach. However, its exact determination is in need of clarification and there is still some question as to whether K_{ISCC} is a fundamental material parameter. Various specimen types used to determine K_{ISCC} are presented, and dissolution at the crack tip (change in crack contour) is discussed from a fracture mechanics point of view.

Next, various models of stress corrosion cracking are reviewed with particular emphasis on hydrogen embrittlement. The critical crack tip

opening displacement $(\delta_t)_c$ is utilized to compute the duration of time for the subcritical crack extension due to stress corrosion. The usefulness of the phenomenon of acoustic emissions during stress corrosion studies is pointed out and its application in the determination of stress corrosion mechanisms discussed. Specifically, a theoretical model explaining hydrogen embrittlement is reviewed. Interesting correlations with experimental results using acoustic emissions can be obtained despite the crudeness of the model. Some inhibiting agents to the stress corrosion process are highlighted. Finally the possibility is pointed out that tensile stresses may form at a crack tip due to corrosion products with the application of a compressive stress field. This area requires further study, particularly in hydrostatic environments.

Fatigue in conjunction with stress corrosion is then discussed. A model that uses superposition of the corrosive action during one cycle to the fatigue growth during that cycle is reviewed. The model is promising but at present its applicability is restricted to cycling above the K_{ISCC} value. Other theories are mentioned but as yet, there is none that can satisfactorily explain the action of corrosion with fatigue. Finally an overview of the implications of the existence of striations is presented.

Additionally, the effect of ambient pressure is to have potentially beneficial effects. This aspect and the need for considerable effort to determine the effect of ambient pressure is also pointed out.

Further, the effect of corrosion on the plasticity effects at the notch tip is discussed. In regions of high cycle, low stress, for example, the corrosion effect greatly enhances the crack growth rate. Future effort might therefore be directed to correlation studies between the effect of corrosion and its effect on the strain-hardening coefficient immediately at the crack tip.

Finally, some specific metals and environments are reviewed. More specifically, steel, aluminum, and titanium alloys are highlighted in some detail although the quantity of available information required considerable condensation.

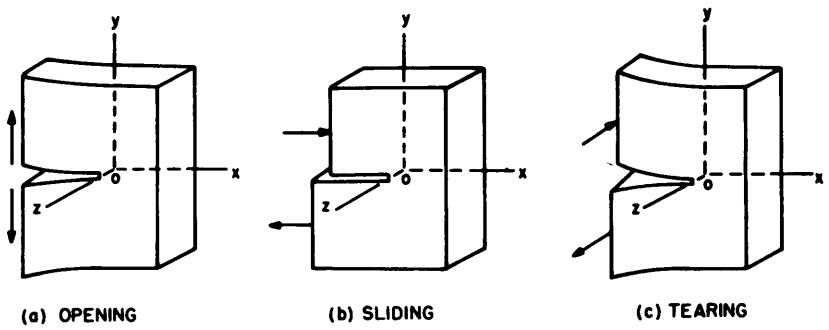

Figure 1 - Basic Modes of Crack Extension
(From Sih and Liebowitz, 1968)

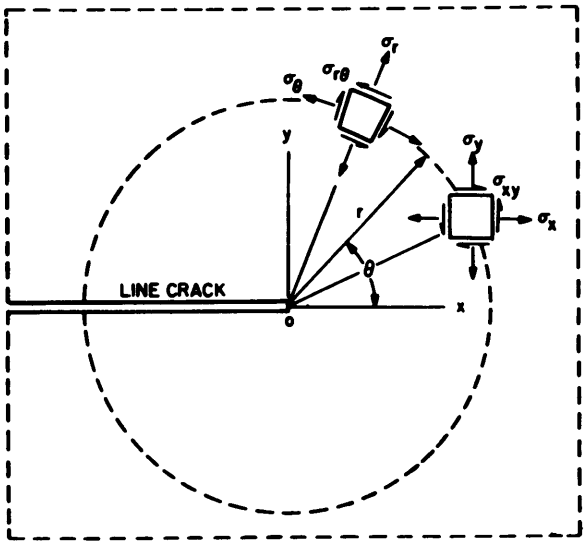

Figure 2 - Polar and Rectangular
Components of Stress Around
Crack Tip
(From Sih and Liebowitz, 1968)

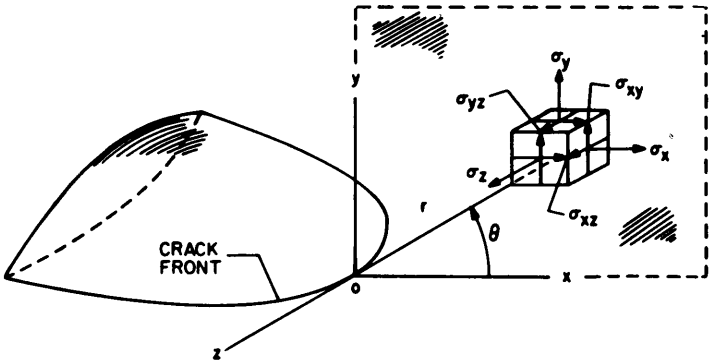

Figure 3 - Local Coordinate System of
Crack-border Stress Components
(From Sih and Liebowitz, 1968)

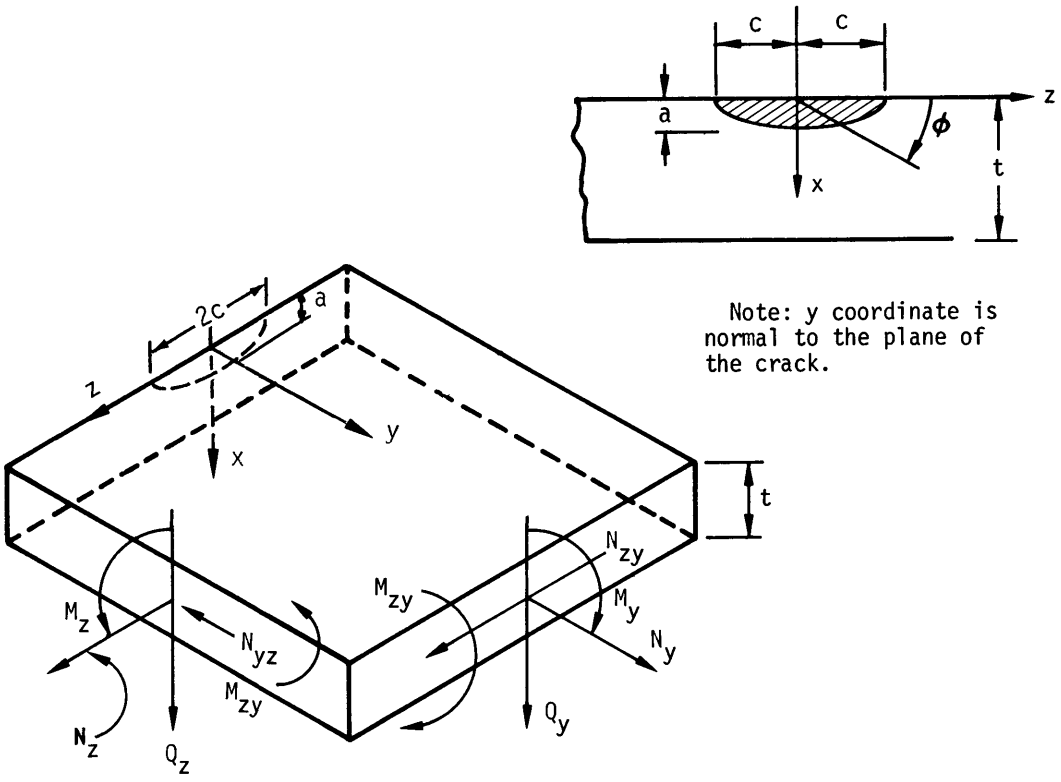

Figure 4 - Shell Element with Elliptical Flaw under General Loading

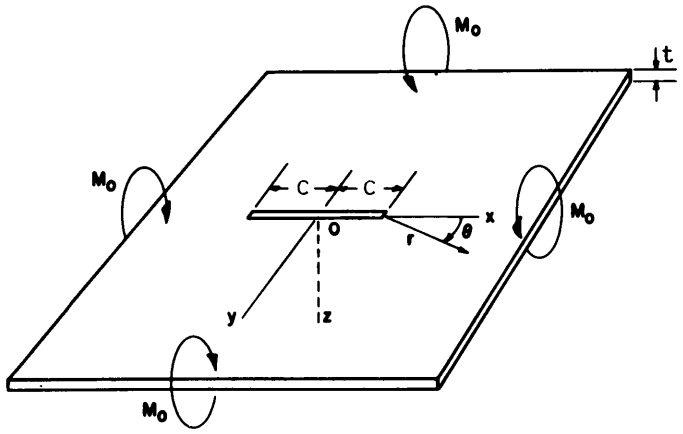

Figure 5 - All-Around Bending of Straight Crack in Flat Plate

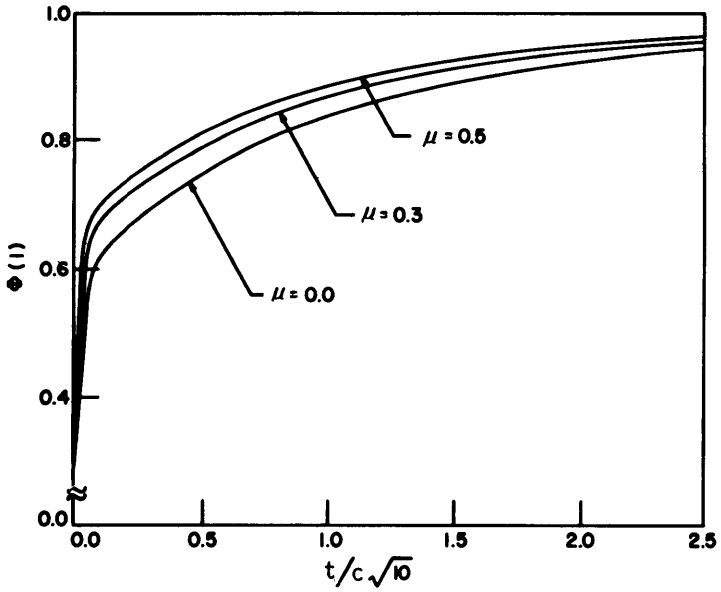

Figure 6 - Magnitude of Local Stresses in Reissner Plate
(From Sih and Liebowitz, 1968)

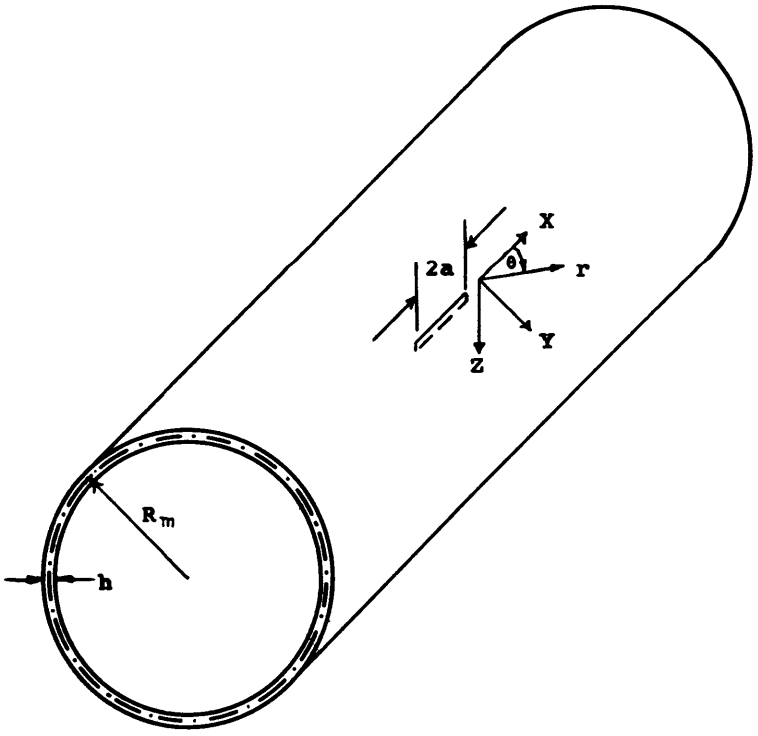

Figure 7 - Internally Pressurized Cylinder with a Through Crack

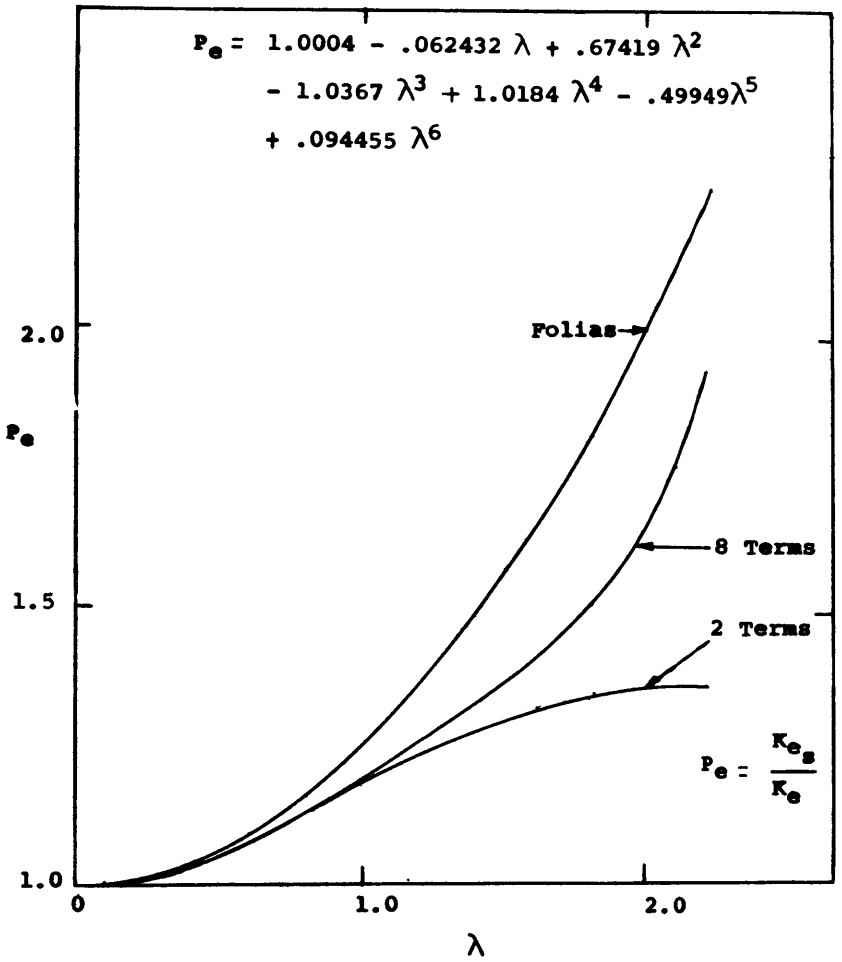

Figure 8 - Stress Intensity Ratio P_e versus λ (Tension)

(From Catanach, 1967)

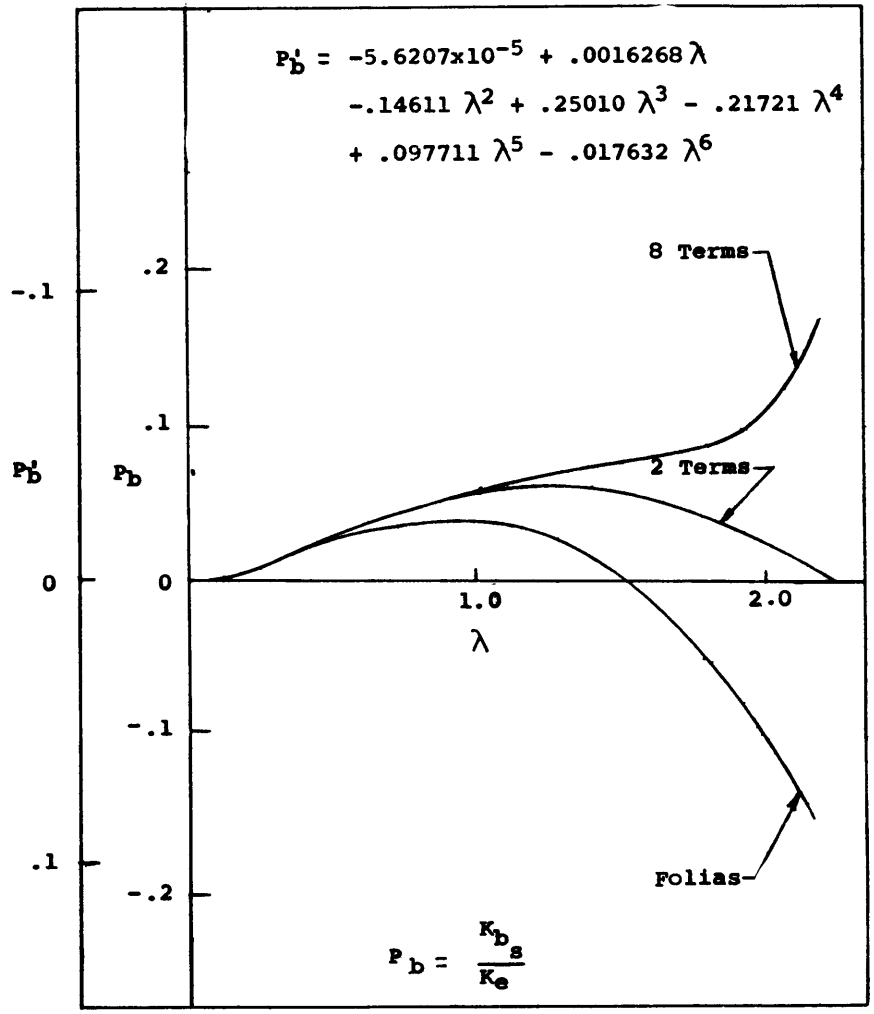

Figure 9 - Stress Intensity Ratio P_b versus λ (Bending)

(From Catanach, 1967)

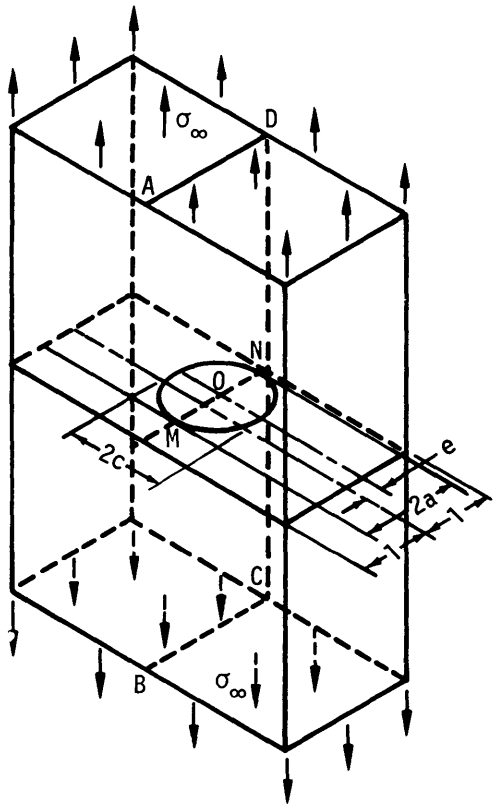

Figure 10 - Elliptical Crack Embedded in a Wall Subjected to Uniaxial Tension

(From Kobayashi et al., 1965)

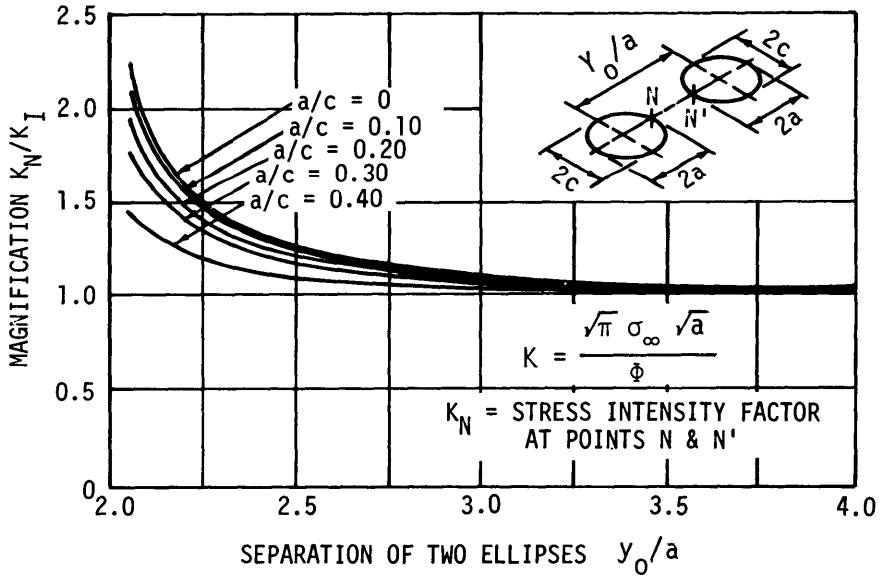

Figure 11 - Magnification Factor for Stress Intensity Factor for Two Coplanar Cracks in Infinite Solid Subjected to Uniaxial Tension

(From Kobayashi et al., 1965)

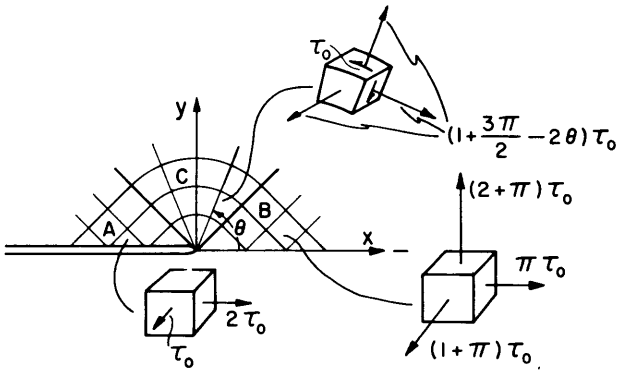

Figure 12 - Slip Line Field Near a Crack Tip in a Plane Strain

(From Rice, 1968 and Drucker and Rice, 1968)

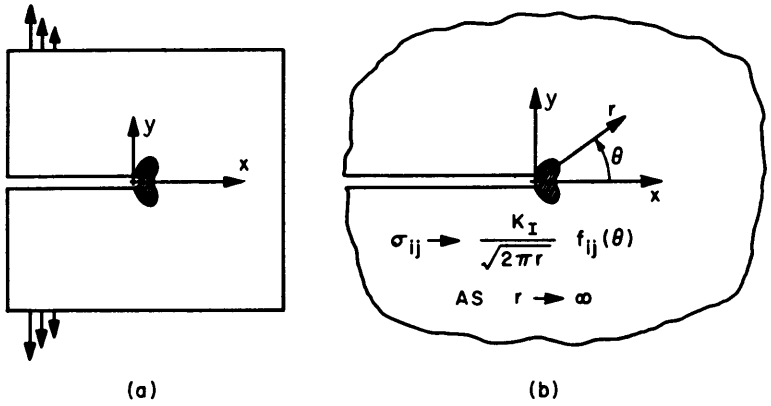

Figure 13 - Small Scale Yielding Formulation

(From Rice, 1968)

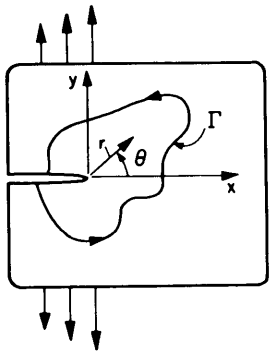

Figure 14 - Crack in Two-Dimensional Deformation Field

(J integral has same value for all paths such as Γ)

(From Rice (1968) and Drucker and Rice (1968))

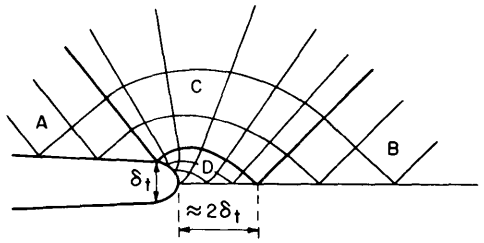

Figure 15a - Large Geometry Changes in Progressive Blunting Create a Small Region D of Intense Deformation which is not Included in a Sharp Crack Analysis Based on Conventional Small Strain Assumptions

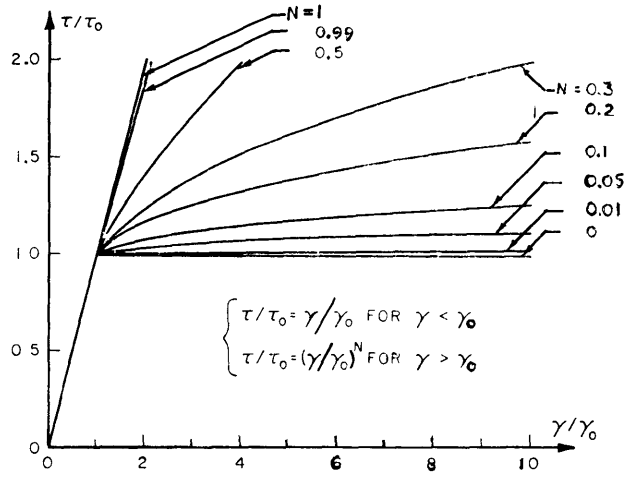

Figure 15b - Power Hardening Law

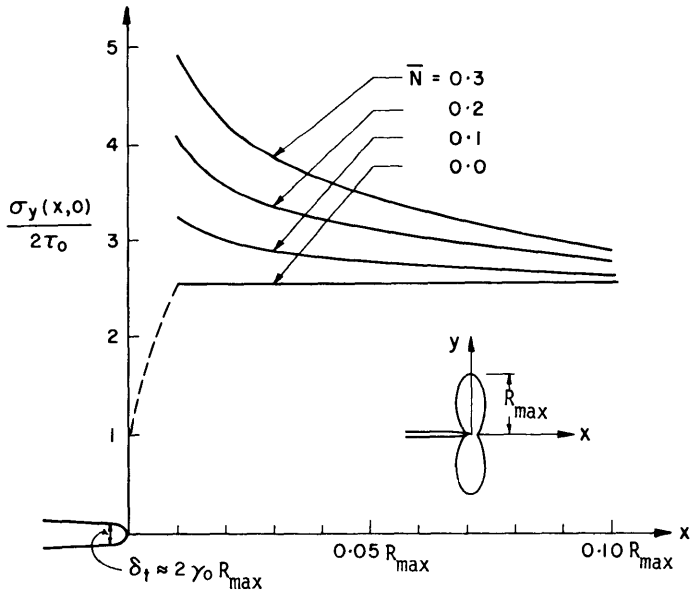

Figure 15c - Tensile Stress Acting Directly Ahead of the Crack Tip for Various Hardening Exponents; Dashed Line Indicates Falloff of Stress in Region Affected by Blunting

Figure 15 - Details of the Very Near Tip Deformation in Plane Strain
(From Rice (1968) and Drucker and Rice (1968))

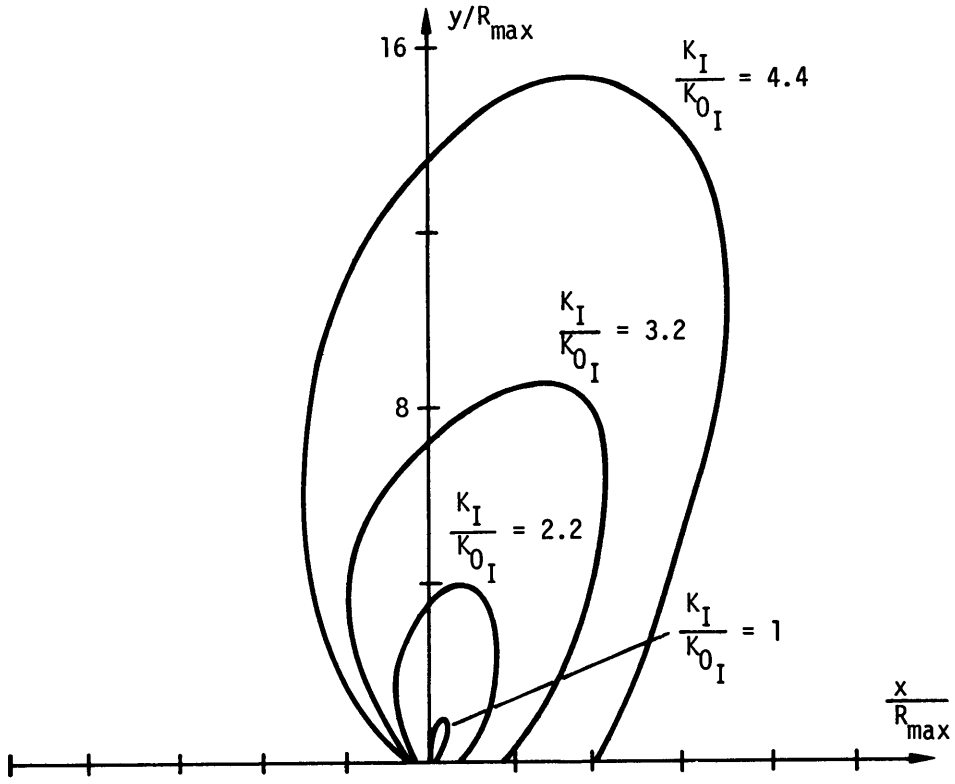

Figure 16 - Extent of the Elastic-Plastic Boundary for Increasing Loading in Plane Strain

(From Ostergren, 1968)

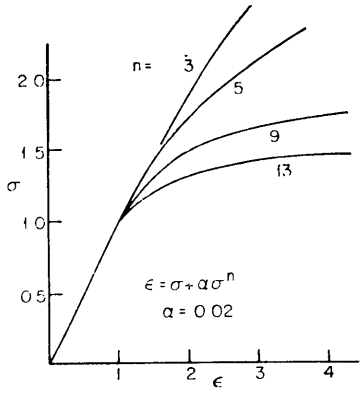

Figure 17 - Ramberg-Osgood-Type Stress-Strain Relation

(From Hutchinson, 1968)

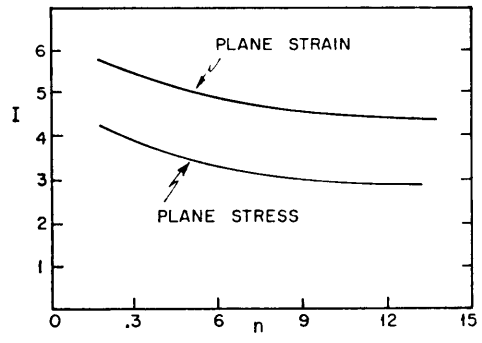

Figure 18 - Values of I versus n (for Equation 23)

(From Hutchinson, 1968)

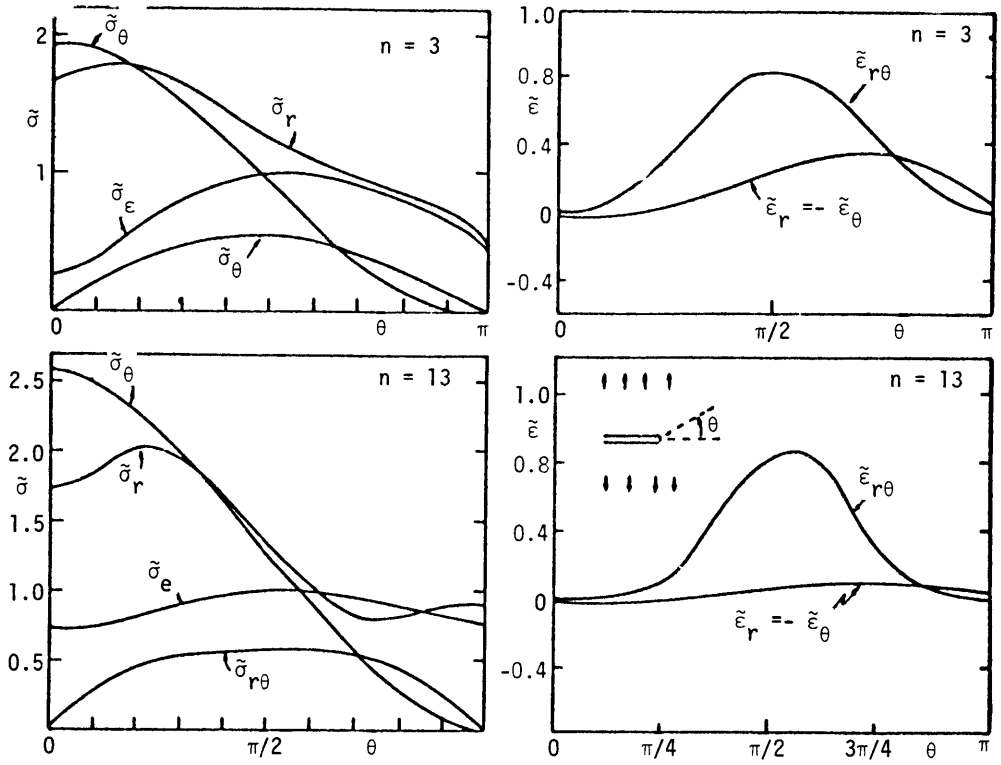

Figure 19 - Angular Variations of Stresses and Strains at the Tip of a Tensile Crack for Plane Strain
(From Hutchinson, 1968)

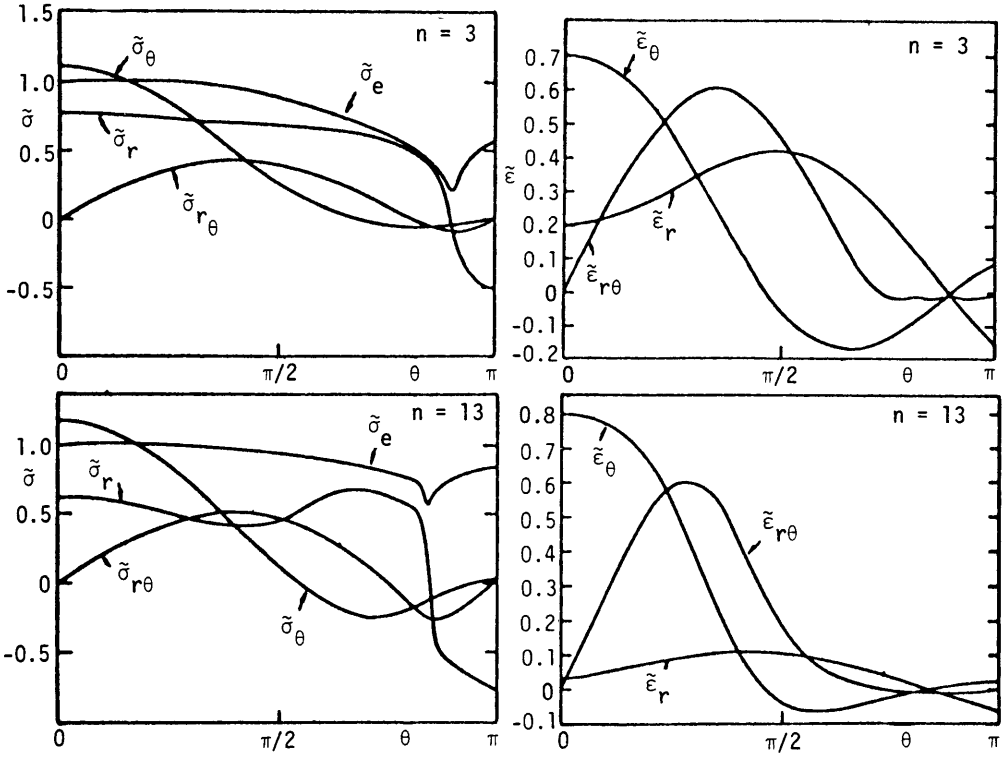

Figure 20 - Angular Variation of Stresses and Strains at the Tip of a Tensile Crack for Plane Stress
(From Hutchinson, April 1968)

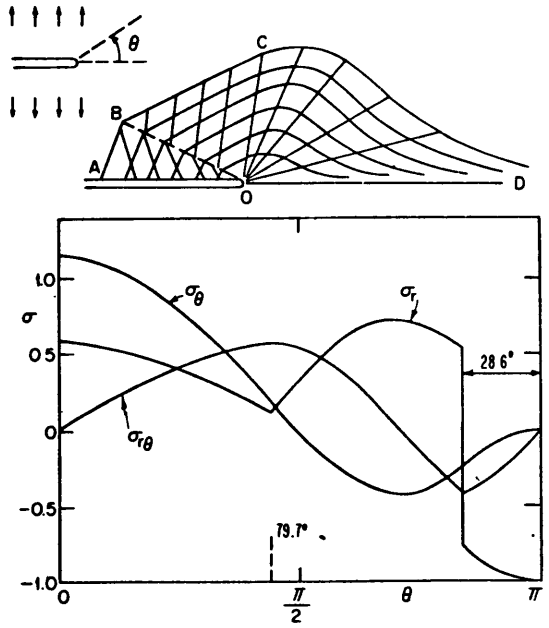

Figure 21 - Stress Characteristics and Stress Distribution at the Tip of a Tensile Crack in a Perfectly Plastic Material for Plane Stress

(From Hutchinson, April 1968)

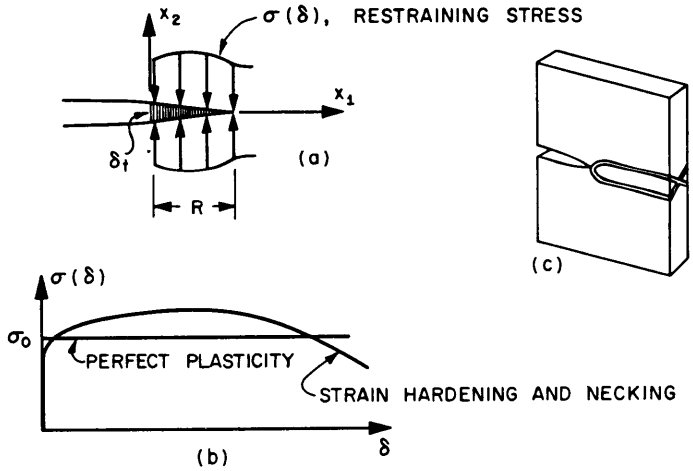

Figure 22 - Dugdale-Barenblatt Model for Plane Stress Yielding

(From Rice, 1968. In (a) above, yielding is viewed as confined to a narrow zone in front of the crack where stresses oppose separation of extended crack surfaces. The sketch labeled (b) shows restraining stress versus separation distance. The sketch labeled (c) gives the physical justification in terms of through-the thickness slip in fully developed plane stress yielding).

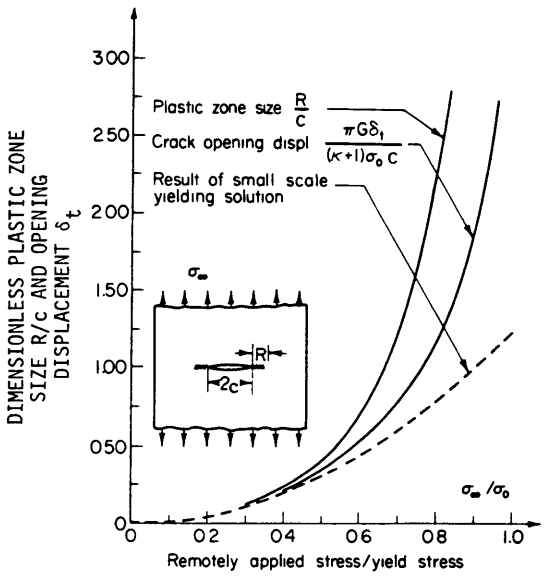

Figure 23 - Variation of Plastic Zone Size and Crack Opening Displacement with Applied Stress for Centrally Notched Plate

(From Rice, 1968 for perfectly plastic Dugdale-Barenblatt model. The dashed line is the result of small-scale yielding approximation.)

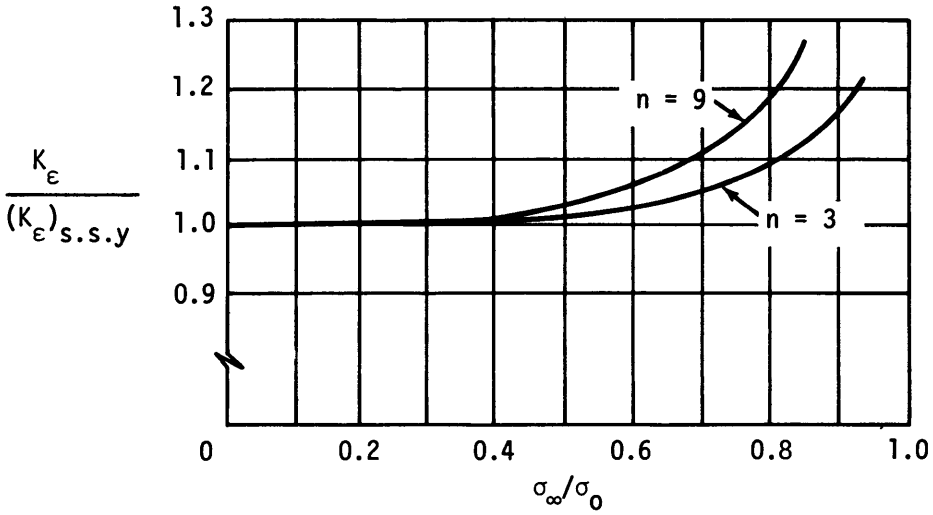

Figure 24 - The Plastic Strain Intensity Factor as a Function of the Applied Stress for Tensile Loading

(From Hilton and Hutchinson, 1969)

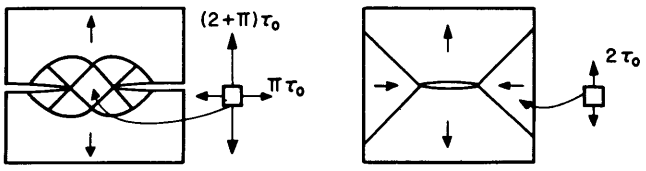

Figure 25 - Fully Plastic Flow Fields in Tension (Plane Strain)

(From Drucker and Rice, 1968)

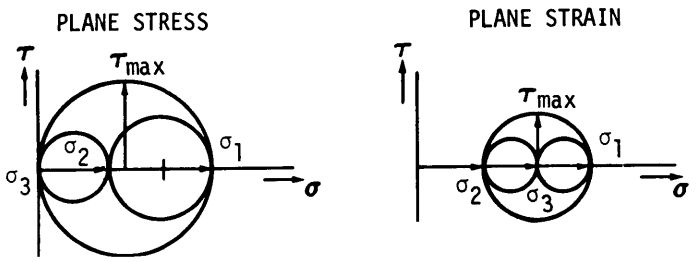

Figure 26a - Stress Condition near the Crack Tip

(Diagrammatically close to the crack tip σ_1 is in the longitudinal direction)

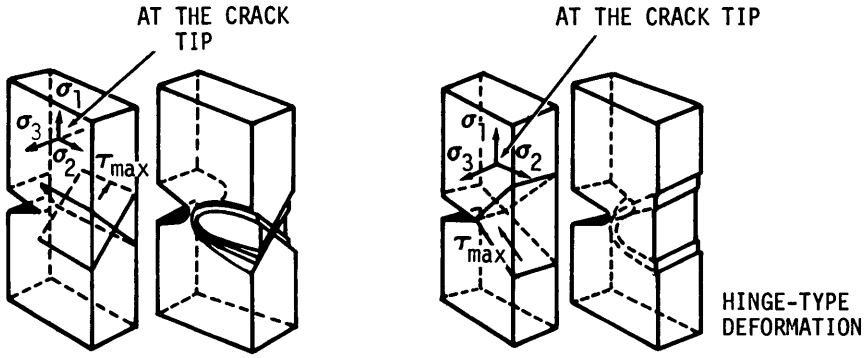

Figure 26b - Plane of τ_{max} and Resulting Shear Deformation

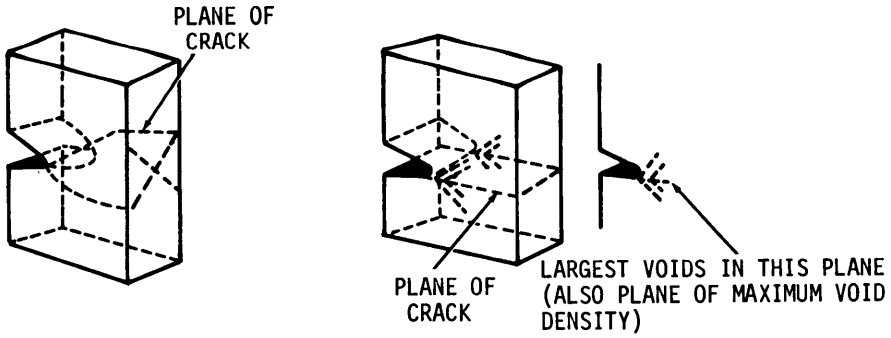

Figure 26c - Microvoid Formation on Planes of Most Extensive Slip and Crack Growth in Planes of Largest Void Concentration

Figure 26 - Slant and Square Fractures as a Result of the State of Stress

(From Broek, 1966)

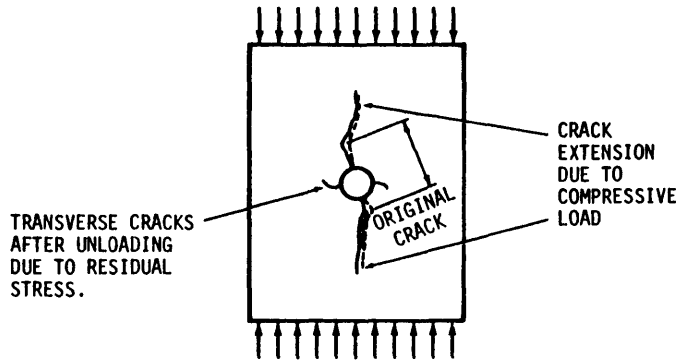

Figure 27 - Crack-Propagation in PMMA under Compression (From Guinand (1961) and the McClintock discussion of a Erdogan and Sih paper, J. Basic Eng., December 1963).

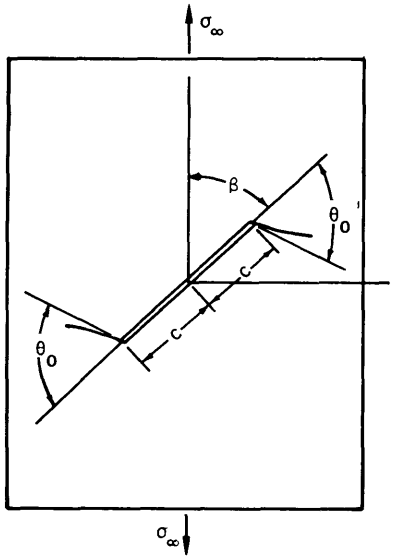

Figure 28a - Cracked Plate under Uniform Tension

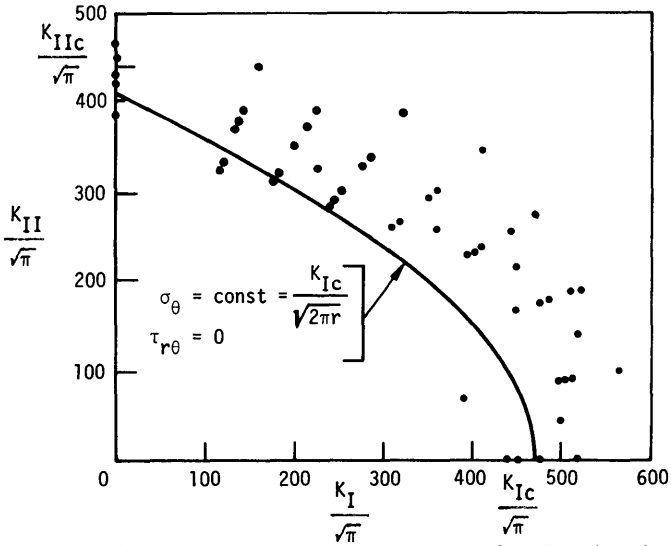

Figure 28b - K_I versus K_{II} at the Beginning of Crack Extension in a Cracked Plate Under Plane Loading

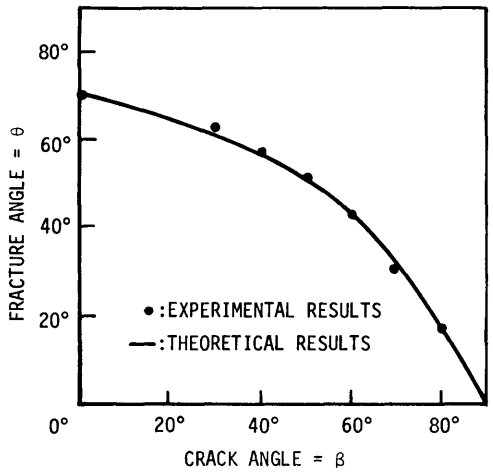

Figure 28c - Fracture Angle versus Crack Angle in Cracked Plate under Uniform Tension

Figure 28 - Crack Propagation for Arbitrarily Inclined Cracks in Brittle Plates under Uniform Tension

(From Erdogan and Sih, 1963)

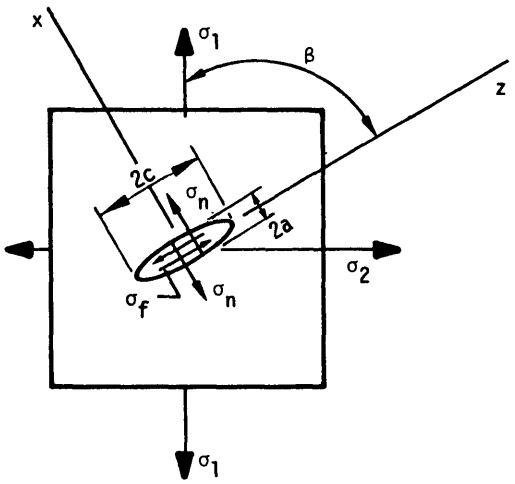

Figure 29a

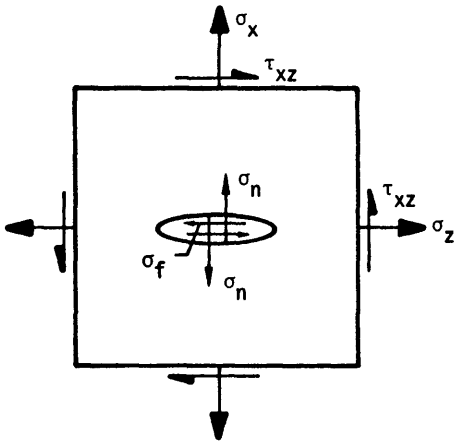

Figure 29b

Figure 29 - Stress Components Referred to Principal Axes of Crack under Combined Shear and Normal Loading

(From McClintock and Walsh, 1963)

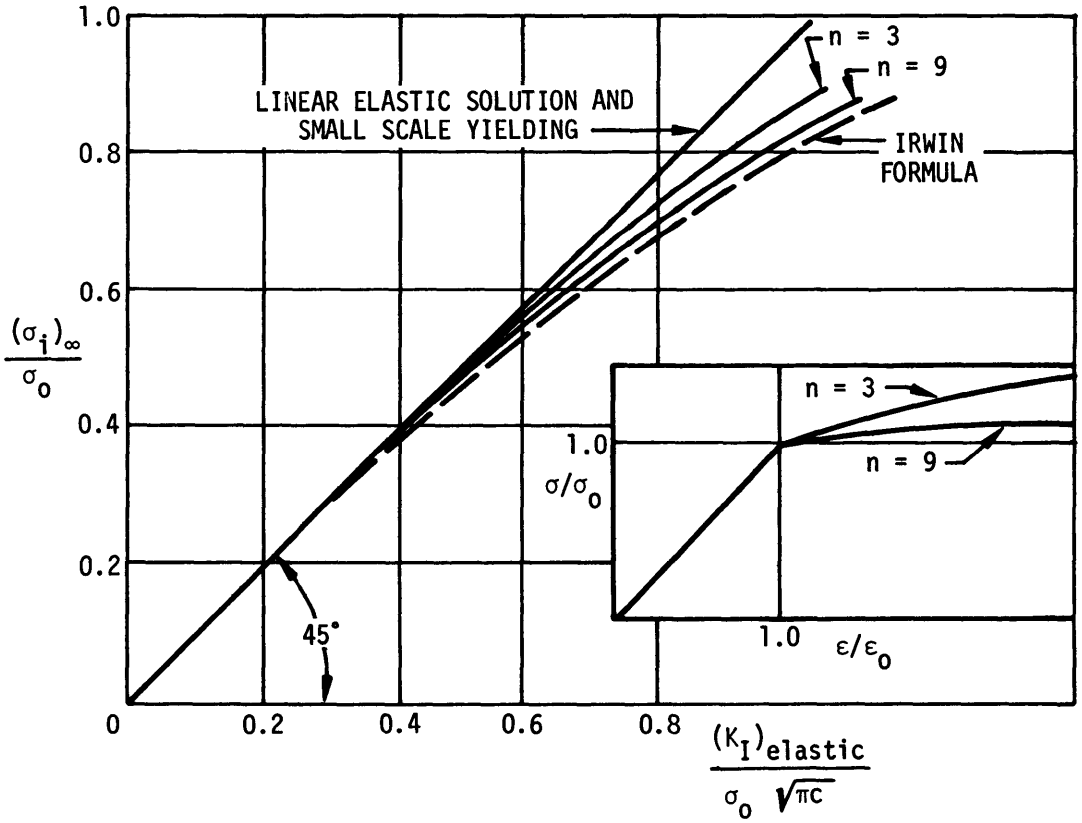

Figure 30 - Critical Initiation Stress for Large Scale Yielding, Tension

(From Hilton and Hutchinson, 1969)

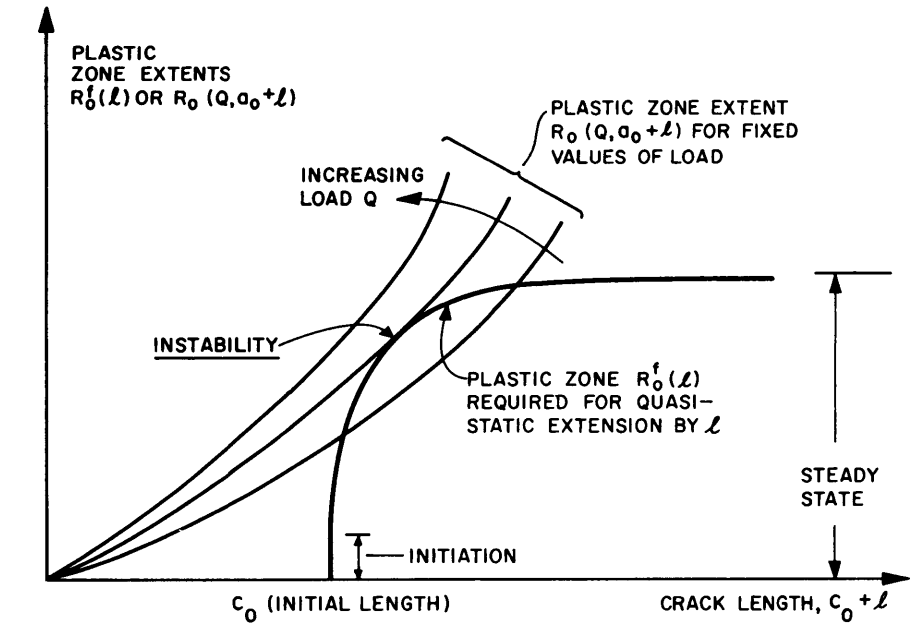

Figure 31 - Elastic-Plastic Stable Crack Extension and Final Instability, from Antiplane Shear Theory

(From Rice, 1968 and Drucker and Rice, 1968)

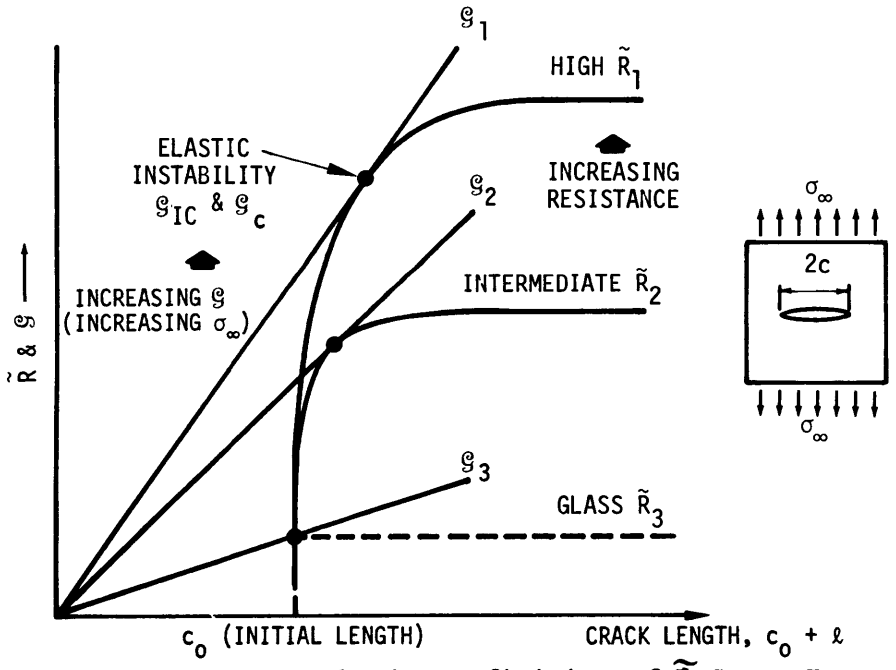

Figure 32 - Fracture Mechanics Definition of $\widetilde{R}$-Curve Features in Terms of Rising $\mathcal{G}$ to the Point of Instability ($\mathcal{G}_c$)

(Rice (1968) The mathematical analyses apply for the case of elastic loading, but the basic concepts may be extended to visualize $\widetilde{R}$-curve aspects in plastic fracture. (Pellini and Judy, 1970).

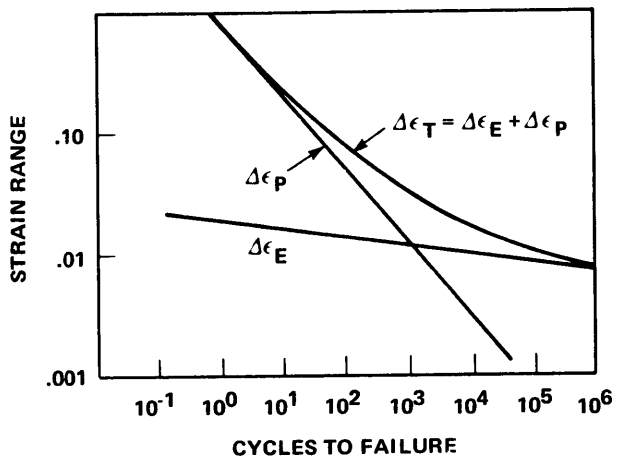

Figure 33 - Total Strain as a Combination of Two Linear Relations

(From Manson, 1965, 1966)

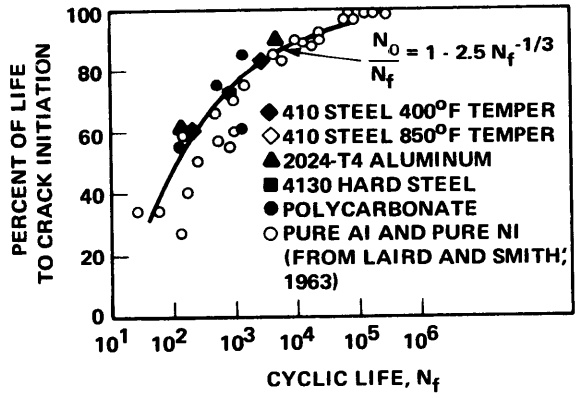

Figure 34 - Relation between Percent of Life to Crack Initiation N_o and Fatigue Life N_f

(From Manson, 1965)

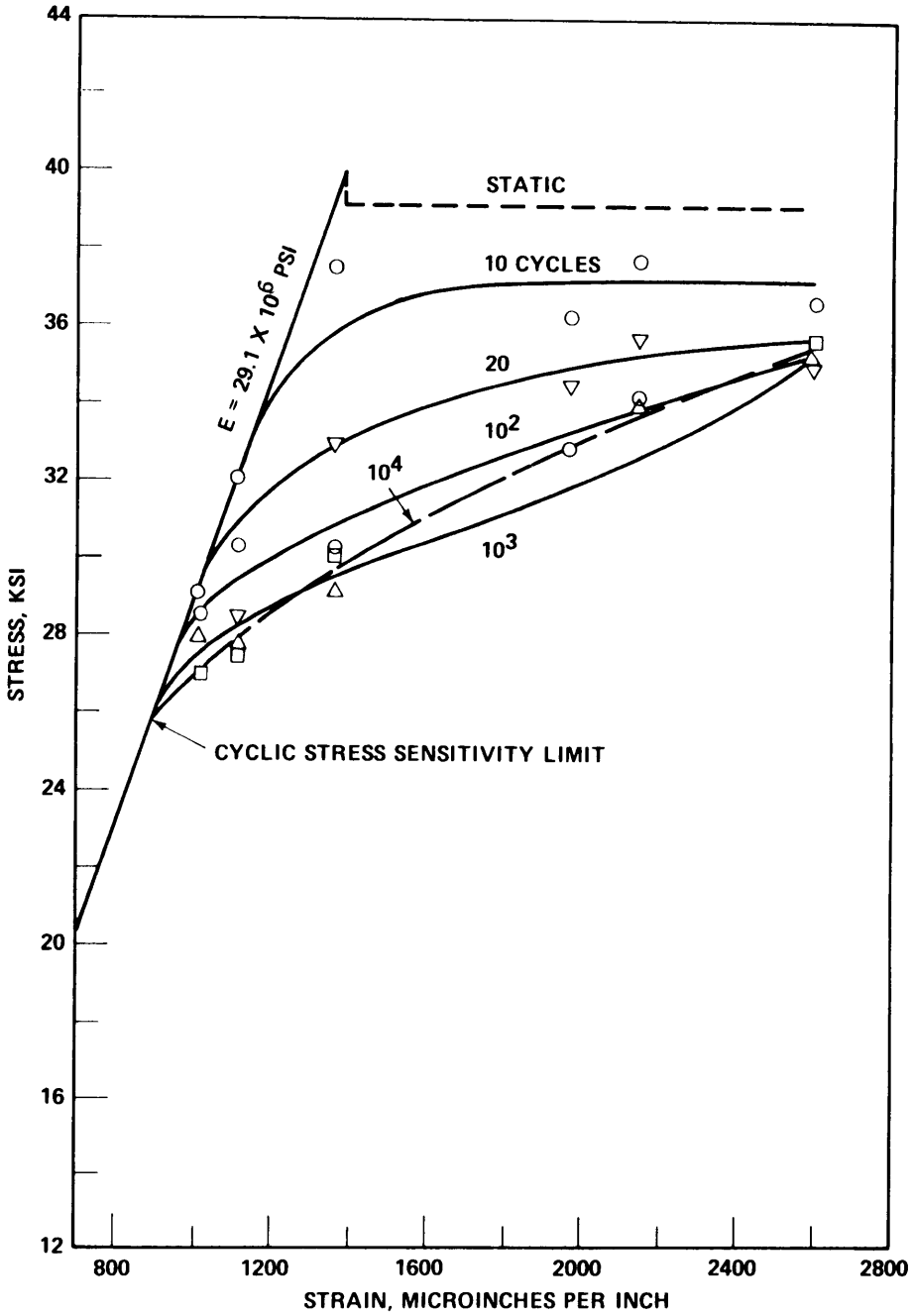

Figure 35 - Cyclic Stress-Strain Curves for SAE 1018 Steel at Various Numbers of Cycles

(From Blatherwick and Olson, 1968)

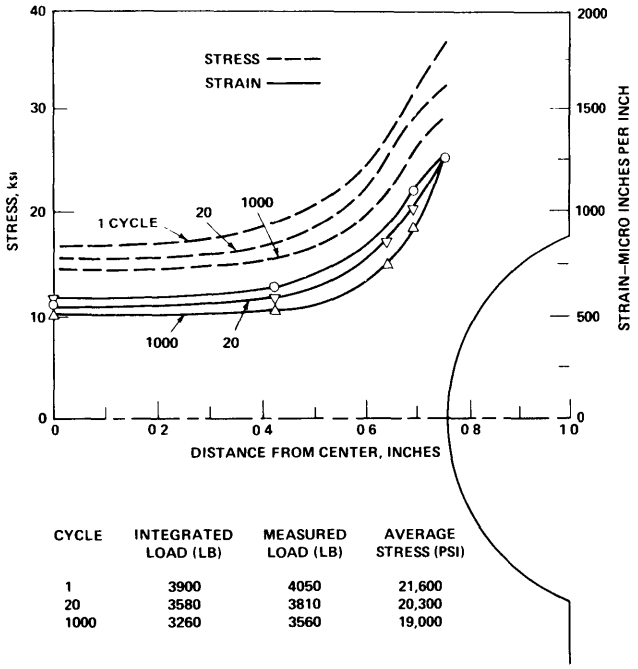

CYCLE	INTEGRATED LOAD (LB)	MEASURED LOAD (LB)	AVERAGE STRESS (PSI)
1	3900	4050	21,600
20	3580	3810	20,300
1000	3260	3560	19,000

Figure 36 - Stress and Strain Distributions in Notched Specimen under Controlled Strain Amplitude

(From Blatherwick and Olson, 1968)

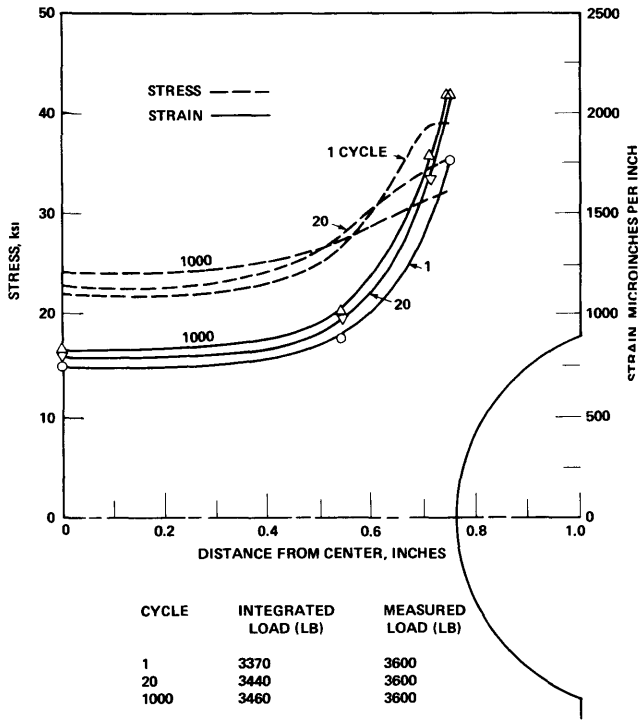

CYCLE	INTEGRATED LOAD (LB)	MEASURED LOAD (LB)
1	3370	3600
20	3440	3600
1000	3460	3600

Figure 37 - Stress and Strain Distributions in Notched Specimen under Controlled Force Amplitude

(From Blaterwick and Olson, 1968)

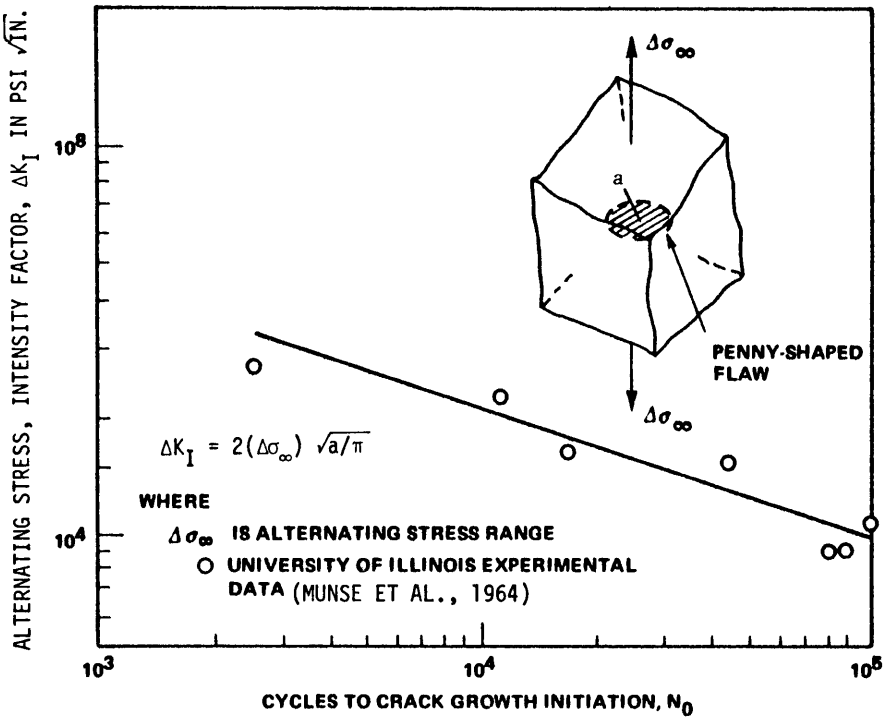

Figure 38 - Variation of ΔK_I with N_o, for Flaws in Butt-Welded 3/4-Inch-Thick HY-80 Steel Strips
(From Forman, 1968)

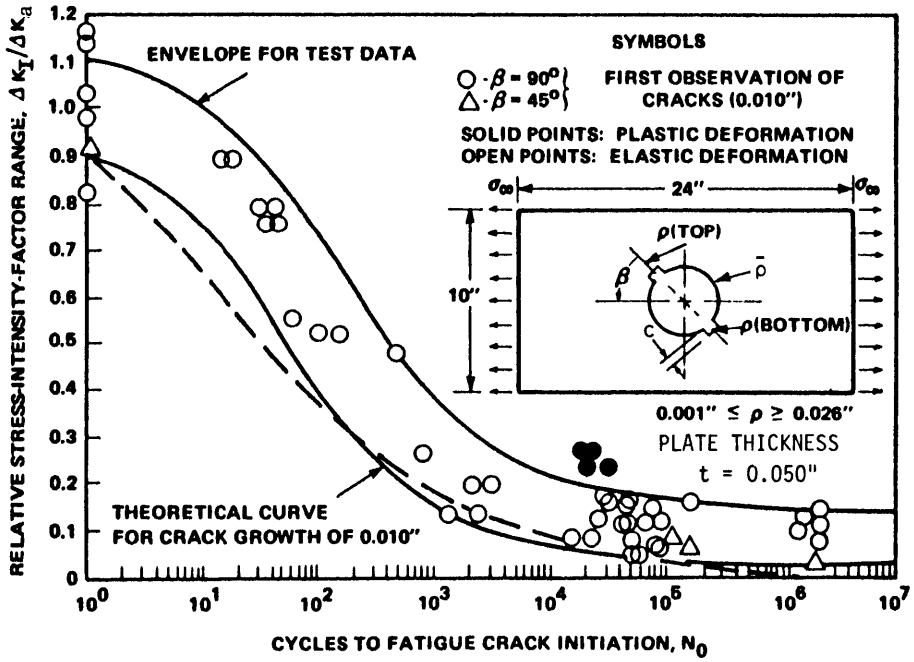

Figure 39 - Comparison of Theoretical Crack Growth of 0.010-Inch with First Observation of 0.010-Inch Fatigue Cracks in Notched Sheets of 7075-T6 Aluminum
(From Forman, 1968)

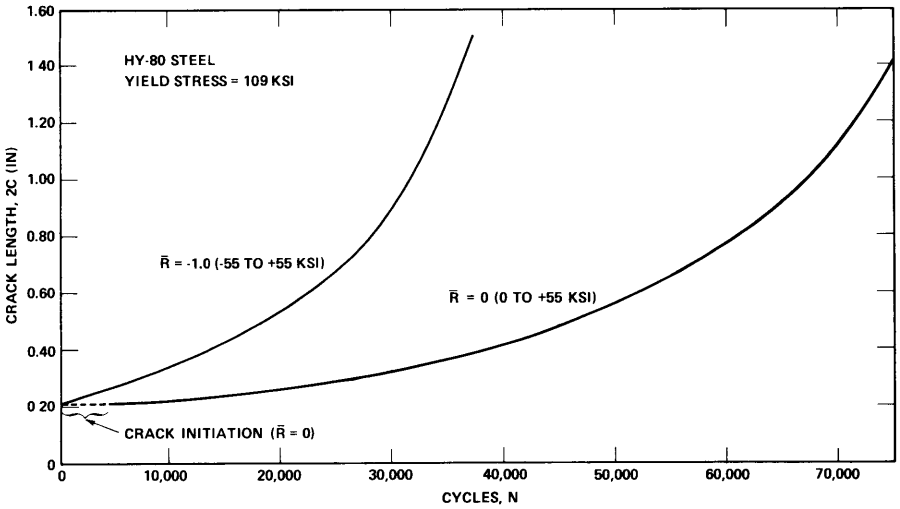

Figure 40 - Surface Length versus Number of Cycles of Repeated Load for HY-80 Plate Specimens Cycled Zero-Tension (R = 0) and Tension-Compression ($\bar{R}$ = -1)

(From Crooker, 1971)

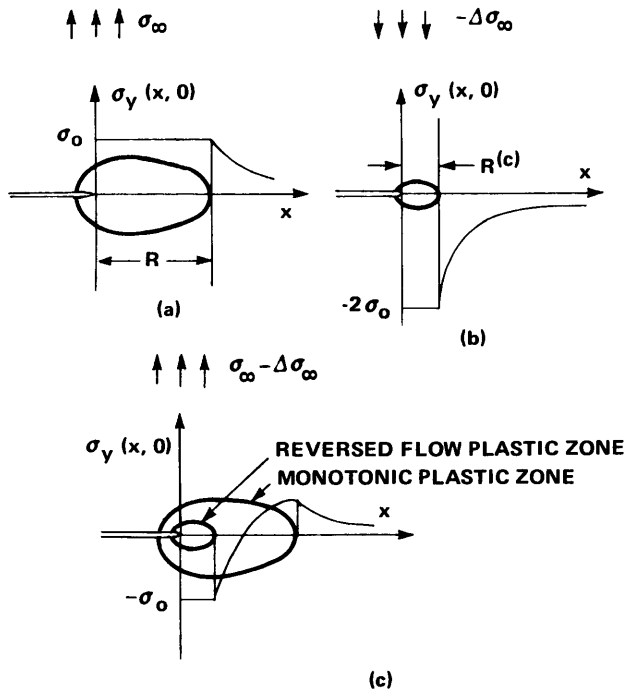

Figure 41 - Plastic Superposition for Unloading

(From Rice, 1967. Adding (b) for load $\Delta\sigma_\infty$ with a double yield stress to (a) gives the solution (c) resulting after unloading from σ_∞ to σ_∞ - $\Delta\sigma_\infty$ reloading $\Delta\sigma_\infty$ - $\Delta\sigma_\infty$ to σ_∞ restores (a).

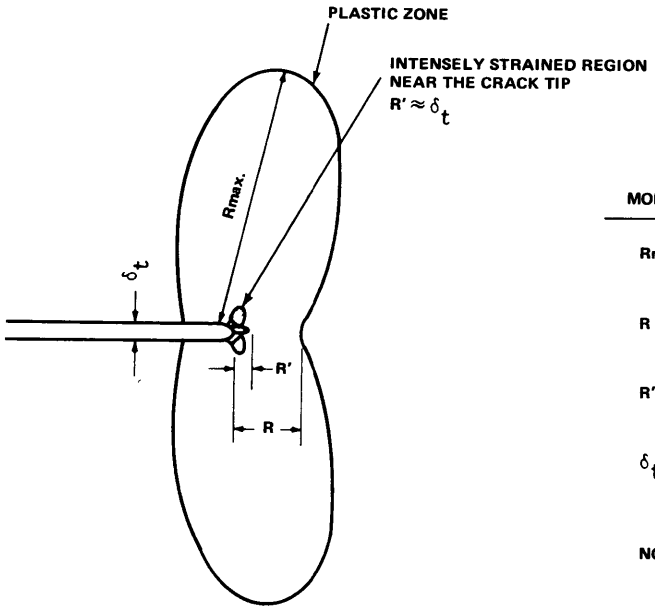

MONOTONIC ZONE	CYCLIC ZONE
$R_{max.} \approx 0.2\left(\frac{K_I}{\sigma_o}\right)^2$	$R^{(c)}_{max.} \sim 0.2\left(\frac{\Delta K_I}{2\,\sigma_o^{(c)}}\right)^2$
$R \approx 0.03\left(\frac{K_I}{\sigma_o}\right)^2$	$R^{(c)} \sim 0.03\left(\frac{\Delta K_I}{2\,\sigma_o^{(c)}}\right)^2$
$R' \approx \delta_t$	$R^{(c)} \sim \delta_t$
$\delta_t \approx \frac{K_I^2}{2E\,\sigma_o}$	$\delta_t(c) \sim \frac{\Delta K_I^2}{4E\,\sigma_o^{(c)}}$

NOTE: SUFFIX "c" IS ASSOCIATED WITH CYCLIC PLASTICITY

Figure 42 - Plasticity Estimates near Monotonically and Cyclically Loaded Cracks in Plane Strain

(From Hahn et al., December 1969)

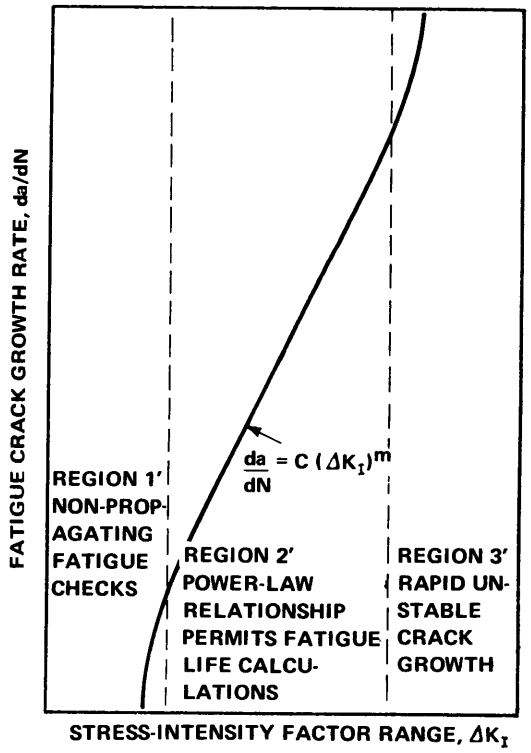

Figure 43 - Fatigue Crack Growth Curve on Log-Log Coordinates
(From Crooker and Lange, Dec 1969)

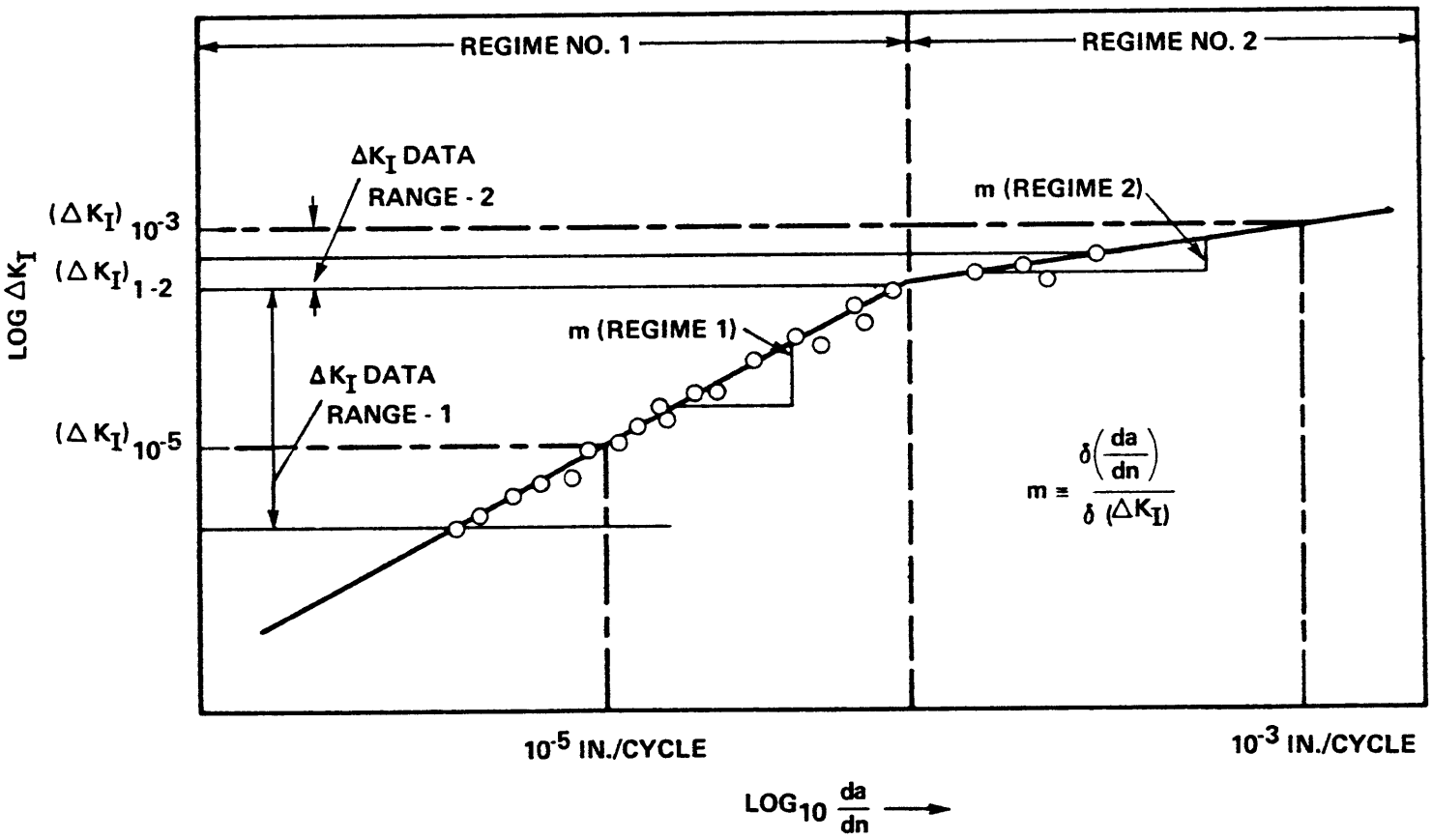

Figure 44 - Stress-Intensity-Growth Rate Spectrum with Two Regimes and Definitions in Table 2

(From Hahn et al., 1969)

Figure 45 - Specimen Configuration and Result of Crack Propagation Studies on 7075-T6 Aluminum Plates Loaded Tension

(From Hartman and Schijve, 1970)

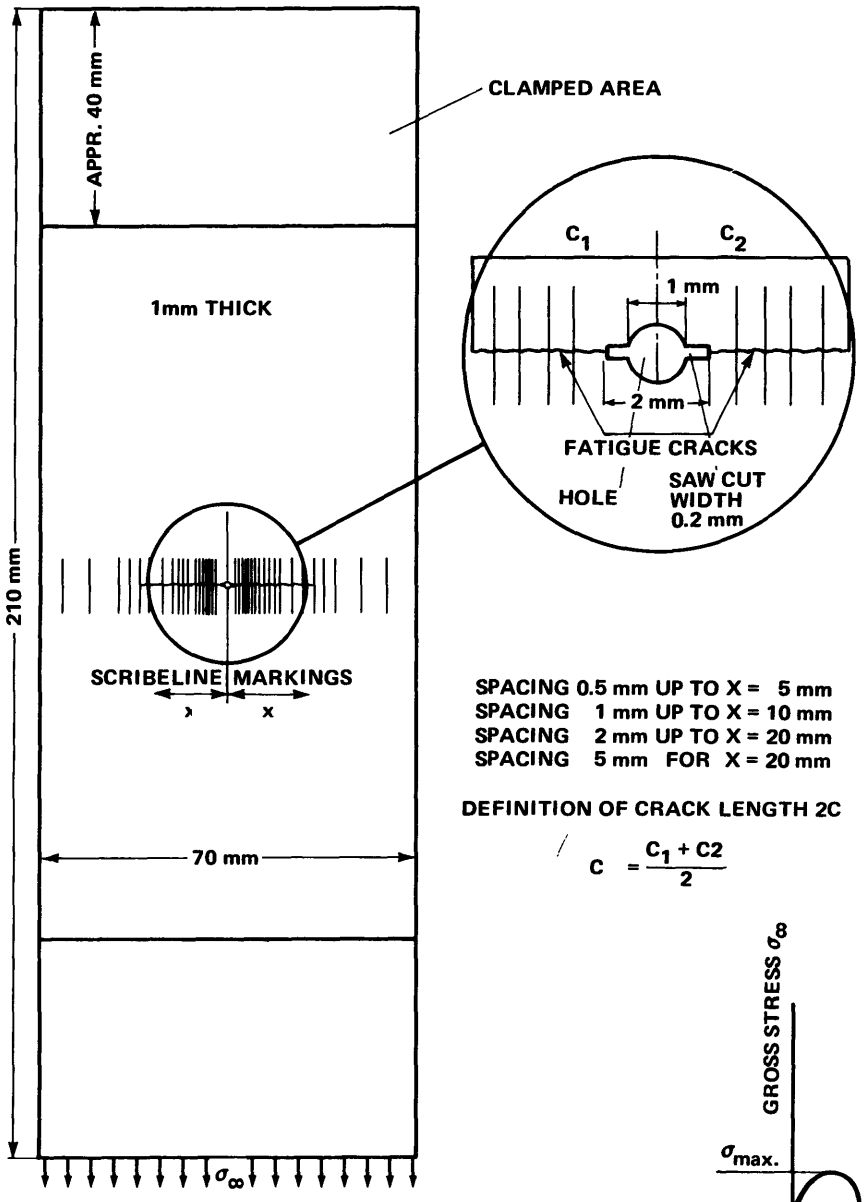

(a) Figure 45a - Specimen Configuration

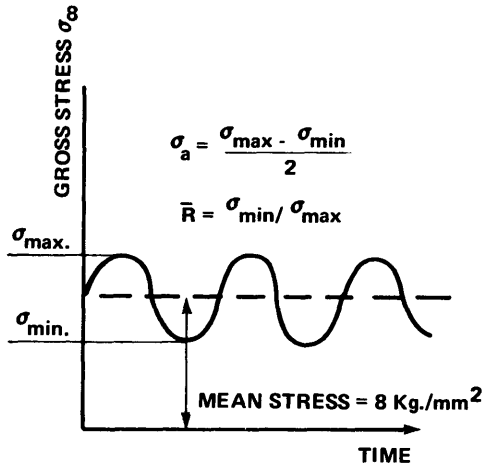

Figure 45b - Stress Cycle Definitions

(Frequency approx. 3400 cycles/in in., environment - dry air)

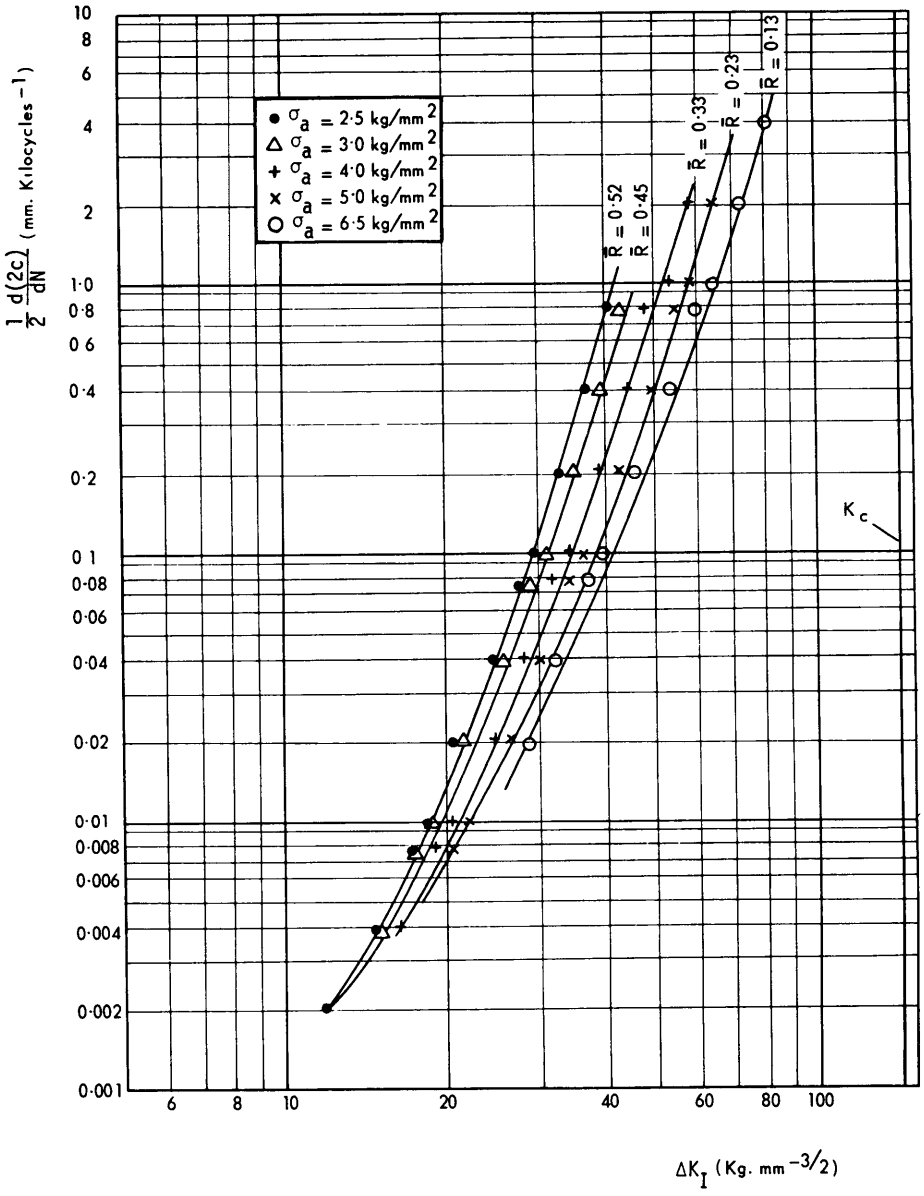

Figure 45c - Crack Propagation Data

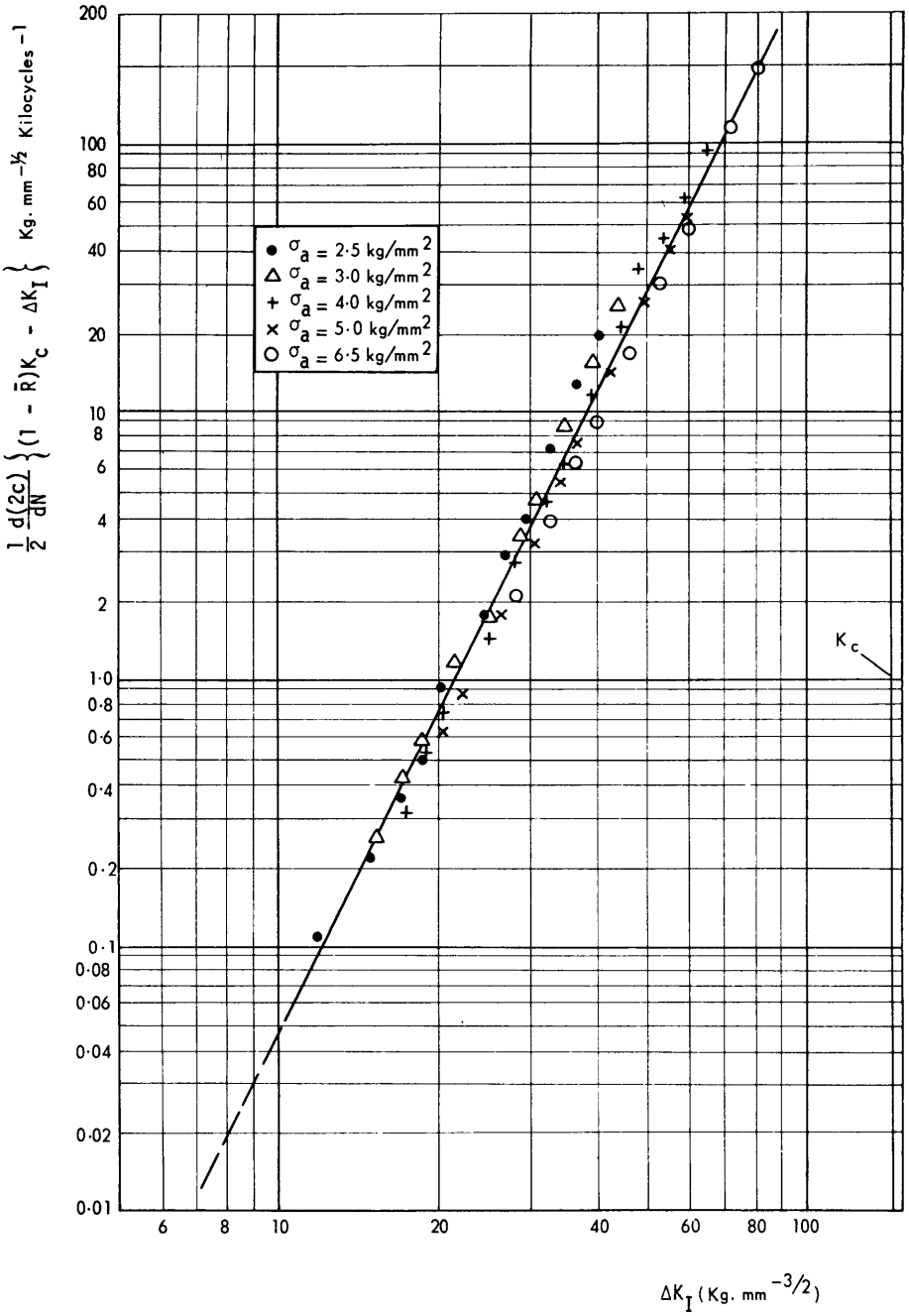

Figure 45d - Crack Propagation Data Plotted in Terms of Equation (52)

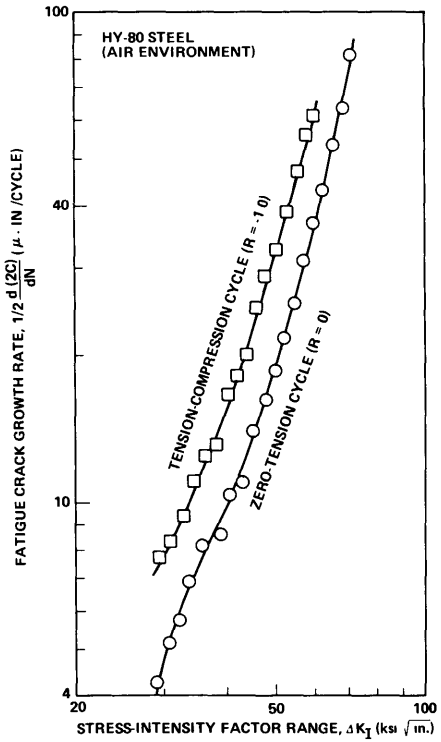

Figure 46 - Fatigue Crack Propagation Data for Specimens Cycled Zero-to-Tension ($\bar{R}$ = 0) and Fully Reversed Tension-to-Compression ($\bar{R}$ = -1)

(From Crooker and Lange, 1971)

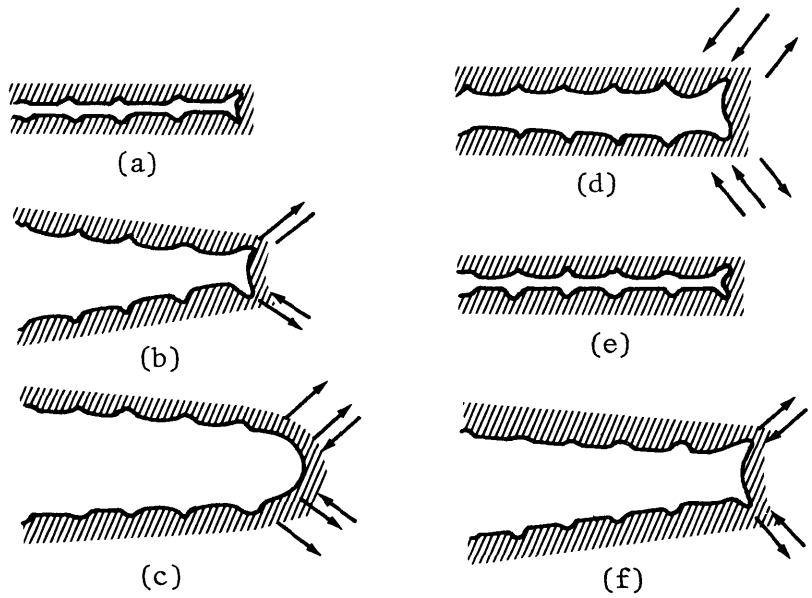

Figure 47 - The Plastic Blunting Process of Fatigue Crack Propagation According to Laird (1967)

(Letter designations indicate: (a) zero load, (b) small tensile load, (c) maximum tensile load, (d) small compressive load, (e) maximum compressive load, and (f) small tensile load. The double arrowheads in (c) and (d) signify the greater width of slip bands at the crack in these stages of the process. The stress axis is vertical.)

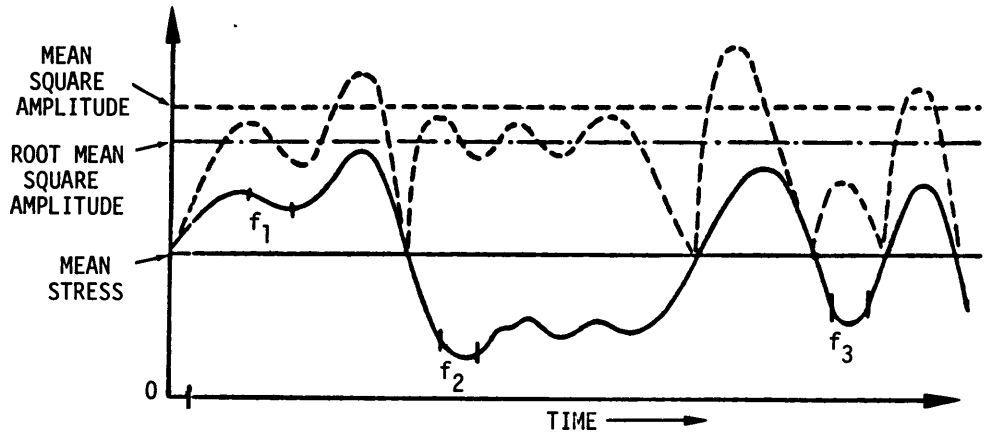

Figure 48a - Stress Time History

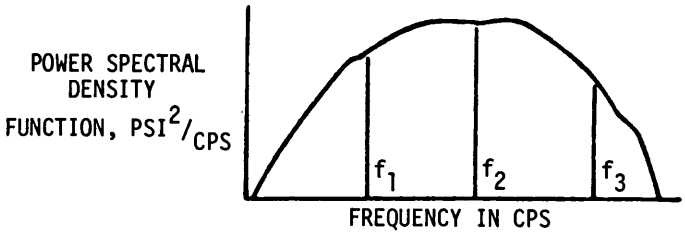

Figure 48b - Power Spectral Density Plot
(From Swanson, 1968)

Figure 48 - Typical Random Load Trace Showing Derivation of RMS and Associated PSD Diagram

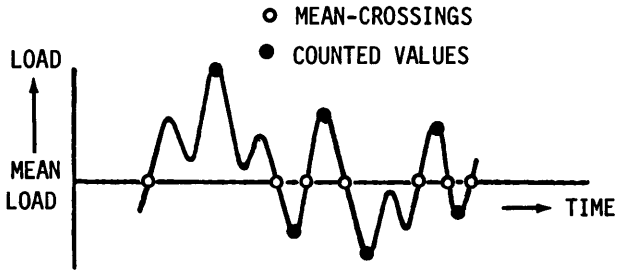

Figure 49a - Mean-Crossing Peak Count Method

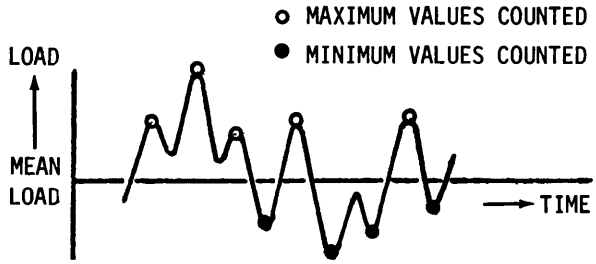

Figure 49b - Peak Count Method

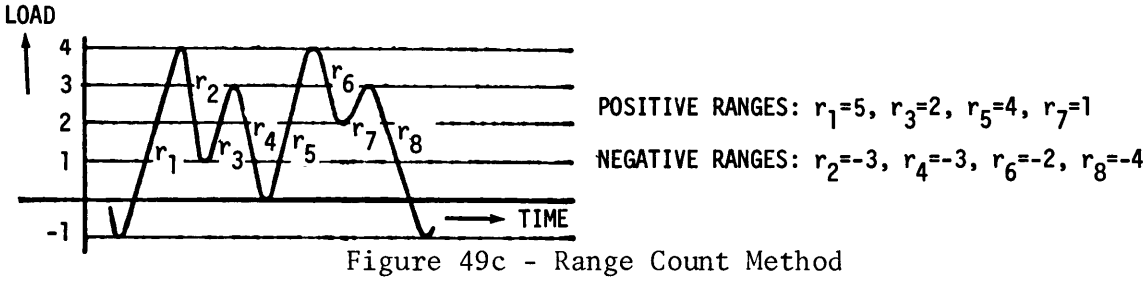

Figure 49c - Range Count Method

Figure 49 - Examples of Statistical Counting Methods
(From Schijve, 1961)

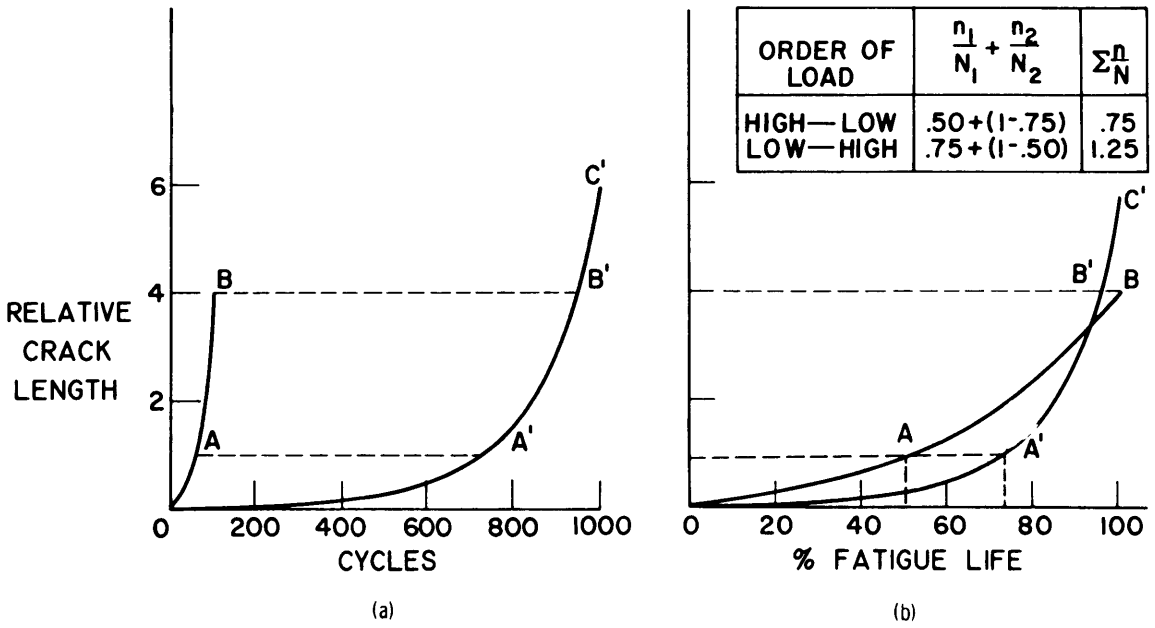

Figure 50 - Idealized Crack-Growth Behavior under Two-Level Loading

(From Manson, 1965)

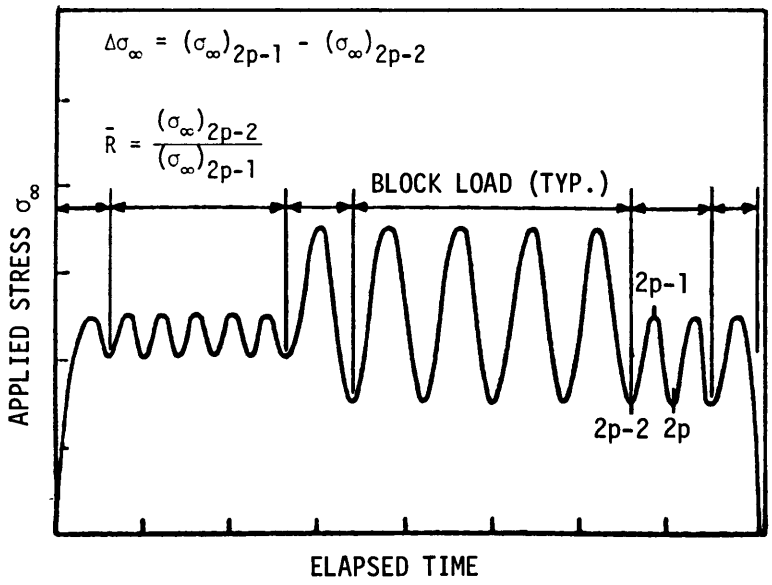

Figure 51 - Cyclic Stress and Stress Ratio for Block-Loading Problem

(From Forman and Hudson, 1967)

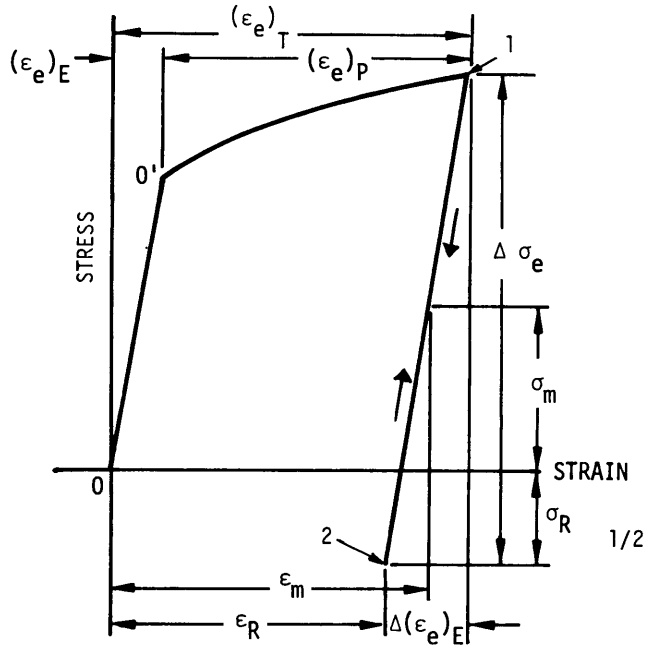

Figure 52a - Elastic Strain Range Cycling

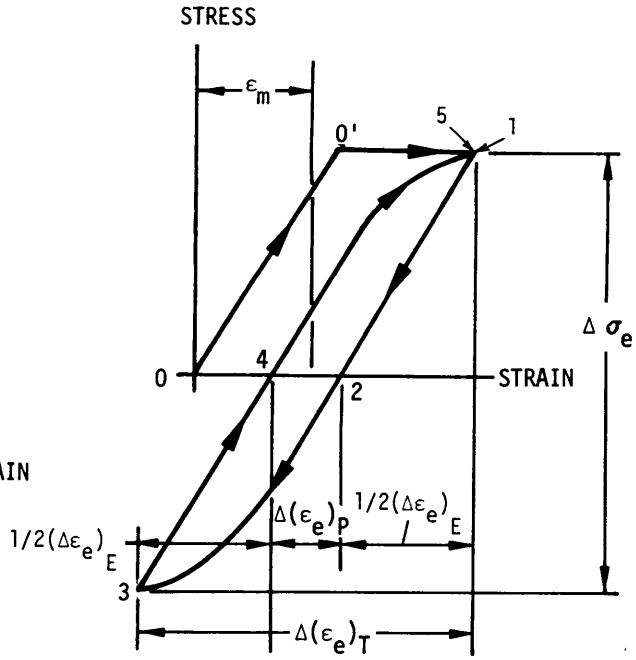

Figure 52b - Inelastic Strain Range Cycling

Figure 52 - Hypothetical Cyclic Strain Histories at a Notch

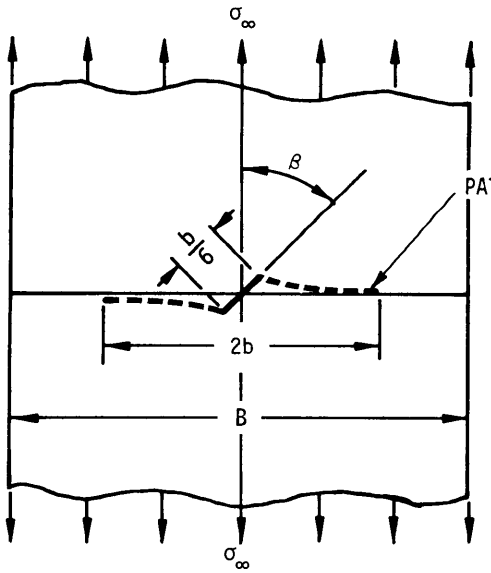

Figure 53a - Initial Crack Orientation
β = 45 Deg

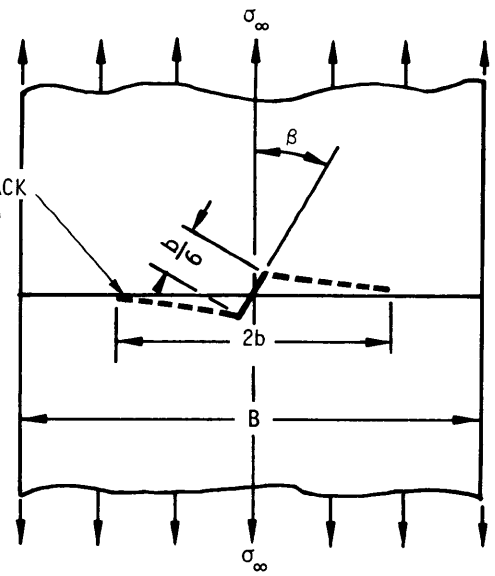

Figure 53b - Initial Crack Orientation
β = 30 Deg

Figure 53 - Crack Extension Pattern of an Initially Slanted Crack in a Tension Plate

(From Kobayashi and Iida, 1969)

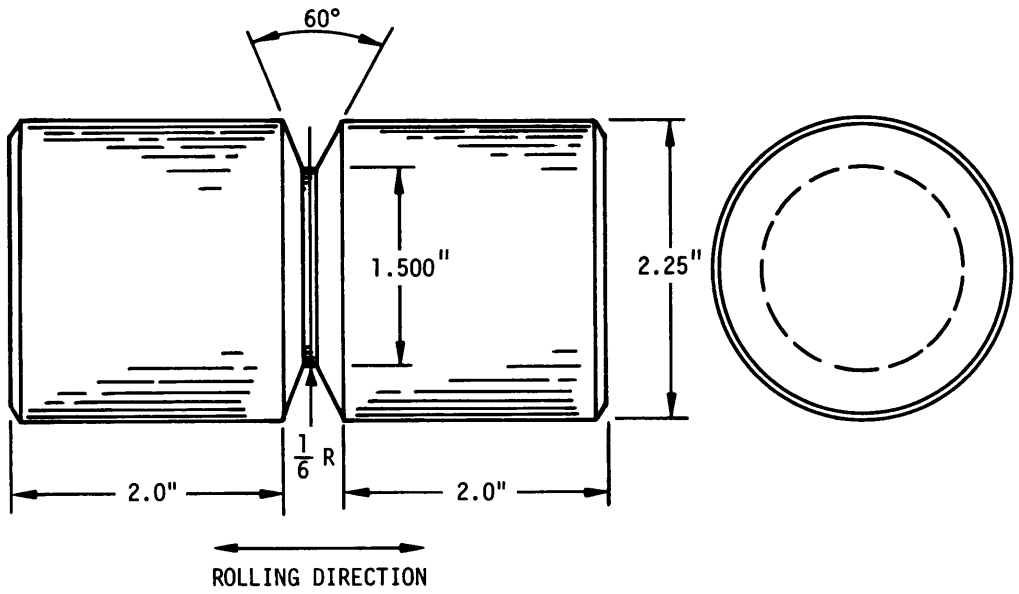

Figure 54 - Compressive Specimen Design
(From DeHart et al., 1968)

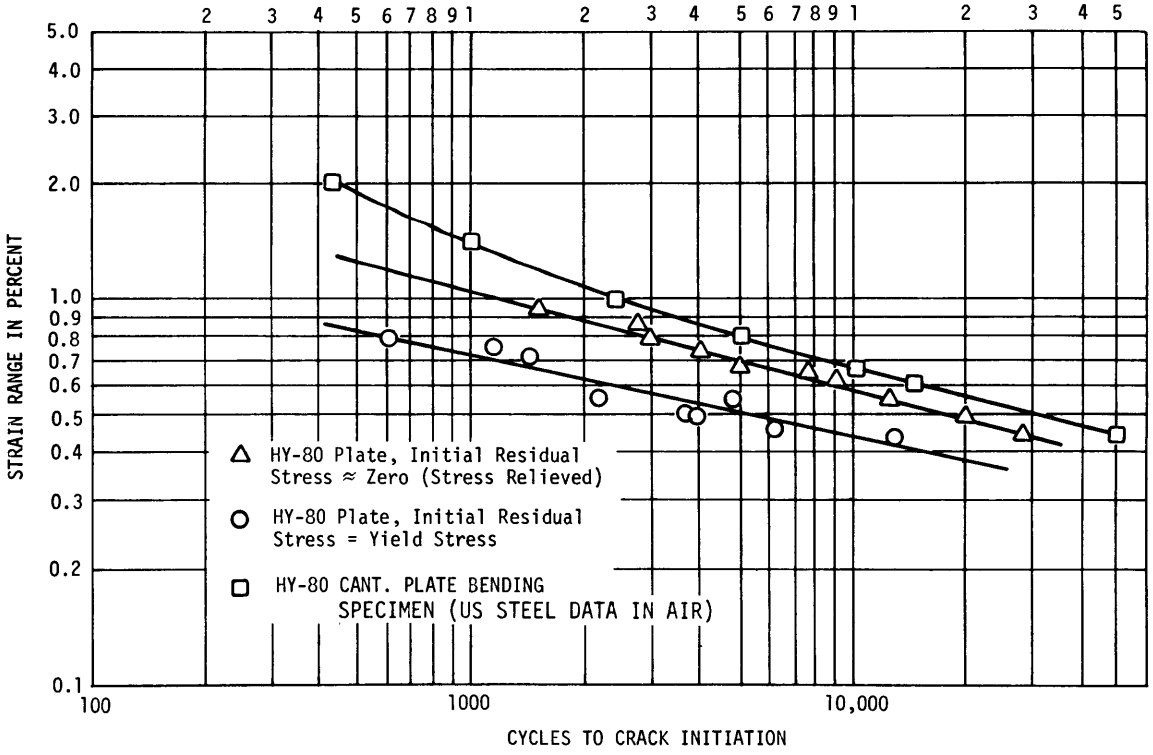

Figure 55 - Compressive Specimen Fatigue Data
(HY-80 plate material with high residual stress and zero residual stress. From DeHart et al., 1968; U.S. steel data from Boblenz and Rolfe, 1966).

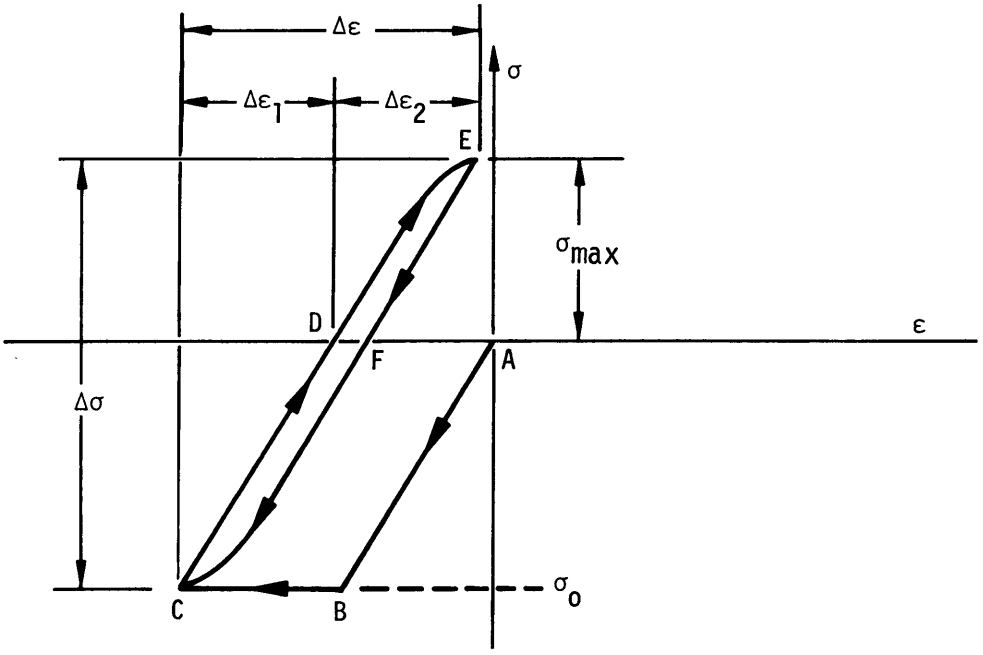

Figure 56a

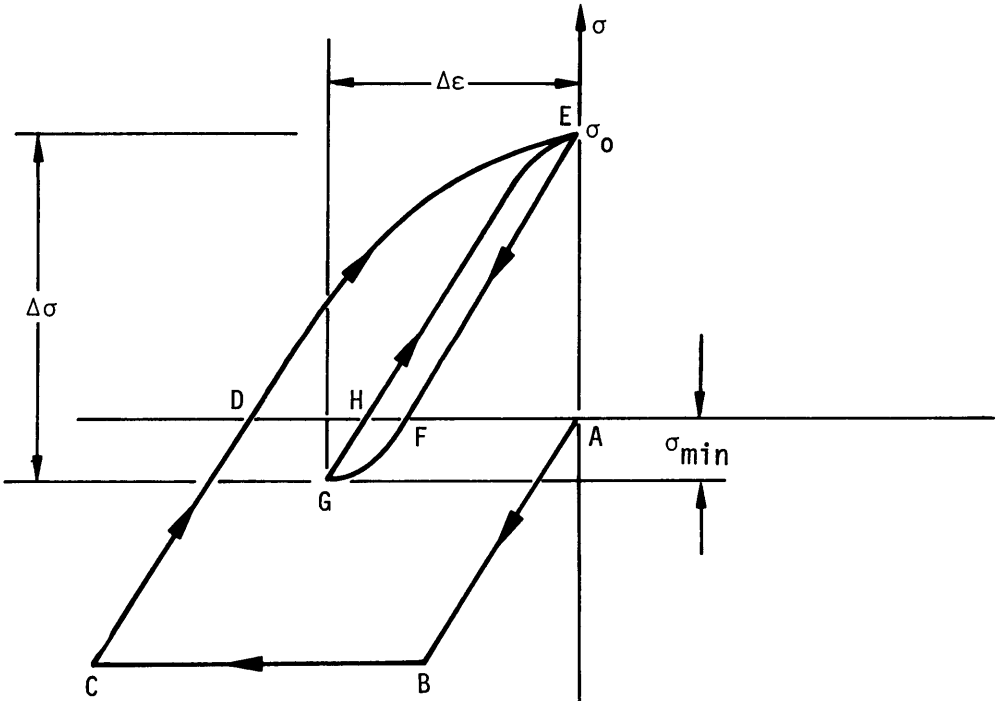

Figure 56b

Figure 56 - Qualitative Notch Stress-Notch Strain under Compressive Cycling

(From DeHart et al., 1968)

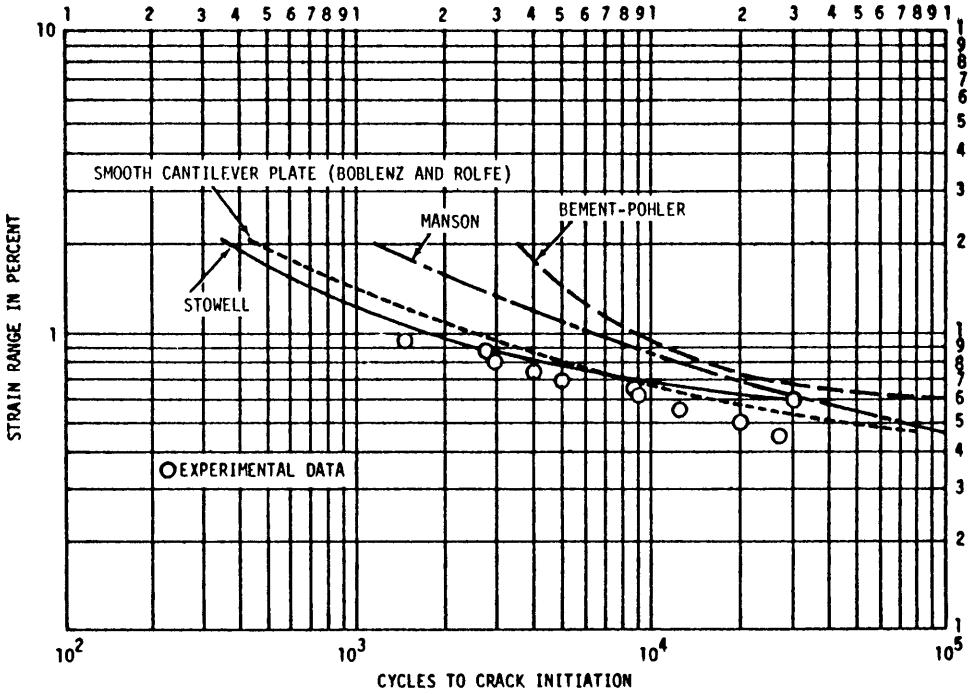

Figure 57 - Predicted Fatigue Curves for Notched Compression Specimens with No Residual Stress
(From DeHart et al., 1968)

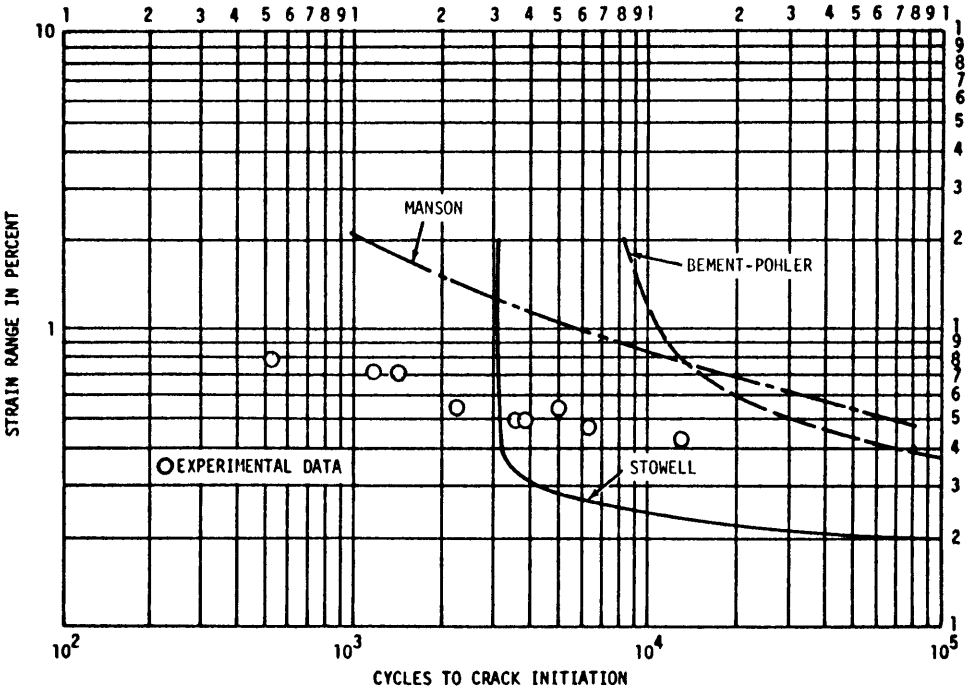

Figure 58 - Predicted Fatigue Curves for Notched Compression Specimens with Initial Residual Stress
(From DeHart et al., 1968)

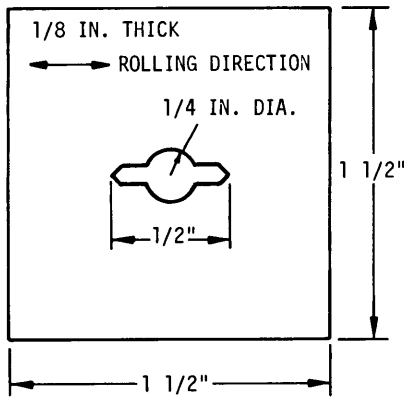

Figure 59a - Specimen Geometry

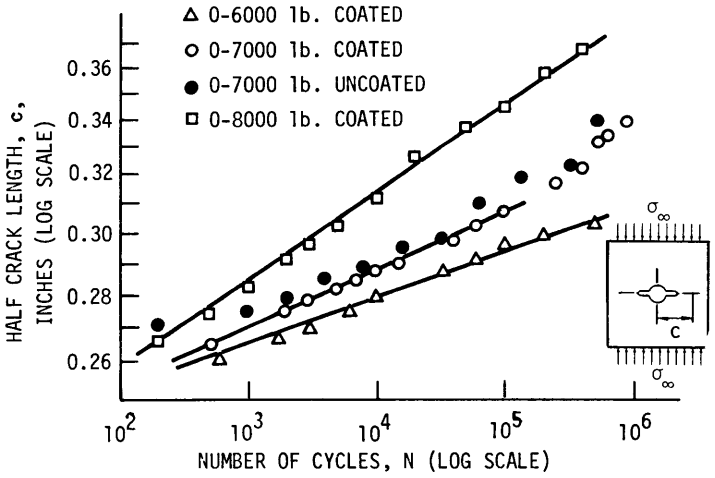

Figure 59b - Crack Length versus Number of Cycles for Notched Specimens

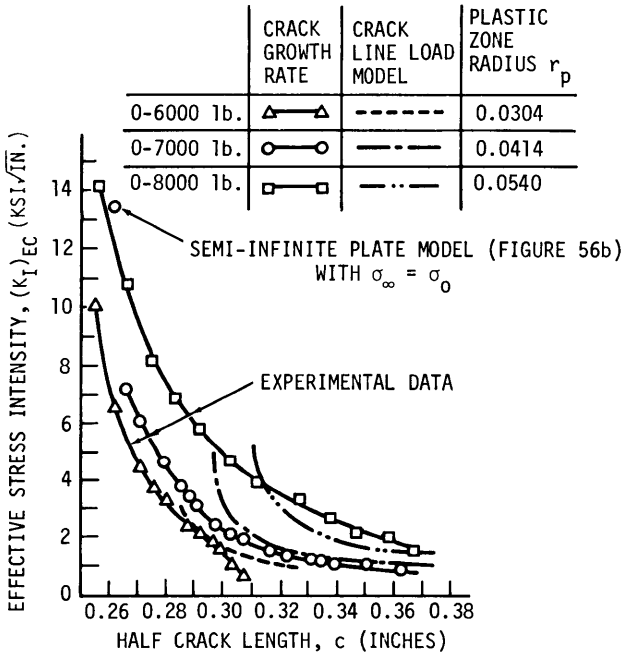

Figure 59c - Stress Intensity versus Crack Length

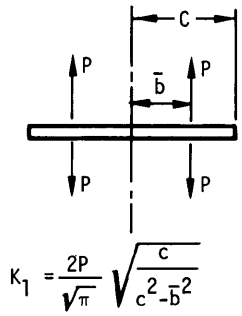

$$K_1 = \frac{2P}{\sqrt{\pi}} \sqrt{\frac{c}{c^2 - \bar{b}^2}}$$

c = NOTCH LENGTH PLUS CRACK LENGTH

$\bar{b}$ = NOTCH LENGTH PLUS R/2

Figure 59d - Concentrated Force Model

Figure 59 - Specimen Configuration and Results of Crack Propagation Studies on 7075-T6 Aluminum Plates Loaded in Compression

(From Hubbard, 1969)

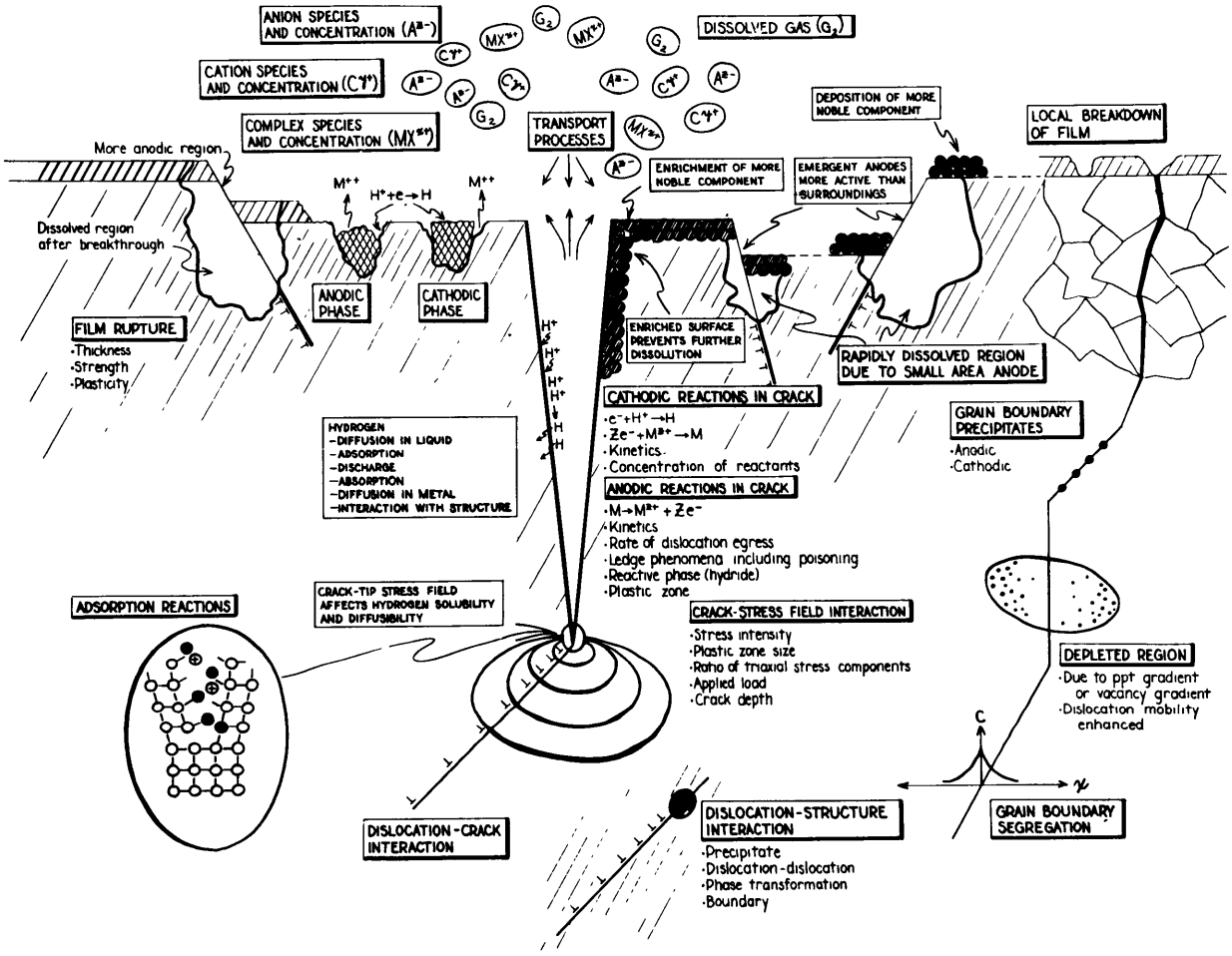

Figure 60 - Important Processes that Operate to Affect Stress Corrosion Cracking

(From Staehle, 1967)

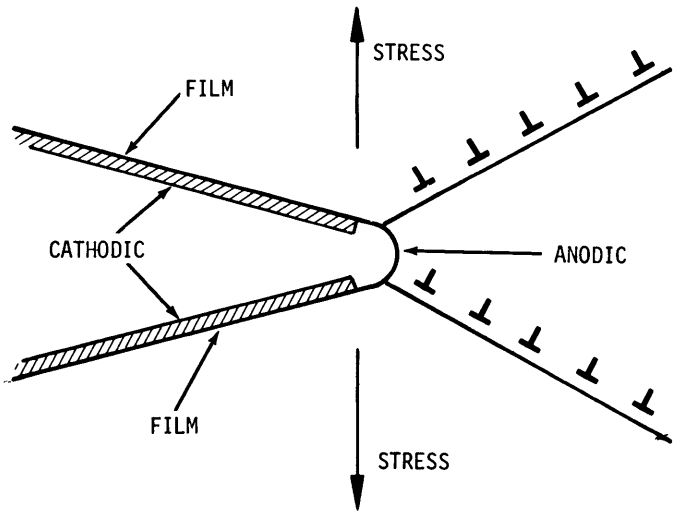

Figure 61 - Film-Rupture Model

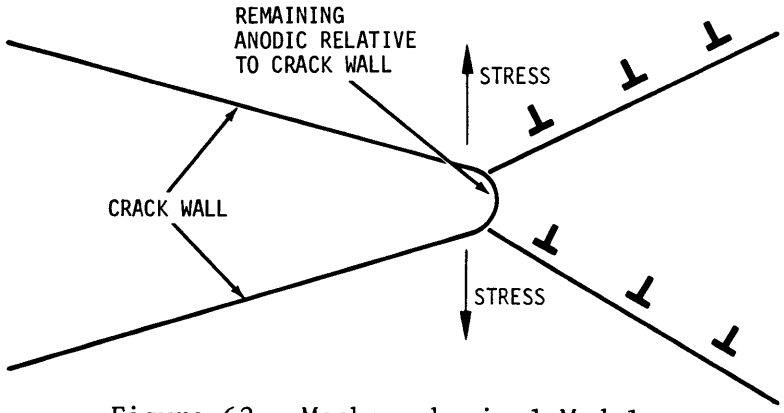

Figure 62 - Mechanochemical Model

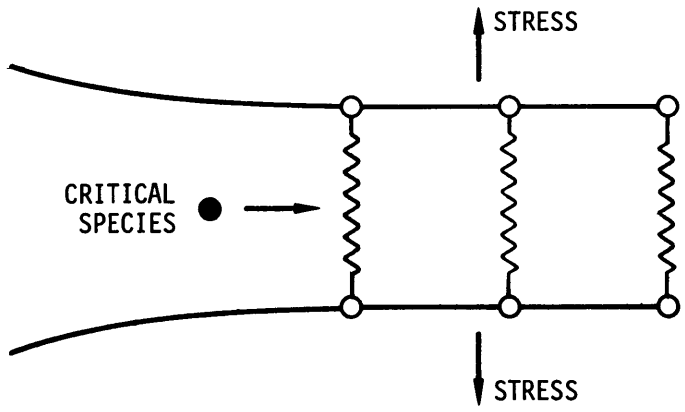

Figure 63 - Adsorption Model

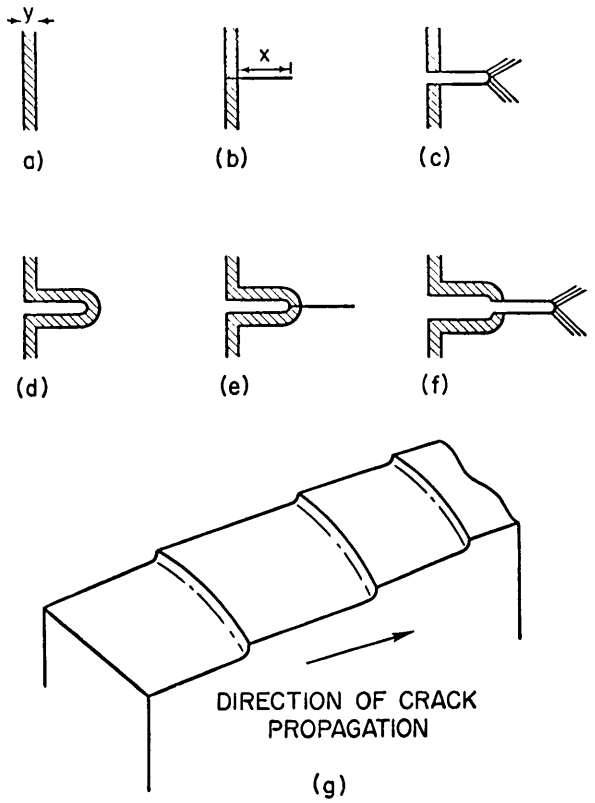

Figure 64 - Brittle Film Model and Resulting Fracture Surface
(From Pugh et al., 1969)

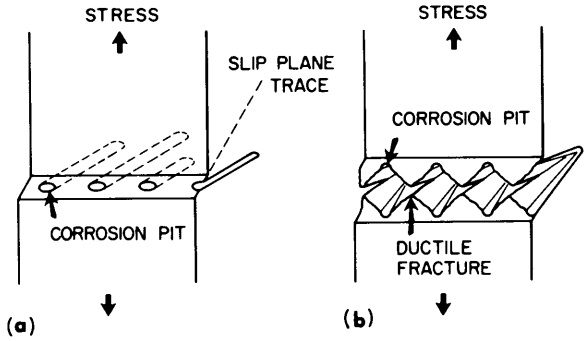

Figure 65 - Mechanism of Stress
Corrosion Cracking

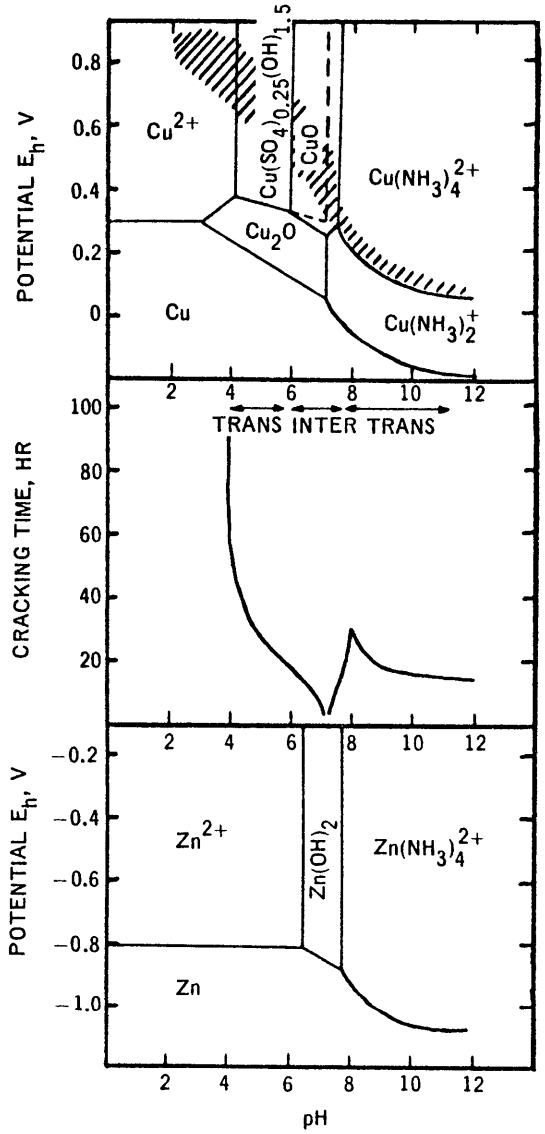

Figure 66 - Potential-pH Diagram and Stress Corrosion Cracking of Brass in Ammoniacal Solutions

(a) Potential-pH diagram for the system Cu-NH_3-H_2O at 50 mM dissolved $CuSO_4$ and 1 M total (NH_4^+ + NH_3); (b) Dependence of stress corrosion cracking susceptibility upon pH; and (c) Potential-pH diagram for the system Zn-NH_3-H_2O at 10 mM dissolved Zn and 1 M total (NH_4^+ + NH_3). From Booker, 1967).

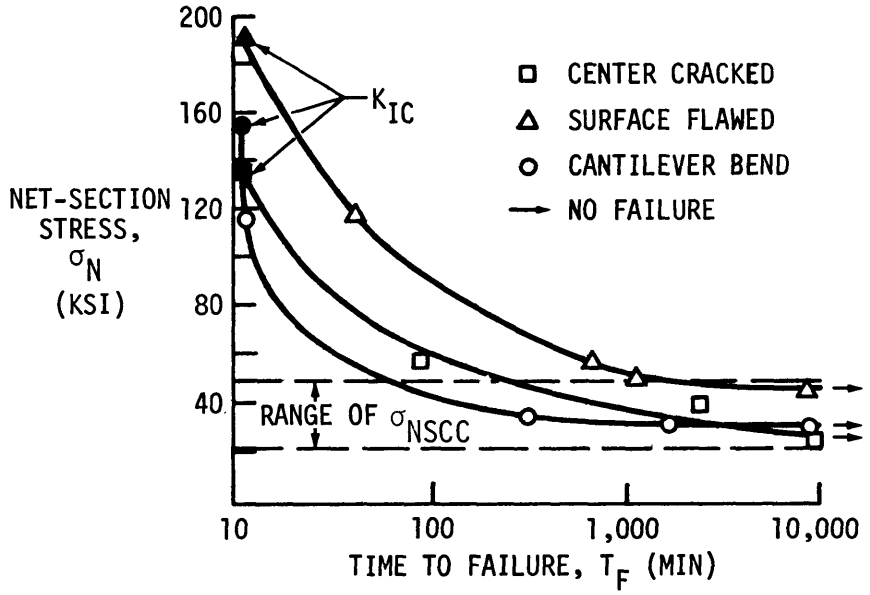

Figure 67 - Determination of σ_{NSCC} for 4340 Steel Using Three Different Specimen Configuration

(From Smith et al., 1968)

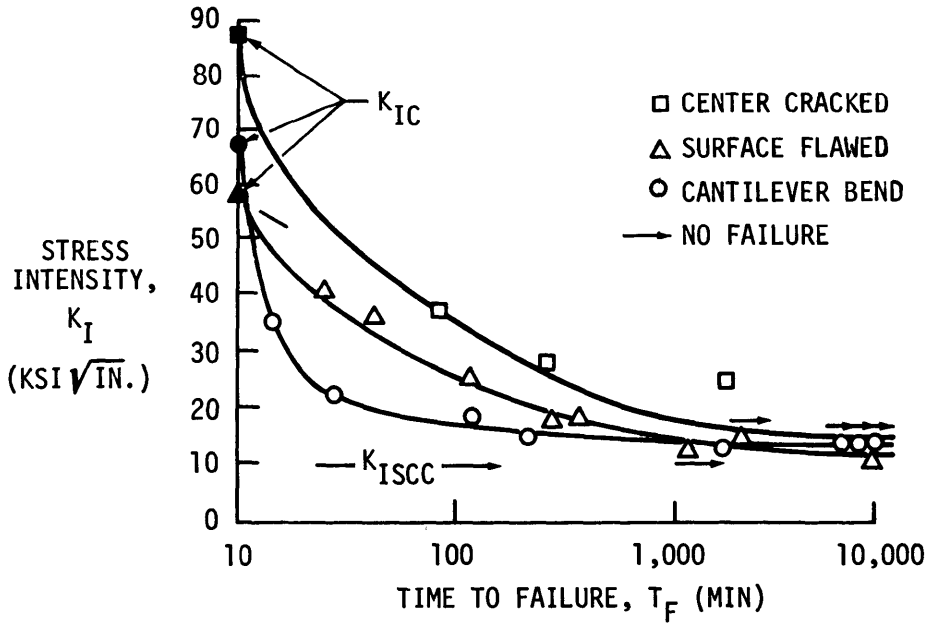

Figure 68 - Determination of K_{ISCC} for 4340 Steel Using Three Different Specimen Configuration

(From Smith et al., 1968)

Figure 69 - Fracture Specimens

SPECIMEN TYPE	SPECIMEN DESIGNATION	SPECIMEN GEOMETRY	EQUATION FOR K_I
TENSILE	CENTER-CRACKED PLATE UNDER UNIFORM TENSION	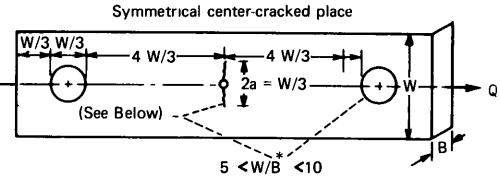 * Surfaces must be symmetric to specimen center line within W/1000	$K_I = \frac{Q}{B}\frac{a^{1/2}}{W}\left[1.77 + 0.227\left(\frac{2a}{W}\right) - 0.510\left(\frac{2a}{W}\right)^2 + 2.7\left(\frac{2a}{W}\right)^3\right]$ for range $\frac{2a}{W}$ = 0 to 0.7 FROM WESSEL et al (1966)
TENSILE	DOUBLE EDGE CRACKED PLATE	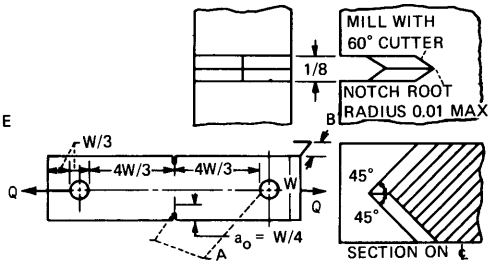	$K_I = \frac{Q}{B}\frac{a^{1/2}}{W}\left[1.98 + 0.36\left(\frac{2a}{W}\right) - 2.12\left(\frac{2a}{W}\right)^2 + 3.42\left(\frac{2a}{W}\right)^3\right]$ FROM BROWN AND SRAWLEY (1966)
TENSILE	SINGLE EDGE CRACKED PLATE	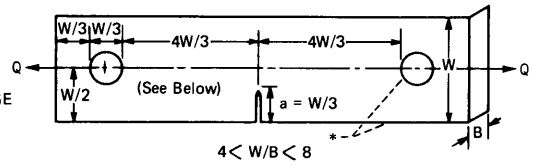 *-Surfaces must be true to specimen center line within W/1000.	$K_I = \frac{Q}{B}\frac{a^{1/2}}{W}\left[1.99 - 0.4124\left(\frac{a}{W}\right) + 18.70\left(\frac{a}{W}\right)^2 - 38.48\left(\frac{a}{W}\right)^3 + 53.85\left(\frac{a}{W}\right)^4\right]$ for range $\frac{a}{W}$ = 0 to 0.6 FROM WESSEL et al (1966)
TENSILE	SURFACE CRACKED PLATE	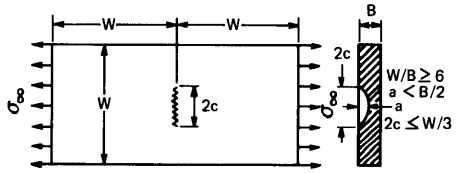	$K_I^2 = \frac{1.2\pi Q^2 a}{W^2 B^2}\left[\frac{1}{\phi^2 - 0.212\left(\frac{P^2}{W^2 B^2 \sigma_o^2}\right)}\right]$ WHERE $\phi = \int_0^{\pi/2}\sqrt{1 - \frac{c^2 - a^2}{c^2}\,\mathrm{Sin}^2\Theta}\; d\Theta$ $Q = WB\sigma_\infty$ FROM WESSEL et al (1966)
TENSILE	TAPERED DOUBLE CANTILEVER BEAM	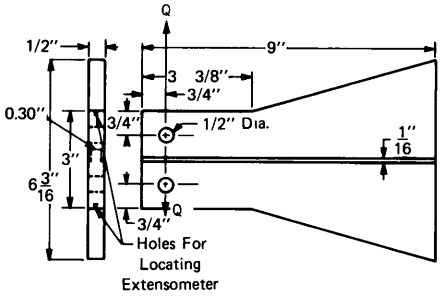	$K_I = \frac{2Q\left[3(a + a_o)^2 + h^2\right]^{1/2}}{\sqrt{b_n b}\, h^{3/2}\,(1 - \mu^2)^{1/2}}$ FROM WESSEL et al (1966)
BENDING	CANTILEVER BEAM	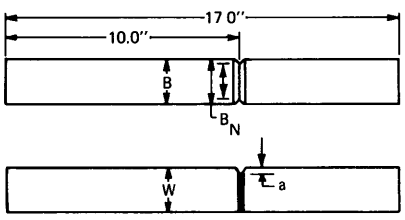	$K_I = \frac{4.12M\sqrt{\frac{1}{\alpha^3} - \alpha^3}}{BW^{3/2}}$ $\alpha \equiv 1 - \frac{a}{W}$ WHERE M = BENDING MOMENT AT THE NOTCH FROM KIES et al (1965)

Figure 69 Continued

SPECIMEN TYPE	SPECIMEN DESIGNATION	SPECIMEN GEOMETRY	EQUATION FOR K_I
BENDING	THREE-POINT BENDING	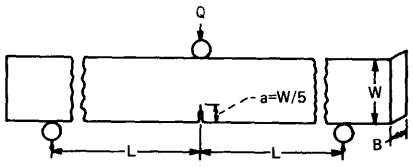 $2 < W/B < 8$	$K_I = \frac{6Ma^{1/2}}{B\,W^2}\left[1.96 - 2.75\left(\frac{a}{W}\right) + 13.66\left(\frac{a}{W}\right)^2 - 23.98\left(\frac{a}{W}\right)^3 + 25.22\left(\frac{a}{W}\right)^4\right]$ FOR L = 4W AND $K_I = \frac{6Ma^{1/2}}{B\,W^2}\left[1.93 - 3.07\left(\frac{a}{W}\right) + 14.53\left(\frac{a}{W}\right)^2 - 25.11\left(\frac{a}{W}\right)^3 + 25.80\left(\frac{a}{W}\right)^4\right]$ FOR L = 2W FROM WESSEL et al (1966)
BENDING	PURE BENDING FOUR POINT LOADING	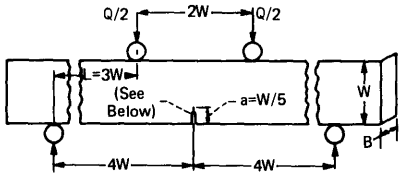 $2 < W/B < 8$	$K_I = \frac{6M}{B}\frac{a^{1/2}}{W^2}\left[1.99 - 2.47\left(\frac{a}{W}\right) + 12.97\left(\frac{a}{W}\right)^2 - 23.17\left(\frac{a}{W}\right)^3 + 24.80\left(\frac{a}{W}\right)^4\right]$ for $\frac{a}{W}$ = 0 to 0.6 where $M = \frac{PL}{2}$ FROM WESSEL et al (1966)
	DOUBLE TORSION PLATE	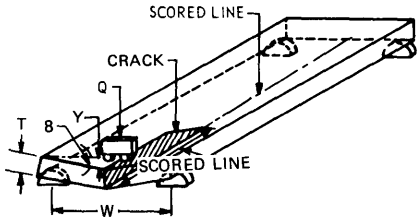	$K_I = \frac{QW}{2}\left[\frac{3E}{8GWtT^3}\right]^{1/2}$ WHERE t = T - depth of SCORED Line E = YOUNG'S MODULUS G = SHEAR MODULUS FROM KIES AND CLARK (1968)
CRACK ARREST	CENTER CRACKED WEDGE FORCE PANEL	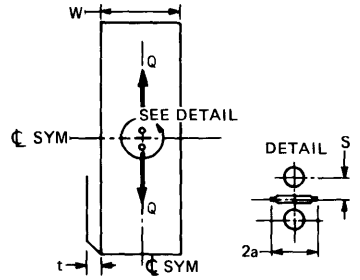	$K_I = \frac{Q}{2t}\left(\frac{a}{\pi}\right)^{1/2}\left[\frac{(3+\mu)\,s^2 + 2a^2}{(a^2+s^2)^{3/2}}\right]\left(\frac{W}{2\pi a}\sin\frac{2\pi a}{W}\right)^{-1/2}$ for $\frac{2a}{W} \leq 0.5$ FROM DOWNEY et al (1968)
SELF-STRESSED	MODIFIED WOL SPECIMEN FOR S.C.C.	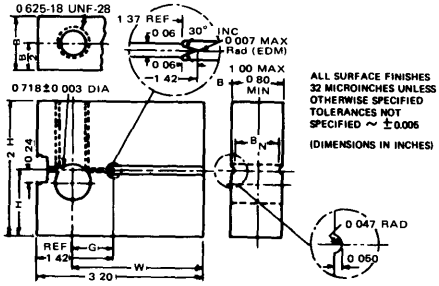	$K_I = \frac{Q}{Ba^{1/2}}\left[30.96\left(\frac{a}{W}\right) - 195.8\left(\frac{a}{W}\right)^2 + 730.6\left(\frac{a}{W}\right)^3 - 1186.3\left(\frac{a}{W}\right)^4 + 754.6\left(\frac{a}{W}\right)^5\right]$ $\frac{H}{W}$ = 0.486 Q = APPLIED LOAD FROM NOVAK AND ROLFE (1970)
SELF-STRESSED	WOL SELF-STRESSED SPECIMEN	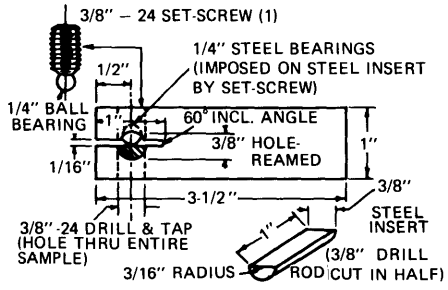	FROM DAHLEBERG (1966)

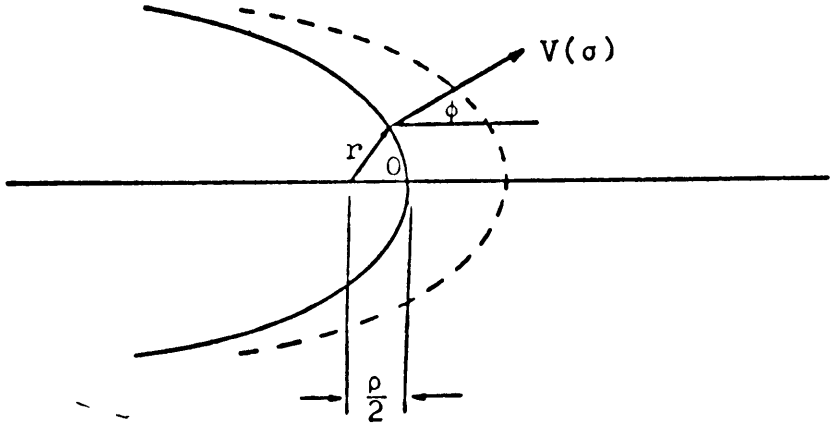

Figure 70 - Crack Extension Due to Stress Corrosion

(From Creager, 1970)

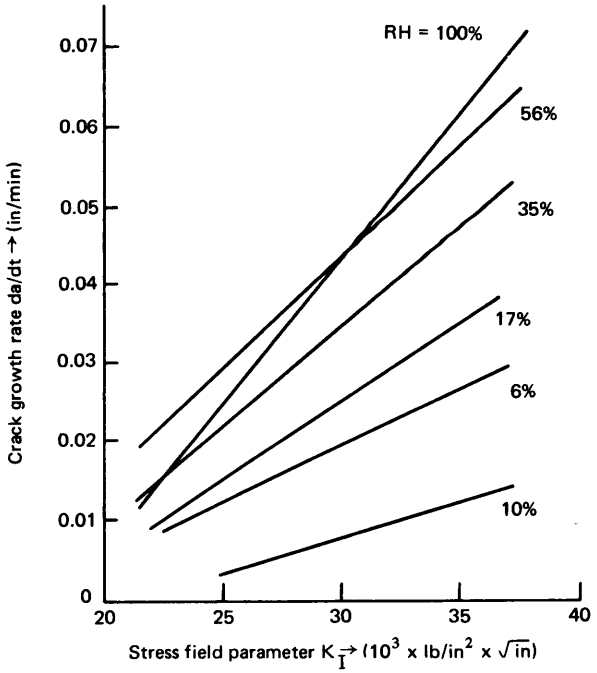

Figure 71 - Crack Growth Rates versus Stress Intensity for H-11 Steel in Humidified Argon

(From Johnson and Wilner, 1965)

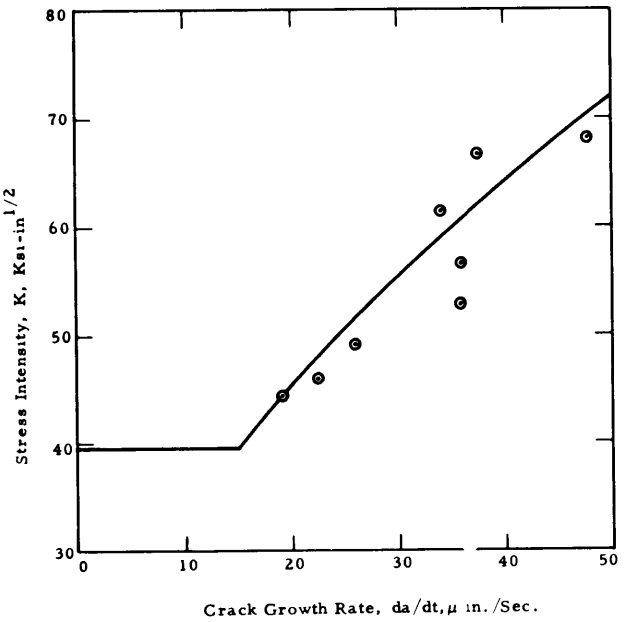

Figure 72 - Comparison of Actual and Predicted Crack Growth Rates for Hydrogenated D6aC Steel

(From Gerberich and Hartbower, 1967)

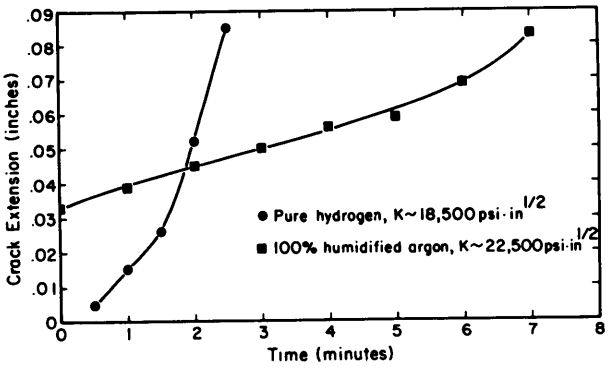

Figure 73 - Subcritical Crack Growth in Molecular Hydrogen at Atmospheric Pressure and Humidified Argon, H-11 Steel

(From Johnson, 1967)

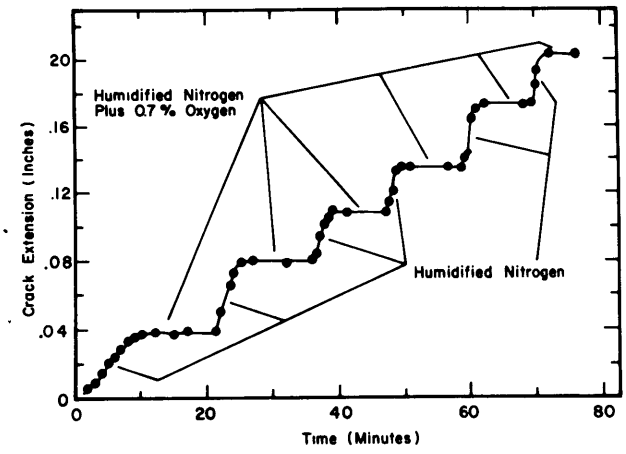

Figure 74 - Oxygen and Subcritical Crack Growth in Humidified Nitrogen, H-11 Steel

(From Johnson, 1967)

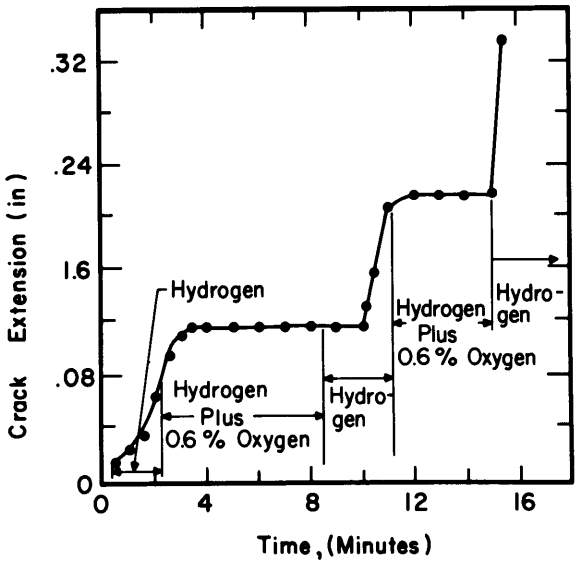

Figure 75 - Hydrogen-Oxygen Mixtures and Subcritical Crack Growth, H-11 Steel

(From Johnson, 1967)

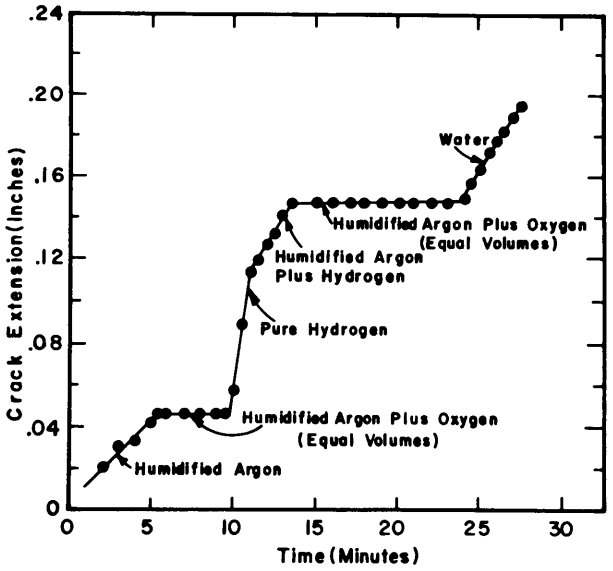

Figure 76 - Subcritical Crack Growth in Different Water, Water Vapor Hydrogen, and Oxygen Environments, HY-11 Steel

(From Johnson, 1967)

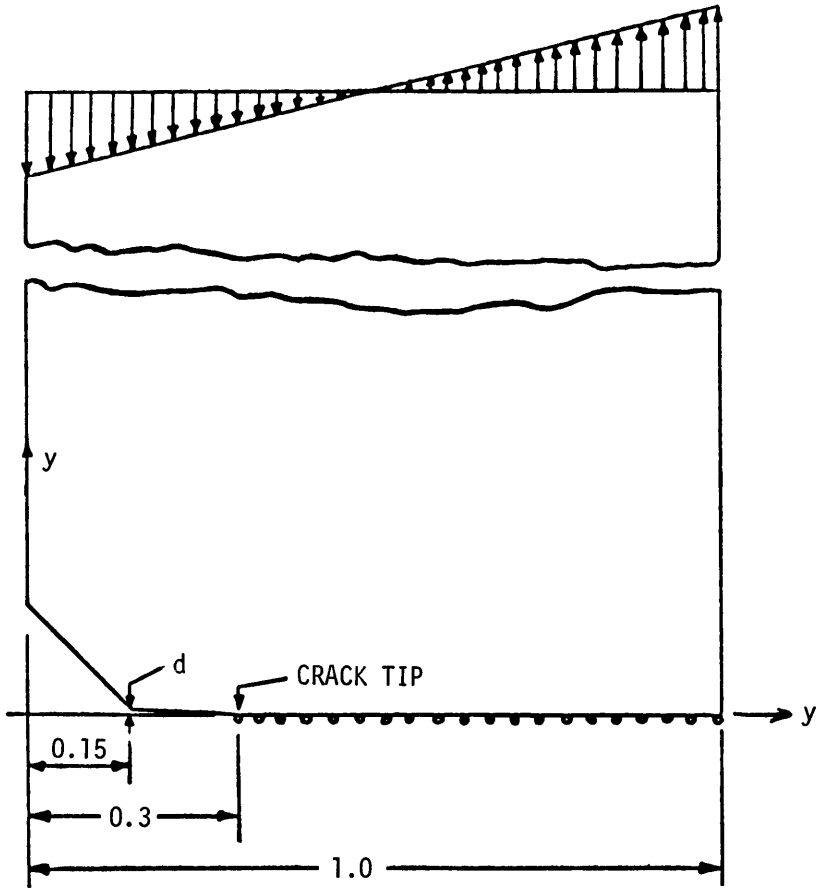

Figure 77 - Crack Tip Idealization Considering Corrosion Product Wedging Action

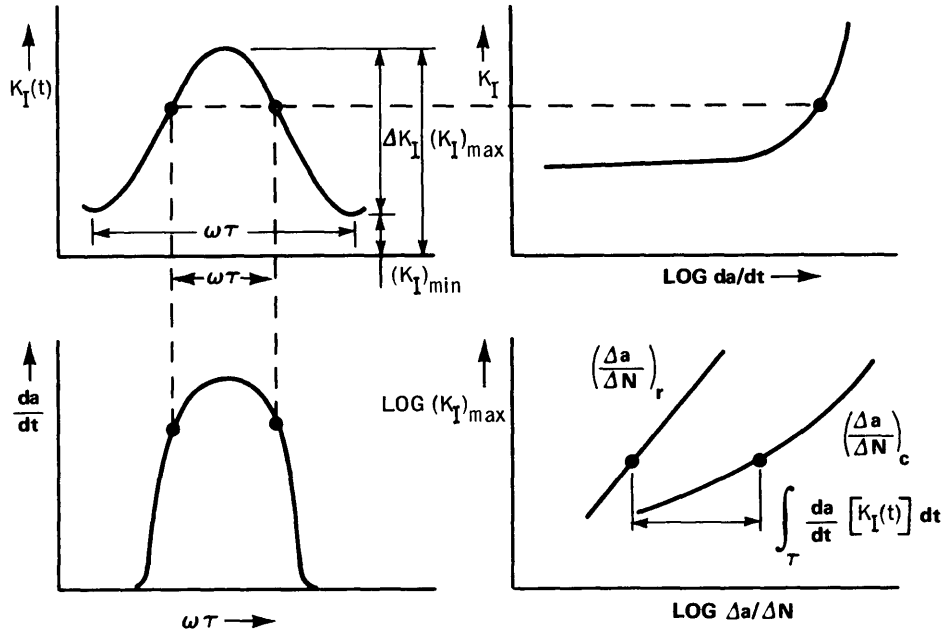

Figure 78 - Suggested Method of Analyzing the Effect of Environment on Fatigue Crack Growth Rate

(Stress intensity spectrum in fatigue (top left) rate of crack growth under sustained load in an aggressive environment (top right) environmental contribution to crack growth in fatigue (bottom left) and integrated effects of environment and K_{max} on fatigue crack growth rate. (bottom right). From Wei and Landes, 1969.

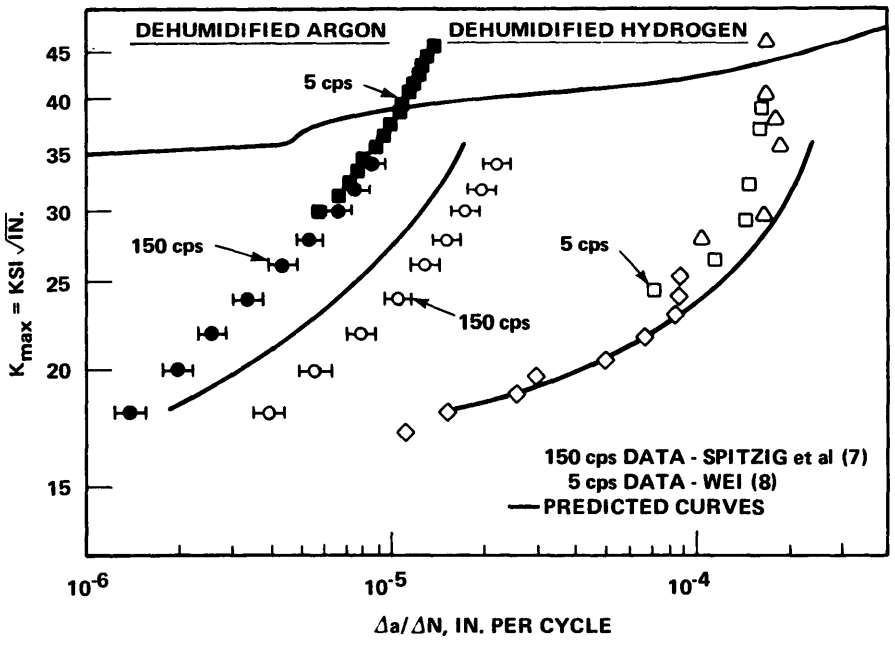

Figure 79 - Fatigue-Crack Growth in 18 Ni (250) Maraging Steels Tested in Dehumidified Argon and Hydrogen (From Wei and Landes, 1969)

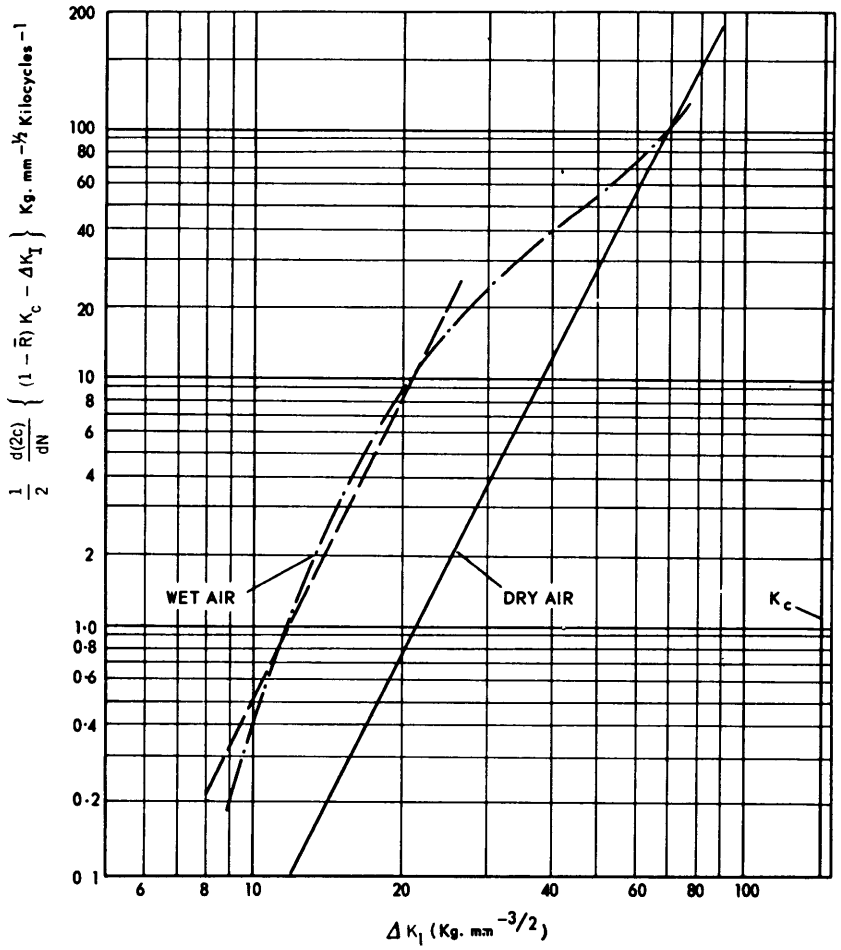

Figure 80 - Fatigue Crack Propagation of 7075-T6 Alclad Aluminum in Wet and in Dry Air High Load Frequency
(From Hartman and Schijve, 1970)

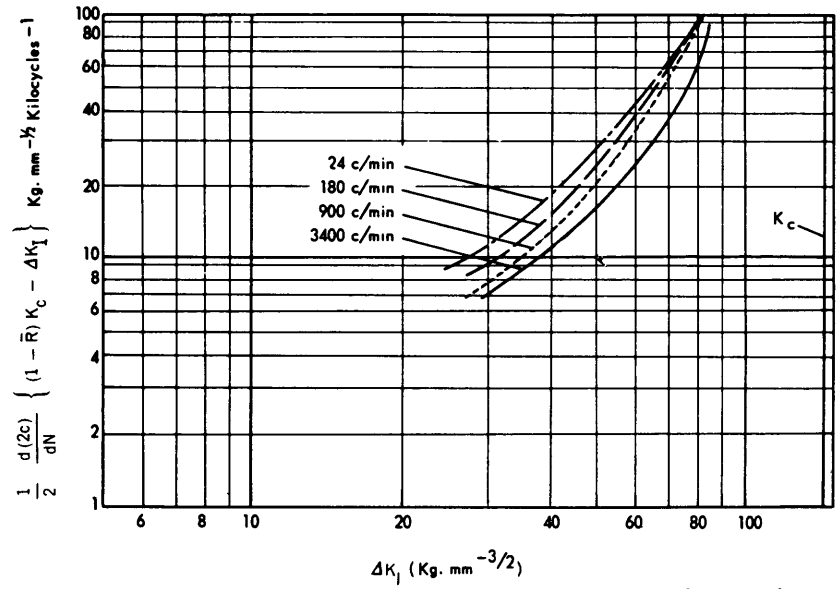

Figure 81 - Effect of Load Frequency for 2024-T3 Alclad Aluminum in Wet Air
(From Hartman and Schijve, 1970)

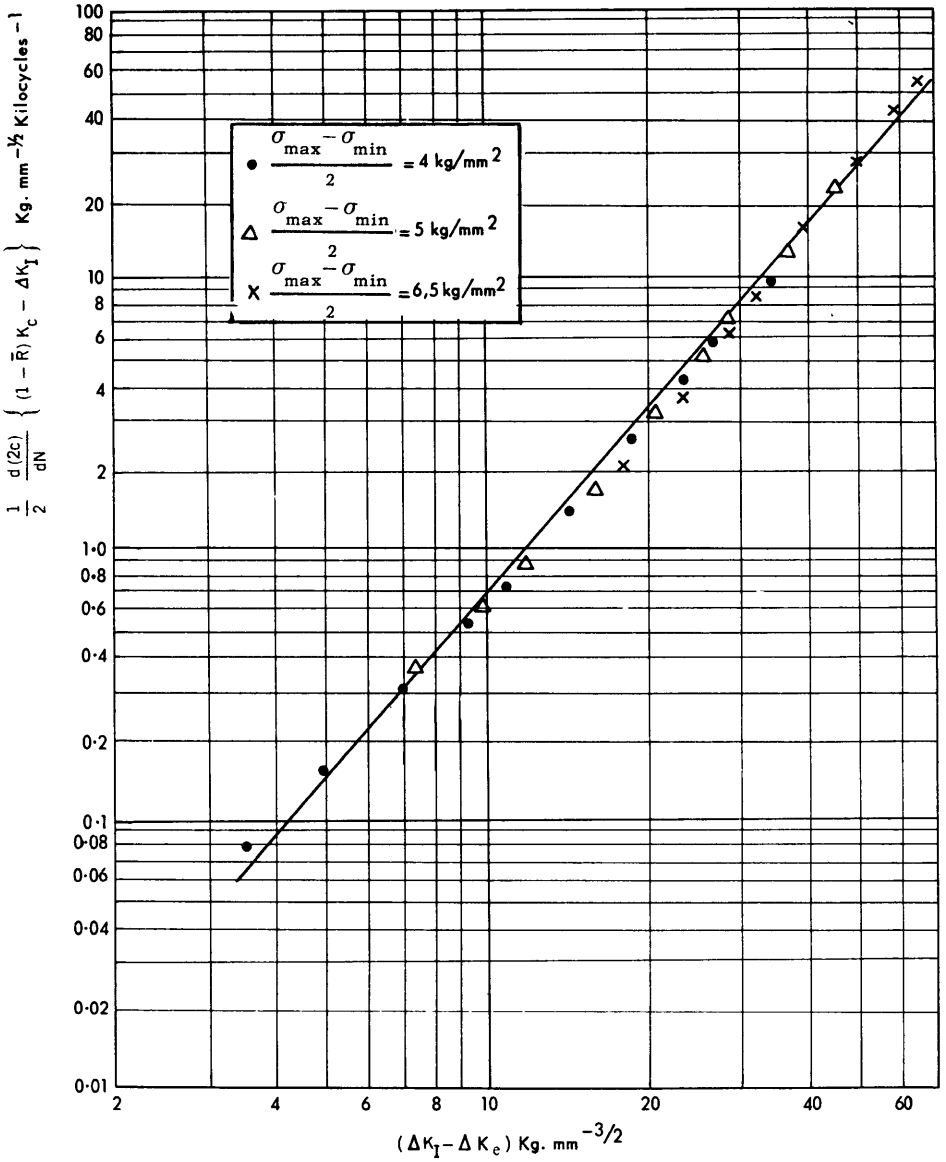

Figure 82 - Fatigue Crack Propagation of 2024-T3 Alclad Aluminum in Dry Argon
(From Hartman and Schijve, 1970)

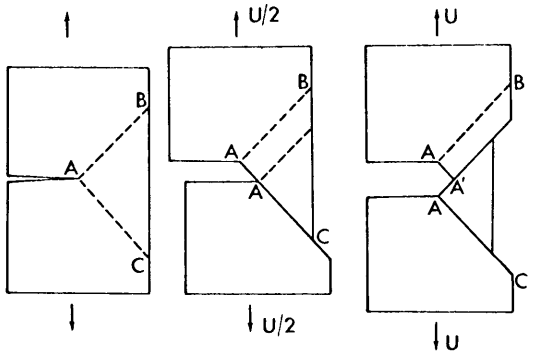

Figure 83 - Crack Extension by Alternating Shear
in a Singly Grooved Tensile Specimen
(From Pelloux, 1969)

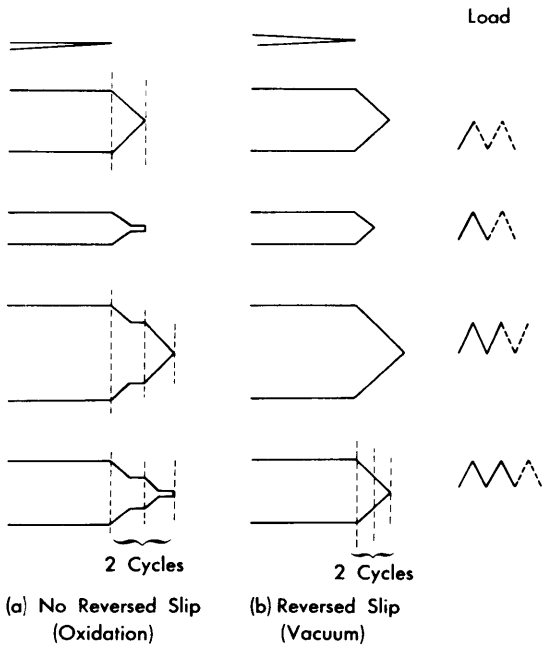

Figure 84 - Comparison of Crack Tip Extension after Two Load Cycles in Air and in Vacuum

(From Pelloux, 1969)

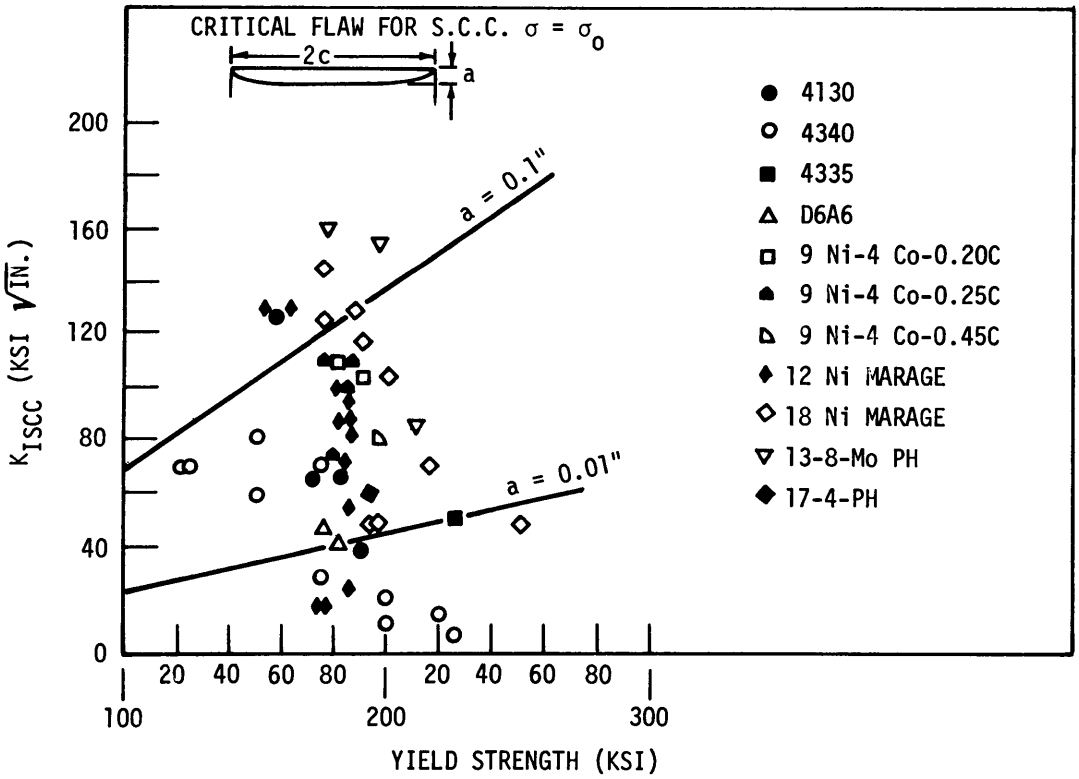

Figure 85 - K_{ISCC} Data for Several Alloy Steels

(From Sandoz, 1970)

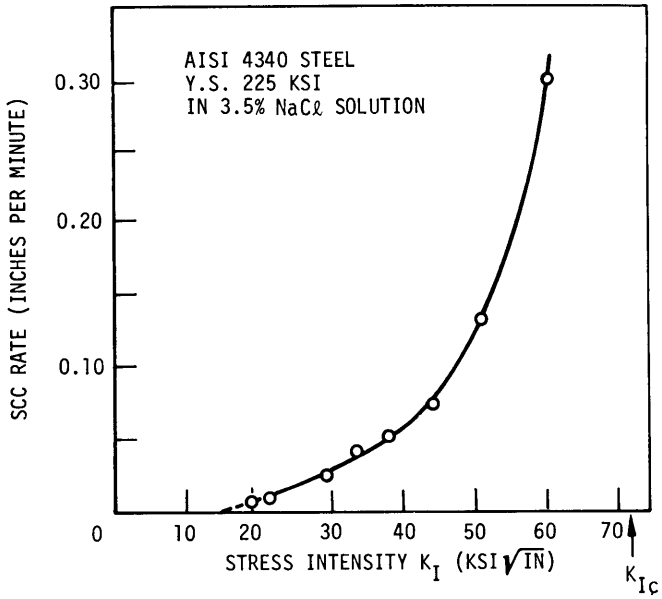

Figure 86 - Stress-Corrosion Crack Growth Rate of AISI 4340 Steel in Salt Water as a Function of Stress Intensity

(From Peterson et al., 1967)

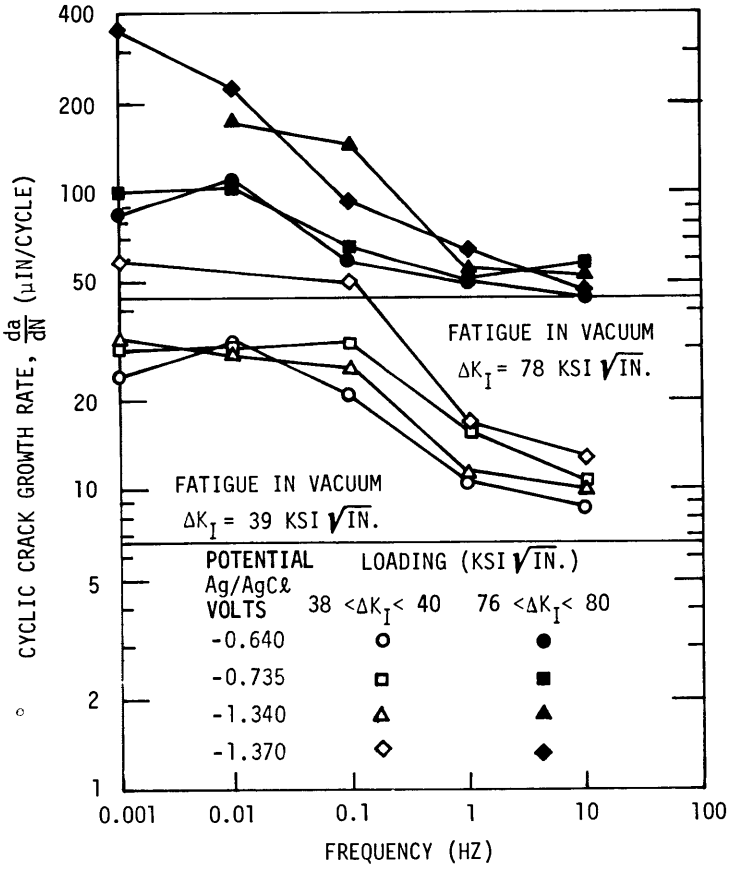

Figure 87 - Corrosion Fatigue Cyclic Crack Growth Rates in HY-80 Steel as a Function of Frequency

(From Gallagher, 1970)

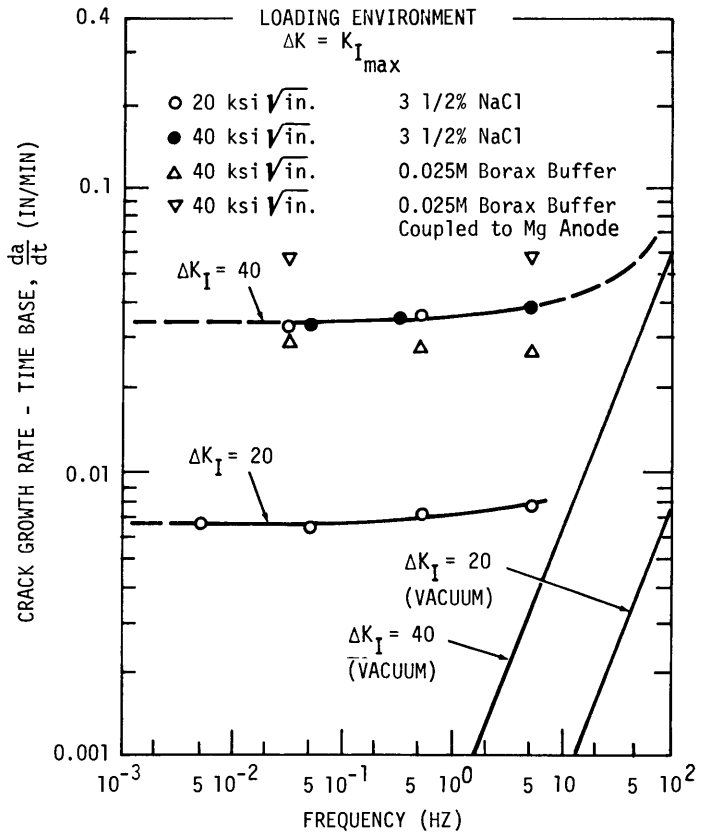

Figure 88 - Time-Based Crack Growth Rates in 4340 Steel as a Function of Frequency

(From Gallagher, 1970)

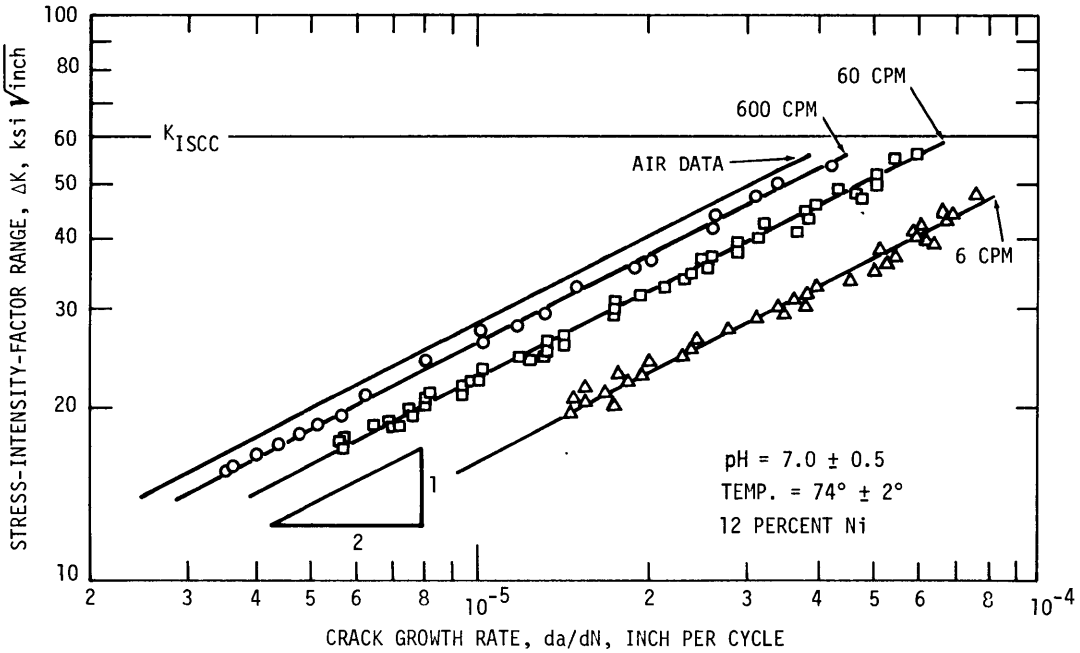

Figure 89 - Effect of Frequency on the Crack Growth Rate of 12 Ni-5 Cr-3 Mo Maraging Steel in a 3-Percent NaCl Solution

(From Barsom, 1969)

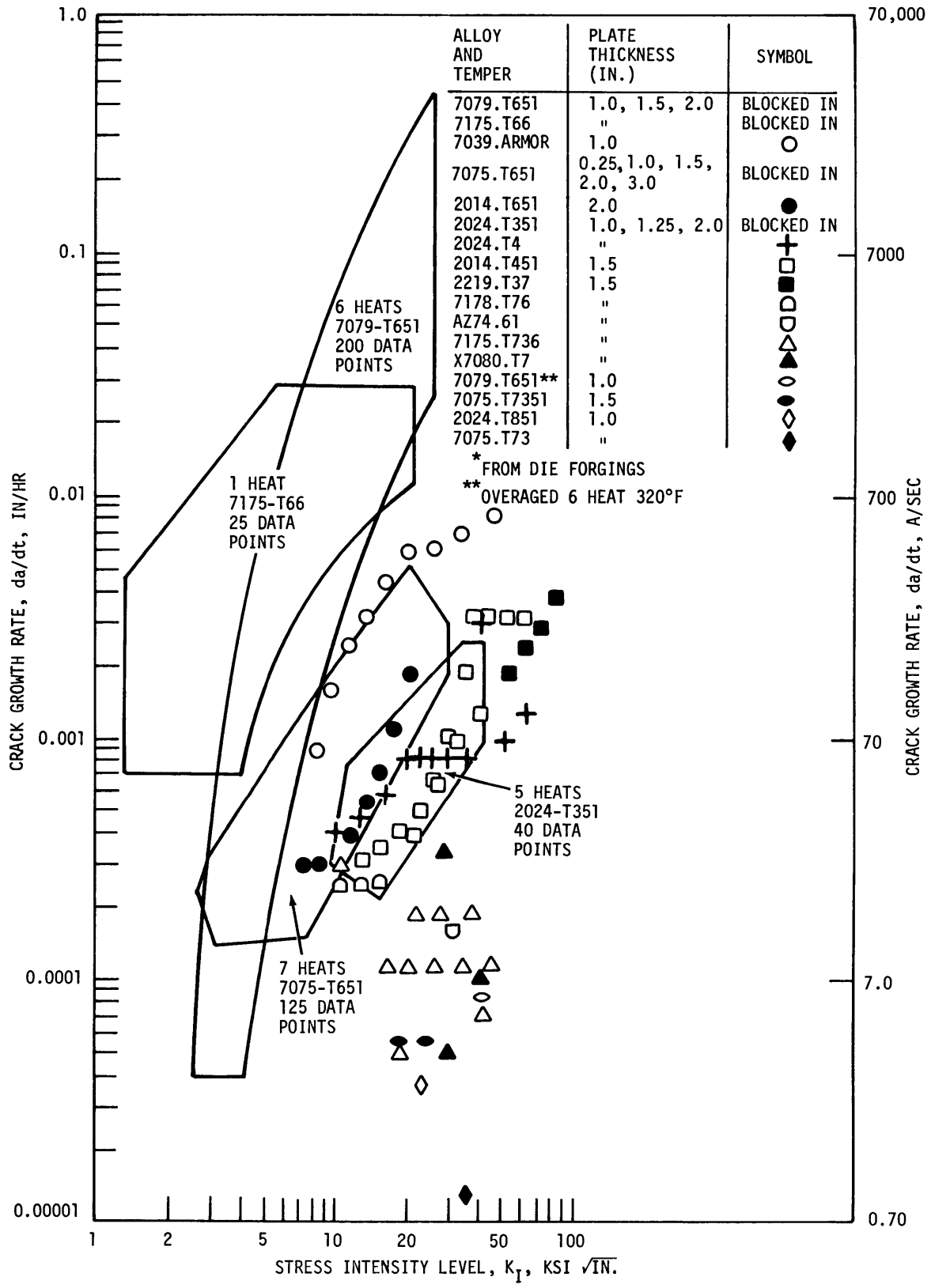

Figure 90 - Stress-Corrosion Crack Growth Rates for Aluminum Alloys as a Function of Stress Intensity
(From Hyatt, 1967)

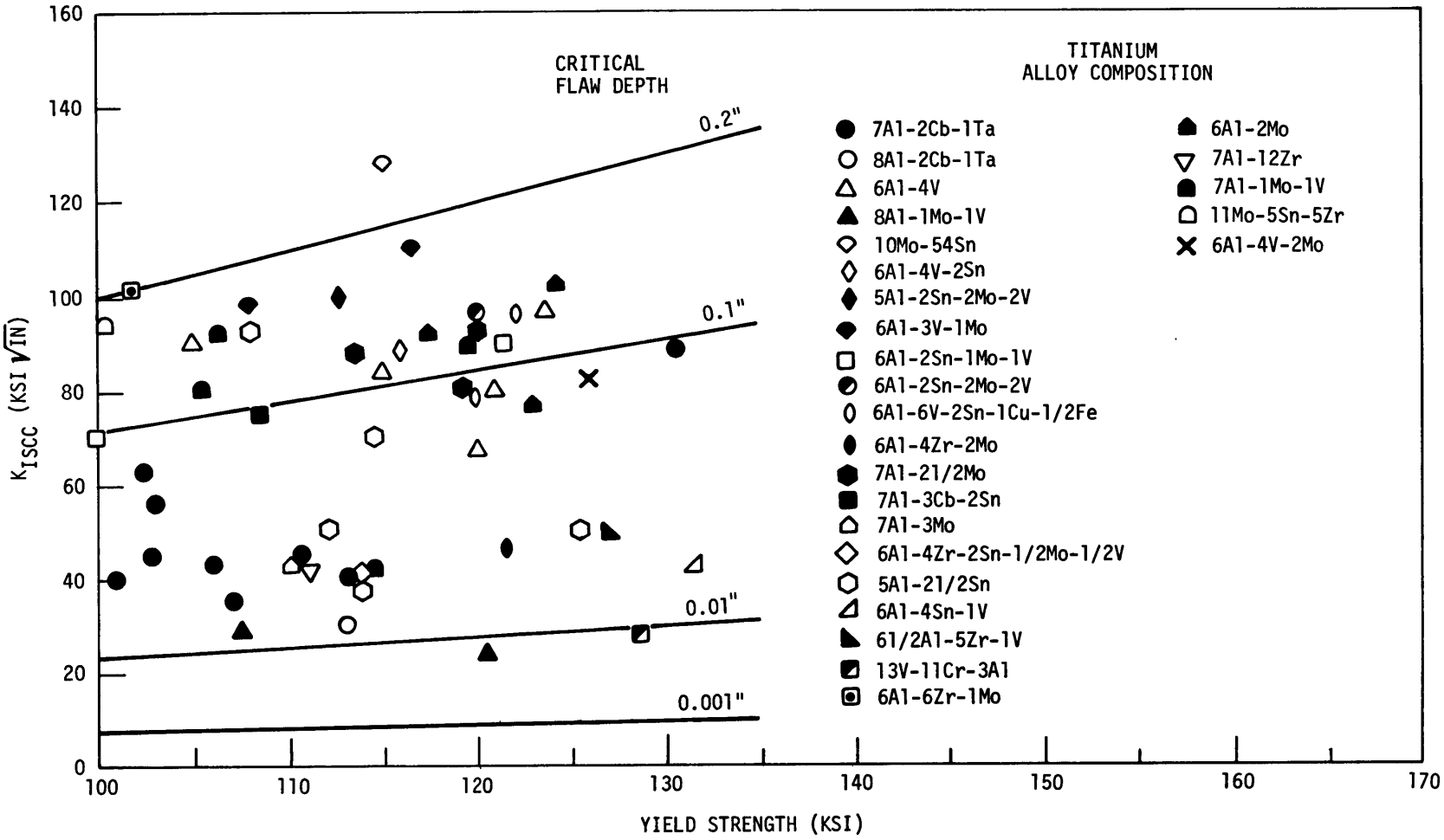

Figure 91 - Summary of Stress Corrosion Cracking Resistance Index for Titanium Alloys in 3.5-Percent NaCl Solution

(From Goode et al., 1967)

TABLE 1

Criteria for the Extension of Axial Through Cracks in Unstiffened Pressure Vessels

(From Hahn et al., 1969)

Category	Specifications $\frac{R_m}{t}\left(\frac{K_c}{\sigma_o}\right)^2\frac{1}{c}$	Criterion	M	Applications
1. Intermediate wall thickness, low-to medium-toughness vessels with relatively long cracks	5-50 > 7	$\sigma_H^* = \frac{K_c}{(\pi c \phi_3)^{\frac{1}{2}}} M^{-1}$	$\left[1 + 1.61\frac{c^2}{R_m t}\right]^{\frac{1}{2}}$	Steel pipe lines and pressure vessels operating below the shear-to cleavage-fracture transition temperature
2. Intermediate wall thickness high-toughness vessels with relatively short cracks	5-50 > 7	$\sigma_H^* = \bar{\sigma} M^{-1}$ and $\bar{\sigma}(\text{ksi}) = 1.04\sigma_o(\text{ksi}) + 10.0$ $\bar{\sigma}(\text{ksi}) = 1.23\sigma_o(\text{ksi})$ $\bar{\sigma}(\text{ksi}) = 0.66[\sigma_o(\text{ksi}) + \sigma_U(\text{ksi})] - 18.1$ $\bar{\sigma}(\text{ksi}) = 0.51[\sigma_o(\text{ksi}) + \sigma_U(\text{ksi})]$	$\left[1 + 1.61\frac{c^2}{R_m t}\right]^{\frac{1}{2}}$	Steel pipe lines and pressure vessels that fail by 100% shear fracture
3. Very thin wall low and medium toughness vessels with relatively long cracks	> 5-50 > 7	$\sigma_H^* = \frac{K_c}{(\pi c \phi_3)^{\frac{1}{2}}} M^{-1}$	$\left[1 + 1.61\frac{c^2}{R_m^2}\left(50 \tanh \frac{R_m}{50t}\right)\right]^{\frac{1}{2}}$	Thin walled rocket propeller tanks

A Vessel radius

t Wall thickness

2c Crack length

K_c Fracture toughness

σ_H^* Critical hoop stress

σ_U Ultimate tensile stress

$\bar{\sigma}$ Average flow stress. Note that more than one definition of $\bar{\sigma}$ is used. The value of $\bar{\sigma}$ appropriate for the failure criterion of Category 2 vessels is reasonably well established only for low- and medium-strength steel vessels. The value of $\bar{\sigma}$ to be inserted into ϕ_3 cannot be defined as precisely. At present, only the following estimates of the upper and lower bound are employed: $\sigma_o < \bar{\sigma} < \sigma_U$.

ϕ_3 Plasticity correction

$$\begin{cases} \phi_3 = \left(\frac{\pi\sigma_H^* M}{2\bar{\sigma}}\right) \ln\left[\sec\frac{\pi\sigma_H^* M}{2\bar{\sigma}}\right] \\ \sigma_o < \bar{\sigma} < \sigma_U \end{cases}$$

TABLE 2 - SUMMARY OF CYCLIC CRACK GROWTH DATA

Material	Regime No. 1				Transition		Regime No. 2			References
	Yield Stress σ_o (Ksi)	ΔK_I Data Range (Ksi $\sqrt{in.}$)	$(\Delta K_I)_{10^{-5}}$ (Ksi $\sqrt{in.}$)	m	$(\Delta K_I)_{1-2}$ (Ksi $\sqrt{in.}$)	$\frac{(\Delta K_I)_{1-2}}{\sigma_o}$ ($\sqrt{in.}$)	ΔK_I Data Range (Ksi $\sqrt{in.}$)	$(\Delta K_I)_{10^{-3}}$ (Ksi $\sqrt{in.}$)	m	
Steels										
Fe-3Si	54	-	38	-	-	-	-	-	-	Hahn, et al Dec 1969
A-302B[c]	59	-	-	-	-	-	40-120	~ 165	3.1	Mobray, et al 1968
A-302B[d]	51	-	-	-	~ 40	~ 0.8	40-110	~ 130	4.2	Mobray, et al 1968
A-508-2[e]	65	-	-	-	-	-	45-90	~ 200	~ 2.9	Mobray, et al 1968
A-508-2[d]	67	-	-	-	-	-	60-110	~ 150	~ 3.2	Mobray, et al 1968
A-533	73	30-100[e]	38/40[e]	2.1/2.2[e]	-	-	-	-	-	Bates and Clark 1968
3Ni-Mo-V	93	30-150	34	~ 1.85	-	-	-	-	-	Bates and Clark 1968
HY-80[a]	87	21-61	38	2.48	-	-	-	-	-	Barsom, et al 1968
HY-80[b]	95	23-50	33	2.54	-	-	-	-	-	Barsom, et al 1968
HY-100 Steel	109	5.6-26	20/23	2.3/2.6	-	-	-	-	-	Yokobori, et al 1967
HY-130[a]	139	19-68	28	2.16	-	-	-	-	-	Barsom, et al 1968
HY-130[b]	140	42-92	29.5	2.13	92	0.66	92-150	~ 140	6/8	Barsom, et al 1968
4340 (ANNEALED)	60	14-20/25	20	2.2/2.6	20/25	0.3/0.4	20/25-35	-	4.0	Liu and Lino 1969
4340 (Q & T @ 1400F)	63	-	35	-	-	-	25-70	~ 120	4/3.2[e]	Miller 1968, 1969
4340 (Q & T @ 1000F)	163	20-80	33	2.4/2.26[e]	~ 80	0.49	80-110	~ 120	-	Miller 1968, 1969
4340 (Q & T @ 500F)	221	20-80	33	2.6	~ 80	0.36	80-90	~ 95	-	Miller 1968, 1969
4340 (Q & T @ 200F)	193	-	-	-	-	-	20-45	~ 50	6.73	Miller 1968, 1969
9Ni-4Co-0.25C	180	-	-	-	-	-	40-100	90	3.7	Crooker, et al May 1968
9Ni-4Co-0.25C	175/180	45-80	~ 34	~ 1.85	-	-	-	-	-	Bates and Clark 1968
10Ni-Cr-Mo-Co[a]	191	5.5-80	35	2.25	86	0.45	86-140	~ 165	3.8	Barsom, et al 1968
10Ni-Cr-Mo-Co[b]	182	30-60	30	2.24	-	-	-	-	-	Barsom, et al 1968
12Ni-5Cr-3Mo[a]	185	21-60	31	2.16	-	-	-	-	-	Barsom, et al 1968
12Ni-5Cr-3Mo[b]	184	25-60	28	2.18	-	-	-	-	-	Barsom, et al 1968
12Ni-5Cr-3Mo	194	33-80	33	2.3	80	-	80-105	~ 130	~ 5.0	Schwab July 1968
12Ni-5Cr-3Mo (NaCl,600CPM)	184	15-53	26	~ 2.0	-	-	-	-	-	Barsom 1969
12Ni-5Cr-3Mo (NaCl,60CPM)	184	18-55	23	~ 2.0	-	-	-	-	-	Barsom 1969
12Ni-5Cr-3Mo (NaCl,6CPM)	184	20-47	16	~ 2.0	-	-	-	-	-	Barsom 1969
12Ni-Maraging	180	25-100	25	2.3	-	-	-	-	-	Crooker and Lange Sep 1968
18Ni-Maraging	180	42-90	~ 16	2.3	-	-	-	-	-	Crooker and Lange Sep 1968
18Ni-Maraging	218	20-80	31	2.3/2.5/1.42[e]	~ 80	-	80-100	~ 110		Miller 1968, 1969
18Ni-Maraging	245	20-100	35	2.88/1.74[e]	-	-	-	~ 150	-	Miller 1968, 1969
18Ni-Maraging	246/252	20-80	36	2.4	80	0.32	80-100	-	-	Wei, et al 1967 and Carman and Katlin 1966
18Ni-Maraging	295/308	18-60	35	2.6	-	-	-	-	-	Wei, et al 1967 and Carman and Katlin 1966
H 11	208	-	-	-	-	-	21-29	~ 50	6.62	Miller 1968, 1969
H 11	242	-	34				27-60	~ 120	~ 4.0	Carman and Katlin 1966
D6AC	241	32-80	32	~ 2.8	~ 70	-	-	-	-	Carman and Katlin 1966

(a) 1-in.-thick plate
(b) 2-in.-thick plate
(c) Thickness direction
(d) Axial direction
(e) Based on striation spacing

TABLE 3

Stress Corrosion Characteristics of Some Titanium Alloys

(From Judy and Goode, 1967)

Titanium Alloys	Code	YS (ksi)	DWTT (ft-lbs)	K_{Ix} (ksi $\sqrt{in.}$)	K_{ISCC} (ksi $\sqrt{in.}$)	Specimen Dimensions			Remarks
						Depth (in.)	Width (in.)	Side Groove Depth (in.)	
5Al-2.5Sn	3	112	2750	130	50	1	3/4	1/10	
5Al-2.5Sn	7	125.5	2000	119	50	1	3/4	1/8	
13V-11Cr-3Al	9	128.5	1000	88	28	1	3/4	1/8	
Unalloyed	17	83	500	69	40	1	3/4	1/32	High interstitial
5Al-2.5Sn	18	--	1750	112	50	1	3/4	1/10	
5Al-2.5Sn	18	114.7	1750	128	72	1	11/16	1/8	
8Al-1Mo-1V	19	120.4	--	88	23	1	1/2	--	1700°F/1 hr/AC-1200°F/2 hr/WQ
8Al-1Mo-1V	19	107.9	--	112	28	1	1/2	--	1825°F/1 hr/AC
6Al-4Sn-1V	20	131.4	2250	114	42	1	11/16	1/32	1825°F/1 hr/WQ-1100°F/2 hr/AC
6Al-6V-2.5Sn	21	179.6	--	55	21	1	3/4	--	1550°F/1 hr/WQ-900°F/4 hr/AC
6Al-2Mo	22	124.4	3333	122	102	1	11/16	1/32	1750°F/1 hr/AC-1100°F/4 hr/WQ
8Al-2Cb-1Ta	23	113	1750	102	31	1	3/4	1/32	
6Al-2Sn-1Mo-1V	25	100	2250	109	70	1	3/4	1/10	
6Al-4V	27	120	931	88	67	1	11/16	1/32	
6Al-4V	32	121	660	101	80	1	3/4	1/10	High interstitial
6.5Al-5Zr-1V	36	127	1480	99	49	1	3/4	1/10	
6Al-2Sn-1Mo-1V	37	121.5	1660	112	90	1	3/4	--	
7Al-2Cb-1Ta	39	106	2086	105	43	1	11/16	--	
6Al-6Zr-1Mo	41	102	2646	106	102	1	1/2	1/16	
7Al-3Mo	46	103.9	2808	128	45	1	--	--	
3Al	52	71.3	>5000	81	64	1	1/2	1/16	
6Al-4Zr-2Mo	55	121.4	1478	117	46	1	3/4	1/32	
6Al-4V	56	123.7	--	116	95	1/2	1/2	--	
5Al-2.5Sn	57	113.6	--	112	39	1/2	1/2	--	
7Al-2Cb-1Ta	58	113.0	--	42	40	1/2	1/2	--	
6Al-2Mo	59	123.0	--	116	76	1/2	1/2	--	
7Al-12Zr	62	110.5	870	108	42	1	3/4	1/8	Laminate structure
6Al-4V-2Sn	67	115.8	1173	97	88	1	3/4	1/8	
6Al-4Zr-2Sn-0.5Mo-0.5V	68	113.5	1784	124	40	1	3/4	1/8	
10Mo-5.4Sn	69	115	1905	129	128	1	1/2	1/16	1200°F/48 hr/WQ
7Al-2Cb-1Ta	70	102.4	2114	110	63	1	1/2	--	Distilled water
7Al-2Cb-1Ta	70	100.8	2294	118	40	1	11/16	--	Sea water
7Al-2.5Mo	71	113.5	1751	112	88	1	3/4	1/32	
7Al-2Cb-1Ta	72	102.8	2174	134	45	1	5/8	1/10	2200°F/lge reduction/AC
7Al-2Cb-1Ta	73	103	2206	130	56	1	5/8	1/10	
7Al-2Cb-1Ta	74	--	2206	122	50	1	5/8	1/10	Planetary rolled
7Al-2Cb-1Ta	75	--	2902	118	43	1	5/8	1/10	
7Al-3Cb-2Sn	76	108.5	2026	146	75	1	5/8	1/10	
7Al-2Cb-1Ta	78	--	3281	129	88	1	1/2	1/16	
6Al-2Mo-2V-2Sn	80	120	1540	99	96	1	3/4	1/10	
7Al-1Mo-1V	88A	--	--	94	90	1/2	1/2	1/16	1750°F/1 hr/vac. FC
7Al-1Mo-1V	88B	--	--	90	78	1/2	1/2	1/16	
7Al-1Mo-1V	88C	105.6	2443	111	80	1	1/2	1/32	
7Al-1Mo-1V	88D	106.4	2026	122	92	1	1/2	1/32	1850°F/1 hr/He cool
7Al-1Mo-1V	88E	119.8	1228	117	90	1	1/2	1/32	1750°F/1 hr/He cool
7Al-1Mo-1V	88	113.7	--	118	42	1	3/4	1/32	1800°F/1 hr/He cool
7Al-2Cb-1Ta	89	110.6	2146	119	45	1	5/8	1/8	
5Al-2V-2Mo-2Sn	90	112.7	1723	108	100	1	3/4	1/10	
6Al-4V	91	104.9	1228	118	90	1	3/4	1/10	
6Al-6V-2Sn-1Cu-0.5Fe	92	122.1	681	111	96	1	3/4	1/10	
6Al-6V-2Sn-1Cu-0.5Fe	92	120.1	--	102	78	1	3/4	1/32	1660°F/1 hr/He cool
6Al-3V-1Mo	93	116.5	1173	116	110	1	3/4	1/10	
6Al-3V-1Mo	93	--	--	112	98	1	3/4	1/32	1850°F/1 hr/He cool
7Al-2.5Mo	94	119.2	1540	101	80	1	1/2	1/32	
7Al-2.5Mo	94B	99.0	2086	118	93	1	1/2	1/32	1800°F/1 hr/He cool
7Al-2.5Mo	94	108	--	123	92	1	3/4	1/32	1800°F/1 hr/He cool
6Al-4V	95	--	811	94	68	1	1/2	1/32	ELI Grade (<0.12%O_2)
6Al-4V (ELI)	95	--	--	112	84	1	3/4	1/32	1850°F/1 hr/He cool
6Al-2Cb-1Ta-0.8Mo	96	--	2384	117	98	1	1/2	1/32	
11Mo-5Sn-5Zr	97	100.5	1021	117	94	1	1/2	1/32	
3.5Al	98	74.0	397	90	80	1	1/2	1/32	
3.5Al	98	70.9	4724	101	80	1	1/2	1/32	1660°F/1 hr/He cool
6Al-4V	100E	--	1052	107	100	1	1/2	1/32	
6Al-2Mo	R1	117.6	1601	107	94	1	3/4	1/32	
6Al-4V-2Mo	R2	126.0	1052	96	82	1	3/4	1/32	
6Al-6V-2Sn-2Mo	R4	138.2	514	71	65	1	3/4	1/32	
6Al-6V-2Sn-2Mo	R4	126.8	681	91	82	1	3/4	1/32	1660°F/2 hr/He cool
Unalloyed = A-70	--	78-84	--	65	44	1/2	1/4	--	High interstitial
7Al-2Cb-1Ta	--	105-110	--	100	35	7/8	1/2	--	Mat'l from DTMB NSRDC
8Al-1Mo-1V	--	130	--	54	18	1/8	--	--	
6Al-4V	--	165	--	64	55	3/4	1/10	--	Minuteman Casing Mat'l

REFERENCES

Achter, M.R., "Effect of Environment on Fatigue Cracks," ASTM STP 415 (Fatigue Crack Propagation), pp. 181-202 (1967).

American Society for Testing Materials, "Plane Strain Crack Toughness Testing of High Strength Metallic Materials," ASTM STP 410 (1966).

American Society of Mechanical Engineers, "Criteria of Section III of the ASME Boiler and Pressure Vessel Code for Nuclear Vessels," ASME 22 (1964).

Ang, A.H.-S. and Amin, M., "Development of a Probabilistic Reliability Model for Evaluating Structural Safety and Design of Deep Submersibles," University of Illinois Annual Report to Department of Structural Mechanics, NSRDC, Contract N00014-69-C-0436 (Sep 1970).

Ayres, D.J., "A Numerical Procedure for Calculating Stress and Deformation near a Slit in a Three-Dimensional Elastic-Plastic Solid," NASA Tech. Memo TMX-52410 (1968).

Barenblatt, G.I., "Mathematical Theory of Equilibrium Cracks in Brittle Fracture," Advances in Appl. Mech., Vol. VII, Academic Press, New York (1962).

Barsom, J.M., "Investigation of Subcritical Crack Propagation," M.Sc. Thesis, University of Pittsburgh (1969).

Barsom, J.M., "Corrosion-Fatigue Crack Propagation below K_{ISCC}," presented to the Third National Symposium on Fracture Mechanics, Lehigh University (1969).

Barsom, J.M., "Mechanisms of Corrosing Fatigue below K_{ISCC}," Fourth National Symposium on Fracture Mechanics, Pittsburgh, Pa. (1970).

Barsom, J.M. et al., "Fatigue-Crack Propagation in High Yield-Strength Steels," U.S. Steel Applied Research Laboratory Report 39-018-007(27), B-23103, B-63103 (Dec 1968).

Bates, R.C. and Clark, W.G., "Fractography and Fracture Mechanics," 68-107-RPAFC-P1, Westinghouse Research Laboratory, Pittsburgh, Pa (1968).

Beeuwkes, Jr. R., "Characteristics of Crack Failure," Proc. 14th Sagamore Army Materials Research Conference, Syracuse Univ. Press, p. 277 (1968).

Beeuwkes, Jr. R., "On Status of Correlation of Crack Failure with Material Properties in Metals," AMMRC TN 69-01 (Mar 1969).

Bement, A.A. and Pohler, C.H., "Fracture Mechanics - A Basic Solution to Fatigue Using Energy Principles," J. Ship Res., Vol. 10, No. 2 (Jun 1966).

Bieniawski, Z.T., "Mechanism of Brittle Fracture of Rock, Part 1 - Theory of the Fracture Process," Int. J. Rock Mech. Min. Sci. (Great Britain), Vol. 4, pp. 395-406 (1967).

Blatherwick, A.A. and Olson, B.B., "Stress Redistribution in Notched Specimens during Fatigue Cycling," presented at Meeting Soc. Exper. Stress Anal. (SESA), Albany, New York (May 1968).

Boblenz, T.L. and Rolfe, S.T., "Corrosion-Fatigue Characteristics of HY-80 15 Ni-Cr-Mo-V, 12 Ni-5Cr-3Mo and 18 Ni-8Co-3Mo Steels," U.S. Steel Appl. Res. Lab. Report 39018-002(37), (S-23008-2) (1 Jan 1966).

Booker, C.J.L., "Some Electrochemical Factors in the Stress Corrosion of α-Brass," Proc. Conf. on Fundamental Aspects of Stress Corrosion Cracking, published by NACE, pp. 178-184 (1967).

Broek, D., "The Effect of the Sheet Thickness on the Fracture Toughness of Cracked Sheet," Report NLR-TR M2160, Delft, Netherlands (Jan 1966).

Broek, D., "Some Considerations on Slow Crack Growth," Int. J. Fract. Mech., Vol. 4, No. 1, p. 20 (Mar 1968).

Broek, D., "A Critical Note on Electron Fractography, Eng. Frac. Mech., Vol. 1, No. 4, pp. 691-695 (1970).

Brown, B.F., "A New Stress-Corrosion Cracking Fest for High Strength Alloys," ASTM Mat. Res. Stand., Vol. 66, p. 129 (1966).

Brown, B.F., "Implication of Cathodic Reduction of Hydrogen to Stress-Corrosion Cracking," presented to the Electrochemical Society, Detroit, Michigan (Oct 1969).

Brown, B.F., "Application of Fracture Mechanics and Fracture Technology to Stress Corrosion Cracking," Conf. on Fract. Control, Philadelphia, Pennsylvania (1970).

Brown, B.F. and Beachem, C.D., "A Comparison of Three Precracked Specimens for Evaluating the Susceptibility of High Strength to Stress Corrosion Cracking," Stress Corrosion Testing, ASTM STP 425, p. 31 (1967).

Brown, B.F. et al., "Marine Corrosion Studies," NRL Memorandum Report 1634 (Jul 1965).

Brown, B.F. et al., "Method for Studying the Solution Chemistry within Stress Corrosion Cracks," J. Electrochem. Soc., Vol. 116, p. 218 (1969).

Brown, W.F. Jr. and Srawley, J.E., "Plane Strain Crack Toughness Testing of High Strength Metallic Materials," ASTM STP 410, 1966, p. 12.

Carman, C.M. and Katlin, J.M., "Low Cycle Fatigue Crack Propagation of High Strength Steels," ASME 66-MET-3 (Apr 1966).

Carter, C.S., "Stress Corrosion Crack Branching in High Strength Steels," Boeing Company Report D6-23871 (Mar 1969).

Catanach, W.M., "A Study of Fatigue Crack in the Cylindrical Shells Containing a Meridional Crack," Ph.D. Dissertation, Lehigh University (1967).

Champion, F.A., "Symposium on International Stresses in Metals and Alloys," Inst. of Metals, London, p. 468 (1948).

Chan, S.K. et al., "On the Finite Element Method in Linear Elastic Fracture Mechanics," Scientific Paper 68-ID7-FMPWR-P1, Second National Fracture Mechanics, Lehigh University (17-19 Jun 1968).

Chin, L.L.J., "A Model for Toughness Studies of Welds," Welding Res. Suppl., p. 290 (Jul 1969).

Christensen, R.H., "Growth of Fracture in Metal Under Random Cyclic Loading," First Conf. on Fracture, Sendai, Japan (Sep 1965).

Christensen, R.M. and Harmon, M.B., "Limitations of Fatigue Crack Research in the Design of Flight Vehicle Structures," ASTM STP 415, p. 5 (1967).

Clark, W.G., Jr., "Subcritical Crack Growth and Its Effect upon the Fatigue Characteristics of Structural Alloys," Eng. Fract. Mech., Vol. 1, No. 2, p. 385 (Aug 1968).

Coe, F.R. and Moreton, J., "Estimation of Diffusibility Coefficients for Hydrogen in Ferrous Materials," British Welding J., Vol. 43 (1967).

Coffin, L.F., Jr., "A Study of the Effects of Cyclic Thermal Stresses on a Ductile Metal," Trans. ASME, Vol. 76, pp. 931-950 (1954).

Coleman, E. et al., "On a Surface Energy Mechanism for Stress Corrosion Cracking," Act. Metallurgical, Vol. 9, p. 491 (May 1961).

Cotterell, E., "The Paradox between the Theories for Tensile and Compressive Fracture," Reports of Current Research, Int. J. Fract. Mech., Vol. 5, p. 241 (1969).

Creager, M., "The Elastic Stress Field near the Tip of a Blunt Crack," M.Sc. Thesis, Lehigh University (1966).

Crichlow, W.J. et al., "An Engineering Evaluation of Methods for the Prediction of Fatigue Life in Airframe Structures," Air Force Systems Command, Aeronautical Systems Division, Technical Report ASD-TR-61-43 (1962).

Crisci, J.R. and Foster, M.L., "Determination of Mechanical Properties and Causes of Failure of Autec-Toto II Deep Sea Moor Wire Rope," NASL Progress Report 3 on Project SF 51-541-007 (Sep 1968).

Crooker, T.W., "Effects of Tension-Compression Cycling on Fatigue Crack Growth in High-Strength Alloys," NRL Report 7220 (1971).

Crooker, T.W. and Lange, E.A., "Low Cycle Fatigue Crack Propagation Resistance of Materials for Large Welded Structures," ASTM STP 415, p. 121 (Jun 1967).

Crooker, T.W. and Lange, E.A., "Fatigue Crack Growth in Three 180-KSI Yield Strength Steels in Air and in Saltwater Environments," NRL Report 6761 (Sep 1968).

Crooker, T.W. and Lange, E.A., "Fatigue Crack Propagation in a High-Strength Steel under Constant Cyclic Load with Variable Mean Loads," NRL Report 6805 (Nov 1968).

Crooker, T.W. and Lange, E.A., "The Influence of Salt Water in Fatigue Crack Growth in High-Strength Structural Steels," ASTM STP 462, p. 258 (1968).

Crooker, T.W. and Lange, E.A., "The Influence of Yield Strength and Fracture Toughness on Fatigue Design Procedures for Structural Steels, NRL Report 7036 (Dec 1969).

Crooker, T.W. et al., "Subcritical Flaw Growth in 9Ni-4Co-0.25C Steel - A Fatigue and Fractographic Investigation and Its Relationship to Plane Strain Fracture Toughness," NRL Report 6698 (May 1968).

Crooker, T.W. et al., "Subcritical Crack Growth in Several Titanium Alloys," NRL Memorandum Report 2160 (Sep 1970).

Crosby, J.R. et al., "Effect of Stress Biaxiality on the High-Strain Fatigue Behavior of an Aluminum Copper Alloy," Exper. Mech., p. 305 (Jul 1969).

Dahlberg, E.P., "A Self-Stressed Specimen for Measuring Stress-Corrosion Cracking in Aluminum Alloys," NRL Progress Report, April (1966).

Davis E.A., "Extension of Iteration Method for Determining Strain Distribution to the Uniformly Stressed Plate with a Hole," J. Appl. Mech., Vol. 30E, No. 2 (1963).

DeHart, R.C. et al., "Study of the Low Cycle Fatigue Life on HY-80 Steel Specimens," Final Report SWRI Project 03-1754-01, Contract NObs92531 (Nov 1968).

DeHart, R.C. and Liebowitz, H., "The Influence of Ambient Pressure on the Stress Corrosion Susceptability of Metals," Eng. Frac. Mech., Vol. 1, No. 1, pp. 129-135 (1968).

Dixon, J.R., "Stress and Strain Distribution around Cracks in Sheet Materials Having Various Work-Hardening Characteristics," Int. J. Fract. Mech., No. 3 (Sep 1965).

Drucker, D.C. and Rice, J.R., "Plastic Deformation in Brittle and Ductile Fracture," Brown University Report ARPA E57 (Jul 1968).

Dugdale, D.S., Yielding of Steel Sheet Containing Slits," J. of Mech. Phys. Solids, Vol. 8 (1960).

Erdogan, F., "Crack Propagation Theories," Ch. 5, Vol. II (Fracture) edited by H. Liebowitz, Academic Press, New York, p. 497 (1968).

Erdogan, F. and Sih, G.C., "On the Crack Extension in Plates under Plane Loading and Transverse Shear," J. Basic Eng., ASME (Dec 1963).

Eringen, A.C., "Theory of Micropolar-Elasticity," Ch. 7, Vol. II of "Fracture," edited by H. Liebowitz, Academic Press, New York (1968).

Feeney, J.A. et al., "Environmental Fatigue Crack Propagation of Aluminum Alloys at Low Stress Intensity Levels," Boeing Company Report D6-60114 (1969).

Feltner, C.E. and Morrow, Jo Dean, "Micro-Plastic Strain Hysteresis Energy as a Criterion for Fatigue Fracture," Trans. J. Basic Eng., Trans. ASME, Vol. 83, Series D, p. 15 (Mar 1961).

Fleck, W.G. and Anderson, R.B., "A Model Study of the Characteristics of Fatigue Crack Extension," Proc. USAF Conference on Fatigue and Fracture of Aircraft Structures and Materials, Miami Beach, Florida (15-18 Dec 1969).

Folias, E.S., "A Finite Line Crack in a Pressurized Spherical Shell," Int. J. Fract Mech., pp. 20-46 (1965).

Folias, E.S., "An Axial Crack in a Pressurized Cylindrical Shell," Int. J. Fract. Mech., pp. 104-113 (1965).

Folias, E.S., "Cracked Spherical Shell," J. Math. and Phys., Vol. 44, No. 2, pp. 164-176 (1965).

Folias, E.S., "A Circumferential Crack in a Pressurized Cyclindrical Shell," Int. J. Fract. Mech., pp. 1-11 (1967).

Forman, R.G., "Study of Fatigue Crack Initiation from Flaws Using Fracture Mechanics Theory," Air Force Flight Dynamics Laboratory, AD 842809 (Sep 1968).

Forman, R.G. and Hudson, J.P., "Digital Computer Program for the Analysis of Crack Propagation in Cyclic Loaded Structures," Air Force Flight Dynamics Laboratory, Tech Report 67-5, AD 832042 (Apr 1967).

Forman, R.G. et al., "Numerical Analysis of Crack Propagation in Cyclic-Loaded Structures," J. Basic Eng. ASME, pp. 459-464 (Sep 1967).

Forty, A.J., "Physical Metallurgy of Stress Corrosion Fracture," Edited by T.N. Rhodin, Interscience, New York (1959) p. 99.

Freedman, A.H., "An Accelerated Stress Corrosion Test for High-Strength Ferrous Alloys," J. of Materials, JMLSA, Vol. 5, No. 2, pp. 431-466 (Jun 1970).

Freudenthal, A.M., "Fatigue Mechanisms; Fatigue Performance and Structural Integrity," Columbia University Institute for the Study of Fatigue and Reliability, Final Report for Contract Nonr 266(91) (Dec 1969).

Frost, N.E., "Notch Effects and the Critical Alternating Stress Required to Propagate a Crack in an Aluminum Alloy Subject to Fatigue Loading," J. Mech. Eng. Sci., Vol. 2, No. 2, p. 103 (1960).

Frost, N.E. and Denton, K., "Effect of Sheet Thickness on the Rate of Growth of Fatigue Cracks in Mild Steel," J. Mech. Eng. Sci. No. 3 (1961).

Frost, N.E. and Dixon, J.R., "A Theory of Fatigue Crack Growth," Int. J. Fract. Mech., Vol. 3, No. 4, p. 30 (Dec 1967).

Frost, N.E. and Dugdale, D.S., "The Propagation of Fatigue Cracks in Sheet Specimens," J. Mech. Phys. of Solids, p. 52 (1958).

Gall, H.J., "Corrosion Control for Manned Space Flight Network Facilities," NASA CR1492 (Feb 1970).

Gallagher, J.P., "Corrosion Fatigue Crack Growth Behavior above and below K_{ISCC}," NRL Report 7064 (May 1970).

Gardner, J.E. and Royster, D.M., "Influence of Salt and Elevated-Temperature Exposure on the Maximum Compressive Strength of Titanium-Alloy Skin-Stringer Panels," NASA TN D-5670 (Feb 1970).

Garrison, D.R. and Salive, M.L., "Correlation of the Bement-Pohler Fatigue Theory with Experimental Fatigue Data and Its Extension to Notched Specimens," NSRDC Report 3343 (Jun 1970).

Gerber, T.L. and Fuchs, H.O., "Analysis of Nonpropagating Fatigue Cracks in Notched Parts with Compressive Mean Stress," J. Materials, JMLSA, Vol. 3, No. 2, pp. 359-374 (1968).

Gerberich, W.W., "Plastic Strains and Energy Density in Cracked Plates," Ch. I. (Experimental Techniques and Results) of Vol. 4 (Experimental Mechanics) (1964).

Gerberich, W.W. and Hartbower, C.E., "Monitoring Crack Growth of Hydrogen Embrittlement and Stress Corrosion Cracking by Acoustic Emission," Proc. Conf. on Fundamental Aspects of Stress Corrosion Cracking, Ohio State University, published by NACE, pp. 420-438 (1967).

Goode, R.J. et al., "Metallurgical Characteristics of High Strength Structural Materials," NRL Report 6607 (Sep 1967).

Goodier, J.N. and Field, F.A., "Plastic Energy Dissipation in Crack Propagation," in "Fracture of Solids," edited by D.C. Drucker and J.J. Gilman, Interscience, New York (1963).

Gough, H.J. and Sopurith, D.G., "Atmospheric Action as a Factor in Fatigue of Metals," J. Inst. Metals, Vol. 49, No. 2, pp. 92-112 (1932).

Green, A.E. and Sneddon, I.N., "The Distribution of Stress around an Elliptical Crack in an Elastic Solid," Proc. Cambridge Phil. Soc., Vol. 46, p. 159 (1950).

Griffith, A.A., "The Phenomena of Rupture and Flow in Solids," Trans. Roy. Soc. London, Ser. A, Vol. 221, p. 163 (1921).

Griffith, A.A., "Theory of Rupture," Proc. Eleventh Int. Cong. Appl. Mech., Delft, Holland, pp. 53-64 (1925).

Gross, M.R., "Low-Cycle Fatigue of Materials for Submarine Construction," Eng. Exper. Sta. Report 91 (Feb 1963).

Gross, M.R., "Broad Spectrum Fatigue-Crack Growth Studies," NSRDL Annapolis Report 8-629 (Nov 1970).

Guinand, E.F., "Propagation of Cracks," Course 237 (Mechanical Behavior of Materials Laboratory) Dept. Mech. Eng., MIT (1961).

Hahn, G.T. and Rosenfield, A.R., "Experimental Determination of Plastic Constraint ahead of a Sharp Crack under Plane Strain Conditions," U.S. Navy Report, Ship Structures Committee Report SSC-180 (1966).

Hahn, G.T. and Rosenfield, A.R., " Sources of Fracture Toughness: The Relation between K_{IC} and the Ordinary Tensile Practices in Metals," in ASTM Special Technical Publication 432 (Applications Related Phenomena in Titanium Alloys), p. 5 (Mar 1968).

Hahn, G.T. et al., "Observations of Yielding Accompanying Crack Growth," Battelle Colloquium on the Inelastic Behavior of Solids, Columbus and Atwood Lake (15-19 Sep 1969).

Hahn, G.T. et al., "Criteria for Crack Extension in Cylindrical Pressure Vessels," Int. J. Fract. Mech., Vol. 5, No. 3, p. 187 (Sep 1969).

Hahn, G.T. et al., "Experiments on the Nature of the Fatigue Crack Plastic Zone," Proc. U.S. Air Force Conf. on Fatigue and Fracture of Aircraft Structures and Material, Miami Beach, Florida (15-18 Dec 1969).

Hancock, G.G. and Johnson, H.H., "Hydrogen Oxygen and Subcritical Crack Growth in a High-Strength Steel," Trans. of the Metallurgical Soc. of AIME, Vol. 236, p. 513 (Apr 1966).

Hardrath, H.F., "Cumulative Damage," Proc. Sagamore Army Mat. Res. Conf. on Fatigue, an Interdisciplinary Approach, Syracuse University Press, p. 345 (1964).

Hardrath, H.F. and Ohman, L., "A Study of Elastic and Plastic Stress Concentration Factors Due to Notches and Fillets in Flat Plates," NACA TR-1117 (1953).

Hardrath, H.F. and Naumann, E.C., "Variable Amplitude Fatigue Tests of Aluminum-Alloy Specimens," ASTM STP 274 (Fatigue in Aircraft Structures) (1959).

Hartmann, A. and Schijve, J., "The Effects of Environment and Load Frequency on the Crack Propagation Law for Macro-Fatigue Crack Growth in Aluminum Alloys," Eng. Fract. Mech., Vol. 1, No. 4, pp. 615-631 (1970).

Hartranft, R.J. and Sih, G.C., "An Approximate Three-Dimensional Theory of Plates with Application to Crack Problems," Lehigh University Tech. Report 7 (May 1969).

Head, A.K., "The Growth of Fatigue Cracks," Phil. Mag., Vol. 44, 7th Series, p. 925 (1953).

Hertzberg, R.W. and Paris, P.C., "Application of Electron Fractography and Fracture Mechanics to Fatigue Crack Propagation," Proc. First Int. Conf. on Fracture, Sendai, Japan, Vol. 1, p. 466 (1965).

Hilton, P.D. and Hutchinson, J.W., "Plastic Stress Intensity Factors for Cracked Plates," Harvard University Report SM-35 (May 1969).

Hoar, T.P. and Hines, J.G., "Stress Corrosion Cracking and Embrittlement," edited by W.D. Robertson, Wiley, New York (1956) p. 107.

Hubbard, R.P., "Crack Growth under Cyclic Compression," J. Basic Eng., Trans. ASME, p. 615 (Dec 1969).

Hudson, C.M., "Effect of Stress Ratio on Fatigue-Crack Growth in 7075-T6 and 2024-T3 Aluminum-Alloy Specimens," NASA TN-D-5390 (Aug 1969).

Hult, A.J. and McClintock, F.A., "Elasto-Plastic Stress and Strain Distribution around Sharp Notches under Repeated Shear," 9th Int. Cong. Appl. Mech., Brussels, Vol. 8 (1956).

Hutchinson, J.W., "Plastic Stress and Strain Fields at a Crack Tip," Harvard University Report SM-23 (Apr 1968).

Hutchinson, J.W., "Singular Behavior at the End of a Tensile Crack in a Hardening Material," J. Mech. and Phys. of Solids, Vol. 16 (1968).

Hyatt, M.V., "Data Taken under the ARPA Stress-Corrosion Project," The Boeing Company.

Illg, W. and McEvily, A., "The Rate of Fatigue-Crack Propagation for Two Aluminum Alloys Under Completely Reversed Loading," NASA TN D-52 (Oct 1959).

Irwin, G.R., "Analysis of Stresses and Strains near the End of a Crack Traversing a Plate," Trans. ASME, J. Appl. Mech., Vol. 79, Series E, p. 361 (Mar 1957).

Irwin, G.R., "Fracture Testing of High-Strength Sheet Materials under Conditions Appropriate for Stress Analysis," NRL Report 5486 (Jul 1960).

Irwin, G.R., "Fracture Mechanics in Structural Mechanics, Pergamon Press, New York (1960).

Irwin, G.R., "Crack Extension Force for a Part-Through Crack in a Plate," J. Appl. Mech., Trans. ASME, Series E, Vol. 29, pp. 651-654 (1962).

Irwin, G.R. et al., "Basic Aspects of Crack Growth and Fracture," NRL Report 6598 (Nov 1967).

Ives, K.D. et al., "Equibiaxial Low-Cycle Fatigue Properties of Typical Pressure Vessel Steels," J. Basic Eng., Trans. ASME, p. 745 (Dec 1966).

Jack, A.R. and Price A.T., "The Initiation of Fatigue Cracks in Mild Steel Plates," Int. J. Fract. Mech., Vol. 6, No. 4, p. 409 (Dec 1970).

Jacoby, G.H., "Fractographic Methods in Fatigue Research," Experimental Mechanics (Mar 1965).

Johnson, H.H., "On Hydrogen Brittleness in High Strength Steels," Proc. Conf. on Fundamental Aspects of Stress Corrosion Cracking, Ohio State University, published by NACE, pp. 439-444 (1967).

Johnson, R.E., "Some Observations of Cyclic Crack Propagation from a Fracture Mechanics Viewpoint," ASM Symposium of Metallurgical Aspects of Fatigue Fracture, Materials Engineering Congress, Philadelphia, Pennsylvania (Oct 1969).

Johnson, H.H. and Paris, P.C., "Sub-Critical Flaw Growth," Eng. Fract. Mech., Vol. 1, pp. 3-45 (1968).

Johnson, H.H. and Wilner, A.M., "Moisture and Stable Crack Growth in a High Strength Steel," Appl. Math. Res., Vol. 4, p. 34 (1965).

Johnson, H.H. et al., "Hydrogen, Crack Initiation and Delayed Failure in Steel," Trans. of the Metallurgical Soc. of AIME, Vol. 212, No. 4, p. 528 (Aug 1958).

Judy, R.W., Jr. and Goode, R.J., "Stress-Corrosion Cracking Characteristics of Alloys of Titanium in Salt Water," NRL Report 6564 (Jul 1967).

Kaechele, Lloyd, "Review and Analysis of Cumulative Fatigue-Damage Theories," Rand Corporation Report RM-3650-PR (Aug 1963).

Kassir, M.K. and Sih, G.C., "Three-Dimensional Stress Distribution around an Elliptical Crack under Arbitrary Loadings," J. Appl. Mech., p. 601 (Sep 1966).

Kassir, M.K. and Sih, G.C., "Griffith's Theory of Brittle Fracture in Three Dimensions," Lehigh University Tech. Report 207 (Mar 1967).

Katz, Y. and Gerberich, W.W., "On the Discontinuous Nature of Stress-Corrosion Cracking in Titanium Alloys," Int. J. Frac. Mech., Vol. 6, pp. 219-221 (1970).

Kibler, J.J. and Roberts, R., "The Effect of Biaxial Stresses on Fatigue and Fracture," Paper 70-PVP-17, Petroleum Mech. Eng. and Pressure Vessels and Piping Conf., Denver, Colorado (Sep 1970).

Kies, J.A. and Clark, A.B.J., "Mechanical Strength Degradation and Prediction of Times to Fail for Bulk Glass," Prescribed at ASTM, Atlanta, Ga., Sep 1968.

Kies, J.A. et al. "Fracture Testing of Weldments," ASTM STP 381, (1965).

Knowles, J.K. and Wang, N.M., "On the Bending of an Elastic Plate Containing a Crack," J. Math. and Phys., Vol. 39, pp. 223-236 (1960).

Kobayashi, A.S., "On the Magnification Factors for Deep Surface Flaws," Boeing Company Struct. Dev. Res. Memo 16 (Dec 1965).

Kobayashi, A.S. and Iida, S., "Crack Propagation Rate in 7075-T6 Plates under Tensile and Transverse Shear Loadings," University of Washington Contract Nonr-477(39), NR064.478, Tech Report 6 (Jan 1969).

Kobayashi, A.S. and Moss, W.L., "Stress Intensity Magnification Factors for Surface Flawed Tension Plate and Notched Round Tensile Bar," Proc. Second Int. Conf. on Fracture, Brighton, England (Apr 1969).

Kobayashi, A.S. et al., "Approximate Stress Intensity Factor for an Embedded Elliptical Crack near Two Parallel Free Surfaces," Int. J. Fract. Mech., Vol. I, No. 2 (Jun 1965).

Kobayashi, A.S. et al., "Crack Opening Displacements and Normal Strains in Centrally Notched Plates," University of Washington, Tech. Report 4, Contract Nonr-477(39), NR064478 (Jan 1968).

Kobayashi, A.S. et al., "Application of the Methods of Finite Element Analysis to Two-Dimensional Programs in Fracture Mechanics," University of Washington Contract Nonr-477(39), NR064478, Tech. Report 5 (Oct 1968).

Kobayashi, A.S. et al., "Elastic-Plastic State in a Plate with an Extending Crack," Proc. Army Symposium on Solid Mech., Watertown, Mass. (13-14 Oct 1970).

Krafft, J.M., "Correlation of Plane Strain Crack Toughness with Hardening Characteristics of a Low, a Medium, and a High Strength Steel," Appl. Mat. Res., Vol. 3 p. 88 (Apr 1964).

Krafft, J.M., "Application of Tensile Ligament Model to Fatigue Crack Propagation," Presented to ASTM Cmt E24, Atlanta, Georgia (3 Mar 1971).

Krafft, J.M. et al., "Effect of Dimensions on Fast Fracture Instability of Notched Sheets," Proc. Crack Propagation Symposium, College of Aeronautics, Cranfield (England), Vol. 1 p. 8 (Sep 1961).

Laird, C. and Smith, G.C., "Initial Stages of Damage in High Stress Fatigue in Some Pure Metals," Phil. Mag. 8, p. 1945 (Nov 1963).

Laird, C., "The Influence of Metallurgical Structure on the Mechanisms of Fatigue Crack Propagation," ASTM STP 415, p. 131 (Jun 1967).

Langer, B.F., Memorandum to Members of ASME Boiler and Pressure Vessel Committee, Special Committee to Review Code Stress Basis, Task Group on Fatigue (17 Jul 1957).

LaQue, F.L., "Deterioration of Metals in an Ocean Environment," Ocean Eng., Vol. 1, pp. 299-312 (1969).

Lawrence, F.V., Jr. and Radziminski, J.B., "Fatigue Crack Initiation and Propagation in High-Yield Strength Steel Weld Metal," Welding Res. Suppl., Vol. 35, No. 10, p. 445S (Oct 1970).

Leckie, H.P., "Effect of Environment on Stress Induced Failure of High Strength Maraging Steels," Proc. Conf. on Fundamental Aspects of Stress Corrosion Cracking, Ohio State University, published by NACE, pp. 411-419 (1967).

Lehr, K.R. and Liu, H.W., "Fatigue Crack Propagation and Strain Cycling Properties," Int. J. Fract. Mech., Vol. 5, No. 45 (1969).

Levy, N., "Application of the Finite Element Method to 2- and 3-Dimensional Elastic-Plastic Problems of Fracture Mechanics," Ph.D. Dissertation, Brown University (Jun 1970).

Li, C.Y. et al., "Subcritical Crack Growth in an Inert Environment," ASTM Meeting, Note E-24, Washington, D.C. (31 Jan-3 Feb 1966).

Liu, H.W., "Crack Propagation in Thin Metal Sheet under Repeated Loading," J. Basic Eng., Trans. ASME, Series D, Vol. 83, p. 23 (1961).

Liu, H.W. and Lal, D.N., "Shear Crack Propagation in HY-80, HY-130, and 18Ni (180) Maraging Steels under Cyclic Biaxial Loading," Syracuse University Research Institute Report Met-E 1415-969 (Sep 1969).

Liu, H.W. and Lino, N., "A Mechanical Model for Fatigue Crack Propagation," Proc. Second Int. Conf. on Fract., Brighton, England (Apr 1969).

Logan, H.L., "Film Rupture Mechanism of Stress Corrosion," J. of Res. of the National Bureau of Standards, Vol. 236, p. 513 (Apr 1966).

Lomacky, O., "Status Report on Submarine Hull Reliability Program," NSRDC Report 3287 (Feb 1970).

Lomacky, O. et al., "Fatigue and Fracture Reliability Analysis of Pressure Vessels," First National Congress on Pressure Vessels and Piping, ASME, San Francisco, California (10-12 May 1971).

Love, A.E.H., "A Treatise on the Mathematical Theory of Elasticity," Fourth Edition, University Press, Cambridge (1927).

Mager, T.R., "Notch Preparation in Compact Tension Specimens," Westinghouse Electric Heavy Section Steel Technology Program Tech. Report 11 (Nov 1970).

Manson, S.S., "Behavior of Materials under Conditions of Thermal Stress," NACA TN 2933 (1954).

Manson, S.S., "Fatigue: A Complex Subject - Some Simple Approximations," Exper. Mech., Vol. 5, No. 7, pp. 193-226 (Jul 1965).

Manson, S.S., "Thermal Stress and Low Cycle Fatigue," McGraw-Hill, New York (1966).

Manson, S.S. and Hirschberg, M.H., "Low Cycle Fatigue of Notched Specimens by Consideration of Crack Initiation and Propagation," NASA TN D-3146 (1966).

Manson, S.S. et al., "Further Investigation of a Relation for Cumulative Fatigue Damage in Bending," NASA TMX-52002 (1964).

Manson, S.S. et al., "Application of a Double Linear Damage Rule to Cumulative Fatigue," ASTM STP 415, p. 384 (1967).

Marcal, P.V., "Finite Element Analysis with Material Nonlinearities - Theory and Practice," Brown University Report 0014-0007-3 (Aug 1969).

Marcal, P.V. and Turner, C.E., "Limited Life of Shells of Revolution Subjected to Severe Local Bending," J. Mech. Eng. Sci., Vol. 17, No. 4, p. 408 (1965).

Marcal, P.V. et al., "Three-Dimensional Elastic-Plastic Stress and Strain Analyses for Fracture Mechanics," Oak Ridge National Laboratory Heavy Section Steel Technology Program, Semiannual Progress Report ORNL-4590 (28 Feb 1970).

Mattawi, J.C., "Low-Cycle Fatigue Behavior under Biaxial Strain Distribution," J. Basic Eng., Trans. ASME, p. 23 (Mar 1969).

Mattsson, E., "Stress Corrosion in Brass Considered Against the Background of Potential/pH Diagrams," Electrochem. Acta, Vol. 3, p. 279 (1961).

McClintock, F.A., "On the Plasticity of the Growth of Fatigue Cracks," (Proceedings of the Maple Valley Fracture Conference); published in "Fracture of Solids," Edited by D.C. Drucker and J.J. Gilman, Interscience, New York, p. 65 (1963).

McClintock, F.A., "Effects of Root Radius, Stress, Crack Growth, and Rate on Fracture Instability," Proc. Roy. Soc., Vol. 285, No. 1400, p. 58 (Apr 1965).

McClintock, F.A., "A Criterion for Ductile Fracture by the Growth of Holes," J. Appl. Mech., p. 363 (Jun 1968).

McClintock, F.A. and Irwin, G.R., "Plasticity Aspects of Fracture Mechanics," Fracture Toughness Testing and Its Applications, ASTM 381, p. 84 (Jun 1964).

McClintock, F.A. and Pelloux, R.M.N., "Crack Extension by Alternating Shear," Boeing Company Sci. Res. Lab. Report AD 669531 (Feb 1968).

McClintock, F.A. and Walsh, J.B., "Friction on Griffith Cracks in Rocks under Pressure," Proc. Fourth U.S. Cong. Appl. Mech., Am. Soc. Mech. Eng., p. 1015 (1963).

McEvily, A.J., "Fatigue Crack Growth and the Strain Intensity Factor," USAF Conf. on Fatigue and Fracture of Aircraft Structure and Materials, Miami Beach, Florida (15-18 Dec 1969).

McEvily, A.J. et al., "On the Formation and Growth of Fatigue Cracks in Polymers," Proc. Sagamore Army Mat. Res. Conf. on Fatigue, an Interdisciplinary Approach, Syracuse University Press (1964).

McMillan, J.C. and Pelloux, R.M.N., "Fatigue Crack Propagation under Program and Random Loads," ASTM STP 415, p. 505 (Jun 1967).

Miller, G.A., "The Dependence of Fatigue-Crack Growth Rate on Stress Intensity Factor and the Mechanical Properties of Some High-Strength Steels," Trans. Am. Soc. for Metals, Vol. 61, p. 442 (1968).

Miller, G.A., "Fatigue Fracture Appearance and the Kinetics of Striation Formation in Some High-Strength Steels," Trans. Am. Soc. for Metals. Vol. 62, p. 651 (1969).

Miner, M.A., "Cumulative Damage in Fatigue," J. Appl. Mech. No. 12, pp. A159-A164 (1945).

Morrow, Jo Dean, "Speculative Remarks and Analysis Concerning Mechanical Hysteresis Energy as a Criterion for Fatigue Failure," presented at General Electric Company, Evendale, Ohio (Mar 1959).

Morrow, Jo Dean, "An Investigation of Plastic Strain Energy as a Criterion for Finite Fatigue," report to the Garrett Corporation, Phoenix, Arizona (Aug 1960).

Morrow, Jo Dean, "Cyclic Plastic Strain Energy and Fatigue of Metals," ASTM STP 378, p. 45 (Jun 1964).

Morrow, J., R.M. Wetzel, and T.H. Topper, "Laboratory Simulation of Structural Fatigue Behavior," in Effects of Environment and Complex Load History on Fatigue Life, American Society for Testing and Materials, STP 462, 1970.

Mowbray, D.F. et al., "Fatigue-Crack Growth-Rate Studies of Low-Alloy Pressure-Vessel Steels," ASME Paper 68 PVP-23 (1968).

Munse, W.H. et al., "Studies of the Fatigue Behavior of Butt-Welded Joints in HY-80 and HY-100 Steels," University of Illinois Report 285, AD 452-191 (Nov 1964).

Mylonas, C., "The Mechanics of Brittle Fracture," Proc. Eleventh Int. Cong. Appl. Mech., Springer, p. 652 (1966).

Mylonas, C., "Strain Embrittlement and Fracture of Mild Steel,"

Solid Mechanics Seminar, Brown University (8-17 Jun 1967).

Mylonas, C. and Beaulieu, R.J., "Restoration of Ductility of Pre-strained Steel by Heat Treatment at 700 to 1150°F," Welding Res. Suppl. (Jul 1969).

Mylonas, C. and Kobayashi, A.S., "Notch Brittleness after Pre-straining," U.S. Navy Ship Structures Committee Report SSC-192 (Jan 1969).

Neuber, H., "Theory of Notch Stresses, Principles for Exact Stress Calculations," J.N. Edwards Co., Ann Arbor, Michigan (1946).

Nielsen, N.A., "Physical Metallurgy of Stress Corrosion Fracture," Conf. Metallurgical Society, Vol. 4, Interscience, New York, pp. 121-154 (1959).

Nielsen, N.A., "Observations and Thoughts on Stress Corrosion Mechanisms," 1970 Gillett Memorial Lecture, J. Mat., JMLSA, Vol. 5, No. 4, pp. 794-829 (Dec 1970).

Novak, S.R. and Rolfe, S.T., Modified WOL Specimen for K_{ISCC} Environmental Testing, Submitted to ASTM, (1970).

Ohji, K., Miller, W.R. and Marin, J., "Cumulative Damage and Effect of Mean Strain in Low-Cycle Fatigue of a 2024-T351 Aluminum Alloy," J. Basic Eng. (ASME), p. 801 (Dec 1966).

Orowan, E., "Fracture and Strength of Solids," Report on Progress in Physics, Vol. 12, p. 185 (1947).

Ostergren, W., "Small-Scale Plastic Yielding near a Crack in Plane Strain: A Finite Element Analysis," M.Sc. Thesis, Brown University (1968).

Packman, P.F., "Multiple Crack Interactions and Fracture," Proc. of a Symposium on Weld Imperfections, Lockheed, Palo Alto, California (19-21 Sep 1968).

Packman, P.F. et al., "The Applicability of a Fracture Mechanics-Nondestructive Testing Design Criterion," Air Force Materials Lab. Tech. Report 68-32 (May 1968).

Palmgren, A., "Die Lebensdauer von Kugellagern," Ver. Dtech. Ing., Vol. 68, pp. 339-341 (1924).

Paris, P.C., "The Fracture Mechanics Approach to Fatigue," in "Fatigue - an Interdisciplinary Approach," Syracuse University Press, Syracuse, New York (1964).

Paris, P.C., "Testing for Very Slow Growth of Fatigue Cracks," Closed Loop (MTS Magazine), Vol. II, No. 5 (1970).

Paris, P.C. and Erdogan, F., "A Critical Analysis of Crack Propagation Laws," J. Basic Eng., Trans. ASME, Series D, Vol. 85, p. 528 (1963).

Paris, P.C. and Sih, G.C., "Stress Analysis of Cracks," Fracture Toughness Testing and Its Applications, ASTM 381, p. 30 (Jun 1964).

Paris, P.C. and Wei, R.P., "Fracture Mechanics in Fatigue," ASTM Symposium on Engineering Aspects of Fatigue, 1969 Materials Engineering Congress, Philadelphia, Pennsylvania (Oct 1969).

Pascoe, K.J. and deVilliers, J.W.R., "Low Cycle Fatigue of Steels under Biaxial Straining," J. Strain Analy., Vol. 2, No. 2, p. 117 (1967).

Paul, B., "Macroscopic Criteria for Plastic Flow and Brittle Fracture," in "Fracture," edited by H. Liebowitz, Academic Press, New York, p. 313 (1968).

Payne, W.R., "Incorporation of Fracture Information in Specification," ASTM 381 (Fracture Toughness Testing and Its Applications), p. 357 (Jun 1964).

Pellini, W.S. and Judy, W.R., "Significance of Fracture Extension Resistance (R-Curve) Factors in Fracture-Safe Design for Nonfrangible Metals," NRL Report 7187 (Oct 1970).

Pelloux, R.M., "Review of Theories and Laws of Fatigue Crack Propagation," Proc. USAF Conf. on Fatigue and Fracture of Aircraft Structures and Materials, Miami Beach, Florida (15-18 Dec 1969).

Pelloux, R.M.N., "Mechanisms of Formation of Ductile Fatigue Striations," Trans. ASM, 62, 281 (1969).

Petch, N.J. and Stables, P., "Delayed Fracture of Metals under Static Load," Nature, Vol. 169, p. 842 (May 12, 1952).

Peterson, R.E., "Stress Concentration Design Factors; Charts and Relations Useful in Making Strength Calculations for Machine Parts and Structural Elements," John Wiley and Sons, Inc., New York (1953).

Peterson, M.H. et al., "Stress Corrosion Cracking of High Strength Steels and Titanium Alloys in Chloride Solutions at Ambient Temperature," Corrosion, Vol. 23, No. 5 (1967).

Petrak, G.J., "An Investigation of Stress Corrosion Crack Arrest and Crack Propagation in a Titanium Alloy," USAF Materials Laboratory Report TR-70-244 (Oct 1970).

Pickering, H.W. and Swann, P.R., "Electron Metallography of Chemical Attack upon Some Alloys Susceptible to Stress Corrosion Cracking," Corrosion, Vol. 19, p373 (1963).

Pickering, H.W. et al., "Corrosion," CORRA, Vol. 18, No. 6, pp. 230-239 (1962).

Pickett, A.G. and Grigory, S.C., "Prediction of the Low Cycle Fatigue Life of Pressure Vessels," J. Basic Eng., Trans. ASME, p. 860 (Dec 1967).

Pickett, A.G. et al., "A Study of Low-Cycle Fatigue Strength of Compressive Specimens Made of Submarine Hull Materials," Southwestern Res. Inst. Final Report for Contract Nobs 88598 (Oct 1964).

Pinnow, K.E. and Moskowitz, A., "Corrosion Resistance of Stainless Steel Weldments," Welding J. Suppl., pp. 278S-184S (Jun 1970).

Pourbaix, M.J.N., "Atlas d' equilibres electrochimiques," Gauthier-Villars, Paris (1963).

Prager, W. and Hodge, P.C., "Theory of Perfectly Elastic Solids," Dover Publications (1968).

Pugh, E.N., "On the Mechanism(s) of Stress-Corrosion Cracking," Environment-Sensitive Mechanical Behavior, Gordon and Breach, New York (1966) pp. 351-401.

Pugh, E.N. et al., "Current Understanding of Stress-Corrosion Phenomena," Proc. Int. Conf. on Interfaces, Melbourne, Austrailia (1969); also RIAS Technical Report 69-3 (Mar 1969).

Randall, P.N., "Severity of Natural Flaws as Fracture Origins and a Study of the Surface-cracked Specimen," TRW Space Technology Laboratories Report AFML-TR-66-204 (Aug 1966).

Reissner, R.J., "The Effect of Transverse Shear Deformation on the Bending of Elastic Plates," J. Appl. Mech., Vol. 12, A69(1945).

Reuter, W.G. and Hartbower, C.E., "Stress Corrosion Cracking in an Air-Melted and Vacuum-Arc-Rewelded Grade-250 Maraging Steel," Fourth National Symposium on Fracture Mechanics, Pittsburgh, Pa. (1970).

Rice, J.R., "Plastic Yielding at Crack Tip," Proc. First Int. Conf. on Fracture, Sendai, Japan (1965).

Rice, J.R., "Mechanics of Crack Tip Deformation and Extension by Fatigue," ASTM STP 415, p. 247 (Jun 1967).

Rice, J.R., "A Path Independent Integral and the Approximate Analysis of Strain Concentration by Notches and Cracks," J. Appl. Mech., Vol. 35, p. 379 (1968).

Rice, J.R., "Mathematical Analysis in the Analysis of Fracture," Ch. 3, Vol. II, in "Fracture," edited by H. Liebowitz, Academic Press, New York (1968).

Rice, J.R. and Tracey, D.M., "On the Ductile Enlargement of Voids in Triaxial Stress Fields," J. Mech. Phys. of Solids, Vol. 17, p. 201 (1969).

Rice, J.R. and Johnson, M.A., "The Role of Large Crack Tip Geometry Changes in Plane Strain Fracture," Brown University Report 38 (Sep 1969).

Rice, J.R. and Rosengren, G.F., "Plane Strain Deformation near a Crack Tip in a Power Law Hardening Material," J. Mech. and Phys. of Solids (Jan 1968).

Rice, J.R. et al., "On the Prediction of Some Random Loading Characteristics Relevant to Fatigue," in "Acoustical Fatigue in Aerospace Structures," Syracuse University Press, Syracuse, New York (1965).

Roberts, R. and Erdogan, F., "The Effect of Mean Stress on Fatigue Crack Propagation in Plates Under Extension and Bending," Proc. First Int. Conf. on Fracture, Sendai, Japan, Vol. 1 (Sep 1965).

Romine, H.E. and Smith, H.L., "K_{ISCC} Stress-Corrosion Tests of HY-140 Welds for DSRV-2," NRL Memorandum Report 1923 (Sep 1968).

Rooke, D.P. and Bradshaw, F.J., "Fracture," Chapman and Hall, London (1969), p. 46.

Rosenfield, A.R. et al., "Crack Extension and Propagation under Plane Stress," Proc. First Int. Conf. on Fracture, Sendai, Japan (1965).

Sandoz, G., "The Resistance of Some High Strength Steels to Slow Crack Growth in Salt Water," submitted for publication (1970).

Saunders, S.C., "On the Analytical Basis for Fatigue Life Prediction," Proc. USAF Conf. on Fatigue and Fracture of Aircraft Structures and Materials, Miami Beach, Florida (15-18 Dec 1969).

Schijve, J., "The Analysis of Random Load-Time Histories with Relation to Fatigue Tests and Life Calculations," presented at Second ICAF-AGARD Symposium, Paris, France, p. 115 (16-18 May 1961).

Schijve, J., "Significance of Fatigue Cracks in Micro-Range and Macro-Range," ASTM STP 415, p. 415 (Jun 1967).

Schwab, R.C., "The Use of Tapered Double-Cantilever-Beam Specimens for Fatigue-Crack Growth Studies, NSRDC Report 2689 (Jul 1968).

Schwab, R.C. and Czyryca, E.J., "Effects of Notches and Salt Water Corrosion on the Flexural Fatigue Behavior of High Strength Structural Alloys," ASTM STP 462, p. 203 (1968).

Shah, R.C. and Kobayashi, A.S., "On the Parabolic Crack in an Elastic Solid," Eng. Fracture Mech., Vol. I, No. 2 (Aug 1968).

Shah, R.C. and Kobayashi, A.S., "Stress Intensity Factors for an Elliptical Crack under Arbitrary Loading," University of Washington Report submitted for publication in J. Eng. Fract. Mechanics.

Sih, G.C. et al., "Three-Dimensional Stress Distribution near a Sharp Crack in a Plate of Finite Thickness, Air Force Materials Laboratory, Wright-Patterson Air Force Base, AFML-TR-66-242 (1966).

Sih, G.C., "Three-Dimensional Stress-State in a Cracked Plate," Proc. USAF Conf. on Fatigue and Fracture of Aircraft Structures and Materials, Miami Beach, Florida (15-18 Dec 1969).

Sih, G.C. and Liebowitz, H., "Mathematical Theories of Brittle Fracture," Ch. 2, Vol. II of "Fracture," edited by H. Liebowitz, Academic Press, New York (1968), p. 67.

Sih, G.C. et al., "Crack Tip Stress-Intensity Factors for Plane Extensional Plate Bending Problems," J. Appl. Mech. (Jun 1962).

Smith, S.H., "Fatigue Crack Growth under Axial Narrow and Broad Band Random Loading," in "Acoustical Fatigue in Aerospace Structures," Syracuse University Press, New York, New York (1965).

Smith, F.W., "Stress Intensity Factors for a Semi-Elliptical Surface Flaw," Boeing Company, Struct. Dev. Res. Memo 17 (Aug 1966).

Smith, F.W. et al., "Stress Intensity Factors for Penny Shaped Cracks, Part 1 - Infinite Solid," J. Appl. Mech. (Dec 1967), pp. 947-951.

Smith, F.W. et al., "Stress Intensity Factors for Semicircular Cracks, Part 2 - Semi-infinite Solid," J. Appl. Mech., pp. 953-959 (Dec 1967).

Smith, H.R. et al., "A Study of Stress-Corrosion Cracking by Wedge-Force Loading," Eng. Frac. Mech., Vol. 1, No. 1, pp. 123-128 (1968).

Sorensen, Arthur, Jr., "A General Theory of Fatigue Damage Accumulation," J. Basic Eng., Trans ASME (Mar 1967).

Spretnak, J.W. and Griffis, C.A., "Research on Notch Plasticity May Contribute to the Understanding of Stress Corrosion Cracking," Corrosion, Vol. 25, No. 5, p. 193 (1969).

Srawley, J.E. and Brown, W.F., "Fracture Toughness Testing," ASTM 381, p. 133 (Jun 1964).

Staehle, R.W., "Evaluation of the Current State of Stress Corrosion Cracking," Proc. Conf. on Fundamental Aspects of Stress Corrosion Cracking, Ohio State University, published by NACE, pp. 1-14 (1967).

Stowell, E.Z., "Stress and Strain Concentration at a Circular Hole in an Infinite Plate," NACA TN 2073 (Feb 1950).

Stowell, E.Z., "A Study of the Energy Criterion for Fatigue," Nuclear Engineering and Design, No. 3, pp. 32-40 (1966).

Sutton, H. et al.; Joint Discussion on W.A. Baker's Paper, "Microporosity in Magnesium Alloy Casting," and F.A. Fox's Paper, "The Properties of Some Alloys and the Incidence of Microporosity," Journal of the Institute of Metals, Vol. 71, pp.630-631 (1945).

Swanson, R., "Load Fatigue Testing, State of the Art Survey," Materials Research and Standards, p. 11 (Apr 1968).

Swanson, R., "Random Load Fatigue Testing, Parts I and II," Closed Loop (MTS magazine), Vol. 1, No. 8 and Vol. 11, No. 4 (1968).

Swedlow, J.L., "Elastic-Plastic Cracked Plates in Plane Strain," Int. J. Fract. Mech., Vol. 5, No. 1 (Mar 1969).

Swedlow, J.L. et al., "Elastic-Plastic Stresses and Strains in Cracked Plates," Proc. First Int. Conf. on Fracture, Sendai, Japan (1965).

Tetelman, A.S., "The Mechanism of Hydrogen Embrittlement in Steel," Proc. Conf. on Fundamental Aspects of Stress Corrosion Cracking, Ohio State University, published by NACE, pp. 446-460 (1967).

Tetelman, A.S. and Robertson, W.D., "The Mechanism of Hydrogen Embrittlemen Observed in Iron-Silicon Single Crystal," Trans. of Metallurgical Soc. of AIME, Vol. 224, p. 775 (Aug 1962).

Tetelman, A.S. and Wilshaw, T.R., "A Criterion for Plastically Induced Cleavage after General Yield in Notched Bend Specimens," Second Int. Conf. on Fract. Mech., Brighton, England (Apr 1969).

Tiffany, C.F. and Masters, J.N., "Applied Fracture Mechanics," ASTM STP 381, p. 249 (Jun 1964).

Tiffany, C.F. et al., "Investigation of Plane Strain Flaw Growth in Thick Walled Tanks," Boeing Company Report prepared for NASA under Contract NASA-4194 (Feb 1966).

Tomkins, B., "Fatigue Crack Propagation - An Analysis," Phil. Mag., Vol. 18, p. 1056 (1968).

Uhlig, H., "Physical Metallurgy of Stress Corrosion Fracture," edited by T.N. Rhodin, Interscience, New York (1959) pp. 1-16.

Uhlig, H.H., "An Evaluation of Stress Corrosion Cracking Mechanism," Proc. Conf. on Fundamental Aspects of Stress Corrosion Cracking, Ohio State University, published by NACE, pp. 86-91 (1967).

Valluri, S.R., "Fracture under Biaxial Conditions in the Presence of a Crack," Proc. First Int. Conf. on Fract., Sendai, Japan (1965).

Vasques, J.A. and Paris, P.C., "A Plastic Zone Instability Phenomena Leading to Crack Propagation," Fourth Nat. Symposium on Fract. Mech., Pittsburgh, Pa. (1970).

Visser, C. and Tuba, I.S., "Stress Analysis of Fracture Test Specimens," Third Semiannual Information Meeting, Oak Ridge National Laboratory Heavy Section Standard Technology Program (15-16 Apr 1969).

Visser, C. et al., "A Two-Dimensional Elastic-Plastic Analysis of Fracture Test Specimens," Oak Ridge National Laboratory Heavy Section Steel Technology Program, Westinghouse Electric Corporation Subcontract 3088, Technical Report 4 (Oct 1969).

Watkinson, F., "Hydrogen Cracking in High Strength Weld Metals," Welding J. Suppl., pp. 417S-424S (Sep 1969).

Weertman, J., "Theory of Rate of Growth of Fatigue Cracks under Combined Static and Cyclic Stresses," Int. J. Fract. Mech., Vol. 5, No. 1 (Mar 1969).

Wei, R.P., "Some Aspects of Environment-Enhanced Fatigue Crack Growth," Eng. Fract. Mechanics, Vol. 1, No. 4 (Apr 1970).

Wei, R.P. and Landes, J.D., "Correlation between Sustained-Load and Fatigue Crack Growth in High-Strength Steels," Mat. Res. and Stand., Vol. 9, No. 7, p. 25 (Jul 1969).

Wei, R.P. et al., "Fatigue Crack Propagation in Some High Strength Steels,: ASTM STP 415, p. 460 (Jun 1967).

Wells, A.A., "Application of Fracture Mechanics at and beyond General Yielding," Brit. Welding J., Vol. 10, pp. 563-570 (1963).

Wessel, E.T. et al., "Engineering Methods for the Design and Selection of Materials against Fracture," Westinghouse Final Tech. Report on U.S. Army Contract DA-30-069-AMC-602(T) (1966).

Wilhelm, D.P., "Investigation of Cyclic Crack Growth Transitional Behavior," ASTM STP 415, p. 363 (1966).

Williams, M.C., "The Bending Stress Distribution at the Base of a Stationary Crack," J. Appl. Mech., Vol. 28 (1961).

Wilshaw, T.R. et al., "A General Model to Predict the Elastic-Plastic Stress Distribution and Fracture Strength of Notched Bars in Plane Strain Bending," J. Eng. Fract. Mech., Vol. I, No. 19 (Jun 1968).

Wilson, W.K. et al., "Fracture Mechanics Technology for Combined Loading and Low-to-Intermediate Strength Metals," Westinghouse Research Laboratories Technical Report 10276 (Nov 1968).

Wood, W.A. and Reimann, W.H., "Some Direct Observations of Cumulative Fatigue Damage in Metals," Columbia University Institute for the Study of Fatigue and Reliability, Technical Report 11 (Oct 1964).

Yang, C.T., "A Study of the Law of Crack Propagation," J. Basic Eng., Trans. ASME, Series D, Vol. 89, p. 487 (1967).

Yokobori, T. et al., "Fatigue Crack Propagation Behavior of Mild Steel and High Strength Steels," Tohoku Univ. Reports of Res. Inst. Strength Fract. Mat., Vol. 3, p. 39 (1967).

Younger, G.D., "The Cyclic State of Materials and the Relationship to Mechanical Properties and Fatigue," Air Force Flight Dynamics Lab. Tech. Report 66-125 (Nov 1966).

Younger, D.G., "Cyclic Plasticity and Fatigue at Stress Concentrations," presented at Meeting of SESA, Albany, New York (May 1968).

INITIAL DISTRIBUTION

Copies	
1	DIR DEF, R&E Attn: Tech Lib
4	CNO 1 Plans, Prgms & Req Br (OP 311) 1 Tech Analy & Adv Gr (OP 098T) 1 Sub Program Br (OP 981G) 1 Tech Support Br (OP 916)
3	CHONR 1 Struc Mech Br (Code 439) 1 Undersea Prog (Code 466) 1 Res Coord (Code 104)
7	DIR, NRL 1 W. F. Brown 1 W. S. Pellini 1 P. P. Puzak 1 J. M. Krafft 1 E. A. Lange 1 T. W. Crooker 1 H. L. Smith
6	NAVMAT 1 MAT 033 1 MAT 033B 1 MAT 034B 1 MAT 03L4 1 PM-17 1 CNM 395
1	NAVAIR (320N)
1	NAVFAC (03211)
1	NAVORD (035)
14	NAVSHIPS 1 SHIPS 031 1 SHIPS 034 1 SHIPS 0342 1 SHIPS 03421 1 SHIPS 03422 1 SHIPS 03423 2 SHIPS 2052 1 SHIPS 425 1 PMS 381 1 PMS 391 1 PMS 393 1 PMS 395 1 PMS 396

Copies	
2	NADC 1 Code STD 1 Code ST-3
1	NELC
2	CDR, NOL
1	NAVSTIC (Code 10)
1	NURDC
1	NUSC
1	CDR, NWC
1	Supt, US Naval Academy
1	CO, USNROTC & NAVADMINU, MIT
1	Supt, PGSC, Monterey
19	NAVSEC 1 SEC 6101 1 SEC 6101D 1 SEC 6101E 1 SEC 6110 1 SEC 6110D 1 SEC 6111 1 SEC 6113 1 SEC 6113B4 1 SEC 6114 1 SEC 6120 1 SEC 6120D 1 SEC 6122 1 SEC 6128 1 SEC 6128E 2 SEC 6129 1 SEC 6140 1 SEC 6144 1 SEC 6147C
1	NAVSHIPYD CHASN
1	NAVSHIPYD PTSMH
1	NAVSHIPYD SFRAN BAY VJO
1	SUPSHIP, Camden
1	SUPSHIP, Newport News
1	SUPSHIP, Pascagoula
2	CDR, DDC

Copies	
1	AMMRC, Warminster, Pa. Attn: Dr. Burke, Code AMXMR-T
1	AFFDL, WPAFB Attn: Dr. R. G. Forman
1	USCG (CDR S. Loosmore)
1	MARAD (Mr. J. Nachtschein)
1	NASA, Lewis Research Center Attn: Mr. S. S. Manson
1	NASA, Goddard Space Flight Center Attn: Mr. P. Stern
1	NAS, Attn: Comm on Undersea Warfare
1	DIR, APL, Univ of Wash., Seattle
1	Dr. R. DeHart, SWRI
1	Prof. J. R. Rice, Brown Univ
1	Prof. G. R. Irwin, Lehigh Univ
1	Prof. R. P. Wei, Lehigh Univ
1	Prof. A. S. Kobayashi, Univ of Washington
1	Prof. P. Hilton, Lehigh Univ
1	Prof. P. C. Paris, Lehigh Univ
1	Prof. G. C. Sih, Lehigh Univ

Copies	
1	Dr. G. T. Hahn, Battelle Memorial Institute
1	Dr. S. R. Heller, Catholic Univ of America
1	Dr. H. Liebowitz, George Washington Univ
1	Dr. F. A. Mellinbock, MIT
1	Prof. W. H. Munse, Univ of Illinois
1	Prof. A. H.-S. Ang, Univ of Illinois
1	Prof. A. M. Freudenthal, George Washington Univ
1	Prof. A. J. McEvily, Univ of Connecticut
1	EB Div, Gen Dyn Corp
1	NNSB & DD Co.
1	Ingalls Shipbldg Corp
2	Mr. C. F. Larson Sec., Welding Res Council

CENTER DISTRIBUTION

1	17
1	172
1	173
1	174
1	177
1	1721
4	1727
1	28
1	2814
1	282
5	2823
1	2802

UNCLASSIFIED

Security Classification

DOCUMENT CONTROL DATA - R & D

(Security classification of title, body of abstract and indexing annotation must be entered when the overall report is classified)

1 ORIGINATING ACTIVITY (Corporate author)	2a. REPORT SECURITY CLASSIFICATION
Naval Ship Research & Development Center Washington, D.C. 20034	UNCLASSIFIED
	2b. GROUP

3 REPORT TITLE

CRITICAL REVIEW OF FRACTURE AND FATIGUE ANALYSIS

4 DESCRIPTIVE NOTES *(Type of report and inclusive dates)*

Final

5. AUTHOR(S) *(First name, middle initial, last name)*

O. Lomacky
H. Vanderveldt

6. REPORT DATE	7a. TOTAL NO OF PAGES	7b. NO. OF REFS
March 1972	274	304

8a. CONTRACT OR GRANT NO.	9a. ORIGINATOR'S REPORT NUMBER(S)
b. PROJECT NO. SF 35.422.210, Task 15055	3655
c.	9b. OTHER REPORT NO(S) *(Any other numbers that may be assigned this report)*
d.	

10 DISTRIBUTION STATEMENT

Approved for public release: Distribution unlimited.

11. SUPPLEMENTARY NOTES	12. SPONSORING MILITARY ACTIVITY
	Naval Ship Systems Command Code 0342

13 ABSTRACT

The state of knowledge in fracture and fatigue analysis is reviewed in order to provide a technical background for the development of fatigue design procedures for submarine hulls. Special emphasis is placed on analytical fracture mechanics approach. Results are presented for the stress and strain distribution near the crack tip. Current fracture criteria and subcritical crack initiation and propagation laws are summarized including the environmental effects.

DD FORM 1 NOV 65 1473 (PAGE 1)

S/N 0101-807-6801

UNCLASSIFIED

Security Classification

14 KEY WORDS	LINK A		LINK B		LINK C	
	ROLE	WT	ROLE	WT	ROLE	WT
Submarine hull application						
Crack stress analysis						
Fracture criteria						
Crack fatigue initiation						
Crack propagation						
Cumulative damage						
Environmental effects						
Hydrogen embrittlement						